



College of Engineering, Design and Physical Sciences  
Department of Electronic and Computer Engineering  
Wireless Networks and Communications Centre

# Enhancement and Performance Analysis for 3D Beamforming Systems

A thesis submitted in fulfilment of the requirements for the degree of  
Doctor of Philosophy (PhD)

By:

**Cheng Xu**

Department of Electronic and Computer Engineering, Brunel University  
London

Supervisor:

**Prof. John Cosmas**

February 2018

# Publications and Presentations

## Publications

### Journals:

1. Cheng Xu, John Cosmas and Yue Zhang, “Minimal Mean-Square Error for 3D MIMO Beamforming Weighting”, published in IET Electronics Letters, vol. 52, pp: 2019 – 2021, November 2016.

### Conferences

1. Cheng Xu, John Cosmas, Yue Zhang, Pavlos Lazaridis, Giuseppe Araniti and Zaharias D. Zaharis, “3D MIMO radio channel modelling of a weighted linear array system of antennas for 5G cellular systems”, 2016 International Conference on Telecommunications and Multimedia (TEMU), IEEE, Heraklion, Greece, July 2016.
2. Cheng Xu and John Cosmas, “Comparison of Isotropic and 3D Beamforming LTE Systems using Simulation”, The 1st EAI International Conference on 5G for Future Wireless Networks (5GWN), Springer, Beijing, China, December 2017.

# Abstract

This thesis is about the researching for 5<sup>th</sup> generation (5G) communication system, which focus on the improvement of 3D beamforming technology in the antenna array using in the Full Dimension Multiple-Input Multiple-Output (FD-MIMO) system and Millimeter-wave (mm-wave) system. When the 3D beamforming technology has been used in 5G communication system, the beam needs a weighting matrix to direct the beam to cover the UEs, but some compromises should be considered. If the narrow beams are used to transmit signals, then more energy is focused in the desired direction, but this has a restricted coverage area to a single or few User Equipments (UEs). If the BS covers multiple UEs, then multiple beams need to be steered towards more groups of UEs, but there is more interference between these beams from their side lobes when they are transmitted at same time. These challenges are waiting to be solved, which are about interference between each beam when the 3D beamforming technology is used.

Therefore, there needs to be one method to decrease the generated interference between each beam through directing the side lobe beams and nulls to minimize interference in the 3D beamforming system. Simultaneously, energy needs to be directed towards the desired direction. If it has been decided that one beam should cover a cluster of UEs, then there will be a range of received Signal to Interference plus Noise Ratio (SINR) depending on the location of the UEs relative to the direction of the main beam. If the beam is directed towards a group of UEs then there needs be a clustering method to cluster the UEs.

In order to cover multiple UEs, an improved K-means clustering algorithm is used to cluster the multiple UEs into different groups, which is based on the cosine distance. It can decrease the number of beams when multiple UEs need be covered by multiple beams at same time.

Moreover, a new method has been developed to calculate the weighting matrix for beamforming. It can adjust the values of weighting matrix according to the UEs' location and direct the main beam in a desired direction whilst minimizing its side lobes in other undesired directions. Then the minimum side lobe beamforming system only needs to know the UEs' location and can be used to estimate the Channel State Information (CSI) of UEs. Therefore, the scheme also shows lower complexity when compared to the beamforming methods with pre-coding.

In order to test the improved K-means clustering algorithm and the new weighting method that can enhance the performance for 3D beamforming system, the two simulation systems are simulated to show the results such as 3D beamforming LTE system and mm-wave system.

# Contents

<b>Abstract.....</b>	<b>i</b>
<b>Glossary of Abbreviations .....</b>	<b>ix</b>
<b>List of Figures.....</b>	<b>xi</b>
<b>List of Tables.....</b>	<b>xxi</b>
<b>Acknowledgments .....</b>	<b>xxiv</b>
<b>1. Introduction.....</b>	<b>25</b>
1.1 Motivation .....	26
1.2 Challenges .....	29
1.3 Aims of research.....	30
1.4 Methodology .....	31
1.5 Research Contribution.....	32
1.6 Thesis organization.....	33
<b>2. Technical Background and Literature Review .....</b>	<b>36</b>
2.1 Introduction to LTE System .....	37
2.1.1 AMC Technology .....	38
2.1.2 OFDM Technology.....	39
2.1.3 MIMO Technology .....	39
2.1.4 Channels Model of LTE System.....	40
2.2 Antenna Array .....	42
2.2.1 Point Sources .....	42
2.2.2 Linear Unit Antenna Array .....	43
2.2.3 Rectangular Array.....	43
2.2.4 Other Different Shape Antenna Arrays.....	44
2.3 Clustering Algorithms .....	50

2.3.1 Density-based Clustering .....	51
2.3.2 Hierarchical Clustering .....	51
2.3.3 Grid-Based Clustering .....	51
2.3.4 Partition Clustering .....	51
2.4 The Road to 5G .....	53
2.4.1 Introduction of 5G.....	54
2.4.2 Comparison LTE and Verizon Wireless 5G .....	55
2.4.3 Carrier Frequency .....	55
2.4.4 Multi-user MIMO Technology .....	57
2.4.5 Beamforming Technology .....	58
2.4.6 Massive MIMO Theory .....	58
2.4.7 Mm-wave .....	59
2.5 3D Beamforming .....	59
2.5.1 The Beam Pattern.....	60
2.5.2 Dolph-Tchebyscheff optimum distribution for the linear arrays .....	62
2.5.2 3D LTE Channel Model.....	67
2.5.3 The Weighting of MxN antenna .....	69
2.5.4 FD-MIMO Beamforming.....	70
2.5.5 Constant Beamwidth Beamforming.....	71
2.5.6 Minimum Side-lobe Beamforming in Spherical Antenna Array .....	72
2.6 Millimetre-wave .....	72
2.6.1 Analogue Beamforming.....	73
2.6.2 Digital Beamforming .....	73
2.6.3 Hybrid Beamforming in MIMO.....	74

2.6.4 Millimetre-Wave Channel Model .....	76
2.7 Conclusion.....	80
<b>3. Innovation Schemes for 3D Beamforming Technology .....</b>	<b>81</b>
3.1 Introduction .....	82
3.2 Grouping UEs based on K-meansAlgorithm.....	83
3.3 Calculatingthe Power of Each User in the Same Beam .....	85
3.4 Calculating the Weighting Matrix .....	86
3.4.1 The Direction Matrix calculation.....	87
3.4.2 The Weighting Vector in x-Direction .....	88
3.4.3 The Weighting Vector in y-Direction .....	91
3.4.4 Calculation of the Weighting Matrix .....	91
3.5 Calculation of the Receive Signal .....	93
3.6 Conclusion.....	93
<b>4. Minimal Side Lobe 3D LTE Beamforming System towards a Group of UEs..</b>	<b>95</b>
4.1 Introduction .....	96
4.2 The Analysis of Simulation Results .....	96
4.2.1 Introduction.....	96
4.2.2 The network environment .....	98
4.2.3 The beams .....	98
4.2.4 The BER results compared .....	99
4.2.5 The testing for different environments.....	106
4.2.6 Conclusion .....	108
<b>5. Optimal Minimum Side lobe Hybrid Beamforming in Millimeter Wave System</b>	<b>110</b>
.....	
5.1 Introduction .....	111

5.2 The Analysis of Simulation results.....	112
5.2.1 Introduction.....	112
5.2.2 The network environment.....	113
5.2.3 The beams.....	114
5.2.4 The BER results compared in different mm-wave systems.....	118
5.2.5 CDF of BER in different mm-wave systems.....	126
5.3 Compare the different size of antenna arrays and the different numbers of beams .....	127
5.5.1 32×32 antenna arrays.....	128
5.5.2 16×16 antenna arrays.....	135
5.5.3 8×8 antenna arrays.....	141
5.5.4 Comparison of the results.....	151
5.6 Conclusion.....	156
<b>6. Discussion, Conclusions and Future Work.....</b>	<b>158</b>
6.1 Discussion.....	159
6.2 Conclusions.....	160
6.3 Future Work.....	162
<b>Reference.....</b>	<b>164</b>
<b>Appendices:PhD programs.....</b>	<b>176</b>
<b>Appendix A: Simulation Design for Minimal Side Lobe 3D Beamforming LTE System towards a Group of User Equipment.....</b>	<b>177</b>
A.1 UML Modeling for Simulation System.....	177
A.1.1 Introduction.....	177
A.1.2 SimStart Use-case.....	179
A.1.3 ReadStart Use-case.....	184

A.1.4 BeamStart Use-case .....	186
A.1.5 CBERStart Use-case .....	192
A.1.6 ReadBERStart Use-case.....	197
A.1.7 BERCellUEsStart Use-case .....	202
A.1.8 Plot3DStart Use-case .....	208
A.2 The Simulation System design .....	210
A.2.1 Data Class .....	210
A.2.2 Output Class.....	211
A.2.3 Interactive Interface .....	211
A.3 Function SimStart_Callback (hObject, eventdata, handles).....	213
A.3.1 Function EstCommEnv .....	213
A.3.2 Function networkEnv3D .....	218
A.4 Function ReadStart_Callback (hObject, eventdata, handles) .....	220
A.5 Function BeamStart_Callback (hObject, eventdata, handles).....	221
A.5.1 Function WeightSIRmaxLSM.....	221
A.5.2 Function ShowBeamOnFace.....	224
A.5.3 Function ShowBeamOnCell .....	224
A.5.4 Function SinrAndThroughput .....	225
A.6 Function CBERStart_Callback (hObject, eventdata, handles).....	226
A.6.1 Function CalBerPDFOn3DBeam.....	226
A.6.2 Function Beam3DChannel .....	227
A.6.3 Function receivedSignalConv .....	238
A.6.4 Function calculateBER .....	239
A.7 Function ReadBERStart_Callback (hObject, eventdata, handles) .....	240



A.7.1 Function calBERLteSystem .....	240
A.7.2 Function calBERLteSISO .....	241
A.7.3 Function CheckUserOnBeam .....	241
A.7.4 Function calBER3DBeam.....	242
A.7.5 Function readBER.....	243
A.8 Function BERCellUEsStart_Callback (hObject, eventdata, handles).....	244
A.8.1 Function CalBerUEsCell.....	244
A.9 Function Plot3DStart_Callback (hObject, eventdata, handles).....	245
A.9.1 Function readBerUEsCell .....	245
<b>Appendix B: Simulation Design for Optimal Minimum Side lobe Hybrid Beamforming of Millimeter Wave System .....</b>	<b>247</b>
B.1 UML Modeling for mm-wave antenna arrays system .....	248
B.1.1 Introduction .....	248
B.1.2 Same use-case as the simulation of a hexagonal antenna arrays cell in last Section.....	249
B.1.3 mmCBERStart Use-case .....	249
B.1.4 mmReadBERStart Use-case.....	255
B.1.5 CompBERStart Use-case .....	260
B.1.6 ReadCompBER Use-case.....	265
B.2 The Simulation System design .....	268
B.2.1 Data Class.....	268
B.2.2 Output Class .....	268
B.2.3 Interactive Interface.....	268
B.2.4 The simulation systems .....	271
B.3 Function mmCBERStart_Callback (hObject, eventdata, handles).....	272

B.3.1 Function CalBerPDFOn3DBeam .....	272
B.4 mmReadBERStart_Callback (hObject, eventdata, handles) .....	278
B.4.1 Function calBERLteSystem .....	278
B.4.2 Function calBERLteSISO .....	279
B.4.3 Function CheckUserOnBeam.....	280
B.4.4 Function calBER3DBeam .....	280
B.4.5 Function readBER .....	281
B.5 Function CompBERStart_Callback (hObject, eventdata, handles).....	282
B.5.1 Function CalBerOn3DBeam .....	283
B.6 Function ReadCompBER_Callback (hObject, eventdata, handles) .....	283

# Glossary of Abbreviations

Abbreviation	Stands for
1G	First Generation
2G	Second Generation
3G	Third Generation
3GPP	Third Generation Partnership Project
3GPP TR	Third Generation Partnership Project Technical Report
4G	Fourth Generation
5G	Fifth Generation
2D	Two Dimensional
3D	Three Dimensional
3D-Uma	3D Urban Macro
3D-UMi	3D Urban Micro
ABF	Analog Beamforming
AMC	Adaptive Modulation and Coding
AP	Access Point
BLAST	Bell Laboratories Layered Space Time
BER	Bit Error Rate
BS	Base Station
BSS	Basic Service Set
CDF	Cumulative Distribution Function
CDMA	Code Division Multiple Access
CP	Cyclic Prefix
CQI	Channel Quality Indicator
CSI	channel state information
dB <sub>i</sub>	dB(isotropic)
dB <sub>m</sub>	dB(mW)
DBF	Digital Beamforming
DFT	Discrete Fourier Transform
DL	Downlink
DoA	Direction of Arrival
DVB	Digital Video Broadcasting
eMBB	Enhanced Mobile Broadband
EU	European Union
FCC	Federal Communications Commission
FDD	Frequency Division Duplexing
FDMA	Frequency Division Multiple Access
FD-MIMO	Full Dimension Multiple-Input Multiple-Output
FNBW	First Nulls Beam Width
Giga Hertz	GHz
HBF	Hybrid Beamforming

HDA	Hybrid Digital or Analogue
HPBW	Half-power Beam Width
IMT-A	International Mobile Telecommunications Advanced
ITU	International Telecommunication Union
ITU-R	International Telecommunication Union Radio-communication Sector
IoT	Internet of Things
LOS	Line of Sight
IP	Internet Protocol
LTE	Long-Term Evolution
NLOS	Non-line of Sight
MCS	Modulation and Coding Scheme
MIMO	Multiple-Input Multiple-Output
MLD	Maximum likelihood detection
mm-wave	Millimetre Wave
MU-MIMO	Multi-user Multiple-Input Multiple-Output
MVDR	Minimum Variance Distortion less Response
OFDM	Orthogonal Frequency Division Multiplexing
PCB	Printed Circuit Board
PDF	Probability Distribution Function
PHY	Physical layer
PL	Path Loss
PMI	Pre-coding Matrix Indicator
PSO	Particle Swarm Optimisation
QAM	Quadrature Amplitude Modulation
QPSK	Quadrature phase Shift Keying
RF	Radio Frequency
SD	Sphere Decoding
SIC	Sequential Interference Cancellation
SIR	the signal to interference ratio
SINR	Signal to Interference plus Noise Ratio
SISO	Single Input Single Output
SLL	Side-Lobe Level
SNR	Signal to Noise Ratio
SVD	Singular Value Decomposition
TDD	Time Division Duplexing
TDMA	Time Division Multiple Access
TD-SCDMA	Time Division Synchronous Code Division Multiple Access
UE	User Equipment
ULA	Uniform Linear Array
URLLC	Ultra-reliable low-latency communications
WCDMA	Wideband Code Division Multiple Access

## List of Figures

Figure 1- 1: Methods to achieve capacity improvements .....	26
Figure 2- 1: The evolution of different mobile communication standards[28] ....	37
Figure 2- 2: Timeline in 3GPP and commercialization [29].....	38
Figure 2- 3: N-element linear array composed of isotropic radiating antenna elements .....	43
Figure 2- 4: A rectangular array in the x-y plane .....	44
Figure 2- 5: The triangular prism for an antenna array [40].....	44
Figure 2- 6: The antenna array for one cell in this thesis.....	45
Figure 2- 7: The cylindrical antenna arrays [41] .....	45
Figure 2- 8: The one face for an antenna array[42] .....	46
Figure 2- 9: The 8X16 antenna elements[43] .....	46
Figure 2- 10: The antenna arrays with spacing[44] .....	47
Figure 2- 11: Right: top-to bottom view of FD-MIMO antenna array and feed network; left: bottom view of one sub-array with detailed PCB stack-up [44] .....	48
Figure 2- 12: The rectangular planar array .....	48
Figure 2- 13: The beam patterns for sector 1, 2, and 3 of the proposed 3×3 cell [46] .....	50
Figure 2- 14: Three stages of development on the road to 5G[63].....	54
Figure 2- 15: Air interface framework for 5G[68].....	55
Figure 2- 16: Future mobile broadband requirements .....	56
Figure 2- 17: Possible scope of WRC '15 and WRC '19 5G spectrum discussions[66].....	56
Figure 2- 18: Downlink signals [73].....	57
Figure 2- 19: Uplink signals [73].....	58

Figure 2- 20: The beamforming system[75] .....	58
Figure 2- 21: Massive MIMO antenna [76] .....	59
Figure 2- 22: The beam pattern[83] .....	61
Figure 2- 23: The angular beam width at the half-power level[83] .....	61
Figure 2- 24: The FNBW and HPBW[83] .....	62
Figure 2- 25: The two isotropic point sources having equal amplitude and oscillating .....	63
Figure 2- 26: The two isotropic point sources with the origin of the coordinate system coincident with one of the sources .....	64
Figure 2- 27: The linear arrays for the number of the antennas is even .....	64
Figure 2- 28: The linear arrays for the number of the antennas is odd .....	64
Figure 2- 29: The single channel model[10] .....	67
Figure 2- 30: The 3D-UMi: Definition of d2D and d3Dfor outdoor UEs .....	69
Figure 2- 31: The 3D-Uma: Definition of d2D-out, d2D-in and d3D-out, d3D-in for indoor UEs .....	69
Figure 2- 32: The rectangular planar array for MxN antenna[45] .....	69
Figure 2- 33: The beam pattern in a fixed direction [84] .....	70
Figure 2- 34: Right: top-to bottom view of FD-MIMO antenna array and feed network; left: bottom view of one sub-array with detailed PCB stack-up[86] .....	71
Figure 2- 35: Analogue Beamforming Architecture [89] .....	73
Figure 2- 36: Digital Beamforming Architecture[90] .....	74
Figure 2- 37: Hybrid beamforming structure [93] .....	75
Figure 2- 38: The photo of the 60 GHz reference chip antenna resting on a US quarter[99] .....	76
Figure 2-39: The mm-wavesystem model for the multi-user MIMO beamforming [99] .....	77
Figure 2- 40: The measurement locations in NYC at 28 GHz and 73 GHz[100].	77
Figure 3- 1: The four main beams for 16×16 antenna arrays .....	85

Figure 3- 2: The one hexagonal cell .....	85
Figure 3- 3: The rectangular planar array for MxN antenna[45] .....	87
Figure 4- 1: The antenna arrays for one cell (the red squares are the antennas)...97	
Figure 4- 2: The simulation result in UMa antenna arrays system .....	98
Figure 4- 3: The beam for the fourth antenna face in the second simulation running time .....	99
Figure 4- 4: The 3D beam for second simulation running time in one cell .....	99
Figure 4- 5: The constellation figure of the received signals for UE in LTE SISO system .....	100
Figure 4- 6: The constellation figure of the received signals for UE in 3D beamforming LTE system.....	100
Figure 4- 7: The BER for one UE in 3D beamforming LTE system and another UE in LTE SISO system .....	101
Figure 4- 8: The constellation figure of the received signals for UE in LTE MIMO system .....	102
Figure 4- 9: The constellation figure of the received signals for UE in 3D beamforming LTE system.....	102
Figure 4- 10: The BER for one UE in 3D beamforming LTE system and another UE in LTE MIMO system .....	103
Figure 4- 11: The CDF of BER in 3D beamforming LTE system.....	104
Figure 4- 12: The PDF of BER in 3Dbeamforming LTE system.....	105
Figure 4- 13: The comparison BER between 3D beamforming LTE system and LTE MIMO system.....	105
Figure 4- 14: The BER for different environments in 20 dB for different number of UEs.....	107
Figure 5- 1: The hybrid beamforming mm-wave system .....	112
Figure 5- 2: The simulation result in UMa for16x16 antenna arrays system .....	114
Figure 5- 3: The beams in the 16x16 antenna arrays system with 4 beams .....	115

Figure 5- 4: The 3D beam in the 16×16 antenna arrays system with 4 beams...	116
Figure 5- 5: The CDF for the SINR in the two mm-wave systems .....	117
Figure 5- 6: The CDF for the throughput in the two mm-wave systems.....	117
Figure 5- 7: The constellation figure of the received signals for UE in LTE MIMO system .....	119
Figure 5- 8: The constellation figure of the received signals in equal weighting mm-wave system.....	119
Figure 5- 9: The constellation figure of the received signals for UE in new weighting mm-wave system .....	120
Figure 5- 10: The comparison of BER for these three systems .....	120
Figure 5- 11: The comparison of BER for two mm-wave systems .....	121
Figure 5- 12: The CDF of BER for equal weighting mm-wave system.....	122
Figure 5- 13: The CDF of BER for the new weighting mm-wave system .....	122
Figure 5- 14: The PDF of BER for equal weighting mm-wave system.....	123
Figure 5- 15: The PDF of BER for the new weighting mm-wave system.....	124
Figure 5- 16: The comparison of BER for three systems .....	125
Figure 5- 17: The comparison of BER for three systems when the SNR have different value .....	126
Figure 5- 18: In the 4 beams mm-wave system, the CDF of BER .....	127
Figure 5- 19: The simulation result in UMa for 32×32 antenna arrays system ....	129
Figure 5- 20: The beams in the 32×32 antenna arrays system with 4 beams .....	130
Figure 5- 21: The 3D beam in the 32×32 antenna arrays system with 4 beams.	131
Figure 5- 22: The comparison of CDF for the SINR by different methods.....	131
Figure 5- 23: The comparison of CDF for the throughput by different methods	132
Figure 5- 24: The comparison of BER in three system for different SNR value.	133
Figure 5- 25: In the 2 beams system, the comparison of BER .....	134
Figure 5- 26: In the 4 beams system, the comparison of BER .....	134
Figure 5- 27: The simulation analysis in UMa for 16×16 antenna arrays system .....	135
Figure 5- 28: The beams in the 16×16 antenna arrays system with 2 beams .....	136



Figure 5- 29: The 3D beam in the 16×16 antenna arrays system with 2 beams .	136
Figure 5- 30: The CDF for the SINR in mm-wave system obtained by different methods .....	137
Figure 5- 31: The CDF for the throughput in mm-wave system obtained by different methods .....	137
Figure 5- 32: The BER in three systems when the SNR are 0 dB, 10 dB, 20 dB or 30 dB.....	138
Figure 5- 33: In the 2 beams system, the BER in two systems for different SNR .....	139
Figure 5- 34: In the 2 beams system, the CDF of BER in two mm-wave systems .....	140
Figure 5- 35: The simulation result in UMa for 8×8 antenna arrays system .....	141
Figure 5- 36: The beams in the 8×8 antenna arrays system with 2 beams .....	141
Figure 5- 37: The 3D beam in the 8×8 antenna arrays system with 2 beams .....	142
Figure 5- 38: The CDF for the SINR in two mm-wave systems .....	142
Figure 5- 39: The CDF for the throughput in two mm-wave systems.....	143
Figure 5- 40: The BER in three systems when the SNR are 0 dB, 10 dB, 20 dB or 30 dB.....	144
Figure 5- 41: In the 2 beams system, the 90% sample points for BER in two mm-wave systems .....	145
Figure 5- 42: In the 2 beams system, the CDF of BER in two mm-wave systems .....	146
Figure 5- 43: The simulation result in UMa for the 8×8 antenna arrays system with 1 beam.....	147
Figure 5- 44: The 3D beam in the 8×8 antenna arrays system with 1 beam.....	147
Figure 5- 45: The CDF for the SINR in two mm-wave systems .....	148
Figure 5- 46: The CDF for the throughput in two mm-wave systems.....	149
Figure 5- 47: The BER in three systems when the SNR are 10 dB, 20 dB, 30 dB or 40 dB.....	150
Figure 5- 48: The CDF of BER in two mm-wave systems when the SNR is 0 dB to	

15 dB.....	150
Figure 5- 49: The CDF for the SINR in 2 beams mm-wave system .....	152
Figure 5- 50: The CDF for the SINR in 4 beams mm-wave system .....	153
Figure 5- 51: The CDF for the BER in 2 beams mm-wave system.....	154
Figure 5- 52: The CDF for the BER in 4 beams mm-wave system.....	155
Figure A-1: The main function for the simulation.....	177
Figure A-2: UML use-cases model.....	178
Figure A-3: Activity diagram for UML this use-case.....	180
Figure A-4: The static model of the use-case SimStart .....	181
Figure A-5: The description of the entity class.....	181
Figure A-6: Interaction between the entity class “<entity>:Analyzer” and external UEs.....	182
Figure A-7: The dynamic model of the use-case SimStart .....	183
Figure A-8: The activity diagram for use-case .....	184
Figure A-9: The static model of the use-case ReadStart.....	185
Figure A-10: The description of the entity class.....	185
Figure A-11: The interaction between entity class “<entity>:Analyzer” and external UEs.....	185
Figure A-12: The dynamic model of the use-case ReadStart .....	186
Figure A-13: The activity diagram for use-case .....	188
Figure A-14: The static model of the use-case BeamStart .....	189
Figure A-15: The description of the entity class.....	189
Figure A-16: The interaction between entity class “<entity>:Analyzer” and external UEs.....	189
Figure A-17: The dynamic model of the use-case BeamStart .....	191
Figure A-18: The activity diagram for use-case .....	193
Figure A-19: The static model of the use-case CBERStart .....	194
Figure A-20: The description of the entity class.....	194
Figure A-21: The interaction between entity class “<entity>:Analyzer” and	

external UEs.....	194
Figure A-22: The dynamic model of the use-case CBERStart .....	196
Figure A-23: The activity diagram for this use-case .....	198
Figure A-24: The static model of the use-case ReadBERStart.....	199
Figure A-25: The description of the entity class.....	199
Figure A-26: The interaction between entity class “<entity>:Analyzer” and external UEs.....	200
Figure A-27: The dynamic model of the use-case ReadBERStart .....	201
Figure A-28: The sequence for this use-case.....	203
Figure A-29: The static model of the use-case BERCellUEsStart .....	204
Figure A-30: The description of the entity class.....	204
Figure A-31: The interaction between entity class “<entity>:Analyzer” and external UEs.....	205
Figure A-32: The dynamic model of the use-case BERCellUEsStart .....	206
Figure A-33: The activity diagram for use-case .....	208
Figure A-34: The static model of the use-case Plot3DStart .....	209
Figure A-35: The description of the entity class.....	209
Figure A-36: The interaction between entity class “<entity>:Analyzer” and external UEs.....	209
Figure A-37: The dynamic model of the use-case Plot3DStart .....	210
Figure A-38: Data classes in 7 UML use-cases .....	211
Figure A-39: Output classes in 7 UML use-cases .....	211
Figure A-40: 7 UML use-case interactive interfaces.....	211
Figure A-41: GUI function for the interactive interface.....	212
Figure A-42: The flow chart of functions .....	213
Figure A-43: The flow chart of functions of EstCommEnv .....	214
Figure A-44: The flow chart of functions of RunSim .....	215
Figure A-45: The flow chart of functions of AntArray6F4Aream .....	216
Figure A-46: The flow chart of function MoveUserCluster .....	217
Figure A-47: The network environment for the cell.....	219

Figure A-48: The flow chart of function networkEnv3D .....	220
Figure A-49: The flow chart of function ReadStart_Callback.....	220
Figure A-50: The flow chart of function BeamStart_Callback .....	221
Figure A-51: The flow chart of function WeightSIRmaxLSM .....	222
Figure A-52: The flow chart of function AngleofACS.....	222
Figure A-53: The flow chart of function ShowBeamOnFace.....	224
Figure A-54: The flow chart of function ShowBeamOnCell.....	224
Figure A-55: The flow chart of function Sinr And Throughput .....	225
Figure A-56: The flow chart of function CBERStart_Callback .....	226
Figure A-57: The flow chart of function CalBerPDFOn3DBeam.....	227
Figure A-58: The flow chart of function Beam3DChannel .....	228
Figure A-59: The flow chart of the function ChannelMode .....	229
Figure A-60: The flow chart of the function Channel3DMode .....	230
Figure A-61: The flow chart of the function ChannelModel.....	232
Figure A-62: The flow chart of function ArrDepangle.....	233
Figure A-63: The flow chart of the function fieldPattern.....	234
Figure A-64: The flow chart of the function explambda .....	235
Figure A-65: The flow chart of the function xpr .....	236
Figure A-66: The flow chart of the function ChannelLoS.....	237
Figure A-67: The flow chart of the function fieldPatternLoS .....	238
Figure A-68: The flow chart of the function receivedSignalConv .....	239
Figure A-69: The flow chart of function ReadBERStart_Callback.....	240
Figure A-70: The flow chart of function calBERLteSystem .....	241
Figure A-71: The flow chart of the function calBERLteSISO .....	241
Figure A-72: The flow chart of the function calBER3DBeam.....	243
Figure A-73: The flow chart of the function BERCellUEsStart_Callback.....	244
Figure A-74: The flow chart of the function CalBerUEsCell.....	245
Figure A-75: The flow chart of the function Plot3DStart_Callback.....	245
Figure B- 1: The main program for the simulation.....	247

Figure B- 2: The UML use-cases model.....	248
Figure B- 3: The activity diagram for this use-case mmCBERStart .....	251
Figure B- 4: The static model of the use-case mmCBERStart .....	252
Figure B- 5: The entity class of the use-case mmCBERStart.....	252
Figure B- 6: The class chart of the use-case mmCBERStart .....	252
Figure B- 7: The dynamic model of the use-case mmCBERStart .....	254
Figure B- 8: The activity diagram for this use-case mmReadBERStart.....	256
Figure B- 9: The static model of the use-case mmReadBERStart.....	257
Figure B- 10: The entity class of the use-case mmReadBERStart .....	257
Figure B- 11: The class chart of the use-case mmReadBERStart .....	258
Figure B- 12: The dynamic model of the use-case mmReadBERStart .....	259
Figure B- 13: The activity diagram for this use-case CompBERStart.....	261
Figure B- 14: The static model of the use-case CompBERStart .....	262
Figure B- 15: The entity class CompBERStart.....	262
Figure B- 16: The class chart of the use-case CompBERStart .....	262
Figure B- 17: The dynamic model of the use-case CompBERStart .....	264
Figure B- 18: The activity diagram for this use-case ReadCompBER.....	265
Figure B- 19: The static model of the use-case ReadCompBER.....	266
Figure B- 20: The entity class of the use-case ReadCompBER .....	266
Figure B- 21: The class chart of the use-case ReadCompBER .....	267
Figure B- 22: The dynamic model of the use-case ReadCompBER .....	267
Figure B- 23: Data classes for 7 UML use-cases.....	268
Figure B- 24: Output classes for 7 UML use-cases .....	268
Figure B- 25: Interactive interfaces in7 UML use-cases .....	269
Figure B- 26: A GUI function for the interactive interface .....	270
Figure B- 27: sub-systems in the main.m .....	271
Figure B- 28: The flow chart of the function mmCBERStart_Callback .....	272
Figure B- 29: The flow chart of the function CalBerPDFOn3DBeam .....	273
Figure B- 30: The flow chart of the function Beam3DChannelSINR .....	274
Figure B- 31: The flow chart of function mmReadBERStart_Callback.....	278

Figure B- 32: The flow chart of the function calBERLteSystem .....	279
Figure B- 33: The flow chart of the function calBERLteSISO .....	280
Figure B- 34: The flow chart of the function calBER3DBeam .....	281
Figure B- 35: The flow chart of the function CompBERStart_Callback.....	282
Figure B- 36: The flow chart of the function CalBerOn3DBeam .....	283
Figure B- 37: The flow chart of the function ReadCompBER _Callback.....	284

## List of Tables

Table 2- 1: Overview of dl reference measurement channels[39] .....	40
Table 2- 2: The parameters for ULA MIMO correlation matrices[39] .....	42
Table 2- 3: PHY parameter Comparison[69].....	55
Table 2- 4: Parameters in different path for PL[100] .....	79
Table 4- 1: The parameters for running the simulation .....	97
Table 4- 2: The different simulation running times for different numbers of UEs .....	106
Table 4- 3: Parameters for running the simulation system shown in Figure 4-55 .....	107
Table 4- 4: The detailed BER for results in Figure 4-56 .....	108
Table 5- 1: The parameters for running the simulation .....	113
Table 5- 2: The parameters for running simulation .....	128
Table 5- 3: The parameters for comparison systems .....	151
Table 5- 4: The detailed SINR for the simulation results in Figure5-75 .....	152
Table 5- 5: The detailed SINR for results in Figure 5-50 .....	153
Table 5- 6: The detailed CDF for BER in Figure 5- 51 .....	154
Table 5- 7: The detailed CDF for BER in Figure 5-52.....	156
Table A- 1: The UML use-case description for “SimStart” .....	179
Table A- 2: The message description of the dynamic model of the use-case SimStart.....	182
Table A- 3: The read and present data use-cases description for “ReadStart” ...	184
Table A- 4: The message description of the use-case ReadStart .....	186
Table A- 5: The UML use-case description for “BeamStart” .....	187
Table A- 6: The message description of the use-case BeamStart.....	190
Table A- 7: The UML use-case description for “CBERStart” .....	192

Table A- 8: The message description of the use-case CBERStart.....	195
Table A- 9: The description for “ReadBERStart” .....	197
Table A- 10: The message description of the use-case ReadBERStart .....	200
Table A- 11: The UML use-case for “BERCellUEsStart” .....	202
Table A- 12: The message description of the use-case BERCellUEsStart .....	207
Table A- 13: The description for “Plot3DStart” .....	208
Table A- 14: The message description of the use-case Plot 3D Start.....	210
Table A- 15: Parameters about the channel .....	215
Table A- 16: parameters of antenna array and the coordinate’s data .....	216
Table A- 17: The parameters in the function MoveUserCluster.m .....	217
Table A- 18: The parameters in function UserPosit .....	218
Table A- 19: The parameters of function networkEnv3D .....	219
Table A- 20: The parameters in the function Weight_LSM.....	222
Table A- 21: The parameters in the function pathloss.....	225
Table A- 22: The parameters in function CalBerPDFOn3DBeam .....	226
Table A- 23: The parameters in function Beam3DChannel .....	227
Table A- 24: The parameters in function getWeight .....	228
Table A- 25: The parameters in the function ChannelMode .....	229
Table A- 26: The parameters in the function Channel3DMode .....	230
Table A- 27: The parameters in the function ChannelModel .....	231
Table A- 28: The parameters in the function explambda .....	234
Table A- 29: The parameters in the function ChannelLoS .....	236
Table A- 30: The parameters in the function receivedSignalConv.....	239
Table A- 31: The parameters in the function calculateBER .....	239
Table A- 32: The parameters in the function CheckUserOnBeam.....	242
Table A- 33: The parameters in the function calBER3DBeam .....	242
Table A- 34: The parameters in the function readBER .....	243
Table A- 35: The parameters in the function CalBerUEsCell .....	245
Table B- 1: The UML use-case description for “mmCBERStart” .....	250



Table B- 2: The message description .....	253
Table B- 3: The read and present data use-cases description.....	255
Table B- 4: The message description .....	258
Table B- 5: The UML use-case description for “CompBERStart” .....	260
Table B- 6: The message description for use-case CompBERStart.....	263
Table B- 7: The read and present data use-cases description for “ReadCompBER” .....	265
Table B- 8: The message description of use-case ReadCompBER .....	267
Table B- 9: The parameters in the function CalBerPDFOn3DBeam.....	273
Table B- 10: The parameters in the function Beam3DChannelSINR.....	273
Table B- 11: The parameters the function getWeightSINR.....	274
Table B- 12: The parameters in the function pathloss .....	277
Table B- 13: The parameters in the function calBERLteSystem.....	279
Table B- 14: The parameters in the function CheckUserOnBeam .....	280
Table B- 15: The parameters in the function calBER3DBeam.....	281
Table B- 16: The parameters in the function readBER.....	282
Table B- 17: The parameters in the function CalBerOn3DBeam.....	283

# Acknowledgments

I would like to express my appreciation to my PhD supervisor Prof. John Cosmas for his assistance, patience, helpful and encouragement that guided me through my study. I also learnt how to work at a highly efficient level from him.

Finally, my deepest gratitude goes to my parents, Mr. Ming Xu (M.Eng.) and Mrs. Xiaoying Xu for their moral support and financial support during my PhD research. Words are unable to express how I am indebted to them in my life.

# **Chapter 1**

## **Introduction**

## 1.1 Motivation

Future 5G networks are expected to extend the capabilities of previous generations of mobile communication significantly [1]. One important aspect of such developments of 5G and future communication evolution is to provide extreme mobile broadband user experiences [2]. The supported data rate in 5G wireless networks are expected to increase rapidly compared to current Long-Term Evolution (LTE) networks [3]. In order to improve the transmitted rate for the 5G system, broader bandwidths are available at higher carrier frequencies. However, the signals experience severe path loss (PL) and rain fading when the frequency is increased. Then the distance of propagation will be shortened. Therefore, the beamforming should be used to transmit the signals further in the 5G system because it can focus the energy from the antenna array in the desired direction and increase the distance of propagation. Such an improvement will be mainly achieved through beamforming and the use of mm-waves [4]. On one hand, several users can be multiplexed in the same time-frequency resource slot through beamforming techniques, while on the other hand, by using carrier frequencies in the range 10 GHz-100 GHz, larger bandwidths become available [5].

According to the capacity formula, several methods may be applied to achieve capacity improvements and they are shown in Figure 1-1. For 5G system, research and development are focused around frequencies, and re-architecting of the network.

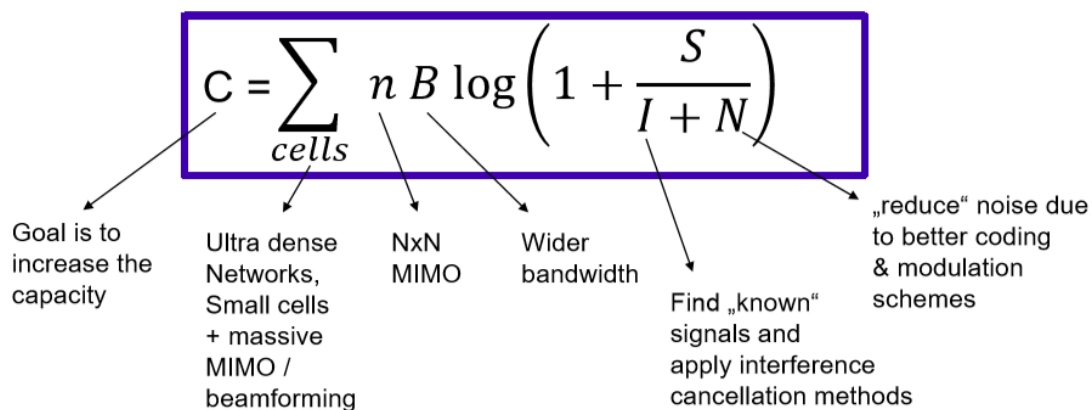


Figure 1- 1: Methods to achieve capacity improvements

Beamforming antennas, where the radio signal is focused to a narrow beam, help to offset the effect of reduced propagation of very high frequency carriers. The beamforming antenna arrays will play an important role in 5G implementations since even handsets can accommodate a larger number of antenna elements at mm-wave frequencies [6]. Aside from a higher directive gain, these antenna types offer complex beamforming capabilities, which allow for an increase in capacity in cellular networks by improving the signal to interference ratio (SIR) through direct targeting of UEs' groups. The narrow transmit beams simultaneously lower the amount of interference in the radio environment while making it possible to maintain sufficient signal power at the receiver terminal at larger distances in rural areas [7].

Massive multiple-input multiple-output (MIMO) wireless technology uses a very large number of antennas with a greater order of magnitude than current LTE systems, thus it is a leading candidate for inclusion in 5G systems. Since it will offer significant improvements in both throughput and energy efficiency. It is that, as the number of antennas increases without limit, the effects of uncorrelated noise and small scale fading can be removed completely[8]. In order to meet the explosive growth of demand for data traffic in mobile broadband networks, it is necessary to identify innovative and practical solutions, which can provide higher spectral efficiency, and a better quality of service [9].

FD-MIMO is one of the key technologies that is currently being studied in the Third Generation Partnership Project (3GPP) [10]. 3GPP is currently making considerable efforts to obtain accurate 3D channel models that support FD-MIMO, which greatly improves the system's performance by exploiting a channel's degrees of freedom in the elevation domain, which enables the use of a various strategies, including sector or user specific, 3D beamforming and cells splitting [11-13]. In an mm-wave system, by deploying many antennas at the Base Station (BS) and UE sides, severe PL problems that traditionally limits the scope of communication over mm-wave frequency bands, can be addressed. However, beam-forming antennas at base stations must track the user equipment in order to remain within the beam; hence, both horizontal and vertical orientations need to be taken into account when beams are

designed [14].

In 4G communication system, the 2D beamforming technology has been used, which is used planar antenna array to generate the beam. Moreover, the Dolph-Tchebyscheff has been used to direct the beam, which is in the horizontal direction [15]. However, in 5G network, the 3D beamforming technology has aroused the interest of the researchers, which need consider about two directions including horizontal and vertical. A 3D beamforming method based on singular value decomposition (SVD) is proposed, however, it is only for single UE [16]. A downlink 3D beamforming scheme is proposed for the 5G multiuser multiple-input multiple-output system. This scheme separates beams in the so-called elevation domain via base station antenna tilt assignment, with the objective of reducing inter-user interference by controlling the vertical radiation pattern of BS antennas [17-19].

In mm-wave communications, a multi-path phenomenon at reasonable implementation cost, several hybrid beamforming techniques are proposed [20, 21]. The main idea is to optimize analog and digital beamforming together on the BS and UE side, either separately or jointly, to achieve the best possible performance. However, such a digital or analog cooperative approach might not be the best method for adapting a fast varying mm-wave propagation environment since it takes a considerable amount of computational resources and time to carry out an optimization process, even if a perfect channel knowledge has already been achieved. Analog beam steering for flexible hybrid beamforming design in mm-wave communications is discussed [22], however, this assumes that a uniform linear array is implemented on both sides.

Multiple beam approaches have been introduced in 5G wireless cellular networks in response to the demand for broader coverage. In beamforming, an array of antennas needs to dynamically adapt the direction and down-tilt towards a receiver by rotating the antenna pattern and transmitting multiple beams to multiple UEs simultaneously. However, when the multiple beams transmit to multiple UE groups in this way, the interference will occur between each beam. In order to solve this problem, a broadband constant beam width beamforming for suppressing main lobe and side lobe interferences will be proposed [23-26]. These methods though can only satisfy a

constant main lobe width, hence performance will degrade severely when main lobe and side lobes interferences occur. However, no effective interference reduction method currently exists that can simultaneously overcome variability in Signal to Noise Ratio (SNR) of UEs in 3D beamforming, which makes this a challenging topic of research.

## 1.2 Challenges

In the FD MIMO system, beamforming technologies are the key technologies in 5G, but there is more interference between these beams from their side lobes when we use them to transmit multiple beams. Moreover, the beamforming in FD MIMO system is hard to change the shape and the direction of beam because it uses the downlink 3D beamforming technology [27], which has a constant beamforming beam width and it usually used to cover one user or one area.

These antenna arrays are essential for beamforming operations that play an important part in next generation networks. However, the mobile environment at these mm-wave bands is far more complex than at the currently used frequencies. Higher propagation losses that greatly vary depending on the environment require an updated network infrastructure and new hardware concepts. In practice, it is very challenging to devise beamforming techniques that are capable of quickly adapting to constantly changing propagation environment in mm-wave frequency bands and at the same time provide extremely high throughput with reasonable cost and energy efficiency. In an mm-wave multiple-input multiple-output system, a large number of antennas can be placed into a very limited space. It is not practical to equip each antenna with one independent radio frequency (RF) chain. Fortunately, the hybrid beamforming (HBF) can be utilized to greatly reduce the number of RF chains, while providing an acceptable performance. However, the conventional multiuser MIMO beamforming algorithms cannot be directly applied to the mm-wave system with HBF structure. Most of researches do not focus on the problem about interference between each beam. The main idea is to optimize analog and digital beamforming together at the BS and UE side, separately or jointly, for achieving the best possible performance. Yet such a

digital or analog cooperation approach might not be the best candidate for adapting fast varying mm-wave propagation environment as it takes some computation resources and time to carry out optimization process even if perfect channel knowledge is already acquired.

Addressing these challenges is the main drive of this research; the presented methods improve the existing 3D beamforming method for large-scale MIMO antennas and hybrid beamforming method for mm-wave. The improved K-means clustering algorithm has been used to cluster the UEs in different groups, which can decrease the number of transmitted beams at same time. Moreover, a new weighting method has been used to direct the beams in a desired direction and minimize its side lobes in undesired directions for 3D beamforming system. Based on the idea that user interference reduction should be performed for both analog beamforming and digital beamforming, we propose a novel hybrid weighting method, which needs the amplifier to adjust the amplitude for beams. In order to test and demonstrate the performance benefits in comparison with traditional schemes, a simulation system has been set up.

### **1.3 Aims of research**

The main aims of this research are to provide a clustering method to cluster the multiple UEs and develop a weighting method for 3D beamforming technology in the 5G communication system. In order to implement these aims, there are four objectives that need to be achieved:

1. The first objective of the thesis is choosing a key technology in 5G communication system to improve. The 5G communication system is a brand-new domain so we must know it first before to improve the related technologies. Moreover, there are a lot of key technologies for 5G communication system so we should choose one key technology for researching the knowledge. In order to comprehensively understand these key technologies in 5G system, there are a lot of books and literatures that need to be researched and read.
2. The second objective of the thesis is that a clustering algorithm is chosen to cluster



the multiple UEs, which can decrease the number of beams when multiple UEs need be covered by multiple beams at same time. For the clustering algorithm, there usually are, density-based clustering, hierarchical clustering, grid-based clustering and partition clustering, 4 kind of clustering methods. Therefore, we should choose one of them that can be used in three-dimensional coordinates to cluster UEs in minimum groups, which is based on the cosine distance between different UEs.

3. The third objective of this research is that a new weighting method should be provided for the 3D beamforming technology, which can produce the maximum SINR values (this means the minimum side lobes for each beams) to calculate the weighting matrix for 3D beamforming technology. It can adjust the values of weighting matrix according to the UEs' location in order to direct the main beam in a desired direction, whilst minimizing its side lobes in other undesired directions.
4. The fourth objective of this research is that a software can be chosen to simulate the 3D beamforming LTE system and the hybrid beamforming mm-wave system, in order to test that our clustering algorithm and new weighting method is successful. Moreover, the comparison of different simulation results has found the advantages and disadvantages about the improved scheme. The operation of this scheme can be found by analysis of simulation results.

## **1.4 Methodology**

The methodology for this PhD research was proposed after detailed analysis of the current challenges with consideration given to multiple parameters in each studied area. This research is based on the simulations, the literature review and is compared to the identified relevant works. In the literature review, the many current works are presented, which are concerned with techniques to avoid the limitations and difficulties that may degrade the systems' performance. The main challenge is that the side lobes are too large and interfere with the other main lobes when the 3D beamforming technology is used to transmit multiple beams. For this research, a well-known clustering algorithm is simulated with the new weighting method, and applied to the current 3D

beamforming LTE and hybrid beamforming mm-wave communication systems.

The simulations of this thesis include the design of 3D beamforming LTE system by using toolbox software at the first step. Afterwards, the 3D channel model has been created according to the structure of LTE and Long Term Evolution Advanced (LTE-A) networks which is based on the 3GPP standard. Finally, the 3D beamforming LTE system and the hybrid beamforming mm-wave system can be simulated and analyzed, which are used to test that the improved scheme has better system performance than LTE system.

## **1.5 Research Contribution**

This research introduces, analyses and proposes the 5G communication system. The proposed simulations are based on the 3GPP standard, which are based on actual measurements and is emerging as an international standard. So the improved scheme can be used in 5G communication system. The research contributions for the novel techniques are:

1. The improved K-means clustering algorithm is a partition clustering method, which was decided to cluster the different UEs in minimum number of groups by researching and comparing these different clustering algorithms. The K-means clustering algorithm can be used to cluster the UEs, which is based on the cosine distance between different UEs and then one beam can cover multiple UEs. In K-mean algorithm, the number of clusters can be set by user so the maximum number of clusters can be controlled and the number of clusters can be decreased by boundary value for cosine distance in 3D coordinate. Therefore, it is a suitable clustering algorithm for 5G communication system. Moreover, the calculation method for K-mean algorithm is applied in the 3D LTE beamforming simulation system and the hybrid beamforming mm-wave simulation system, which has been shown in this thesis.
2. The maximum SINR weighting method as the new weighting method for the 3D beamforming technology is used to minimize all of side lobes for each beam in

specially appointed direction. Therefore, it can keep the value of the main beam as large as possible in a desired direction, whilst minimizing its side lobes in other undesired directions. In this new weighting method, the least-squares solution is used to make the SINR have the maximum value in the 3D beamforming technology. For providing this new weighting method, there are a lot of literature reviews and relevant works researched. This new weighting method is applied in the 3D beamforming LTE simulation system and the hybrid beamforming mm-wave simulation system. The simulation results has shown that the systems' performance have been enhanced.

3. My research chooses the Matlab R2016b to simulate the 3D beamforming LTE system and hybrid beamforming mm-wave system, in order to test that our improved scheme is successful. The Matlab R2016b is one software for engineers in common use, which is best one to test the algorithm among the software due to my ability in using it. The simulations show the results for the 3D beamforming LTE system and the hybrid beamforming mm-wave systems, in which the channel models are based on the 3GPP standard. Moreover, the Matlab R2016b has some LTE communication system models and tools for using, which also are based on the 3GPP standard so all of them are useful to design the Minimal Side Lobe 3D Beamforming LTE System and the Optimal Minimum Side lobe Hybrid Beamforming of Millimeter-Wave System.

## **1.6 Thesis organization**

This thesis consists of a total of six chapters, which include one introduction chapter, one background chapter, one main contributions chapter, two simulation analysis chapters and one conclusion chapter. For Chapter 2 to Chapter 5, there are a chapter introduction and a chapter conclusion for each chapter. In the end of this thesis, there are two Appendix parts for explain about the design processing of the simulation systems. The detailed thesis outline is introduced as follows:

### **Chapter 1: Introduction**

## **Chapter 2: Technical Background and Literature Review**

## **Chapter 3: Innovation Schemes for 3D Beamforming Technology**

## **Chapter 4: Minimal Side Lobe 3D LTE Beamforming System towards a Group of UEs**

## **Chapter 5: Optimal Minimum Side lobe Hybrid Beamforming in Millimeter Wave System**

## **Chapter 6: Conclusions, Discussion and Future Work**

## **Reference**

## **Appendix A: Simulation Design for Minimal Side Lobe 3D Beamforming LTE System towards a Group of User Equipment**

## **Appendix B: Simulation Design for Optimal Minimum Side lobe Hybrid Beamforming of Millimeter Wave System**

Chapter 1 covers general introduction for whole thesis, which expresses the motivation to the research. Moreover, it shows the achievements from the research and provides the outline for this thesis.

Chapter 2 is the literature review chapter, which provides the introduction and background to LTE and 5G technologies. The comparison of LTE system and 5G systems are shown in this chapter, in which some technical challenges, especially the processes that are directly connected to our work are proposed.

Chapter 3 provides the main contributions of this research, which are the K-mean clustering algorithm and the maximum SINR weighting method. It shows how the K-means algorithm how to be applied in 3D beamforming technology and the calculation processing for obtaining the new weighting (maximum SINR weighting). Afterwards, the calculation of the receive signals are shown, which is obtained by the new weighting matrix.

Chapter 4 shows the results from the 3D beamforming LTE simulation system. In this simulation, the design process of the system is presented by the UML software and the simulation results are obtained by the Matlab R2016b software in the 3D beamforming LTE system. The detailed explanation of processing for UML software

and all functions for the Matlab R2016b software are in Appendix A. The simulation results are shown in some figures, which are analyzed in this chapter.

Chapter 5 shows the design of the hybrid beamforming mm-wave system. In this simulation, the design process of the system is presented by the UML software and the simulation results are obtained by the Matlab R2016b software in the hybrid beamforming mm-wave system. The detailed explanation of processing for UML software and all functions for the Matlab R2016b software are in Appendix B. The simulation results are shown in some figures, which are analyzed in this chapter.

Chapter 6 provides a discussion about the research simulation systems, an overall conclusion of the thesis and the future work for further improvements.

# **Chapter 2**

## **Technical Background and Literature Review**

## 2.1 Introduction to LTE System

Since the 80s of the last century, the field of wireless mobile communications has undergone four major changes. The first generation (1G) of mobile communications systems (an analogue communication system) was based on frequency division multiple access (FDMA) technology. The second generation (2G) of mobile communication system used time division multiple access (TDMA) and Code Division Multiple Access (CDMA) as the main access technology. The third generation (3G) of mobile communications systems is based on broadband CDMA technology (such as in the United States, CDMA2000, WCDMA in Europe, TD-SCDMA in China). The fourth generation (4G) of mobile communication system takes the Orthogonal Frequency Division Multiplexing (OFDM) technology as the core. Figure 2-1 shows the general process of the evolution of the above technical standards [28].

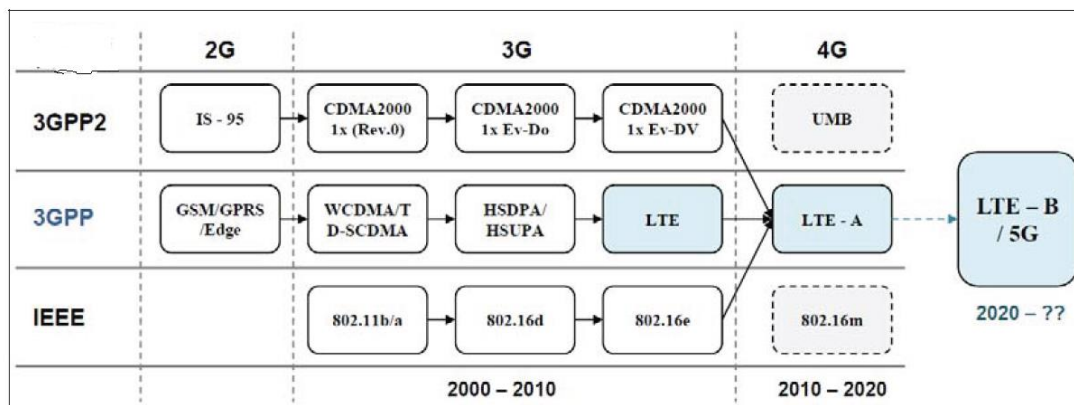


**Figure 2- 1: The evolution of different mobile communication standards [28]**

On December 6, 2010, the International Telecommunication Union (ITU); officially approved that LTE-A was defined as the 4G standard, which was developed by the 3rd Generation Partnership Project. As of August 2013, there are 175 operators in 77 countries and regions that have made investment in and deployment of LTE-A technologies, and the number of LTE-A users worldwide has exceeded 100 million. Figure 2-2 shows the evolution of the 3GPP technology standards and the business schedule [29, 30].

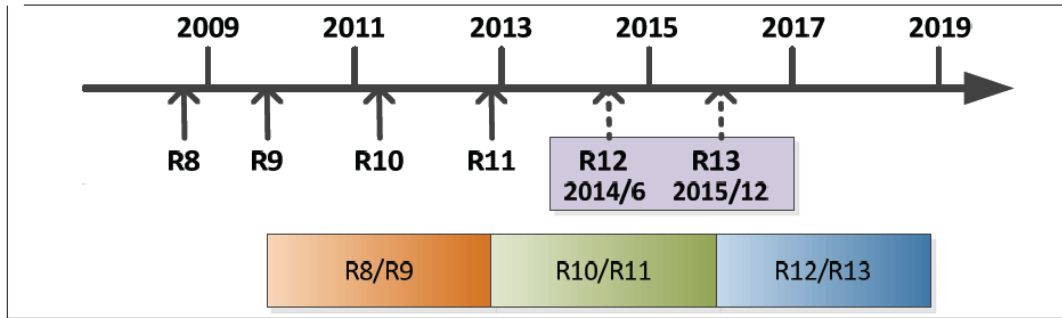


Figure 2- 2: Timeline in 3GPP and commercialization [29]

3GPP launched the LTE version of R8 in early 2009, which is called the 3.9G standard, which supports the maximum 20MHz bandwidth, enabling uplink 50Mbps and downlink 100Mbps peak speeds. At the same time, 3GPP standardisation work on 4G (for the ITU organisation's International Mobile Telecommunications Advanced (IMT-A) proposal requirements) also started in the first half of 2008, called LTE-A, corresponding to 3GPP's R10 and R11 versions. The main features of the LTE-A system are: forward compatible LTE system, but to support bandwidth expansion to 100MHz, so it can achieve higher communication rates (peak rates up to 1Gbps downlink and uplink 500Mbps). In addition, LTE-A can support more commercial providers and achieve a better user experience.

The core technologies of the physical layer of the LTE access network mainly include Adaptive Modulation and Coding (AMC) technology, OFDM technology and MIMO technology.

### 2.1.1 AMC Technology

The core idea of adaptive coded modulation is to adjust the transmission rate according to the quality of the channel. It maximises the use of channel capacity in LTE FDD (Frequency Division Duplexing) mode, because channel reciprocity does not exist, and therefore we need to obtain the channel state information by way of feedback (CSI Channel; State Information). The feedback is generally divided into explicit and implicit feedback; the former refers to the entire channel feedback to the transmitter, and the latter refers to the channel quantised feedback to the originator.

In the actual system, the feedback control channel resource link occupancy is very



valuable. In order to achieve a reasonable compromise between the system performance and complexity, the general implicit overhead feedback strategy is often chosen. By quantifying the quality of the channel, we can get different Channel Quality Indicator (CQI). According to the different CQI, you can use a different Modulation and Coding Scheme (MCS) and achieve a different signal transmission rate, where CQI is a kind of limited feedback of channel information. In the LTE R8 standard, 3GPP provides 15 levels of CQI for implicit feedback. In the 15 level of CQI, channel encoding (Turbo) rate changes from 78/1024 to 948/1024, and modulation includes QPSK, 16QAM, 64QAM [31].

### **2.1.2 OFDM Technology**

OFDM technology was first proposed by Chang [32], which is different from traditional frequency division multiplexing, since it permits the overlap between adjacent sub-carriers, so as to improve the spectrum utilisation rate. In 1971, Weinstein and Ebert proposed the OFDM modem realisation method based on discrete Fourier transform (DFT) [33]. 1980, Peled and Ruiz introduced the cyclic prefix (CP) of this concept, and the problem of two sub-carriers orthogonality was solved [34]. This made the OFDM truly become a practical technology. In addition to the LTE-A standard, the IEEE 802.16 series of standards have chosen OFDM as the core technology of the physical layer. From the perspective of patent, OFDM technology does not have patent barriers as CDMA technology does. This is another factor that led to OFDM technology becoming a supporting technology in the physical layer of LTE and IEEE 802.16 broadband wireless communication.

### **2.1.3 MIMO Technology**

Until the early 1990s, the whole field of wireless communications was against multipath interference. MIMO technology successfully converts multipath interference into a beneficial factor for the communication system. Paulraj and Kailat [35] first put forward the idea of increasing the wireless link capacity using multiple antennas at both ends of a wireless communication system. Telatar studies the capacity [36] of a MIMO system from the point of view of information theory. The main conclusion is that the

capacity of a MIMO channel increases linearly with the increase of the number of antennas.

At the same time, the Bell laboratory developed the Bell Laboratories Layered Space Time (BLAST) structure which the spectrum efficiency can reach 10-20 bps/Hz [37]. MIMO researchers mainly focused on the relationship between channels and transmit pre-coding design and receiver detection technology. The pre-coding operations of LTE in MIMO are implicit feedback, and the standard defines a set of codebooks that are known to both BS and UE PMI (Precoding Matrix Indicator). The detection of MIMO consists of two major categories: linear and nonlinear. With the progress of integrated circuit technology, complex nonlinear detection methods we are adopted, such as sequential interference cancellation (SIC), Sphere Decoding (SD), maximum likelihood detection (MLD), and other programs we are gradually integrated into the receiver [38].

#### 2.1.4 Channels Model of LTE System

Nowadays, the LTE system usually uses the 2×2 or 4×4 LTE MIMO systems to transmit the signals. For the 4×4 LTE MIMO system, the parameters of channel model are from “3GPP TS 36.101” [39]. The system has four ports in the transmitter so the configuration of channel is “R.13 FDD”, which is an antenna for four antenna ports. The parameters for “R.13 FDD” are shown in Table 2-1 and the modulation method can be changed to 16-QAM and 64-QAM in the simulation. Moreover, the simulation for 3D beamforming LTE systems uses R.0 and R.5.

Table 2- 1: Overview of dl reference measurement channels [39]

Reference channels	Reference channels
R.0 (Port0, 1 RB, 16QAM, CellRefP=1, R=1/2)	R.26 (Port5, 50 RB, 16QAM, CellRefP=1, R=1/2)
R.1 (Port0, 1 RB, 16QAM, CellRefP=1, R=1/2)	R.27 (Port5, 50 RB, 64QAM, CellRefP=1, R=3/4)
R.2 (Port0, 50 RB, QPSK, CellRefP=1, R=1/3)	R.28 (Port5, 1 RB, 16QAM, CellRefP=1, R=1/2)
R.3 (Port0, 50 RB, 16QAM, CellRefP=1, R=1/2)	R.43 FDD (Port7-14, 50 RB, QPSK, CellRefP=2, R=1/3)
R.4 (Port0, 6 RB, QPSK, CellRefP=1, R=1/3)	R.43 TDD (SpatialMux, 100 RB, 16QAM, CellRefP=4, R=1/2)

R.5 (Port0, 15 RB, 64QAM, CellRefP=1, R=3/4)	R.44 FDD (Port7-14, 50 RB, QPSK, CellRefP=2, R=1/3)
R.6 (Port0, 25 RB, 64QAM, CellRefP=1, R=3/4)	R.44 TDD (Port7-14, 50 RB, 64QAM, CellRefP=2, R=1/2)
R.7 (Port0, 50 RB, 64QAM, CellRefP=1, R=3/4)	R.45 (Port7-14, 50 RB, 16QAM, CellRefP=2, R=1/2)
R.8 (Port0, 75 RB, 64QAM, CellRefP=1, R=3/4)	R.45-1 (Port7-14, 39 RB, 16QAM, CellRefP=2, R=1/2)
R.9 (Port0, 100 RB, 64QAM, CellRefP=1, R=3/4)	R.48 (Port7-14, 50 RB, QPSK, CellRefP=2, R=1/2)
R.10 (TxDiversity SpatialMux, 50 RB, QPSK, CellRefP=2, R=1/3)	R.50 FDD (Port7-14, 50 RB, 64QAM, CellRefP=2, R=1/2)
R.11(TxDiversity SpatialMux CDD, 50 RB, 16QAM, CellRefP=2, R=1/2)	R.50 TDD (Port7-14, 50 RB, QPSK, CellRefP=2, R=1/3)
R.12 (TxDiversity, 6 RB, QPSK, CellRefP=4, R=1/3)	R.51 (Port7-14, 50 RB, 16QAM, CellRefP=2, R=1/2)
R.13 (SpatialMux, 50 RB, QPSK, CellRefP=4, R=1/3)	R.6-27RB (Port0, 27 RB, 64QAM, CellRefP=1, R=3/4)
R.14 (SpatialMux CDD, 50 RB, 16QAM, CellRefP=4, R=1/2)	R.12-9RB (TxDiversity, 9 RB, QPSK, CellRefP=4, R=1/3)
R.25 (Port5, 50 RB, QPSK, CellRefP=1, R=1/3)	R.11-45RB (CDD, 45 RB, 16QAM, CellRefP=2, R=1/2)

In Table 2-1, R.X is the name of the channel; other parameters: Port 0 = single antenna port, RB = Resource Blocks, CellRefP = number of antenna ports, R = coding rate.

For the four port transmissions, the channel matrix is defined in the frequency domain by [39]:

$$H = \begin{bmatrix} 1 & 1 & j & j \\ 1 & 1 & -j & -j \\ 1 & -1 & j & -j \\ 1 & -1 & -j & j \end{bmatrix} \quad (2-1)$$

where  $H$  is the transfer function for a 4×4 LTE MIMO system.

In the 4×4LTE MIMO system, the antenna configuration uses the uniform linear array at both BS and UE. In order to consider inter-symbol interference, the correlation matrix for the BS and the correlation matrix for the UE have been introduced. The 4×4 MIMO channel spatial correlation matrix  $R_{spat}$  is defined as follows [39]:

$$\mathbf{R}_{\text{spat}} = \mathbf{R}_{eNB} \otimes \mathbf{R}_{UB} \begin{bmatrix} 1 & \alpha^{1/9^*} & \alpha^{4/9} & \alpha \\ \alpha^{1/9^*} & 1 & \alpha^{1/9} & \alpha^{4/9} \\ \alpha^{4/9} & \alpha^{1/9^*} & 1 & \alpha^{1/9} \\ \alpha^* & \alpha^{4/9^*} & \alpha^{1/9} & 1 \end{bmatrix} \otimes \begin{bmatrix} 1 & \beta^{1/9^*} & \beta^{4/9} & \beta \\ \beta^{1/9^*} & 1 & \beta^{1/9} & \beta^{4/9} \\ \beta^{4/9} & \beta^{1/9^*} & 1 & \beta^{1/9} \\ \beta^* & \beta^{4/9^*} & \beta^{1/9} & 1 \end{bmatrix} \quad (2-2)$$

where  $R_{eNB}$  is the correlation matrix for the BS, and  $R_{UB}$  is the correlation matrix for the UE. The  $\alpha$  and  $\beta$  are values for different correlation types given in Table 2-2 [39].

**Table 2- 2: The parameters for ULA MIMO correlation matrices [39]**

<b>Correlation</b>	<b><math>\alpha</math></b>	<b><math>\beta</math></b>
<i>Low</i>	0	0
<i>Medium</i>	0.3	0.3
<i>High</i>	0.9	0.9

In Table 2-2, Low means the channel is ideal, Medium means the channel is suburban and High means the channel is metropolitan.

## 2.2 Antenna Array

Arrays of antennas can assume any geometric form. The various array geometries of common interest are point sources, linear arrays and planar arrays.

### 2.2.1 Point Sources

A point source is a single identifiable localized source of something. A point source has negligible extent, distinguishing it from other source geometries. Sources are called point sources because in mathematical modelling, these sources can usually be approximated as a mathematical point to simplify analysis. The actual source need not be physically small, if its size is negligible relative to other length scales in the problem.

Radio wave sources which are smaller than one radio wavelength are also generally treated as point sources. Radio emissions generated by a fixed electrical circuit are usually polarised, producing anisotropic radiation. If the propagating medium is lossless, however, the radiant power in the radio waves at a given distance will still vary as the inverse square of the distance, if the angle remains constant to the source polarisation.

An antenna is the interface between radio waves propagating through space and electric currents moving in metal conductors, used with a transmitter or receiver. Radio antennas are often smaller than one wavelength, which are also generally treated as point sources.

### 2.2.2 Linear Unit Antenna Array

The simplest array geometry is the linear array. Thus, all elements are aligned along a straight line and generally have a uniform inter-element spacing. Linear arrays are the simplest to analyse and many valuable insights can be gained by understanding their behaviour. The minimum length linear array is the 2-element array.

The more general linear array is the N-element array. For simplification purposes, we will assume that all elements are equally spaced and have equal amplitudes. Later we may allow the antenna elements to have any arbitrary amplitude. Figure 2-3 shows an N-element linear array composed of isotropic radiating antenna elements. It is assumed that the nth element leads the (n-1) element by an electrical phase shift of  $\delta$  radians. This phase shift can easily be implemented by shifting the phase of the antenna current for each element.

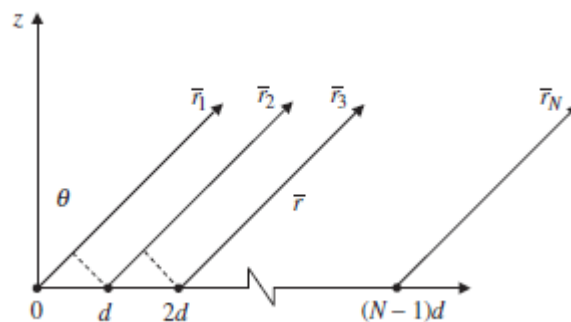


Figure 2- 3: N-element linear array composed of isotropic radiating antenna elements

### 2.2.3 Rectangular Array

Having explored the linear arrays, we can move on to slightly more complex geometries by deriving the pattern for rectangular planar arrays. Figure 2-4 shows a rectangular array in the x-y plane. There are M elements in the x-direction and N elements in the y-direction creating an M×N array of elements. The x-directed elements

are spaced  $dx$  apart and the  $y$ -directed elements are spaced  $dy$  apart. The planar array can be viewed as  $M$  linear arrays of  $N$  elements or as  $N$  linear arrays of  $M$  elements. Since we already know the array factor for an  $M$  or  $N$  element array acting alone, we can use pattern multiplication to find the pattern of the entire  $M \times N$  element array.

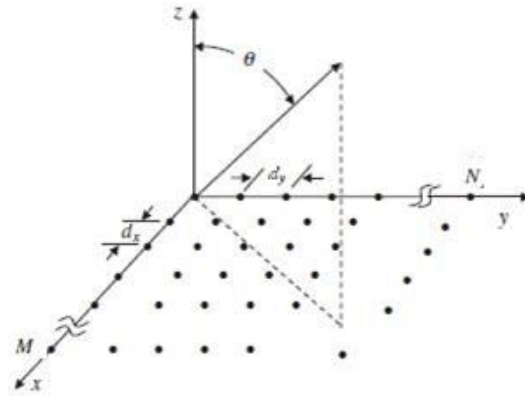


Figure 2- 4: A rectangular array in the x-y plane

## 2.2.4 Other Different Shape Antenna Arrays

The antenna array is a key technology of a 5G system. There are all kinds of shapes of antenna arrays such as triangular prisms or hexagonal prisms.

The Figure 2-5 shows a triangular prism for an antenna array [40]. Figure 2-6 shows a hexagonal prism for an antenna array.

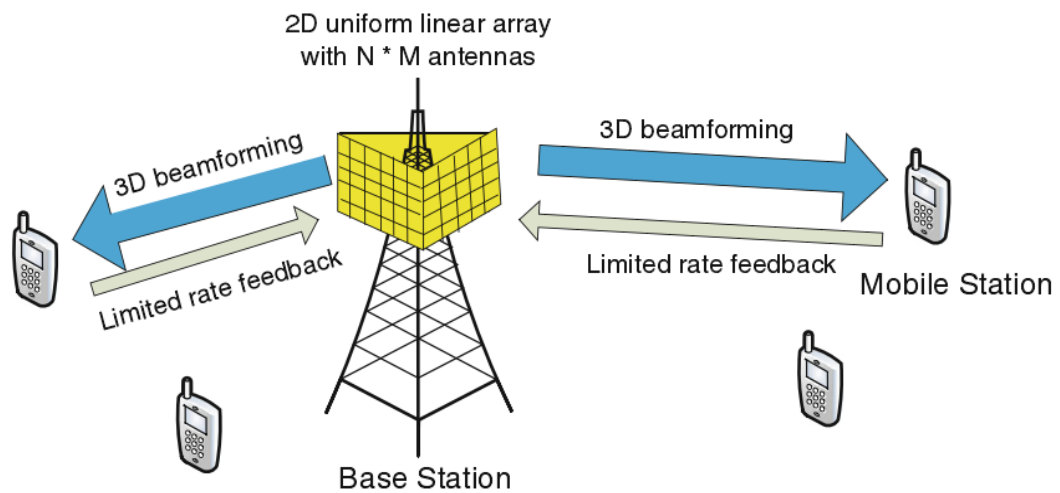
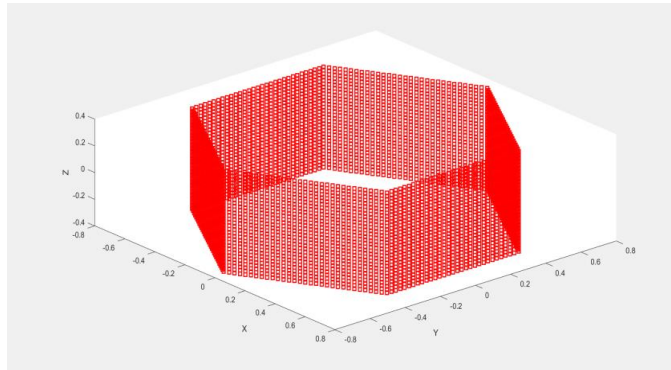


Figure 2- 5: The triangular prism for an antenna array [40]

The antenna arrays for one cell in this thesis are shown in Figure 2-6. In this cell, there are six faces of antenna arrays and 256 antennas for each face, which consists of  $16 \times 16$  antennas for each array face.



**Figure 2- 6: The antenna array for one cell in this thesis**

The special array is the cylindrical antenna array which typically consists of 64 elements of wideband printed dipole antennas that operate at the L-frequency band. The configuration of this antenna array is shown in Figure 2-7 [41].

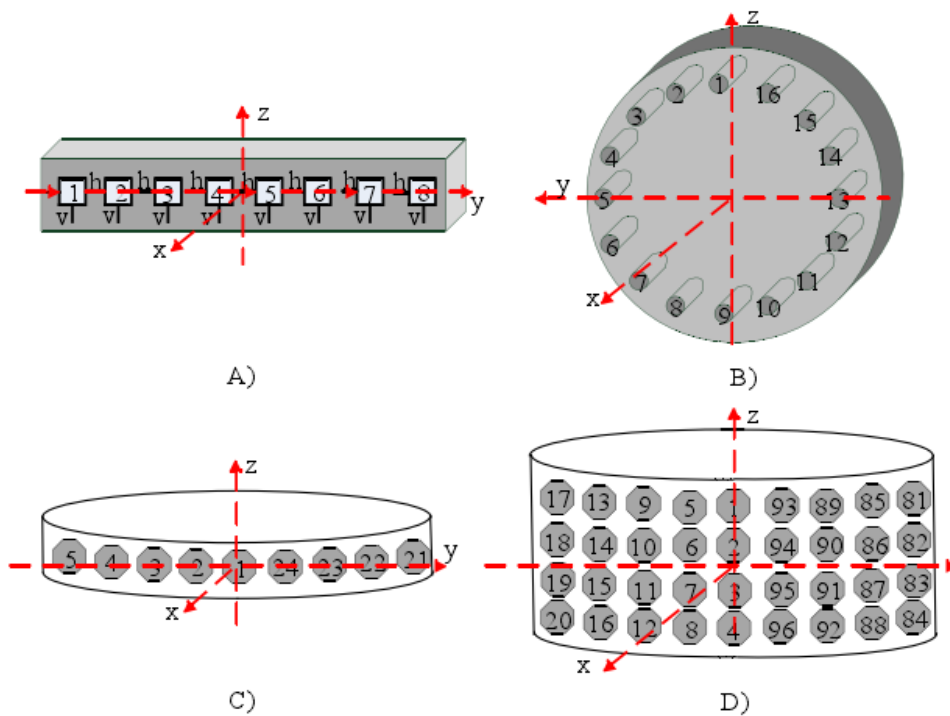


**Figure 2- 7: The cylindrical antenna arrays [41]**

One face for an antenna array is shown in Figure 2-8, which is an  $10 \times 10$  antenna array [42].

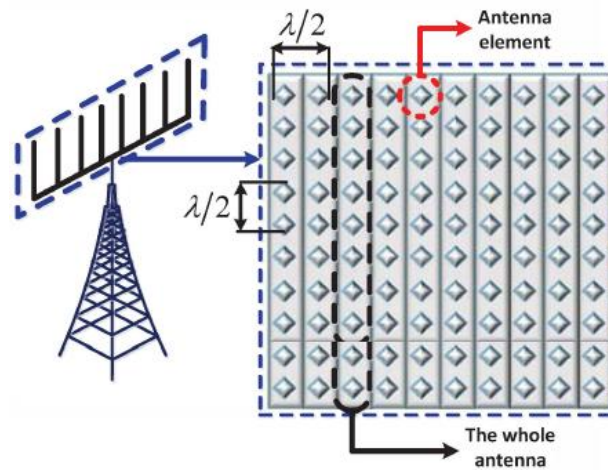


**Figure 2- 8: The one face for an antenna array [42]**

Figure 2-9 is a photo of an  $8 \times 16$  antenna array, which has 128 antenna elements in the board [43].



**Figure 2- 9: The 8X16 antenna elements [43]**

A 2-dimensional antenna array is shown in Figure 2-10. The antenna array with  $\lambda$  spacing consists of  $N_{T-H}$  antenna elements in the horizontal direction and  $N_{T-V}$  antenna elements in the vertical direction [44].



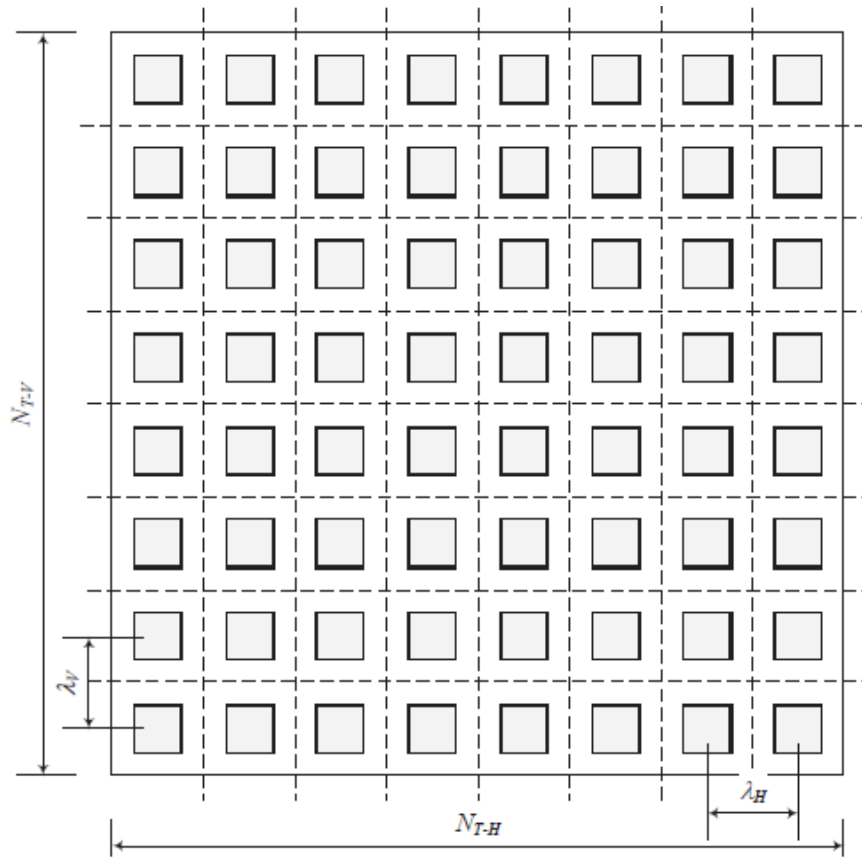


**Figure 2- 10: The antenna arrays with spacing [44]**

The size of antenna arrays can be adjustable such as  $8 \times 1$  (8 horizontal  $\times$  1 vertical) or  $1 \times 4$ , which is shown in Figure 2-11. However, the distance between each antenna element cannot be changed [44].

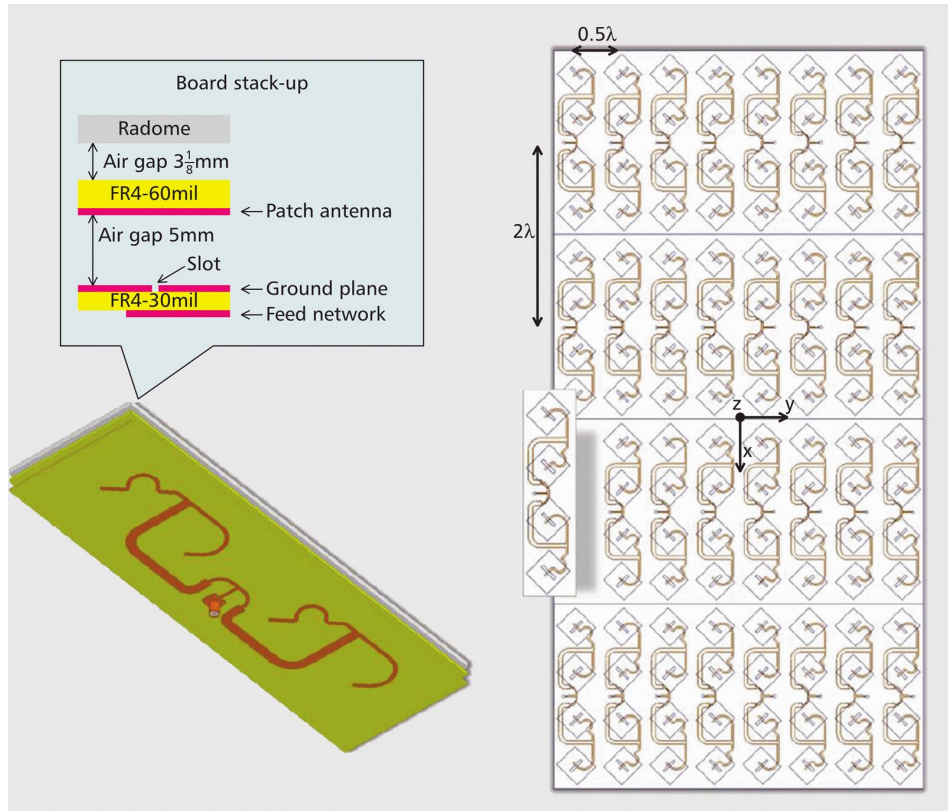


Figure 2- 11: Right: top-to bottom view of FD-MIMO antenna array and feed network; left: bottom view of one sub-array with detailed PCB stack-up [44]

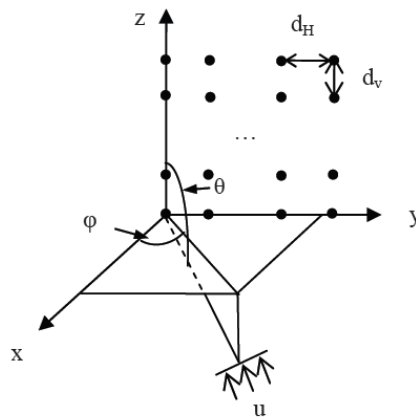


Figure 2- 12: The rectangular planar array

In Figure 2-12, it is assumed that one group of UEs is served by all the antenna elements, and data from a BS is transmitted in a single stream. The BS is equipped with an antenna array that consists of  $N_t \times N_v$  antenna elements. There are  $N_t$  elements in the y-direction and  $N_v$  elements in the z-direction, in which y-direction means the horizontal direction and z-direction means vertical direction. The m-nth element has a

weighting  $w_{mn}$ . The y-directed elements are spaced  $d_H$  apart and the z-directed elements are spaced  $d_V$  apart.

The provided calculation method is for the beam pattern of the  $N_t \times N_v$  rectangular planar array, whose weightings can be uniform or can be in any form according to the designer's needs, such as binomial, Kaiser-Bessel, Hamming, or Gaussian weights. These methods do not consider channel information and only provide the formula for a rectangular planar array in the x-y-plane. The rectangular planar array is extended to the y-z-plane.

The beam pattern of the  $N_t \times N_v$  rectangular planar array in x-y coordinate plane can be obtained by a weighting matrix [45]; then using the same analysis method to determine the beam pattern of the  $N_t \times N_v$  rectangular planar array in y-z-coordinate plane. According to Ref.45, these two beams pattern in two directions can be combined in one equation as follows:

$$AF = \sum_{m=1}^{N_v} \sum_{n=1}^{N_t} w_{mn} e^{j[(m-1)(kd_H \sin \theta \sin \phi + \beta_H) + (n-1)(kd_V \cos \theta + \beta_V)]} \quad (2-3)$$

where  $k = \frac{2\pi}{\lambda}$

$$\beta_H = -\frac{2\pi}{\lambda} d_H \sin \theta_0 \cos \phi_0$$

$$\beta_V = -\frac{2\pi}{\lambda} d_V \cos \theta_0$$

and  $(\theta_0, \phi_0)$  is user direction, and  $0 \leq \theta \leq \frac{\pi}{2}$ ,  $0 \leq \phi \leq 2\pi$ .

The antenna array can use the beam pattern to cover different areas with different directions. In Figure 2-13, the array antenna covered a  $3 \times 3$  cell area, where the available resource is three times that of the  $3 \times 1$  cell and one and a half times that of the  $3 \times 2$  cell. Conversely, the interference in the  $3 \times 3$  cell is three times that of the  $3 \times 1$  cell and one and a half times that of the  $3 \times 2$  cell if the same antenna is used in the three cells [46].

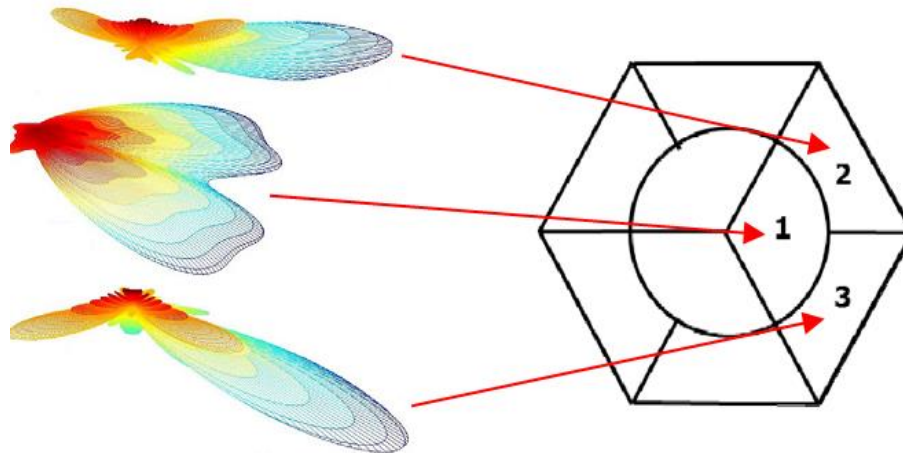


Figure 2- 13: The beam patterns for sector 1, 2, and 3 of the proposed 3×3 cell [46]

## 2.3 Clustering Algorithms

Clustering has been applied in a wide variety of fields, ranging from engineering, computer sciences, life and medical sciences to earth sciences, social sciences and economics [47]. The basic concept of clustering is to divide UEs into different groups (clusters). Cluster analysis emerged as a major topic in the 1960s when the monograph “Principles of numerical taxonomy” by Sokal and Sneath motivated worldwide research on clustering methods [48]. Since clustering algorithms had been proposed by Hartigan, the basic problems and methods of clustering became well-known [49]. Clustering problems arise in many different applications, such as data mining and knowledge discovery data compression and vector quantisation. Clustering is used in data mining techniques in which a group of similar objects is combined together to form clusters, these clusters are different from the objects in other clusters.

This paper describes some clusterisation techniques such as, partitional technique, hierarchical technique, grid-based technique, density-based technique and their algorithms. The Partitional method divides the data set into objects based on some similarity criterion; the hierarchical method creates a hierarchy between clusters by combining the data objects into clusters, and then these clusters are further combined together to form large clusters and so on; the grid based method forms clusters by combining the data objects into grids or cells; and the density-based method is used to separate the high density clusters from low density clusters.

### **2.3.1 Density-based Clustering**

This technique of clustering is suitable for arbitrary shaped clusters. Density-based clustering helps us to separate the low density regions of the clusters from the high density regions. High density regions of objects are combined together to form clusters. It deals with noisy data and scans the whole data in only one scan [50].

### **2.3.2 Hierarchical Clustering**

Hierarchical clustering is a method of cluster analysis in which a hierarchy of clusters is created in such a way that the data objects in clusters are decomposed based on some criteria. The clusters thus obtained in the hierarchy are known as a dendrogram that shows how the clusters are related to each other [51, 52].

### **2.3.3 Grid-Based Clustering**

The Grid-based clustering method maps all the objects in a cluster into a number of square cells, known as grids. These grids are combined together to construct a grid-like format and all the operations of clustering are applied to these cells (grids). The time required to perform clustering operations depends only on the count of cells in each dimension in the space, which means it is only dependent on the x and y dimension, it is not dependent on the number of data objects, and therefore this method is more robust and is performed efficiently.

### **2.3.4 Partition Clustering**

The Partition method is one of the clustering analysis technique in which a number of  $n$  objects is given and the data set is partitioned into a number of  $k$  clusters where  $k \leq n$  to minimise an objective partitioning criterion and each cluster contains similar objects but they are different from the objects outside the clusters. The  $k$  clusters thus obtained must fulfil the following two criteria:

1. Each cluster must contain a minimum of a single object.
2. Every object must relate to absolutely one cluster [53]. The most common method of partitioning technique is the K-means algorithm.

Amongst many different partitioning clustering algorithms, the K-means algorithm is a good algorithm for clustering a low dimensional data set [54-56]. In the K-means algorithm, UEs will be divided into several groups based on the distance between each other. If the distance between a user terminal and one cluster center is smallest among the distances to other cluster centers, then this user terminal will belong to the cluster corresponding to this cluster center. After we divide users into different groups, the UEs in the same group are covered by one beam.

In K-means clustering, we are given a set of  $n$  data points in  $d$ -dimensional space and an integer  $K$  and the problem is to determine a set of  $K$  points in  $d$ -dimensional space, called centers, so as to minimize the mean squared distance from each data point to its nearest center [57]. Two key tasks in the K-means algorithm are the determination of the number of  $K$  and the selected initial cluster central points. Therefore, research all concentrates on these two aspects. A simple and efficient K-means clustering algorithm, which is called the filtering algorithm, has been presented [58]. An energy efficient clustering protocol based on the K-means algorithm named EECPK-means has been proposed where a midpoint algorithm is used to improve the initial centroid selection procedure [59]. A method was proposed to determine the number of clusters for the K-means algorithm for different data sets [60].

Among many different clustering algorithms, the K-means algorithm is a better algorithm for clustering a low dimensional data set.

For the K-means algorithm, there are three common distance measurement methods; suppose there are two points A and B in the Cartesian coordinate system, in which coordinates of the two points are  $(x_1, y_1, z_1)$  and  $(x_2, y_2, z_2)$  respectively, these three distances are as follows.

**(1) Squared Euclidean distance**

The squared Euclidean distance between A and B is:

$$d(A, B) = \sqrt{(x_1 - x_2)^2 + (y_1 - y_2)^2 + (z_1 - z_2)^2} \quad (2-4)$$

In this case, each centroid is the mean of the points in that cluster.

**(2) Hamming distance**

The Hamming distance between A and B is the sum of absolute differences:

$$d(A, B) = |x_1 - x_2| + |y_1 - y_2| + |z_1 - z_2| \quad (2-5)$$

In this case, each centroid is the component-wise median of the points in that cluster.

### (3) Cosine distance

The cosine distance between A  $(x_1, y_1, z_1)$  and B  $(x_2, y_2, z_2)$  is one minus the cosine of the included angle between points (treated as vectors):

$$d(A, B) = 1 - \frac{x_1x_2 + y_1y_2 + z_1z_2}{\sqrt{x_1^2 + y_1^2 + z_1^2} \sqrt{x_2^2 + y_2^2 + z_2^2}} \quad (2-6)$$

In this case, each centroid is the mean of the points in that cluster, after normalising those points to unit Euclidean length.

In the K-means algorithm, samples will be divided into several groups based on the distance between user terminals. If the distance between a user terminal and one cluster centre is smallest among the distances to other cluster centres, then this user terminal will belong to the cluster corresponding to this cluster centre. For the above three distances the K-means algorithm proceeds as follows:

1. Choose  $k$  initial cluster centers (centroid).
2. Compute point-to-cluster-centroid distances of all observations to each centroid.
3. There are two ways to proceed:
  - (1) Batch update — Assign each observation to the cluster with the closest centroid.
  - (2) Online update — individually assign observations to a different centroid if the reassignment decreases the sum of the within-cluster, sum-of-squares point-to-cluster-centroid distances.
4. Compute the average of the observations in each cluster to obtain  $k$  new centroid locations.
5. Repeat steps 2 to 4 until cluster assignments do not change, or the maximum number of iterations is reached.

## 2.4 The Road to 5G

In recent decades, communication system development has been changing

enormously. In upcoming years 3G and 4G technologies will find it difficult to handle the mobile traffic [61]. Therefore, research on 5G mobile wireless technologies has been very active in both academia and industry in the past few years [62].

The three-stage process through which the industry typically progresses can be summarised in the Figure 2-14 below. At present, 5G is somewhere between the first and second stages. The first stage began in 2012 with the ITU-R's launch of its vision work on "IMT for 2020 and beyond" [63] and the EU's METIS project to begin a 5G definition process [64], and in 2013 the "5G White Paper" was published by NGMA [65].

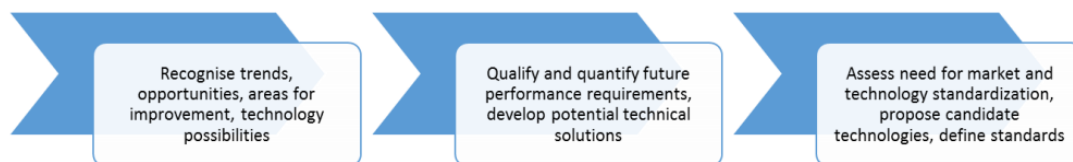


Figure 2- 14: Three stages of development on the road to 5G [63]

### 2.4.1 Introduction of 5G

Two significant trends are driving the wireless industry to develop a fifth generation of network technology: the explosive increase in demand for wireless broadband services needing faster, higher-capacity networks that can deliver video and other content-rich services; and the Internet of Things (IoT) that is fueling a need for massive connectivity of devices, and also a need for ultra-reliable, ultra-low-latency connectivity over Internet Protocol (IP) [66]. Therefore enhanced mobile broadband (eMBB) is needed for 5G applications. Ultra-reliable low-latency communications (URLLC) also is a new feature to be considered for 5G cellular systems [67].

The 5G networks allow the UEs to access the big repository of data and services, which has been considered and studied to achieve these performance targets. For example, the 5G communication system will use 512-QAM or 1024-QAM for modulation, the 28 GHz millimeter waveband and beam adaptation and beamforming for transmission. However, it has been quite clear that there would be no single enabling technology that can achieve all the diverse and even conflicting 5G requirements. Figure 2-15 shows the framework for the 5G system to fulfil multiple scenarios [68].



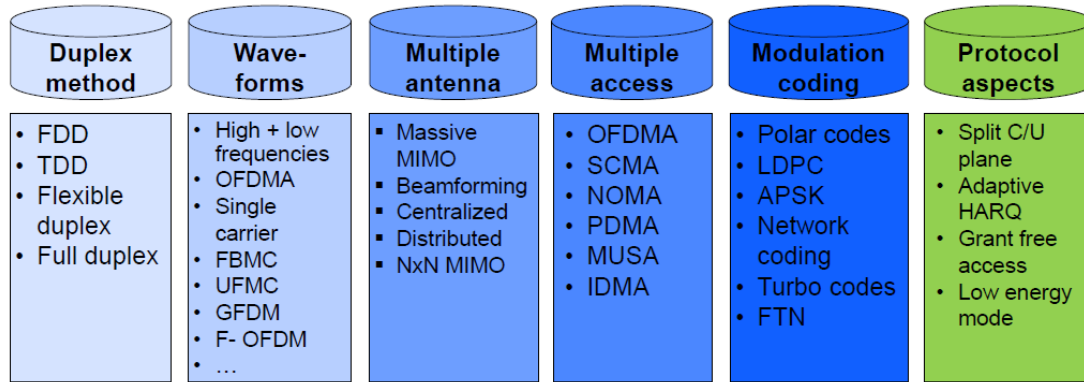


Figure 2- 15: Air interface framework for 5G [68]

### 2.4.2 Comparison LTE and Verizon Wireless 5G

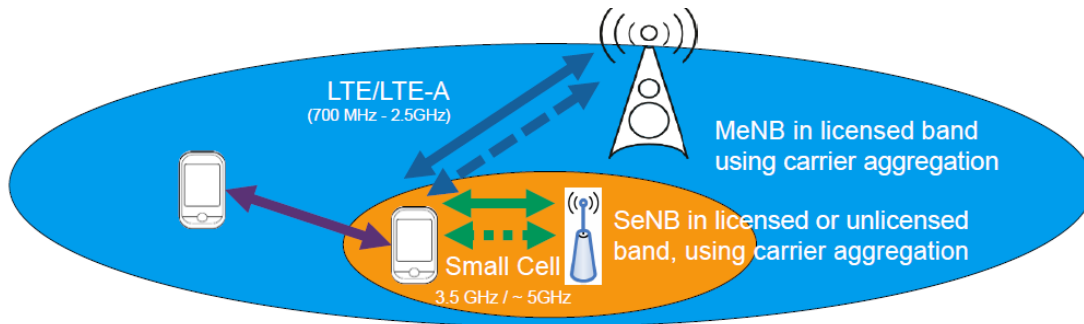
In order to compare the similarities and differences between LTE and wireless 5G, Table 2-3 shows the physical layer (PHY) parameters of LTE and 5G respectively[69, 70]. It shows the main differences between the LTE system and Verizon 5G system.

Table 2- 3: PHY parameter Comparison [69]

PHY parameter	LTE(Rel.8-14)	Verizon 5G
Downlink (DL)	OFDM	OFDM
Uplink (UL)	DFT-s-OFDM(SC-FDMA)	OFDM
Sub-frame Length	1 ms	0.2ms
Sub-carrier Spacing	15 kHz	75 kHz
Sampling Rate	30.72 MHz	153.6 MHz
Bandwidth	20 MHz	100 MHz
NFFT	2048	2048
OFDM symbol duration, no CP	66.67 us	13.33us
Frame Length	10 ms	10 ms
#Sub-frames(#slots)	10(20)	50(100)
CP Type	Normal and Extended	Normal Only
Multiplexing	FDD/TDD	Dynamic TDD
Max RBs	6, 15, 25, 50, 75, 100	100
DL/UL Data Coding	Turbo Code	LDPC Code

### 2.4.3 Carrier Frequency

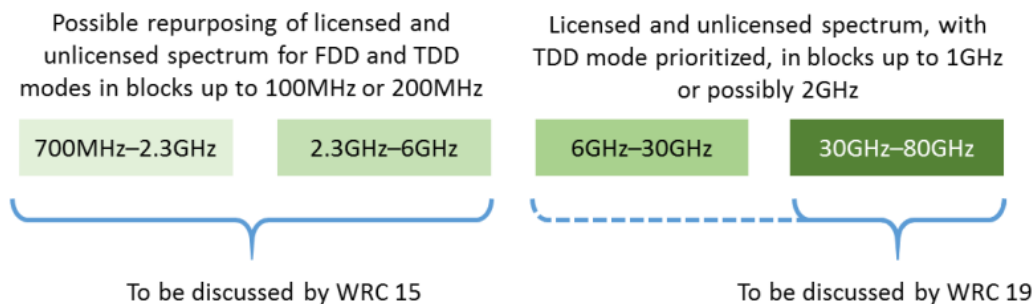
LTE/LTE-A provides the controlling layer and specific enhanced requirements are solved by “adding” – in this case adding small cell peak data rate / capacity using the carrier aggregation feature. The below architecture shown by Figure 2-16 is prepared to addresses future mobile broadband requirements.



**Figure 2- 16: Future mobile broadband requirements**

Using higher frequencies is a major part of 5G development. However, those frequencies – as with all radio spectra – constitute a valuable resource over which different competing interests have a claim. The wireless telecoms services community needs to make a compelling case for access to those frequencies in the face of competition from existing UEs.

While it is widely accepted that 5G networks will make use of spectra in existing wireless communication network bands up to 6GHz, and from 30GHz and upwards, one issue to be decided is the use of spectra bands between 6GHz and 30GHz. Some national bodies (in the UK) have suggested considering spectra from 6GHz as candidate bands for 5G; in the US, the Federal Communications Commission (FCC) has suggested looking only at frequencies from about 24 GHz. Figure 2-17 illustrates possible spectrum allocations for discussion at the WRC '15 and '19 events[66].



There is possible spectrum (with contiguous 300MHz of spectrum) for 5G use in the 6GHz, 10GHz, 12GHz, 15GHz, 18GHz, 22GHz, 24GHz, 28GHz, 31GHz, 39GHz, 45GHz, 48GHz, 51GHz, 60GHz, 70GHz and 80GHz bands

**Figure 2- 17: Possible scope of WRC '15 and WRC '19 5G spectrum discussions [66]**

FCC opens up cm-and mm-wave spectra for 5G. FCC added additional spectra for 5G wireless by an anonymously taken vote [71]. A total of 10.85 GHz will be made available: (1) 28 GHz: 27.5 to 28.35 GHz, (2) 37 GHz: 37.0 to 38.6 GHz, (3)39 GHz:

38.6 to 40 GHz, which are licensed. 64 to 71 GHz frequencies are unlicensed.

The frequency spectrum considerations for 5G in Europe: 700MHz spectrum in particular for IoT use-cases (like sensors) requiring good coverage; 3.4-3.8GHz spectrum for eMBB use-cases supporting existing cell deployments; 24.25-27.5GHz spectrum for eMBB use-cases in small cell deployments [72].

#### 2.4.4 Multi-user MIMO Technology

In the future, one “network” consisting of access point (AP) and one or multiple stations is a basic service set (BSS). AP service areas can overlap (e.g. apartment buildings). The signals are transmitted by spatial multiplexing technology on the same frequency band through the multiple data channels, in which the space dimension is reused more than one time. This technology can be combined with the beamforming technology. All signals are transmitted synchronously [73], which are shown in Figure 2-18.

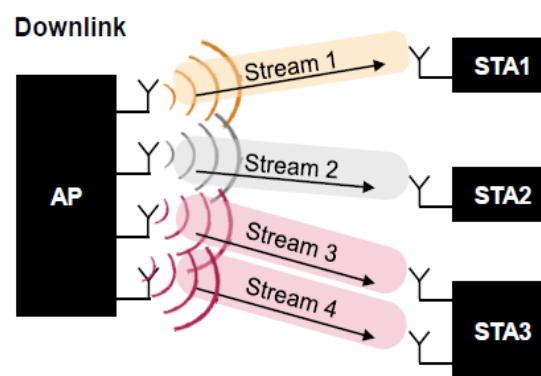


Figure 2- 18: Downlink signals [73]

Various uplink signals are separated due to different Direction of Arrival (DoA) and coding. All signals need to arrive at the AP synchronously. This is shown by Figure 2-19.

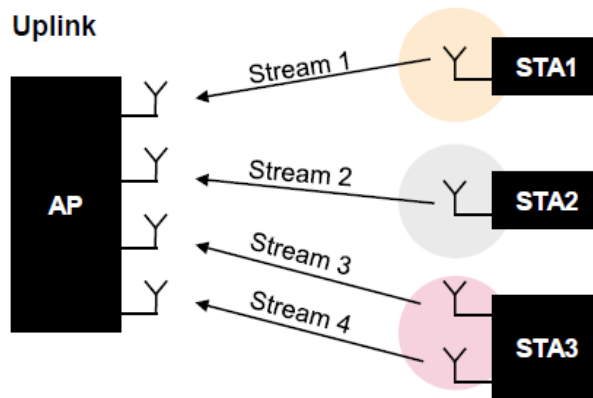


Figure 2- 19: Uplink signals [73]

### 2.4.5 Beamforming Technology

The beamforming technology is a signal processing technique that uses sensor arrays to transmit and receive signals directionally [74]. It can direct the beam in some desired direction by adjusting the phase parameters of the basic unit array as shown in Figure 2-20. Moreover, beamforming can be used not only for the signal transmitter, but also for the signal receiver [75]. The 3D beamforming technology can direct the beam energy to focus on one direction in order to make the signals transmit further distances, which has three types of architecture such as analogue, digital and hybrid.

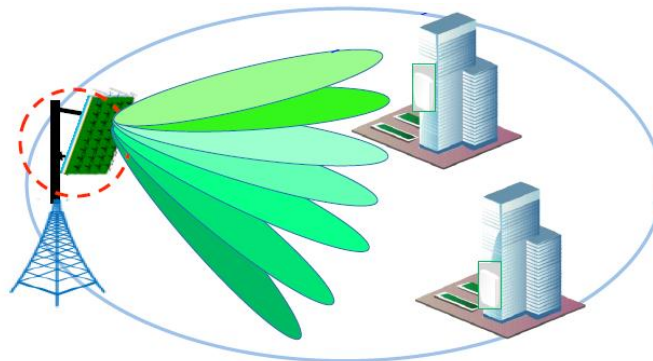


Figure 2- 20: The beamforming system [75]

### 2.4.6 Massive MIMO Theory

Massive MIMO is a hardware perspective of 5G, which is characterised by a very large antenna array at the base station and a large number of UEs served simultaneously [76]. TDD allows channel estimation without UE feedback and leveraging the multiplicity of propagation. It is shown in Figure 2-21.

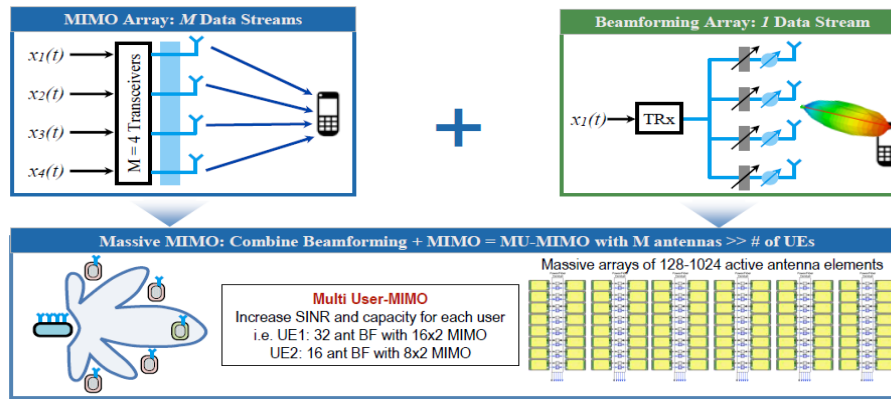


Figure 2- 21: Massive MIMO antenna [76]

### 2.4.7 Mm-wave

The mm-wave communications system has received tremendous interest from both academia and the wireless industry recently since mm-wave spectrum would provide a unique solution to solve the capacity requirements of the future wireless networks. Moreover, the ultra-dense wireless network is a perfect choice to exploit the huge spectrum available in the mm-wave frequency since the high attention in these frequency bands limits the cell size to within a few hundred meters [77, 78]. Importantly, mm-wave could potentially help solve the spectrum shortage problems for both wireless access and backhauls [79, 80].

## 2.5 3D Beamforming

In an application scenario of 3D beamforming called cell splitting is proposed, in which a cell is divided into two sectors served by two beams with different downtilts [81]. The sector with higher downtilt is defined as the near sector and the sector with lower downtilt is defined as the far sector. It remains an issue of finding proper downtilts of the two beams. With the appropriate downtilts, the BS can implement cell-specific 3D beamforming to serve the near and far sectors. A low complexity algorithm based on particle swarm optimization (PSO) to jointly optimize the downtilts and powers of the two beams and then to achieve the optimum or suboptimum cell spectral efficiency is presented in [82]. To solve this problem, a PSO based vertical beamforming optimisation algorithm is proposed, in which the powers and the down

tilts are represented by the positions of particles; and the update direction guiding the movement are mapped to the velocity. We define the cell spectral efficiency as the fitness function. By iteratively updating the positions and velocities of the particles according to some principles considering all constraints, the optimum solution can be obtained to maximize the fitness function. Simulation results show that a high cell spectral efficiency can be achieved with acceptable complexity by the proposed algorithm. Based on SVD decomposition algorithm, a 3D beamforming method is obtained. However, they assumed that one UE is served by all the antenna elements and data from BS is transmitted in a single stream [16].

A novel downlink 3D beamforming scheme is proposed for the 5G multi-user multiple-input multiple-output (MU-MIMO) system. This scheme separates beams in the so-called elevation domain via BS antenna tilt assignment, with the objective of reducing inter-user interference. The key to this scheme is controlling the vertical radiation pattern of BS antennas, which is realized by more efficient use of a two-dimensional (2D) planar antenna array. Moreover, we give the optimal solution of 3D beamforming to maximize the UEs average data rate, including adjustments of the antenna array and the corresponding multi-user selection algorithm. This can be used as a systematic framework for any given 3D scenario to mitigate inter-user interference. Our simulation results demonstrate the performance benefits in terms of transmission rate in comparison with traditional schemes.

### 2.5.1 The Beam Pattern

Figure 2-22 shows the beam pattern in a three-dimensional rectangular coordinate system. The directional antenna has maximum radiation in z-direction at  $\theta=0$ . Most of the radiation is contained in a main beam (or lobe) accompanied by radiation also in minor lobes (side and back). Between the lobes are nulls where the field goes to zero. The radiation in any direction is specified by the angles  $\theta$  and  $\phi$ . The direction of the point P is at the angles  $\theta = 30^\circ$  and  $\phi = 85^\circ$ . This pattern is symmetrical in  $\phi$  and a function only of  $\theta$  [83].

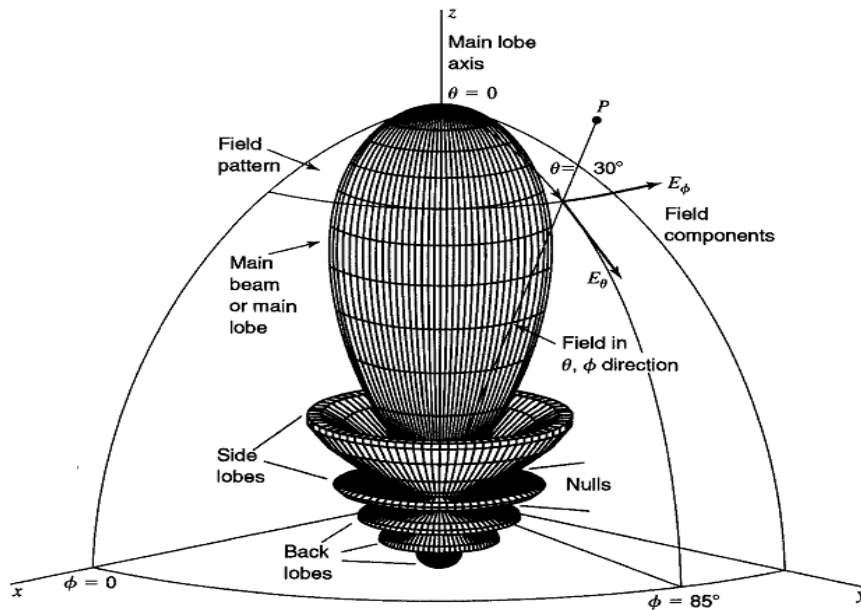


Figure 2- 22: The beam pattern [83]

The angular beam width at the half-power level or half-power beam width (HPBW) (or -3dB beam width), when  $E(\theta) = \frac{1}{\sqrt{2}} = 0.707$  and  $HPBW = 2\theta$  in which  $E(\theta)$  is the field strength. Figure 2-23 shows the HPBW, with  $E(\theta) = \cos^2 \theta = 0.707$  and  $\theta = 33^\circ$  [83].

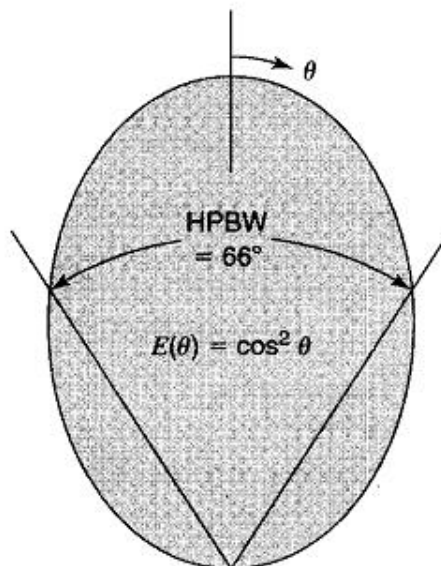


Figure 2- 23: The angular beam width at the half-power level [83]

The First Nulls Beam Width (FNBW) and HPBW are shown in Figure 2-24. If we want the FNBW,  $E(\theta) = 0$  and  $FNBW = 2\theta$ ; so  $\theta$  is  $45^\circ$  [83].

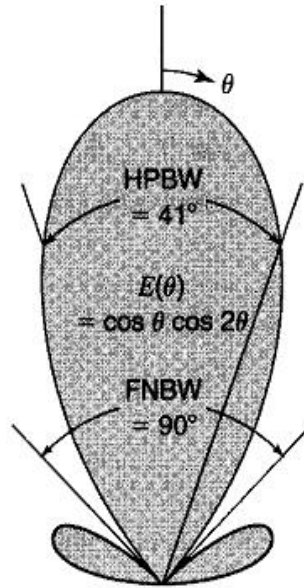


Figure 2- 24: The FNBW and HPBW [83]

### 2.5.2 Dolph-Tchebyscheff optimum distribution for the linear arrays

This section shows how to calculate the beam pattern in linear arrays. In these linear arrays, no uniform amplitude distributions are analysed and the development and application of the Dolph-Tchebyscheff distribution are discussed. It is shown that the far-field pattern of a linear array of isotropic point sources can be expressed as a finite Fourier series of  $N$  terms. Then Dolph's procedure is described for matching the terms of the Fourier polynomial with the terms of like degree of a Tchebyscheff polynomial. This then yields the optimum source amplitude distribution for a specified Side-Lobe Level (SLL) with all side lobes of the same level.

Before using Dolph-Tchebyscheff distribution to calculate the beam pattern, the two point sources, 1 and 2, in an antenna array can be analysed. They are separated by a distance  $d$  and located symmetrically with respect to the origin of the coordinates as shown in Figure 2-25[83].



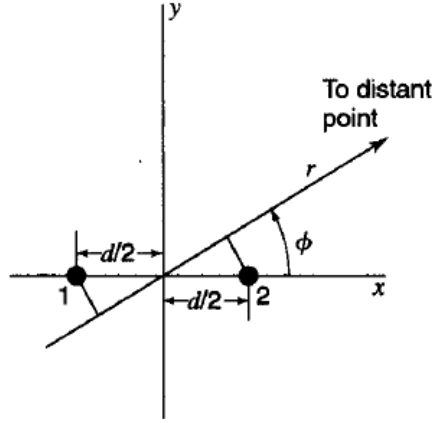


**Figure 2- 25: The two isotropic point sources having equal amplitude and oscillating**

In Figure 2- 25, the angle  $\phi$  is measured counterclockwise from the positive x-axis. The origin of the coordinates is taken as the reference for phase. Then at a distant point in the direction  $\phi$  the field from source 1 is retarded by  $\frac{1}{2}d_r \cos \phi$ , while the field from source 2 is advanced by  $\frac{1}{2}d_r \cos \phi$ , where  $d_r$  is the distance between the sources expressed in radians[83]; that is

$$d_r = \frac{2\pi d}{\lambda} = \beta d \quad (2-7)$$

The total field at a large distance  $r$  in the direction  $\phi$  is then

$$E = E_0 e^{-j\psi/2} + E_0 e^{+j\psi/2} \quad (2-8)$$

where  $\psi = d_r \cos \phi$  and the amplitude of the field components at the distance  $r$  is given by  $E_0$ .

Then obtain:

$$e^{-j\psi/2} = \cos\left(-\frac{\psi}{2}\right) + j \sin\left(-\frac{\psi}{2}\right) = \cos\left(\frac{\psi}{2}\right) - j \sin\left(\frac{\psi}{2}\right) \quad (2-9)$$

$$e^{j\psi/2} = \cos\left(\frac{\psi}{2}\right) + j \sin\left(\frac{\psi}{2}\right) \quad (2-10)$$

$$e^{-j\psi/2} + e^{j\psi/2} = 2 \cos\left(\frac{\psi}{2}\right) \quad (2-11)$$

Thus,

$$\begin{aligned} E &= E_0 e^{-\frac{j\psi}{2}} + E_0 e^{\frac{j\psi}{2}} = E_0 \left( e^{-\frac{j\psi}{2}} + e^{\frac{j\psi}{2}} \right) \\ &= 2E_0 \cos\left(\frac{\psi}{2}\right) = 2E_0 \cos\left(\frac{d_r \cos \phi}{2}\right) \end{aligned} \quad (2-12)$$

For another condition, two isotropic point sources with the origin of the coordinate system coincident with one of the sources are shown in Figure 2-26.

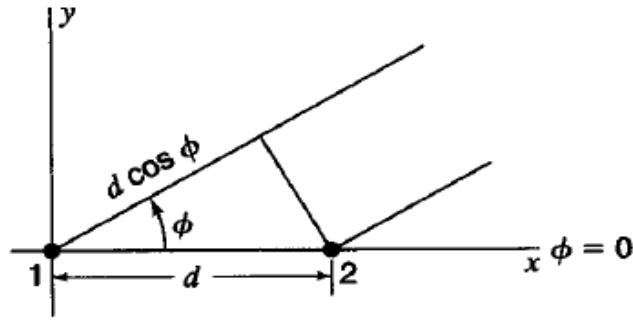


Figure 2- 26: The two isotropic point sources with the origin of the coordinate system coincident with one of the sources

The total field is

$$E = E_0 + E_0 e^{j\psi} = E_0(1 + e^{j\psi}) = E_0 e^{\frac{j\psi}{2}} \left( e^{-\frac{j\psi}{2}} + e^{\frac{j\psi}{2}} \right) = 2E_0 e^{\frac{j\psi}{2}} \cdot \cos\left(\frac{\psi}{2}\right) = 2E_0 \cos\left(\frac{d_r \cos \phi}{2}\right) e^{\frac{j\psi}{2}} \quad (2-13)$$

There are two situations for the linear arrays such as the number of the antennas is even and odd, which is shown in Figure 2- 27 and the number of the antennas is odd, which is shown in Figure 2- 28 [83].

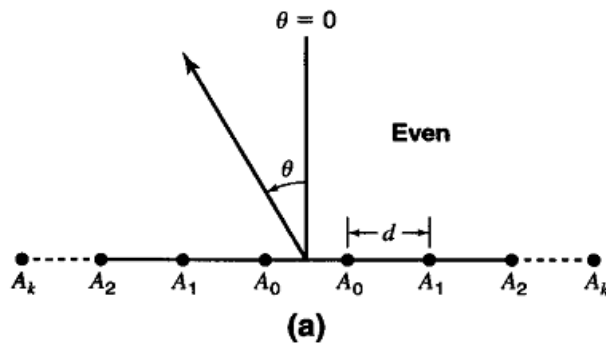


Figure 2- 27: The linear arrays for the number of the antennas is even

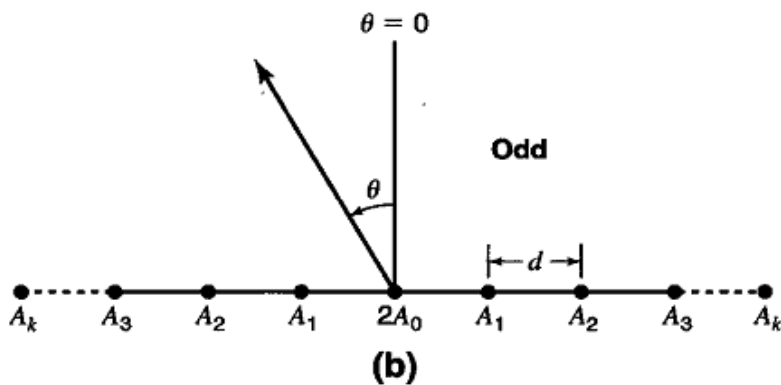


Figure 2- 28: The linear arrays for the number of the antennas is odd

In these two figures,  $\psi = \frac{2\pi d}{\lambda} \sin \theta = d_r \cos \theta$  and  $n_e$  is the number of isotropic

point sources. The individual sources have the amplitudes  $A_0$  to  $A_k$  and the amplitude distribution being symmetrical about the centre of the array. Therefore, the total field  $E_{ne}$  for these two linear arrays are [83]:

1. The number is even:

For the two point sources,

$$E = 2E_0 \cos\left(\frac{d_r \cos \theta}{2}\right) \quad (2-14)$$

Thus,

$$E = 2 \sum_{k=0}^{N-1} A_k \cos\left(\frac{2k+1}{2}\psi\right) \quad (2-15)$$

$$E_{n_e} = 2A_0 \cos\frac{\psi}{2} + 2A_1 \cos\frac{3\psi}{2} + \dots + 2A_k \cos\left(\frac{n_e-1}{2}\psi\right) \quad (2-16)$$

where  $n_e = 2(k+1)$ .

2. The number is odd:

$$E_{n_o} = 2A_0 + 2A_1 \cos \psi + 2A_2 \cos 2\psi + \dots + 2A_k \cos\left(\frac{n_o-1}{2}\psi\right) \quad (2-17)$$

where  $n_o = 2(k+1)$ .

Now, we consider the linear array with the number of isotropic point sources is even.

For  $e^{jm\psi/2}$ ,

$$e^{jm\psi/2} = (e^{j\psi/2})^m = \left(\cos\frac{\psi}{2} + j\sin\frac{\psi}{2}\right)^m \quad (2-18)$$

$$e^{jm\psi/2} = \cos\left(m\frac{\psi}{2}\right) + j\sin\left(m\frac{\psi}{2}\right) \quad (2-19)$$

Thus,

$$\cos\left(m\frac{\psi}{2}\right) + j\sin\left(m\frac{\psi}{2}\right) = \left(\cos\frac{\psi}{2} + j\sin\frac{\psi}{2}\right)^m \quad (2-20)$$

Taking real parts of the above equation, having:

$$\cos\left(m\frac{\psi}{2}\right) = \text{Re}\left(\cos\frac{\psi}{2} + j\sin\frac{\psi}{2}\right)^m \quad (2-21)$$

Expanding as a binomial series gives:

$$\cos\left(m\frac{\psi}{2}\right) = \cos^m\left(\frac{\psi}{2}\right) - \frac{m(m-1)}{2!} \cos^{m-2}\left(\frac{\psi}{2}\right) \sin^2\left(\frac{\psi}{2}\right) + \dots \quad (2-22)$$

Because

$$\sin^2\left(\frac{\psi}{2}\right) = 1 - \cos^2\left(\frac{\psi}{2}\right) \quad (2-23)$$

Substituting particular values of  $m$ , then we have

$$m = 0 \quad \cos\left(m\frac{\psi}{2}\right) = 1$$

$$m = 1 \quad \cos\left(m\frac{\psi}{2}\right) = \cos\frac{\psi}{2}$$

$$m = 2 \quad \cos\left(m\frac{\psi}{2}\right) = 2\cos^2\left(\frac{\psi}{2}\right) - 1$$

$$m = 3 \quad \cos\left(m\frac{\psi}{2}\right) = 4\cos^3\left(\frac{\psi}{2}\right) - 3\cos\frac{\psi}{2}$$

$$m = 4 \quad \cos\left(m\frac{\psi}{2}\right) = 8\cos^4\left(\frac{\psi}{2}\right) - 8\cos^2\left(\frac{\psi}{2}\right) + 1$$

⋮

⋮

Set  $x = \cos\frac{\psi}{2}$  and  $T_m(x) = \cos\left(m\frac{\psi}{2}\right)$ ,

The Tchebyscheff polynomials are:

$$T_0(x) = 1$$

$$T_1(x) = x$$

$$T_2(x) = 2x^2 - 1$$

$$T_3(x) = 4x^3 - 3x$$

$$T_4(x) = 8x^4 - 8x^2 + 1$$

$$T_5(x) = 16x^5 - 20x^3 + 5x$$

$$T_6(x) = 32x^6 - 48x^4 + 18x^2 - 1$$

$$T_7(x) = 64x^7 - 112x^5 + 56x^3 - 7x$$

⋮

⋮

Thus,

$$T_{n+1}(x) = 2xT_n(x) - T_{n-1}(x)$$

Finally, obtain:

$$E = 2A_0 \cos\frac{\psi}{2} + 2A_1 \cos\frac{3\psi}{2} + \dots + 2A_k \left(\frac{2k-1}{2}\psi\right) \quad (2-24)$$

That is

$$E = 2A_0T_1(x) + 2A_1T_3(x) + 2A_2T_5(x) + \dots + 2A_kT_{\frac{2k-1}{2}}(x) \quad (2-25)$$

## 2.5.2 3D LTE Channel Model

The channel coefficients have been obtained from “3GPP TR 36.873” [10]. In the next paragraphs,  $H$  is the channel coefficient matrix. Figure 2-29 shows the two kinds of path in the channel model. One of them is Non-Line of sight (NLOS) and other is Line-of-Sight (LOS).

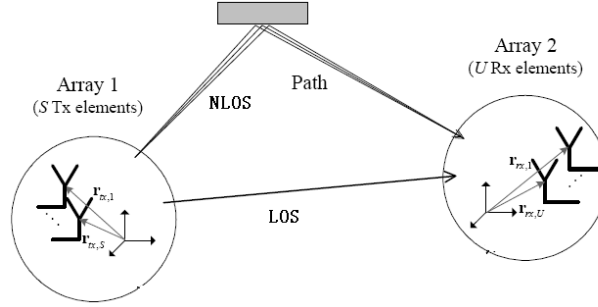


Figure 2- 29: The single channel model [10]

Since the propagation paths over which the signal is transmitted are not deterministic, the probability of existence for each path must be set. The calculation for probability of the LOS is defined in Ref.2 (see Table 7.2-2: LOS probabilities on page 22 of reference). This probability defines how the power is distributed for different paths. If the power is less than -25 dB, this path is ignored [10].

There are two kinds of channel coefficients. The channel coefficient for the NLOS is [10]:

$$\begin{aligned}
 H_{u,s,n}(t) = & \sqrt{P_n/M} \sum_{m=1}^M \left[ \begin{array}{l} F_{rx,u,\theta} \left( \theta_{n,m}, ZOA \cdot \varphi_{n,m}, AOA \right) \\ F_{rx,u,\varphi} \left( \theta_{n,m}, ZOA \cdot \varphi_{n,m}, AOA \right) \end{array} \right]^T \\
 & \left[ \begin{array}{cc} \exp(j\Phi_{n,m}^{\theta\theta}) & \sqrt{\kappa_{n,m}^{-1}} \exp(j\Phi_{n,m}^{\theta\varphi}) \\ \sqrt{\kappa_{n,m}^{-1}} \exp(j\Phi_{n,m}^{\varphi\theta}) & \exp(j\Phi_{n,m}^{\varphi\varphi}) \end{array} \right] \\
 & \left[ \begin{array}{l} F_{tx,s,\theta} \left( \theta_{n,m}, ZOD \cdot \varphi_{n,m}, AOD \right) \\ F_{tx,s,\varphi} \left( \theta_{n,m}, ZOD \cdot \varphi_{n,m}, AOD \right) \end{array} \right] \\
 & \cdot \exp \left( j2\pi\lambda_0^{-1} \left( \hat{r}_{rx,n,m}^T \cdot \bar{d}_{rx,u} \right) \right) \\
 & \cdot \exp \left( j2\pi\lambda_0^{-1} \left( \hat{r}_{tx,n,m}^T \cdot \bar{d}_{tx,s} \right) \right) \cdot \exp(j2\pi\nu_{n,m}t)
 \end{aligned} \tag{2-26}$$

The channel coefficient for the LOS is [10]:

$$\begin{aligned}
H_{u,s,n}(t) &= \sqrt{\frac{I}{K_R + I}} H'_{u,s,n}(t) + \delta(n-1) \sqrt{\frac{K_R}{K_R + I}} \\
&\begin{bmatrix} F_{rx,u,\theta} \left( \theta_{LOS,ZOA} \cdot \varphi_{LOS,AOA} \right) \\ F_{rx,u,\varphi} \left( \theta_{LOS,ZOA} \cdot \varphi_{LOS,AOA} \right) \end{bmatrix}^T \\
&\begin{bmatrix} \exp(j\Phi_{LOS}) & 0 \\ 0 & -\exp(j\Phi_{LOS}) \end{bmatrix} \\
&\begin{bmatrix} F_{tx,s,\theta} \left( \theta_{LOS,ZOD} \cdot \varphi_{LOS,AOD} \right) \\ F_{tx,s,\varphi} \left( \theta_{LOS,ZOD} \cdot \varphi_{LOS,AOD} \right) \end{bmatrix} \\
&\cdot \exp\left( j2\pi\lambda_0^{-1} \left( \hat{r}_{rx,LOS}^T \cdot \bar{d}_{rx,u} \right) \right) \\
&\cdot \exp\left( j2\pi\lambda_0^{-1} \left( \hat{r}_{tx,LOS}^T \cdot \bar{d}_{tx,s} \right) \right) \\
&\cdot \exp(j2\pi\nu_{LOS}t)
\end{aligned} \tag{2-27}$$

In these two equations,  $F_{rx,u}$  and  $F_{rx,u}$  are the receive antenna element  $u$  field patterns for vertical and horizontal polarisations respectively.  $F_{tx,s}$  and  $F_{tx,s}$  are the transmit antenna element  $s$  field patterns for vertical and horizontal polarisations respectively;  $d_s$  and  $d_u$  are the uniform distances [m] between transmitter antenna elements and receiver antenna elements respectively;  $k$  is the cross polarization power ratio in linear scale and the  $\lambda_0$  is the wavelength of the carrier frequency;  $n$  is the cluster number;  $\theta_{n,m}$  and  $\varphi_{n,m}$  are the arrival angle and departure angle of ray  $m$  in cluster  $n$  respectively;  $\{ \phi_{n,m}^{\theta\theta}, \phi_{n,m}^{\theta\varphi}, \phi_{n,m}^{\varphi\theta}, \phi_{n,m}^{\varphi\varphi} \}$  are the random initial phases for four different polarisation combinations ( $\theta\theta, \theta\varphi, \varphi\theta, \varphi\varphi$ );  $\nu_{n,m}$  is the Doppler frequency component;  $K_R$  is the Rician K-factor.

The channel model for 3D beamforming LTE system is based on ‘‘Study on 3D channel model for LTE’’, ‘‘3GPP TR 36.873’’[10]. The PL models can be applied in the frequency range of 2 GHz to 6 GHz and for different antenna heights. The PL models are summarised in 3D urban macro scenario (3D-UMa) and 3D urban micro (3D-UMi) for the 3D channel model from 3GPP. Definition of  $d_{2D}$  and  $d_{3D}$  for outdoor UEs for the 3D-UMi, which are shown in Figure 2-30[10], and definition of  $d_{2D-out}$ ,  $d_{2D-in}$  and  $d_{3D-out}$ ,  $d_{3D-in}$  for indoor UEs for the 3D-Uma, which are shown in Figure 2-31 [10].

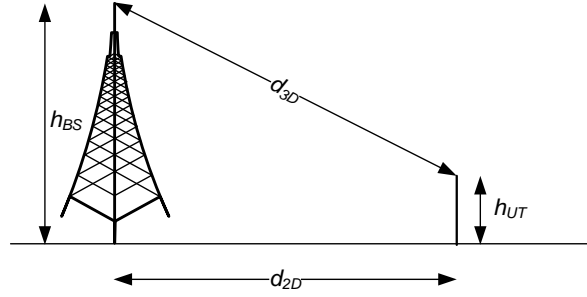


Figure 2- 30: The 3D-UMi: Definition of d2D and d3Dfor outdoor UEs

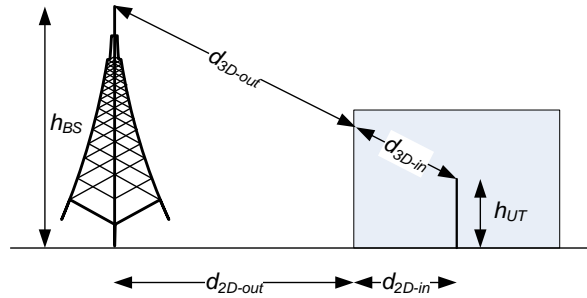


Figure 2- 31: The 3D-Uma: Definition of d2D-out, d2D-in and d3D-out, d3D-in for indoor UEs

### 2.5.3 The Weighting of MxN antenna

A BS is equipped with an antenna array that consists of  $M \times N$  antenna elements. There are N elements in the y-direction and M elements in the x-direction. This is shown in Figure 2-32.

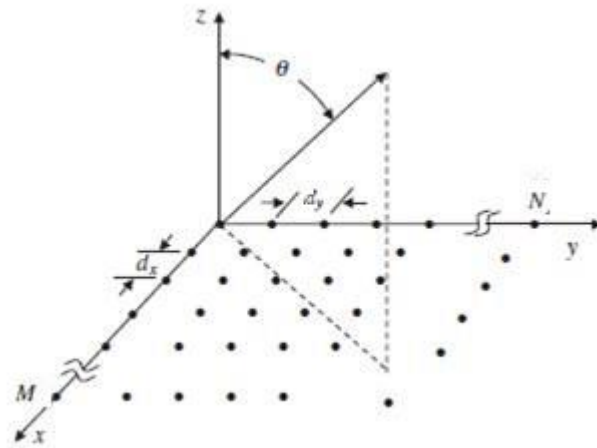


Figure 2- 32: The rectangular planar array for MxN antenna [45]

Using the pattern multiplication, the pattern of the entire  $M \times N$  array has been obtained [45].

$$AF = \sum_{m=1}^M \sum_{n=1}^N w_{mn} e^{j[(m-1)(kd_x \sin \theta \cos \phi + \beta_x) + (n-1)(kd_y \sin \theta \sin \phi + \beta_y)]} \quad (2-28)$$

where  $w_{mn} = a_m b_n$ , the phase delays  $\beta_x$  and  $\beta_y$  are given by:

$$\beta_x = -kd_x \sin \theta_0 \cos \varphi_0, \quad \beta_y = -kd_y \sin \theta_0 \sin \varphi_0.$$

The weights  $a_m$  and  $b_n$  can be uniform or can be in any form according to the designer's needs. This could include the various weights such as the binomial, Kaiser-Bessel, Hamming, or Gaussian weights. The  $a_m$  weights do not have to be identical to the  $b_n$  weights.

### 2.5.4 FD-MIMO Beamforming

The 3D beamforming technology presented in this section is different to FD-MIMO or Massive MIMO systems, since the beam angles in FD-MIMO or Massive MIMO are fixed as shown in Figure 2-33 [84, 85].

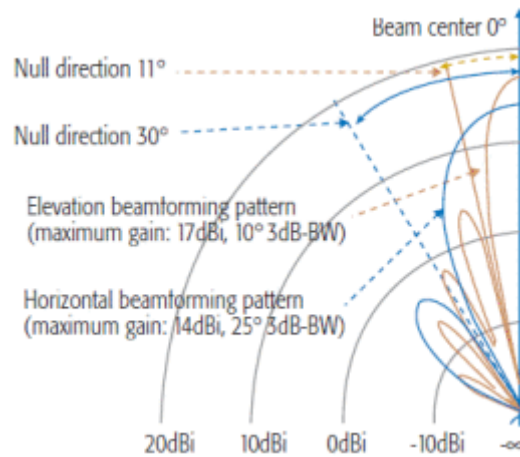
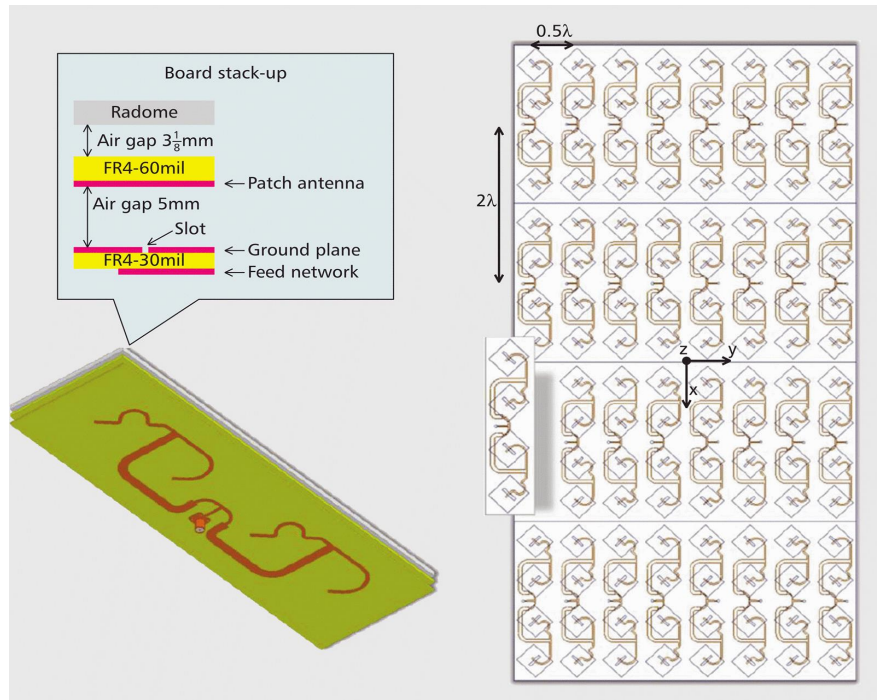


Figure 2- 33: The beam pattern in a fixed direction [84]

Figure 2-33 shows the null direction, an angle to make the magnitude of the beam pattern equal to zero, for the elevation beam pattern is  $11^\circ$  and for the horizontal beam pattern is  $30^\circ$  [84].

If the direction of beam is changed, the direction of the antenna will be changed. For example, the patch antenna elements are disposed in the  $\varphi = \pm 45^\circ$  direction, which results in dual-linear polarization on the two diagonal planes ( $\varphi = 45^\circ$  with reference to the coordinate system shown in Figure 2-34) [86].





**Figure 2- 34: Right: top-to bottom view of FD-MIMO antenna array and feed network; left: bottom view of one sub-array with detailed PCB stack-up [86]**

All sub-arrays are phase matched, which is important, because the difference of electrical lengths from the feed ports to the patch antennas should not exceed more than  $1^{\circ}$ – $2^{\circ}$ . In order to ensure phase matching, every sub-array has the same feed network adjusted to fit both  $\pm 45^{\circ}$  rotated patches by merely mirroring the micro strip sections, as shown in Figure 2-34[86].

However, in this thesis, the beam angles in 3D beamforming can be changed by the weighting matrix and the side-lobes can be minimized towards specified undesired directions even if the locations of UEs changes.

### 2.5.5 Constant Beamwidth Beamforming

The constant beam width beamforming is a key technique and research focus in broadband array signal processing. However, most conventional methods can only satisfy constant main lobe width and the performance will degrade severely when main lobe and side lobe interferences exist. To overcome this problem, a broadband constant beam width beamforming for suppressing main lobe and side lobe interferences is proposed[87]. In the proposed method, the modified blocking matrices of different frequency bins are firstly constructed for main lobe interference cancellation in the data

domain, afterward the minimum variance distortion less response (MVDR) beamformer is adopted to determine the adaptive weight vector of the reference frequency for robust interference suppression. Finally, the adaptive weight vectors of the other frequency bins are calculated using second-order cone programming (SOCP). The proposed method can form the same main lobe width and null characteristics over the entire design frequency range.

### **2.5.6 Minimum Side-lobe Beamforming in Spherical Antenna Array**

An optimal minimum side lobe modal beamforming approach based on the spherical harmonics decomposition for spherical sensor arrays has been proposed; they have provided the ability of three-dimensional broadband beam pattern synthesis [88]. The spherical harmonics domain array processing problem is expressed with a matrix formulation. The weight vector design problem is written as a multiple-constrained problem, so that the resulting beam former can provide a suitable trade-off among mutually conflicting beamforming objectives, such as the lowest side lobe level, beam width, multi-null steering, and robustness. The multiple constrained problem is formulated as a convex form of second-order cone programming, which is computationally tractable. The main advantage of this method over classical element-space array processing approaches is that the frequency dependent components can be pre-decoupled and removed from angular dependent spherical harmonics, so the same beam pattern could be used over a frequency range with a single set of array weights, and the complexity of broadband beamforming optimisation algorithms can be reduced.

## **2.6 Millimetre-wave**

Millimeter-wave bands potentially enable high bandwidths. To date, the limited use of these high frequencies is a result of adverse propagation effects in particular due to obstacles in the channel path. Several transceiver architectures have been developed to compensate these issues by focusing the received or transmitted beams in a desired direction. All these solutions make use of smaller antenna element sizes due to higher carrier frequencies that enable the construction of larger antenna arrays.

With the severe spectrum shortage in conventional cellular bands, millimeter wave frequencies have been attracting growing attention as a possible candidate for the next-generation 5G system. The mm-wave bands offer orders of magnitude greater spectrum than current cellular allocations and enable very high dimensional antenna arrays for further gains via beamforming and spatial multiplexing. This has motivated the study of large-scale antenna arrays for achieving highly directional beamforming.

### 2.6.1 Analogue Beamforming

An analogue beamforming architecture consists of only one RF chain and multiple phase shifters that feed an antenna array. Figure 2-35 shows a basic implementation of an analogue beamforming transmitter architecture.

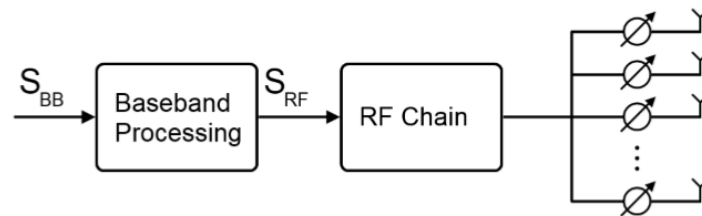
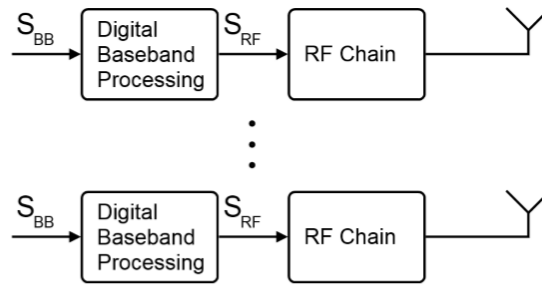


Figure 2- 35: Analogue Beamforming Architecture [89]

This architecture is used today in high-end mm-wave systems as diverse as radar and short-range communication systems like IEEE 802.11ad. Analogue beamforming architectures are not as expensive and complex as the other approaches described in this thesis. On the other hand implementing a multi-stream transmission with analogue beamforming is a highly complex task [89].

### 2.6.2 Digital Beamforming

While analogue beamforming is generally restricted to one RF chain even when using large number antenna arrays, digital beamforming in theory supports as many RF chains as there are antenna elements. If suitable pre-coding is performed in the digital baseband, this yields higher flexibility regarding the transmission and reception. The additional degree of freedom can be leveraged to perform advanced techniques like multi-beam MIMO. These advantages result in the highest theoretical performance possible compared to other beamforming architectures [90]. Figure 2-36 illustrates the general digital beamforming transmitter architecture with multiple RF chains.



**Figure 2- 36: Digital Beamforming Architecture [90]**

Beam squint is a well-known problem for analog beamforming architectures using phase offsets [91]. This is a serious drawback considering current 5G plans to make use of large bandwidths in the mm-wave band. Digital control of the RF chain enables optimisation of the phases according to the frequency over a large band. Nonetheless, digital beamforming may not always be ideally suited for practical implementations regarding 5G applications. The very high complexity and requirements regarding the hardware may significantly increase cost, energy consumption and complicate integration in mobile devices. Digital beamforming is better suited for use in base stations, since performance outweighs mobility in this case. Digital beamforming can accommodate multi-stream transmission and serve multiple users simultaneously, which is a key driver of the technology.

### **2.6.3 Hybrid Beamforming in MIMO**

Hybrid beamforming has been proposed as a possible solution that is able to combine the advantages of both analogue and digital beamforming architectures. First results from implementations featuring this architecture have been presented in prototype level, i.e. in [92]. In order to reduce the number of RF chains for large-scale MIMO systems hybrid beamforming structure has been introduced [93]. Its structure is shown in Figure 2-37.

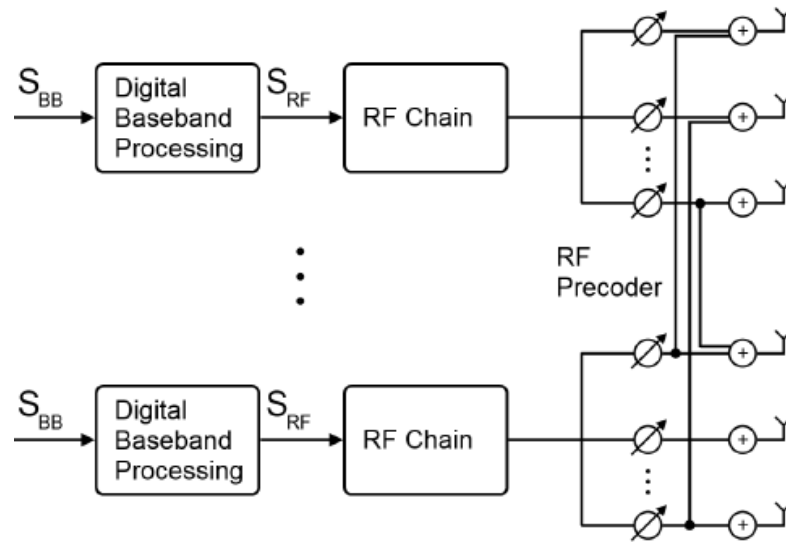


Figure 2- 37: Hybrid beamforming structure [93]

The hybrid beamforming structure combines the advantages of both analogue and digital beamforming architectures but it can reduce the number of complete RF chains. The number of simultaneously supported streams is reduced compared to full blown digital beamforming.

In mm-wave communication systems, to deal with the effect of frequency selective channel fading, we often adopt multiple antennas. However in a traditional MIMO system, full digital beamforming is done at the baseband, and each antenna requires one distinct RF chain. It leads to prohibitive cost or power consumption. In order to reduce the number of RF chains for large-scale MIMO systems hybrid beamforming structure has been introduced [94]. The overall beamforming matrix consists of analogue RF beamforming implemented using phase shifters and baseband digital beamforming of much smaller dimension. When the hybrid structure is used at both the transmitter and the receiver, pre-coder and receiver design for maximising the spectral efficiency were proposed [95].

The design of analogue beam formers for the downlink of multiple UEs massive MIMO systems is considered. They specifically investigate systems where both link ends are equipped with hybrid digital or analogue (HDA) beamforming structures, where the analogue beam formers are adapted based on second-order channel statistics, reducing the training overhead as well as hardware effort [96]. They present a framework for the optimisation of such beam formers operating in mm-wave channels,

exploiting the directional characteristics and sparse nature of such channels. They develop an approximate upper bound of the ergodic sum capacity, based on which efficient beamforming algorithms are devised [97].

#### 2.6.4 Millimetre-Wave Channel Model

The mm-wave has been proposed as a promising candidate for new spectra in 5G cellular networks [98] because it has a good performance with beamforming technology in 60 GHz band [68]. The size of the chip for millimeter-wave could be very smaller such as Figure 2-38 shown [99].

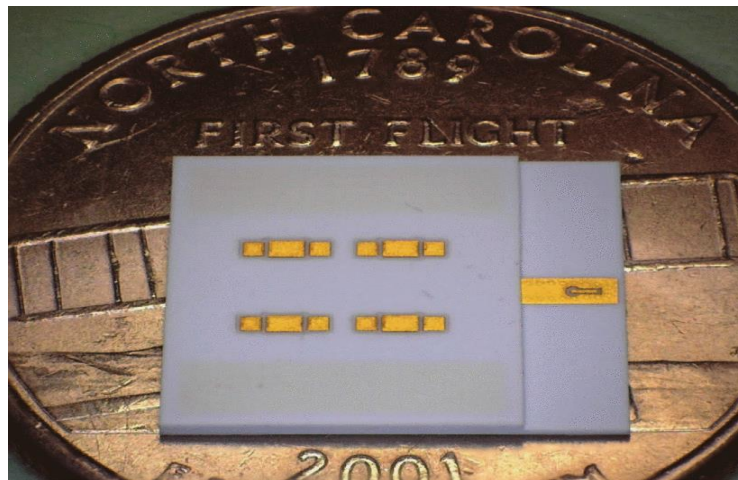


Figure 2- 38: The photo of the 60 GHz reference chip antenna resting on a US quarter [99]

Figure 2-38 shows a photo of a 60GHz reference chip antenna. Overall dimensions of chip are  $430 \times 480 \times 28$  mil<sup>3</sup> or  $10.92 \text{ mm} \times 12.19 \text{ mm} \times 0.71 \text{ mm}$ . The aperture area including EBG structure is  $9.4 \text{ mm} \times 10.92 \text{ mm}$ , or  $1.88\lambda \times 2.18\lambda$  at 60GHz. Radiating elements have an inter-element spacing of 3.05 mm, or  $0.61\lambda$  at 60GHz in both principal planes [99].

One measurement for millimeter-wave system is shown in Figure 2-39. The results show that the reflection coefficient is lower than -15dB ( $VSWR \leq 1.45$ ) within the frequency range from 22.5GHz to 32GHz, which covers the 24.25GHz to 27.5GHz band proposed by ITU and the 27.5GHz to 28.35GHz band proposed by FCC for 5G[99]. The gain of the antenna element varies from 8.2 to 9.6 dBi over the frequency range of 24GHz to 32GHz. The simulated and measured results also illustrate good radiation patterns across the wide frequency band (24-32GHz) [99].

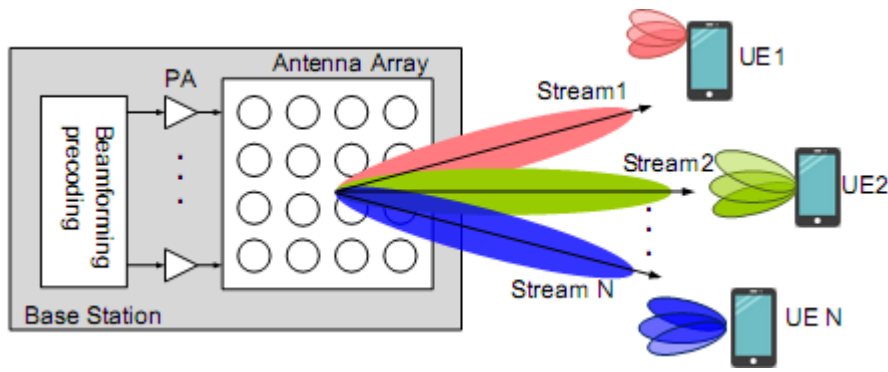


Figure 2-39: The mm-wave system model for the multi-user MIMO beamforming [99]

Other real-world measurements have the frequency at 28GHz and 73GHz, which was in New York, NY, USA, to derive detailed spatial statistical models of the channels and uses these models to provide a realistic assessment of mm-wave and Pico cellular networks in a dense urban deployment [100]. In this measurement, the mm-wave systems can offer an order of magnitude increase in capacity over current state-of-the-art 4G cellular networks with no increase in cell density from current urban deployments as shown in Figure 2-40 [100].

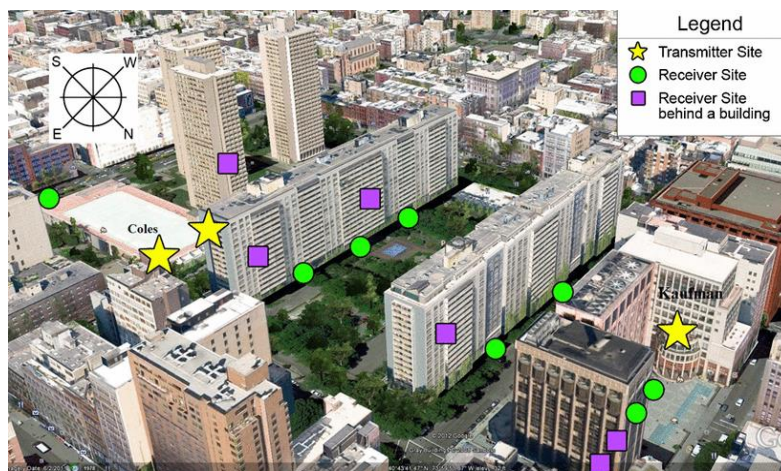


Figure 2- 40: The measurement locations in NYC at 28 GHz and 73 GHz [100]

The PL for this mm-wave system channel has two situations such as NLOS and LOS. The PL equation is from real-world measurements in New York (NY), USA, whose carrier frequencies are at 28GHz and 73GHz. These are used to derive detailed spatial statistical models of the channels and these models are used to provide a realistic assessment of mm-wave and Pico cellular networks in a dense urban deployment [100]. The PL equation is:

$$PL(d) = \alpha + \beta \cdot 10\log_{10}(d) + \xi, \xi \sim N(0, \sigma^2) \text{ (dB)}$$

where  $d$  is the distance in metres,  $\alpha$  and  $\beta$  are the least square best fit of floating intercept and slope over the measured distances (30 m to 200 m), and  $\sigma^2$  is the lognormal shadowing variance [100]. Moreover, the parameters in the PL equation have different values in the two NLOS and LOS situations at 28GHz and 73GHz respectively as shown in Table 2-4 [100]. The PL equation and parameters given in Table 2-4 will be used in Chapter 5 for simulation analysis of the mm-wave system.



Table 2- 4: Parameters in different path for PL [100]

Variable	Model	Model Parameter Variables	
		28 GHz	73 GHz
Omnidirectional path loss, PL and lognormal shadowing, $\zeta$	$PL(d) = \alpha + \beta \cdot 10\log_{10}(d) + \zeta, \zeta \sim N(0, \sigma^2)$	<b>NLOS:</b> $\alpha = 72.0, \beta = 2.92, \sigma = 8.7$ <b>LOS:</b> $\alpha = 61.4, \beta = 2, \sigma = 5.8$	<b>NLOS:</b> $\alpha = 82.7, \beta = 2.69, \sigma = 7.7$ <b>LOS:</b> $\alpha = 69.8, \beta = 2, \sigma = 5.8$
NLOS-LOS-Outage-probability	$p_{out}(d) = \max(0, 1 - e^{-\alpha_{out}d + b_{out}})$ (a) $p_{LOS}(d) = (1 - p_{out}(d)) \cdot e^{-\alpha_{los}d}$ (b) $p_{NLOS}(d) = 1 - p_{out}(d) - p_{LOS}(d)$ (c)	$\frac{I}{\alpha_{out}} = 30 \times 10^{-3}, b_{out} = 5.2, \frac{I}{\alpha_{out}} = 67.1 \times 10^{-3}$	
Number of clusters, K	$K \sim \max\{Poisson(\lambda), 1\}$	$\lambda = 1.8$	$\lambda = 1.9$
Cluster power fraction	$\gamma_k = \frac{\gamma'_k}{\sum_{j=1}^K \gamma'_j} \quad (1)$ $\gamma'_k = U_k^{\gamma_r - 1} \cdot 10^{-0.1Z_k} \quad (2)$	$\gamma_\gamma = 2.8, \zeta = 4$	$\gamma_\gamma = 3, \zeta = 4$
BS and UE horizontal cluster central angles, $\theta$	$\theta \sim U(0, 2\pi)$	None	None
BS and UE vertical cluster central angles, $\phi$	$\phi = \text{LOS elevation angle}$	None	None
BS cluster rms angular spread	$\sigma$ is exponentially distributed, $E(\sigma) = \lambda^{-1}$	Horiz $\lambda^{-1} = 10.2^\circ$ ; Vert $\lambda^{-1} = 0^\circ(*)$	Horiz $\lambda^{-1} = 10.5^\circ$ ; Vert $\lambda^{-1} = 0^\circ(*)$
UE rms angular spread	$\sigma$ is exponentially distributed, $E(\sigma) = \lambda^{-1}$	Horiz $\lambda^{-1} = 15.5^\circ$ ; Vert $\lambda^{-1} = 6^\circ(*)$	Horiz $\lambda^{-1} = 15.4^\circ$ ; Vert $\lambda^{-1} = 3.5^\circ$

- Note:  $d$  is the distance in metres,  $\alpha$  and  $\beta$  are the least square best fits of floating intercept and slope over the measured distances (30m to 200 m), and  $\sigma^2$  is the lognormal shadowing variance [62];  $U_k \sim U[0, 1], Z_k \sim N(0, \zeta^2)$

## 2.7 Conclusion

In the 5G communication system, a large number of novel technologies are applied, but this research thesis cannot show all of them so only some of the relevant literatures about this investigated subject were found and the relevant technologies were introduced in this chapter. Research and development to create the next generation of 5G mobile networks are focused on improving the transmission rate. The main method is supplying the broader bandwidths at higher carrier frequencies and re-architecting of the network. Therefore, the beamforming technology, where the radio signal is focused to a narrow beam, help to offset the effect of reduced propagation of very high frequency carriers. However, the interference between these beams from their side lobes when we use them to transmit multiple beams is hard to be decreased. Moreover, most of beams for the 3D beamforming technology are constant beamwidth beam, which are hard to adjust the shape and direction.

In this thesis, the improved K-means clustering algorithm is used to cluster the different UEs in minimum number of groups, in order to decrease the number of beams when the multiple beams are transmitted. Moreover, the maximum SINR values (means the minimum side lobes for each beams) are chosen to calculate the weighting matrix for 3D beamforming technology, in order to decrease the interference from the side lobes of beams. Our 3D beamforming system is most suited to eMBB and URLLC architectures for 5G. In this research, the performance from the chosen technologies, the improvement K-means clustering algorithm and the new weighting method, are shown by the systems' simulation results. Chapter 3 introduces and explains the specific methods regarding these two technologies.

# **Chapter 3**

## **Innovation Schemes for 3D Beamforming Technology**

### 3.1 Introduction

The beamforming technology is a key technology in 5G communication system, which is a signal processing technique that uses antenna arrays to transmit and receive signals directionally [101-104]. In beamforming, an array of antennas can dynamically adapt the direction and down-tilt towards receiver by rotating the antenna pattern. The array of antennas can transmit the multiple beams to multiple UEs at same time.

In this chapter, the two main improvement technologies for the 3D beamforming technology are explained:

1. The improved K-means clustering algorithm is a partition clustering method. It is supposed that UEs' distributions are uniform and the location of UEs are random. In order to cover all UEs by beams, we need divide UEs into several groups using clustering algorithm, and amongst many different partitioning clustering algorithms, K-means algorithm is a good algorithm for clustering a low dimensional data setting [54-60]. K-means algorithm not only divides UEs into K groups, but also can determine the center of each group, so in this chapter the K-means algorithm can be used. We first divide UEs into K groups, then let each group be covered by a beam and the beam transmit to the center.
2. The maximum SINR weighting method is the new weighting method to direct the 3D beamforming. When the multiple beams transmit to multiple UEs groups at same time, there must be interference between each beam. However, most of researches do not focus on the problem about interference between each beam. In this chapter, vertical dimension of antenna is taken into account and the modeling 3D channel is investigated. Furthermore, an enhanced dynamic beamforming algorithm is proposed where beamforming vector can be obtained according to both UEs' horizontal and vertical directions. The new weighting method not only adjusts the values of weighting matrix to direct the main beam in a desired direction but also minimizes its side lobes in other specific directions.

### 3.2 Grouping UEs based on K-means Algorithm

In order to cover all UEs by beams, we divide UEs into several groups based on the K-means algorithm. In the K-means algorithm we used the Cosine distance, and the detail process of the K-means algorithm is given as follows.

The cosine distance between A and B is one minus the cosine of the included angle between points (treated as vectors).

Suppose the number of UE points  $X^{(i)}(x_i, y_i, z_i)$  is  $m$ ,  $i = 1, 2, \dots, m$ , a cluster centre is  $u_j(x_{c_j}, y_{c_j}, z_{c_j})$ , the distance between UE point  $X^{(i)}$  and cluster centre  $u_j$  is

$$d(X^{(i)}, u_j) = \|X^{(i)} - u_j\| = 1 - \frac{x_{c_j}x_i + y_{c_j}y_i + z_{c_j}z_i}{\sqrt{x_{c_j}^2 + y_{c_j}^2 + z_{c_j}^2} \sqrt{x_i^2 + y_i^2 + z_i^2}}$$

When  $K = 4$ , the method grouping UEs based on K-means algorithm is as follows:

1. Separate the coverage space into 4 parts, choose 4 geometric center become the initial center, cluster centers are denoted respectively as:  $u_1(x_{c1}, y_{c1}, z_{c1})$ ,  $u_2(x_{c2}, y_{c2}, z_{c2})$ ,  $u_3(x_{c3}, y_{c3}, z_{c3})$ ,  $u_4(x_{c4}, y_{c4}, z_{c4})$
2. Calculate the cosine distance between the UE points and centers, then cluster UEs

- 1) First, we calculate the distance between UE  $X^{(1)}(x_1, y_1, z_1)$  and

$$u_1(x_{c1}, y_{c1}, z_{c1}):$$

$$d(X^{(1)}, u_1) = \|X^{(1)} - u_1\| = 1 - \frac{x_{c1}x_1 + y_{c1}y_1 + z_{c1}z_1}{\sqrt{x_{c1}^2 + y_{c1}^2 + z_{c1}^2} \sqrt{x_1^2 + y_1^2 + z_1^2}}$$

- 2) we calculate the distance between UE  $X^{(1)}(x_1, y_1, z_1)$  and  $u_2(x_{c2}, y_{c2}, z_{c2})$ :

$$d(X^{(1)}, u_2) = \|X^{(1)} - u_2\| = 1 - \frac{x_{c2}x_1 + y_{c2}y_1 + z_{c2}z_1}{\sqrt{x_{c2}^2 + y_{c2}^2 + z_{c2}^2} \sqrt{x_1^2 + y_1^2 + z_1^2}}$$

- 3) we calculate the distance between UE  $X^{(1)}(x_1, y_1, z_1)$  and  $u_3(x_{c3}, y_{c3}, z_{c3})$ :

$$d(X^{(1)}, u_3) = \|X^{(1)} - u_3\| = 1 - \frac{x_{c3}x_1 + y_{c3}y_1 + z_{c3}z_1}{\sqrt{x_{c3}^2 + y_{c3}^2 + z_{c3}^2} \sqrt{x_1^2 + y_1^2 + z_1^2}}$$

4) we calculate the distance between UE  $X^{(1)}(x_1, y_1, z_1)$  and  $u_4(x_{c4}, y_{c4}, z_{c4})$ :

$$d(X^{(1)}, u_4) = \|X^{(1)} - u_4\| = 1 - \frac{x_{c4}x_1 + y_{c4}y_1 + z_{c4}z_1}{\sqrt{x_{c4}^2 + y_{c4}^2 + z_{c4}^2} \sqrt{x_1^2 + y_1^2 + z_1^2}}$$

If  $d(X^{(1)}, u_1) = \min \{d(X^{(1)}, u_1), d(X^{(1)}, u_2), d(X^{(1)}, u_3), d(X^{(1)}, u_4)\}$ , where min express its minimum value, then UE  $X^{(1)}(x_1, y_1, z_1)$  is divided in the group which cluster center is  $u_1(x_{c1}, y_{c1}, z_{c1})$ . Using the similar method, then all UEs are divided four groups.

3. Calculate the average of the observations in each cluster to obtain k new centric locations. And UEs will be grouped, which is based on the minimum cosine distance.

1) Re-choose new centric locations based on the following formula:

$$u_j = \frac{\sum_{i=1}^m 1\{c^{(i)} = j\} x^{(i)}}{\sum_{i=1}^m 1\{c^{(i)} = j\}}$$

where  $1\{c^{(i)} = j\}$  is an indicator function, it satisfies:

$$1\{c^{(i)} = j\} = f(x) = \begin{cases} 1, & c^{(i)} = j \\ 0, & c^{(i)} \neq j \end{cases}$$

2) Using new centric locations, we divided UEs into four new groups

4. When the central point coincides with the UE point, this UE will be cluster into other clusters if the cosine distance between the UE and other central points is less than 15 degrees.
5. Repeat steps 2 to 4 until cluster assignments do not change, or the maximum number of iterations is reached. The UEs have been clustered into different groups

For example, let K=4, UEs are divided into four groups.

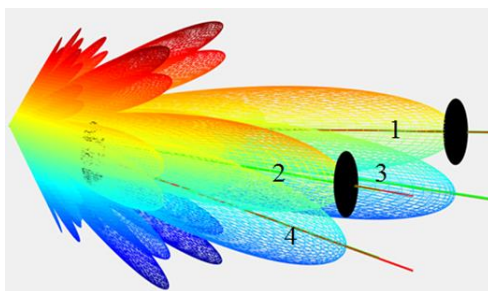


Figure 3- 1: The four main beams for 16×16 antenna arrays

Figure 3-1 shows the four beams in the antenna array, namely: Beam 1 to Beam 4.

### 3.3 Calculating the Power of Each User in the Same Beam

When we divide UEs into different groups, UEs in the same group can be covered by one beam. Because the beam is directed to the group centre, the received signal power of each user in the same group is different, so in the following, the calculation method of the received signal power is proposed.

For example, one cell has six areas and each area is covered by beams as shown in Figure 3-2.

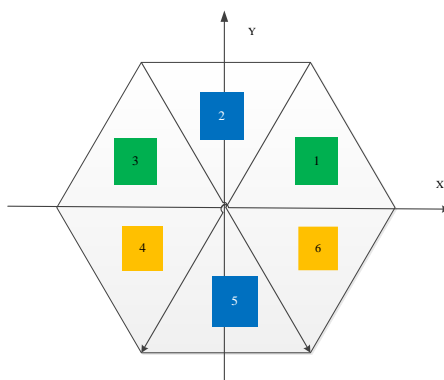


Figure 3- 2: The one hexagonal cell

It is assumed that the UEs in one sector are divided into four groups using the K-means method, which are denoted by  $G_1, G_2, G_3, G_4$  and covered by four beams respectively, and the allocated power of the beams are denoted by  $p_1, p_2, p_3, p_4$ .

Suppose there is one user  $u$  in group  $G_1$ , that is  $u \in G_1$ , and is organised in an array coordinate system, where the coordinates of user  $u$  are  $(x_u, y_u, z_u)$ , the coordinates of the center point of  $G_1$  is  $(x_1, y_1, z_1)$  and the angle between user  $u$  and the

center point of  $G_1$  is denoted by  $\beta_1$ . The angle can be defined by

$$\beta_1 = \arccos \left( \frac{x_u x_1 + y_u y_1 + z_u z_1}{\sqrt{x_u^2 + y_u^2 + z_u^2} \sqrt{x_1^2 + y_1^2 + z_1^2}} \right)$$

In general,  $\beta_1 \neq 0$ , so the power of the received signal of user  $u$  is different from the power of the received signal of the user at the position of the centre point of  $G_1$ . Then we can derive the beam pattern of user  $u$  corresponding first beam is:

$$AF_{1u} = p_1 \cos \beta_1 = \frac{p_1 (x_u x_1 + y_u y_1 + z_u z_1)}{\sqrt{x_u^2 + y_u^2 + z_u^2} \sqrt{x_1^2 + y_1^2 + z_1^2}} \quad (3-1)$$

If the coordinates of the centre point of  $G_2$  is  $(x_2, y_2, z_2)$ , the coordinates of the centre point of  $G_3$  is  $(x_3, y_3, z_3)$ , and the coordinates of the centre point of  $G_4$  is  $(x_4, y_4, z_4)$ . In a similar way, for user  $u$  is in group  $G_2$ , or user  $u$  in group  $G_3$ , user  $u$  in group  $G_4$ , we can obtain the beam pattern of user  $u$  corresponding  $i$ th beam,  $i = 2, 3, 4$ ,  $AF_{iu}$  respectively.

$$AF_{2u} = p_2 \cos \beta_2 = \frac{p_2 (x_u x_2 + y_u y_2 + z_u z_2)}{\sqrt{x_u^2 + y_u^2 + z_u^2} \sqrt{x_2^2 + y_2^2 + z_2^2}} \quad (3-2)$$

$$AF_{3u} = p_3 \cos \beta_3 = \frac{p_3 (x_u x_3 + y_u y_3 + z_u z_3)}{\sqrt{x_u^2 + y_u^2 + z_u^2} \sqrt{x_3^2 + y_3^2 + z_3^2}} \quad (3-3)$$

$$AF_{4u} = p_4 \cos \beta_4 = \frac{p_4 (x_u x_4 + y_u y_4 + z_u z_4)}{\sqrt{x_u^2 + y_u^2 + z_u^2} \sqrt{x_4^2 + y_4^2 + z_4^2}} \quad (3-4)$$

### 3.4 Calculating the Weighting Matrix

In order to calculate the weighting matrix, the weighting vectors are calculated in the x-direction, then using the same method, the weighting vectors can be obtained in the y-direction.

To allow the desired signal to be received without any modification and reject the undesired interfering signals, AF was set to maximum in the desired direction and the values in the undesired interfering directions were set to minimum. There are two



directions for the rectangular planar antenna array, x-direction and y-direction. In the equations (3-5) and (3-6),  $AF_x$  is for x-direction and  $AF_y$  is for y-direction.

$$\begin{aligned}
 AF_x &= \sum_{m=1}^M a_m e^{j(m-1)(kd_x \sin \theta \cos \phi + \beta_x)} \\
 &= \begin{bmatrix} 1 \\ e^{j(kd_x \sin \theta \cos \phi + \beta_x)} \\ \dots \\ e^{j(M-1)(kd_x \sin \theta \cos \phi + \beta_x)} \end{bmatrix} \begin{bmatrix} a_1 \\ a_2 \\ \dots \\ a_M \end{bmatrix} \quad (3-5)
 \end{aligned}$$

$$\begin{aligned}
 AF_y &= \sum_{n=1}^N b_n e^{j(n-1)(kd_y \sin \theta \cos \phi + \beta_y)} \\
 &= \begin{bmatrix} 1 \\ e^{j(kd_y \sin \theta \cos \phi + \beta_y)} \\ \dots \\ e^{j(N-1)(kd_y \sin \theta \cos \phi + \beta_y)} \end{bmatrix} \begin{bmatrix} b_1 \\ b_2 \\ \dots \\ b_N \end{bmatrix} \quad (3-6)
 \end{aligned}$$

### 3.4.1 The Direction Matrix calculation

A BS is equipped with an antenna array that consists of  $M \times N$  antenna elements. There are N elements in the y-direction and M elements in the x-direction. It is shown in Figure 3-3.

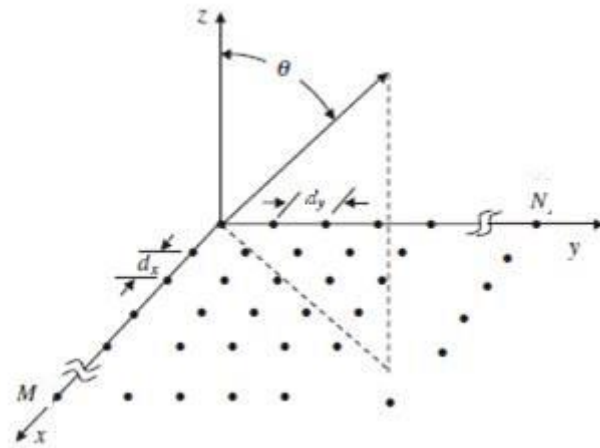


Figure 3- 3: The rectangular planar array for MxN antenna [45]

In order to represent the different locations of antenna elements, the direction matrix  $D$  is introduced according to the method proposed by Ref.45.

$$D = \begin{bmatrix} d_{11} & d_{12} & \cdots & d_{1M} \\ d_{21} & d_{22} & \cdots & d_{2M} \\ \vdots & \vdots & \cdots & \vdots \\ d_{N1} & d_{N2} & \cdots & d_{NM} \end{bmatrix} \quad (3-7)$$

For this matrix:  $d_{ik} = e^{j[(i-1)\beta_x + (k-1)\beta_y]}$ ,  $\beta_x = -\frac{2\pi}{\lambda} d_x \sin \theta_0 \cos \phi_0 = -\pi \sin \theta_0 \cos \phi_0$ ,  
 $\beta_y = -\frac{2\pi}{\lambda} d_y \sin \theta_0 \sin \phi_0 = -\pi \sin \theta_0 \sin \phi_0$ .

In this thesis, we let  $d_x = d_y = \frac{1}{2} \lambda$ .

### 3.4.2 The Weighting Vector in x-Direction

Calculation of the weighting vector is in x-direction  $\begin{bmatrix} a_1 \\ a_2 \\ \cdots \\ a_M \end{bmatrix}$  for the equation (3-

6). For the sake of simplicity, assume there are four beams, so the one desired direction has  $\theta = \theta_0$  and  $\varphi = \varphi_0$ ; three undesired directions are respectively:

$$\theta = \theta_1 \text{ and } \varphi = \varphi_1$$

$$\theta = \theta_2 \text{ and } \varphi = \varphi_2$$

$$\theta = \theta_3 \text{ and } \varphi = \varphi_3$$

In the desired direction, as equation (3-6) shows, the equation is

$$AF_x = \begin{bmatrix} 1 & e^{j(kd_x \sin \theta_0 \cos \varphi_0 + \beta_x)} & \cdots & e^{j(M-1)(kd_x \sin \theta_0 \cos \varphi_0 + \beta_x)} \end{bmatrix} \begin{bmatrix} a_1 \\ a_2 \\ \cdots \\ a_M \end{bmatrix} \quad (3-8)$$

In the undesired directions, from (3-6), the equations are

$$AF_{x1} = \begin{bmatrix} 1 & e^{j(kd_x \sin \theta_1 \cos \varphi_1 + \beta_x)} & \cdots & e^{j(M-1)(kd_x \sin \theta_1 \cos \varphi_1 + \beta_x)} \end{bmatrix} \begin{bmatrix} a_1 \\ a_2 \\ \cdots \\ a_M \end{bmatrix} \quad (3-9)$$

$$AF_{x2} = \begin{bmatrix} 1 & e^{j(kd_x \sin \theta_2 \cos \varphi_2 + \beta_x)} & \cdots & e^{j(M-1)(kd_x \sin \theta_2 \cos \varphi_2 + \beta_x)} \end{bmatrix} \begin{bmatrix} a_1 \\ a_2 \\ \cdots \\ a_M \end{bmatrix} \quad (3-10)$$

$$AF_{x3} = \begin{bmatrix} 1 & e^{j(kd_x \sin \theta_3 \cos \varphi_3 + \beta_x)} & \dots & e^{j(M-1)(kd_x \sin \theta_3 \cos \varphi_3 + \beta_x)} \end{bmatrix} \begin{bmatrix} a_1 \\ a_2 \\ \dots \\ a_M \end{bmatrix} \quad (3-11)$$

In equations (3-9) to (3-11), set  $AF_x$  to be maximized toward the maximum value which is equal to 1, and  $AF_{x1}$ ,  $AF_{x2}$  and  $AF_{x3}$  to be minimized toward the minimum value which is equal to 0. According to the equations (3-9) to (3-11), the matrix equation (3-12) can be obtained:

$$\begin{bmatrix} 1 & e^{j(kd_x \sin \theta_0 \cos \varphi_0 + \beta_x)} & \dots & e^{j(M-1)(kd_x \sin \theta_0 \cos \varphi_0 + \beta_x)} \\ 1 & e^{j(kd_x \sin \theta_1 \cos \varphi_1 + \beta_x)} & \dots & e^{j(M-1)(kd_x \sin \theta_1 \cos \varphi_1 + \beta_x)} \\ 1 & e^{j(kd_x \sin \theta_2 \cos \varphi_2 + \beta_x)} & \dots & e^{j(M-1)(kd_x \sin \theta_2 \cos \varphi_2 + \beta_x)} \\ 1 & e^{j(kd_x \sin \theta_3 \cos \varphi_3 + \beta_x)} & \dots & e^{j(M-1)(kd_x \sin \theta_3 \cos \varphi_3 + \beta_x)} \end{bmatrix} \begin{bmatrix} a_1 \\ a_2 \\ \dots \\ a_M \end{bmatrix} = \begin{bmatrix} AF_x \\ AF_{x1} \\ AF_{x2} \\ AF_{x3} \end{bmatrix} \quad (3-12)$$

If  $AF_x$  is level off to maximum,  $AF_{x1}$ ,  $AF_{x2}$  and  $AF_{x3}$  are minimized toward minimum, the matrix  $\begin{bmatrix} AF_x \\ AF_{x1} \\ AF_{x2} \\ AF_{x3} \end{bmatrix}$  can be close to the matrix  $\begin{bmatrix} 1 \\ 0 \\ 0 \\ 0 \end{bmatrix}$ .

Assume:

$$\begin{bmatrix} a_1 \\ a_2 \\ \dots \\ a_M \end{bmatrix} = X \quad (3-13)$$

$$\begin{bmatrix} 1 \\ 0 \\ \dots \\ 0 \end{bmatrix} = b \quad (3-14)$$

$$A = \begin{bmatrix} 1 & e^{j(kd_x \sin \theta_0 \cos \varphi_0 + \beta_x)} & \dots & e^{j(M-1)(kd_x \sin \theta_0 \cos \varphi_0 + \beta_x)} \\ 1 & e^{j(kd_x \sin \theta_1 \cos \varphi_1 + \beta_x)} & \dots & e^{j(M-1)(kd_x \sin \theta_1 \cos \varphi_1 + \beta_x)} \\ 1 & e^{j(kd_x \sin \theta_2 \cos \varphi_2 + \beta_x)} & \dots & e^{j(M-1)(kd_x \sin \theta_2 \cos \varphi_2 + \beta_x)} \\ 1 & e^{j(kd_x \sin \theta_3 \cos \varphi_3 + \beta_x)} & \dots & e^{j(M-1)(kd_x \sin \theta_3 \cos \varphi_3 + \beta_x)} \end{bmatrix} \quad (3-15)$$

Then the matrix  $AX$  would be close to the matrix  $b$  so gives the following equations:

$$AX = b \quad (3-16)$$

In order to obtain the weighting vector  $\begin{bmatrix} a_1 \\ a_2 \\ \dots \\ a_M \end{bmatrix}$ , the equation (3-16) needs to be

solved. Since  $X = pinv(A)*b$  is the least-squares solution for the matrix equation (3-16), according to the equation (3-12), the weighting vector can be determined in x-direction:

$$\begin{bmatrix} a_1 \\ a_2 \\ \dots \\ a_M \end{bmatrix} = pinv(A)*b \quad (3-17)$$

It should be noted that  $X = pinv(A)*b$  is only the least-squares solution of the matrix equation (3-16). The distance between the two vectors is  $\|A*pinv(A)*b-b\|$ , which is not equal to zero. Therefore, if the weighting vector in x-direction is equal to  $pinv(A)*b$ , the value of  $AF$  can be maximized toward 1 in the desired direction and the value of it can be minimized toward 0 in the undesired interfering direction.

For example, let

$$A = \begin{bmatrix} 0.9953 - 0.0971i & -0.7504 + 0.6610i & 0.2219 - 0.9751i & 0.3904 + 0.9206i \\ 0.9979 - 0.0648i & -0.7714 + 0.6363i & 0.2534 - 0.9674i & 0.3604 + 0.9328i \\ 0.9995 - 0.0324i & -0.7917 + 0.6110i & 0.2847 - 0.9586i & 0.3299 + 0.9440i \\ 1 & -0.8110 + 0.5850i & 0.3156 - 0.9489i & 0.2991 + 0.9542i \\ 0.4151 - 0.9098i & 0.8795 - 0.4824i & -0.5470 + 0.8371i & 0.7936 + 0.6084i \\ 0.7236 - 0.6902i & -0.6338 - 0.7735i & -0.8190 + 0.5738i & 0.5105 + 0.8599i \\ 0.9283 - 0.3718i & -0.3008 - 0.9537i & -0.9736 + 0.2282i & 0.1542 + 0.9880i \\ 1 & 0.0753 - 0.9972i & -0.9887 - 0.1501i & -0.2241 + 0.9746i \end{bmatrix}$$

$$b = [1 \ 1 \ 1 \ 1 \ 0 \ 0 \ 0 \ 0]^T$$

where  $i$  in matrix  $A$  is the imaginary unit, and superscript T represents the transpose of the matrix. The weighting vector is as follows:

$$W = \begin{bmatrix} a_1 \\ a_2 \\ a_3 \\ a_4 \end{bmatrix} = \text{pinv}(A) * b = \begin{bmatrix} 0.1997 - 0.0095i \\ -0.1936 - 0.2395i \\ 0.1449 + 0.2717i \\ 0.0867 - 0.1802i \end{bmatrix}$$

### 3.4.3 The Weighting Vector in y-Direction

Using the same method and according to equation (3-12), the weighting vector in y-direction can be obtained as shown:

$$\begin{bmatrix} b_1 \\ b_2 \\ \dots \\ b_N \end{bmatrix} = \text{pinv}(B) * \begin{bmatrix} 1 \\ 0 \\ \dots \\ 0 \end{bmatrix}$$

where the matrix B is as follows:

$$B = \begin{bmatrix} 1 & e^{j(kd_y \sin \theta_0 \cos \phi_0 + \beta_y)} & \dots & e^{j(N-1)(kd_y \sin \theta_0 \cos \phi_0 + \beta_y)} \\ 1 & e^{j(kd_y \sin \theta_1 \cos \phi_1 + \beta_y)} & \dots & e^{j(N-1)(kd_y \sin \theta_1 \cos \phi_1 + \beta_y)} \\ 1 & e^{j(kd_y \sin \theta_2 \cos \phi_2 + \beta_y)} & \dots & e^{j(N-1)(kd_y \sin \theta_2 \cos \phi_2 + \beta_y)} \\ 1 & e^{j(kd_y \sin \theta_3 \cos \phi_3 + \beta_y)} & \dots & e^{j(N-1)(kd_y \sin \theta_3 \cos \phi_3 + \beta_y)} \end{bmatrix}$$

### 3.4.4 Calculation of the Weighting Matrix

The multiplication of these two weighting vectors are calculated, then combining the derived matrix  $W_A$  and direction matrix  $D$  obtained in Section 3.2 to determine the weighting matrix  $W_A \cdot D$ . Finally, the weighting matrix  $W$  should be normalise to generate the matrix  $W_A \cdot D$ .

$$W_A = \begin{bmatrix} b_1 \\ b_2 \\ \vdots \\ b_N \end{bmatrix} \begin{bmatrix} a_1 & a_2 & \dots & a_M \end{bmatrix} = \begin{bmatrix} a_1 b_1 & a_2 b_1 & \dots & a_M b_1 \\ a_1 b_2 & a_2 b_2 & \dots & a_M b_2 \\ \vdots & \vdots & \dots & \vdots \\ a_1 b_N & a_2 b_N & \dots & a_M b_N \end{bmatrix} \quad (3-18)$$

$$\begin{aligned}
W_A \cdot D &= \begin{bmatrix} a_1 b_1 & a_2 b_1 & \cdots & a_M b_1 \\ a_1 b_2 & a_2 b_2 & \cdots & a_M b_2 \\ \vdots & \vdots & \cdots & \vdots \\ a_1 b_N & a_2 b_N & \cdots & a_M b_N \end{bmatrix} \begin{bmatrix} d_{11} & d_{12} & \cdots & d_{1M} \\ d_{21} & d_{22} & \cdots & d_{2M} \\ \vdots & \vdots & \cdots & \vdots \\ d_{N1} & d_{N2} & \cdots & d_{NM} \end{bmatrix} \\
&= \begin{bmatrix} a_1 b_1 d_{11} & a_2 b_1 d_{12} & \cdots & a_M b_1 d_{1M} \\ a_1 b_2 d_{21} & a_2 b_2 d_{22} & \cdots & a_M b_2 d_{2M} \\ \vdots & \vdots & \cdots & \vdots \\ a_1 b_N d_{N1} & a_2 b_N d_{N2} & \cdots & a_M b_N d_{NM} \end{bmatrix}
\end{aligned} \tag{3-19}$$

Since the sum of weights of all the array elements should be equal to 1, in order to derive the weighting matrix, matrix  $W_A D$  has been normalised and the normalisation matrix is shown:

$$\frac{1}{\sum_{j=1}^N \sum_{i=1}^M a_i b_j d_{ji}} \begin{bmatrix} a_1 b_1 d_{11} & a_2 b_1 d_{12} & \cdots & a_M b_1 d_{1M} \\ a_1 b_2 d_{21} & a_2 b_2 d_{22} & \cdots & a_M b_2 d_{2M} \\ \vdots & \vdots & \cdots & \vdots \\ a_1 b_N d_{N1} & a_2 b_N d_{N2} & \cdots & a_M b_N d_{NM} \end{bmatrix}$$

If the power of one array element is 1 unit, then total energy of the  $M \times N$  array can be equal to  $MN$  units. Therefore the weighting matrix  $W$  is:

$$W = \frac{MN}{\sum_{j=1}^N \sum_{i=1}^M a_i b_j d_{ji}} \begin{bmatrix} a_1 b_1 d_{11} & a_2 b_1 d_{12} & \cdots & a_M b_1 d_{1M} \\ a_1 b_2 d_{21} & a_2 b_2 d_{22} & \cdots & a_M b_2 d_{2M} \\ \vdots & \vdots & \cdots & \vdots \\ a_1 b_N d_{N1} & a_2 b_N d_{N2} & \cdots & a_M b_N d_{NM} \end{bmatrix} \tag{3-20}$$

If the weighting matrix  $W$  is shown as:

$$W = \begin{bmatrix} w_{11} & w_{12} & \cdots & w_{1M} \\ w_{21} & w_{22} & \cdots & w_{2M} \\ \vdots & \vdots & \cdots & \vdots \\ w_{N1} & w_{N2} & \cdots & w_{NM} \end{bmatrix} \tag{3-21}$$

then the equation (3-22) is determined:

$$w_{st} = \frac{MN a_s b_t d_{ts}}{\sum_{j=1}^N \sum_{i=1}^M a_i b_j d_{ji}} \tag{3-22}$$

where  $s = 1, 2, \dots, N, t = 1, 2, \dots, M$

### 3.5 Calculation of the Receive Signal

The channel coefficients matrix  $H$  is determined so the weighting matrix  $W$  can be found. When there only is one receive antenna, the channel coefficients matrix  $H$  and weighting matrix  $W$  are as follows respectively:

$$H = [h_{11} \quad h_{12} \quad \cdots \quad h_{1N} \quad \cdots \quad h_{M1} \quad h_{M2} \quad \cdots \quad h_{MN}] \quad (3-23)$$

$$W = [w_{11} \quad w_{12} \quad \cdots \quad w_{1N} \quad \cdots \quad w_{M1} \quad w_{M2} \quad \cdots \quad w_{MN}]^T \quad (3-24)$$

For each antenna at BS, the transmitted signal is  $T_{sig}$ , denote

$$T_w = W \cdot T_{sig} = \begin{bmatrix} w_{11}T_{sig} \\ w_{12}T_{sig} \\ \vdots \\ w_{1N}T_{sig} \\ w_{21}T_{sig} \\ w_{22}T_{sig} \\ \vdots \\ w_{2N}T_{sig} \\ \vdots \\ w_{M1}T_{sig} \\ w_{M2}T_{sig} \\ \vdots \\ w_{MN}T_{sig} \end{bmatrix} = \begin{bmatrix} T_{w1} \\ T_{w2} \\ T_{w3} \\ \vdots \\ T_{wMN} \end{bmatrix} \quad (3-25)$$

For receiving antennas, the received signal is that the convolution of  $H$  and  $T_w$ , it is as follows:

$$Rx = H * T_w \quad (3-26)$$

### 3.6 Conclusion

The K-means algorithm can cluster UEs in different groups, which reduces the number of beams to cover the UEs. When the number of beams is decreased, the number of side lobes for the beams is decreased so the interference from the side lobes is reduced.

The new weighting matrix is combined with by the horizontal direction weighting vector and the vertical direction weighting vector. These two weighting vectors can be determined by our calculation method, which makes the main beam have the maximum value in the desired direction and its side lobes have the minimum values in other undesired directions. The next chapter describes how the 3D beamforming LTE simulation system is designed and the received signal, which is acquired by the new weighting matrix. The simulation system can use this received signal to compare with the transmitting signal to obtain the BER.



# **Chapter 4**

## **Minimal Side Lobe 3D LTE Beamforming System towards a Group of UEs**

## **4.1 Introduction**

This chapter shows the simulation results for the Minimal Side Lobe 3D LTE Beamforming System towards a Group of UEs, which focuses on the improvement of 3D beamforming technology in 5G system. In the thesis, there are two problems that are solved. One problem of 3D beamforming technology is how to use the beams to cover multiple UEs in different directions. Another problem is that there is interference between each beam when they are transmitted at the same time.

The simulation is of a hexagonal antenna arrays cell for transmitting the beamforming to UEs, which has a 3D channel model in an LTE system. The antenna arrays transmitting the beam are used for the 3D beamforming technology under the maximum SINR weighting method. Moreover, the results from the simulation show the SINR, throughput and BER to prove that the design is a more advanced system than an LTE system. The simulation model is used the UML model language to design, which is shown in Appendix A chapter. Moreover, the Matlab R2016b software is used to be simulate the all systems, in which the functions for the programs are shown in Appendix A chapter.

## **4.2 The Analysis of Simulation Results**

### **4.2.1 Introduction**

In this section, the simulation represents the application of these ideas in an LTE system. For testing, an antenna array is needed to transmit the beams and multiple UEs are needed to be generated in one cell because the testing is focused on how the new weighting method can be used to reduce interference between each beam. Therefore, a hexagonal prism antenna arrays in one cell is generated as shown in Figure 4-1, which has 6 face for antenna arrays. In this cell, there are 256 antennas for each face, each one of which is an  $16 \times 16$  antenna array.

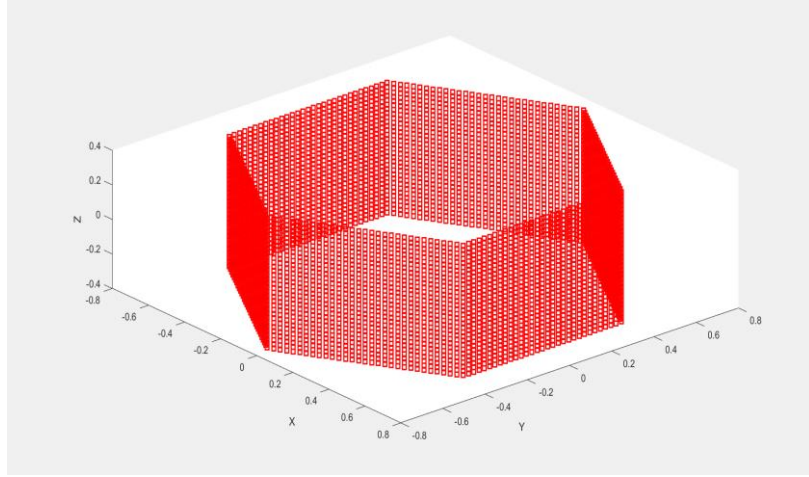


**Figure 4- 1: The antenna arrays for one cell (the red squares are the antennas)**

There are 10 UEs which are randomly distributed in this cell and the parameters for running the simulation are shown in Table 4-1.

**Table 4- 1: The parameters for running the simulation**

<b>Parameter</b>	<b>Value</b>
Height of the base station(m)	25
Height of the UE(m)	$h_{UT}=3(n_{fl} - 1) + 1.5$ (NOTE 1)
RB size	12 sub-carriers
Sub-carrier spacing(kHz)	20
Mobile terminal	Antenna gain 0dBi, Noise 9dBm
Base station	Antenna gain 14dBi, Noise 5dBm
Transmit power for each antenna element (dBm)	43(~20W)
Thermal Noise(dBm/Hz)	-174
The channel model	3GPP TR36.873 (3D UMa or 3D UMi)
The number of time for running simulation	20 times
The number of UEs	10
The size of antenna arrays in each face	16×16
The size of antenna arrays for each beam	8×8
The min of coverage distance(m)	100
The max of coverage distance(m)	2000
The modulation method	R.0 (16-QAM) or R.5 (64-QAM)
The carrier frequency(GHz)	6 GHz
The range of SNR for shown	[10 20 30 40]
The display BER interval (%)	10 to 90
LTE MIMO size	4×4
LTE MIMO channel Correlation	High
SNR for testing(dB)	20

- NOTE 1: 50% of indoor UEs in a macro cell area are assumed to be inside a high-rise building and are associated with the same value of  $N_{fl}$ . The height of a high-rise given by  $N_{fl} \sim$  uniform (20,30). 50% of

indoor UEs in a macro cell area are assumed to be outside the high-rise building and the associated Nfl for each UE ~ uniform (4,8).

## 4.2.2 The network environment

The network environment for the simulation result in the UMa antenna arrays system as shown in Figure 4-2.

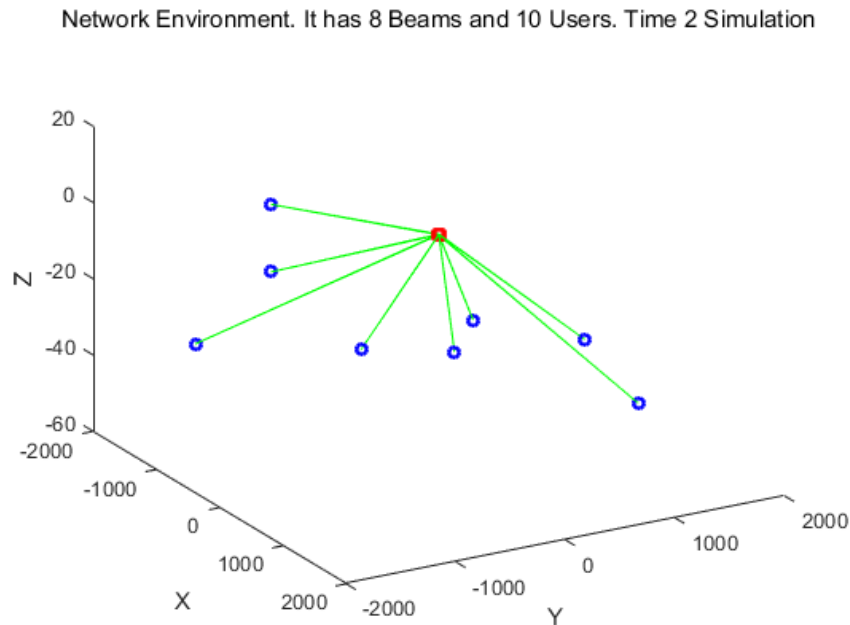


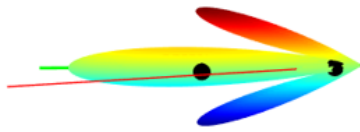
Figure 4- 2: The simulation result in UMa antenna arrays system

In the Figure 4-2, the result shows the twice time among 20 running time, the number of UEs is 10, the number of beam is 8, the modulation is R.5 and the environment is UMa. In this figure, the green lines represent the direction of the beams and the blue points represent the center point for the clusters of UEs.

## 4.2.3 The beams

In this part, the environment parameters can be read from data file. The least square method is used to calculate the weighting matrix under the maximum SINR. Then the beams are shown in Figure 4-3 for the first face. The beams for whole cell are shown in Figure 4-4.

The Atten.Rate = -43.3496dB  $\theta=5.1235$   $\phi=-83.3967$



The Atten.Rate = -18.7045dB  $\theta=15.7014$   $\phi=87.5464$

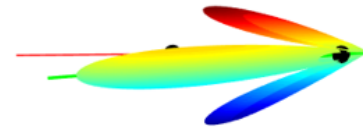


**Figure 4- 3: The beam for the fourth antenna face in the second simulation running time**

Figure 4-3 shows that there are 2 beams in the fourth face to cover two clusters of UEs.

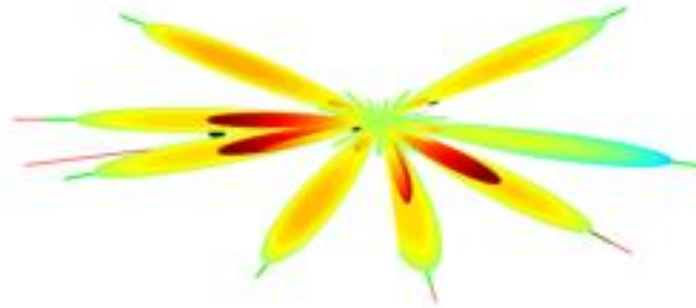


**Figure 4- 4: The 3D beam for second simulation running time in one cell**

The beams for the whole cell are shown in Figure 4-4, in which there are 8 beams for 10 UEs. The main beams are obviously larger than the side lobes.

#### 4.2.4 The BER results compared

In this part, there are two kinds of LTE systems, which are the LTE SISO system and LTE MIMO system. Moreover, the received signals of the 3D beamforming system are obtained and the BER of the transmitted signal and received signal is calculated, which is saved in the different BER data files.

The BER is read from the data files to display the BER and the Cumulative Distribution Function (CDF) of BER for the 3D beamforming LTE system and normal LTE system. Then it calculates the BER by the statistical boundary and the LTE SISO or LTE MIMO system is compared. If the LTE SISO system is chosen, the BER for one UE in the 3D beamforming LTE system is chosen, which can be compared with the

BER in the LTE SISO system. If the LTE MIMO system is chosen, the BER in the LTE MIMO system can be compared with the BER in the 3D beamforming LTE system.

#### 4.2.4.1 The 3D beamforming LTE system compare with LTE SISO system

The constellation figure of received signals for the UE in LTE SISO system is shown in Figure 4-5 at 40 dB for SNR. Figure 4-6 shows the constellation figure of received signals for UE in the 3D beamforming LTE system at 40 dB for SNR.

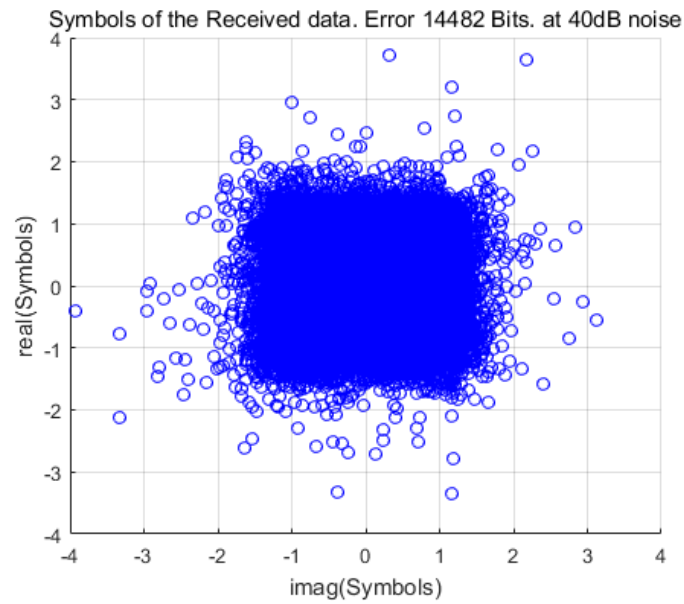


Figure 4- 5: The constellation figure of the received signals for UE in LTE SISO system

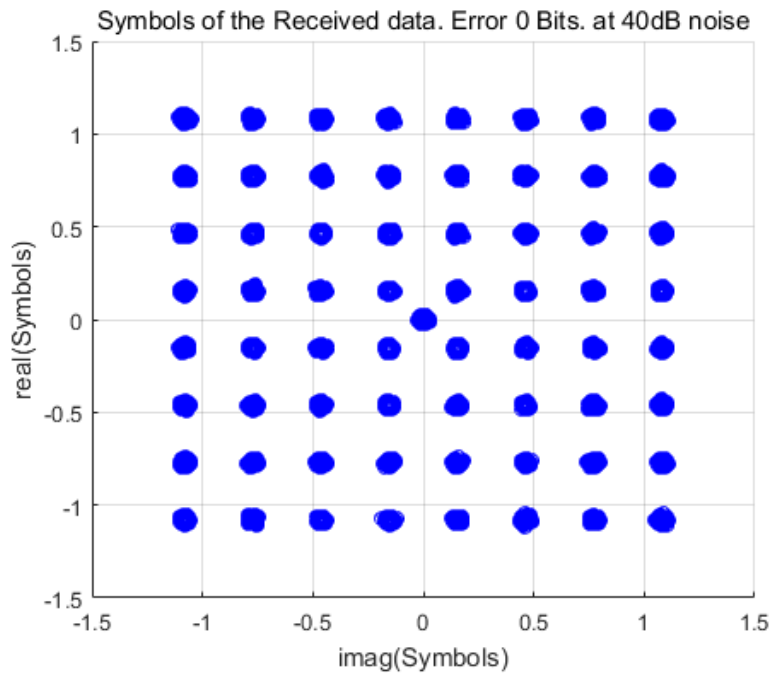
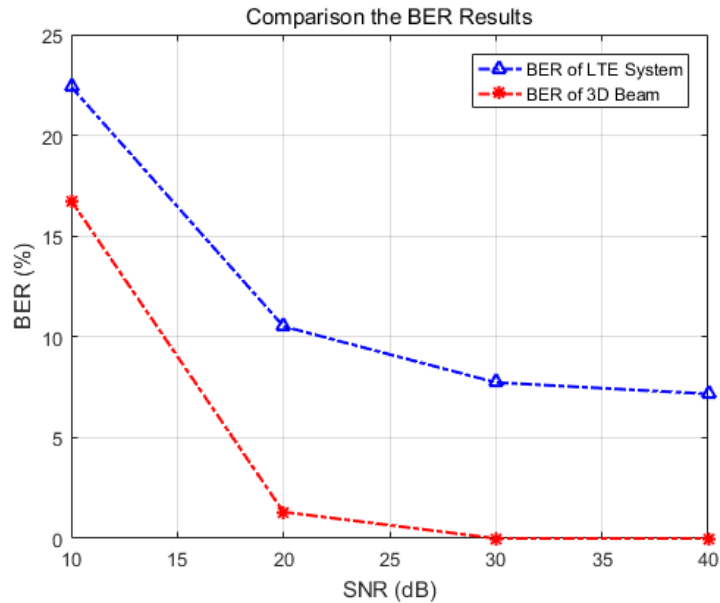


Figure 4- 6: The constellation figure of the received signals for UE in 3D beamforming LTE system

The received signals for the LTE system when the SNR is 40 dB is shown in Figure 4-5, which are disordered and has a bit error of 14482 bits. However, the received signals have a 0 bit error for the 3D beamforming LTE system, which is less than the LTE SISO system, when the SNR is 40 dB as shown in Figure 4-6. Therefore, the design for 3D beamforming LTE system has improved the quality for the received signals in a 64-QAM LTE system. The BER for those two UEs are shown in Figure 4-7.



**Figure 4- 7: The BER for one UE in 3D beamforming LTE system and another UE in LTE SISO system**

In Figure 4-7, the red line is the BER for one UE in the 3D beamforming LTE system and the blue line is the BER in the LTE SISO system. If the modulation method is 64-QAM, when the SNR is from 30 dB to 40 dB, the BER of the 3D beamforming LTE system is close to zero. The BER of the LTE SISO system is more than 7 %, whatever the SNR are 10dB, 20dB, 30dB, or 40 dB.

#### **4.2.4.2 The 3D beamforming LTE system compare with LTE MIMO system**

The constellation figure of received signals for the UE in the LTE MIMO system is shown in Figure 4-8 at 40 dB for SNR.

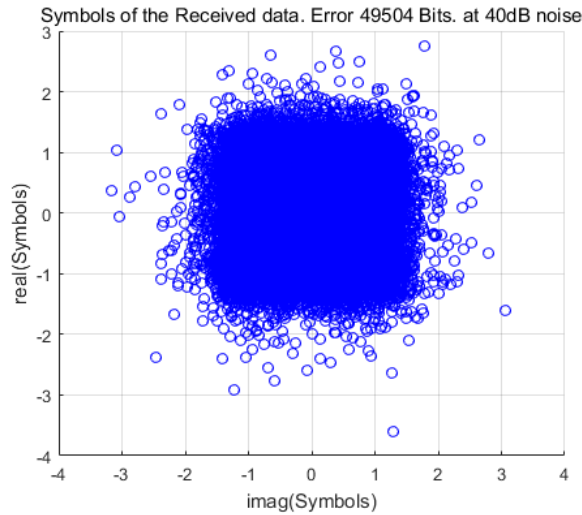


**Figure 4- 8: The constellation figure of the received signals for UE in LTE MIMO system**

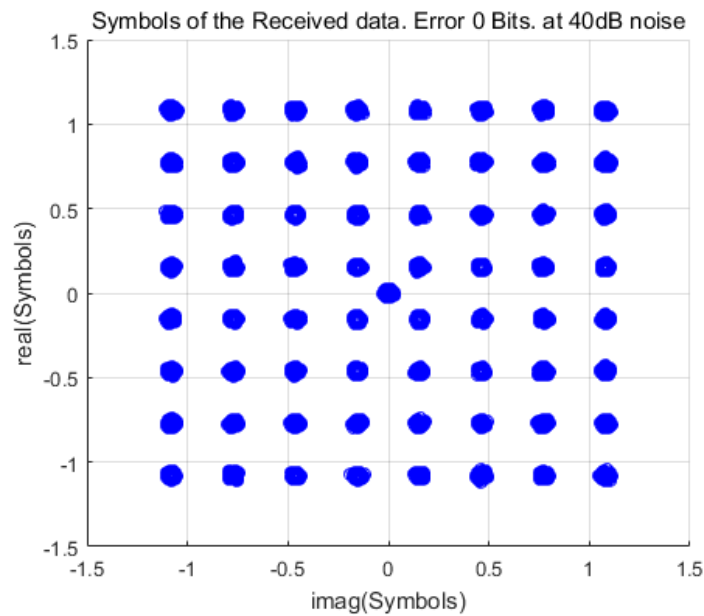


**Figure 4- 9: The constellation figure of the received signals for UE in 3D beamforming LTE system**

The constellation figure of received signals for one UE in the 3D beamforming LTE system has been shown in Figure 4-9 when the SNR is 40 dB. The received signals bit error for the 3D beamforming LTE system still is close to zero, which is less than the 49504 bits error in LTE MIMO system.

Figure 4-10 shows the comparison of BER for these two UEs when the SNR is from 10 dB to 40 dB. In this figure, the red line is the BER for one UE in the 3D beamforming LTE system and the blue line is the BER for the LTE MIMO system. The BER in the 3D beamforming LTE system is smaller than the BER in the LTE MIMO system.



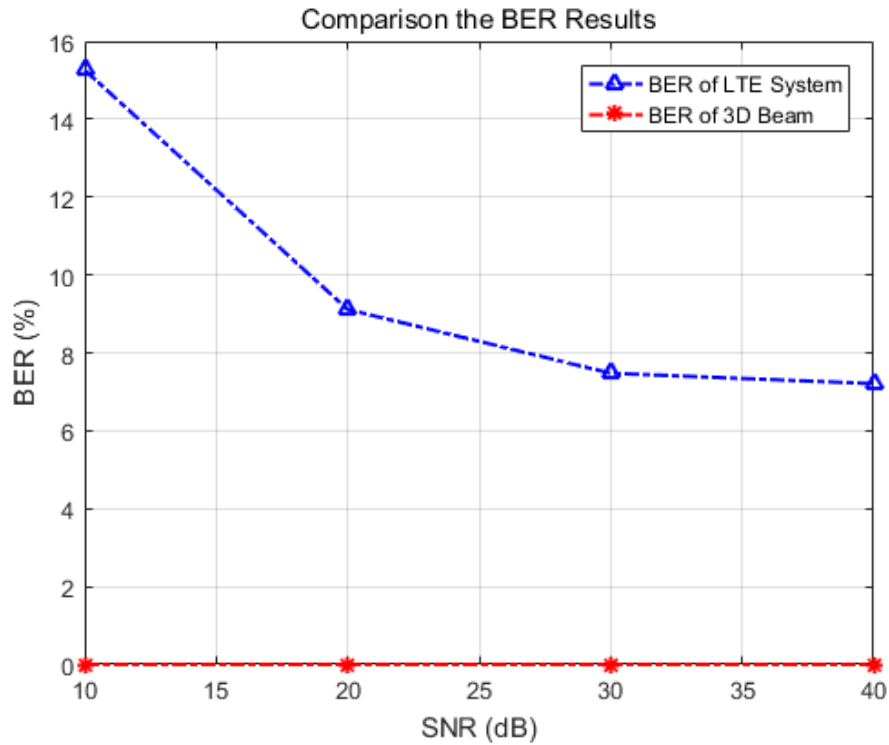


**Figure 4- 10: The BER for one UE in 3D beamforming LTE system and another UE in LTE MIMO system**

Figure 4-11 shows the CDF of BER when the SNR is from 10 dB to 40 dB for the 3D beamforming LTE system. In this figure, the red line is the BER for one UE in the 3D beamforming LTE system and the blue line is the BER for the LTE SISO system. There are a total of 200 data points because there are 10 UEs in one cell and the simulation runs 20 times. In Figure 4-11, the BER can decrease when the SNR is increasing. More than 90% of the BER data points are distributed within 3% BER when the SNR is larger than 20 dB.

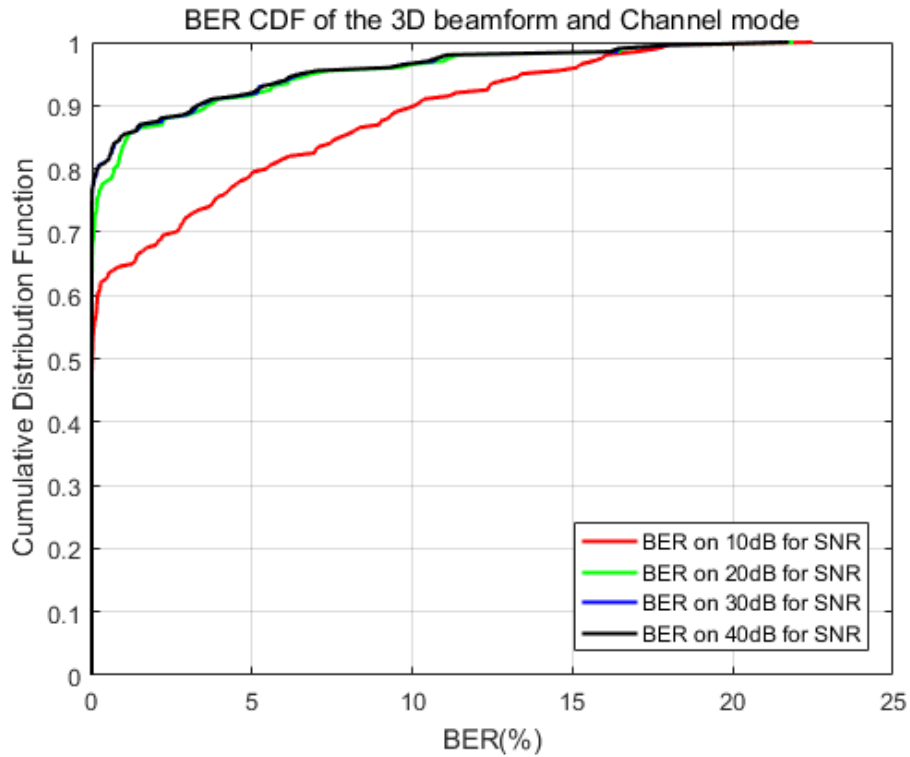


**Figure 4- 11: The CDF of BER in 3D beamforming LTE system**

In Figure 4-11, the red line is the CDF of BER in 10 dB for SNR; the green line is the CDF of BER in 20 dB for SNR; the blue line is the CDF of BER in 30 dB for SNR and the black line is the CDF of BER in 40 dB for SNR 3D beamforming LTE system.

All the Probability Distribution Function (PDFs) of the BER were recorded for each UE in the 3D beamforming LTE system, which are shown in Figure 4-12. In this figure, the BER for UEs has a great probability of being distributed within 2 % BER.

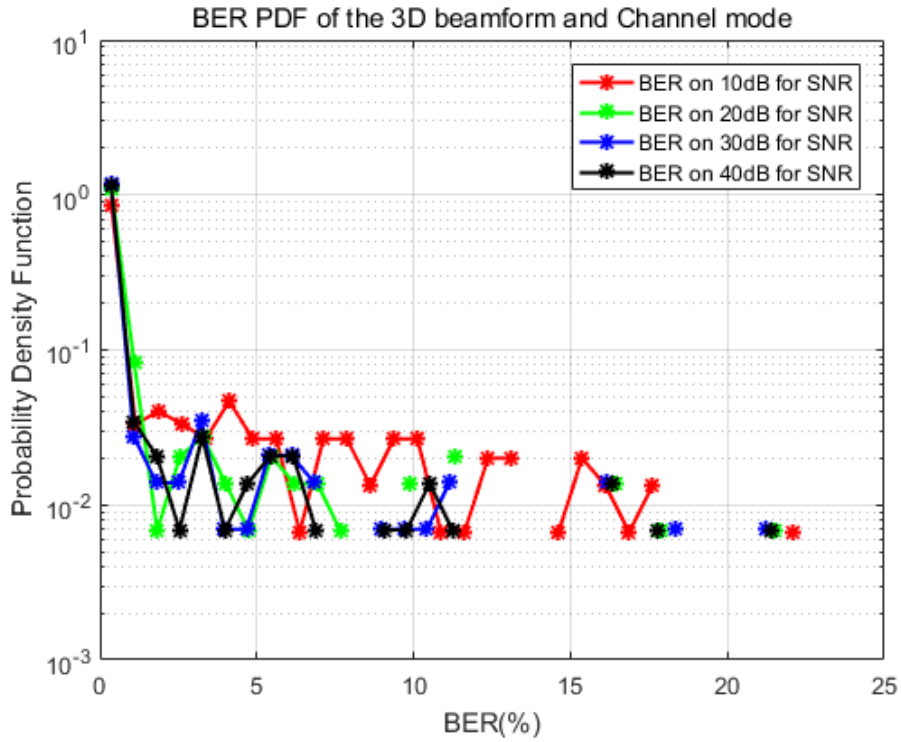


Figure 4- 12: The PDF of BER in 3Dbeamforming LTE system

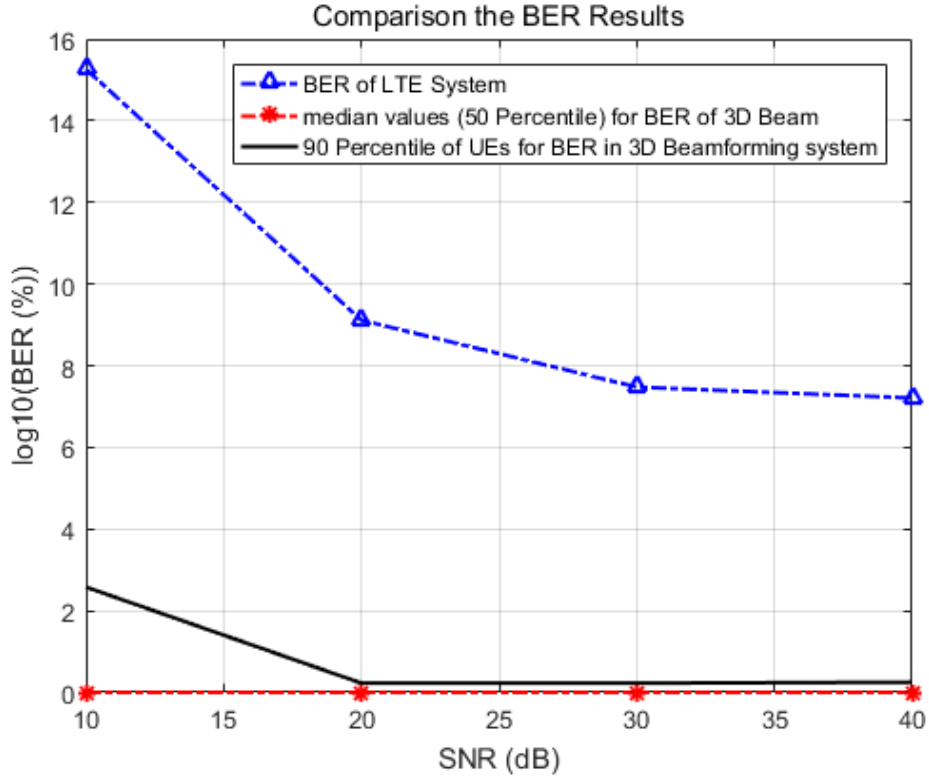


Figure 4- 13: The comparison BER between 3D beamforming LTE system and LTE MIMO system

In Figure 4-13, the red line is the 50% sample points for BER in 3D beamforming

LTE system; the blue line is the BER in LTE MIMO system; the black line is the 90% sample points of BER in 3D beamforming LTE system when the SNR are 10 dB, 20 dB, 30 dB, or 40 dB.

There are 200 sample data points for BER in the 3D beamforming LTE system so the maximum values and minimum values should be abandoned in order to ensure the accuracy because these may be outliers. Then the BER interval is from 10% to 90%.

The 50% sample points for BER in the 3D beamforming LTE system is close to zero in Figure 4-13. The 90 percentile of sample points for BER in the 3D beamforming LTE system is smaller than the BER in the LTE MIMO system as shown in Figure 4-13. Therefore, the 3D beamforming LTE system has a smaller BER than the LTE MIMO system when the modulation method is 64-QAM.

#### 4.2.5 The testing for different environments

In Chapter 2.5.2, the PL models are summarised in 3D urban macro scenario (3D-UMa) and 3D urban micro (3D-UMi) for the 3D channel model from 3GPP. The main difference between those two scenarios is that the UMa is the indoor environment that is passing through the building and the UMi is the outdoor environment that is not passing through the building as Figure 2-30 and Figure 2-31 shows.

This part shows that the effect of the number of UEs and different environments on the BER in the 3D beamforming LTE system when the SNR is 20 dB. The simulation running times for different situations should be different because the numbers of UEs are different in order for the sample data size to be the same for all situations. Table 4-2 shows the different simulation running times for different numbers of UEs and Table 4-3 explains the significance of all parameters. The simulation results are shown in Figure 4-14.

**Table 4- 2: The different simulation running times for different numbers of UEs**

<b>Number of UEs</b>	<b>The simulation running times</b>
2	100
4	50
6	33
8	25

10	20
----	----

**Table 4- 3: Parameters for running the simulation system shown in Figure 4-55**

Parameter	Value
The percentile of sample points for all BER (%)	90
SNR(dB)	20
The number of UEs	[2 4 6 8 10]
The modulation methods (UMiR.5)	64-QAM in UMi
The modulation methods (UMiR.0)	16-QAM in UMi
The modulation methods (UMaR.5)	64-QAM in UMa
The modulation methods (UMaR.0)	16-QAM in UMa

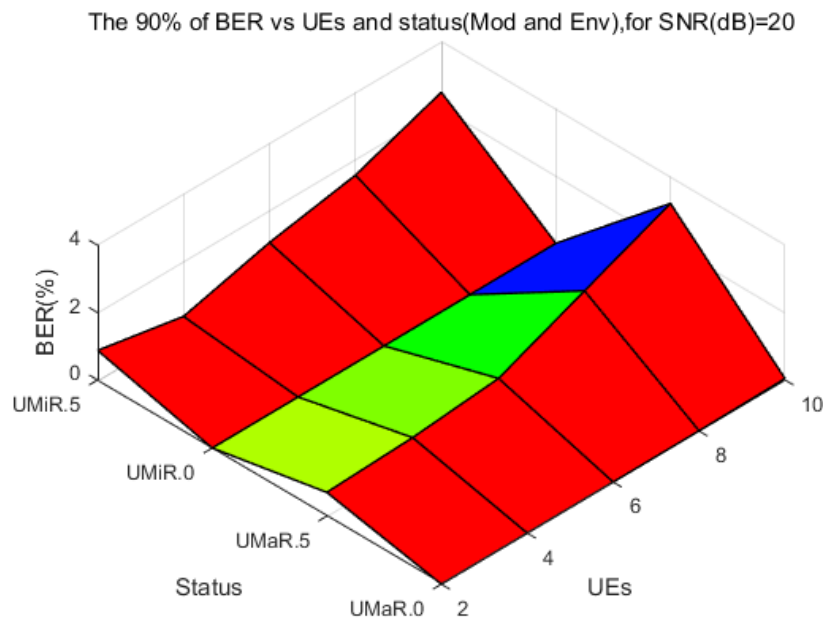


**Figure 4- 14: The BER for different environments in 20 dB for different number of UEs**

In Figure 4-14, the BER for different environments at 20 dB for SNR is shown when the number of UEs are 2, 4, 6, 8 or 10 (UMi is outdoor; UMa is Indoor; R.0 = 16-QAM; R.5 = 64-QAM).

In this figure, the values of BER for the R.0 (16-QAM) system are smaller than the values of BER for the R.5 (64-QAM) system. The detailed BER results for different environments with a different number of UEs are as shown in Table 4-4. Moreover, the number of UEs is another influential parameter for BER in the same environment.

**Table 4- 4: The detailed BER for results in Figure 4-56**

Modulation	Number of UEs				
	2 UEs	4 UEs	6 UEs	8 UEs	10 UEs
<b>UMaR.0</b>	0%	0%	0%	0.005511%	0.03858%
<b>UMaR.5</b>	0.705495%	0.814999%	1.057565%	2.142104%	3.220565%
<b>UMiR.0</b>	0%	0%	0%	0.005511%	0.016534%
<b>UMiR.5</b>	0.877286%	0.370705%	1.048021%	1.532047%	2.480912%

#### 4.2.6 Conclusion

Beamforming is a key technology in 5G. In beamforming, an array of antennas can dynamically adapt the direction and down-tilt towards receivers by rotating the antenna pattern. However, when the multiple beams transmit to multiple UEs' groups at the same time, there can be interference between each beam. The focus of this simulation is the improvement of the 3D beamforming technology in a 5G system.

In order to test that our improvement ideas can be applied in the LTE simulation system, the UEs' distribution is uniform and the locations of UEs are random. To cover all UEs with beams, the UEs are divided into several groups using a K-means algorithm. The K-means algorithm not only divides UEs into K groups, but also can determine the centre of each group, so in this simulation system the K-means algorithm was used. After the UEs have been divided into K groups, each group is covered by a beam and the beam is transmitted towards the centre. In the simulation, the channel coefficients of the 3D channel model are based on the parameters provided by "3GPP TR 36.873", and the power coefficients of antennae arrays are constructed to form the 3D beamforming. This simulation system is achieved by obtaining figures for:

1. The 3D network environment for the 3D beamforming LTE simulation system;
2. The beam patterns for the 3D beamforming LTE simulation system;
3. The constellation of the received signals for one UE in the 3D beamforming LTE simulation system or the LTE simulation system;
4. The comparison of one UE BER in the 3D beamforming LTE simulation system and the LTE simulation system;

5. The CDF and PDF of BER in the 3D beamforming LTE simulation system;
6. The BER of the 3D beamforming LTE simulation system, which is compared with the LTE MIMO simulation system;

The results show that the 3D beamforming LTE system has already obtained a definite improvement for signal quality over the 4G LTE system. Moreover, the new weighting method can minimize the side lobes in other specific directions to the main beam, which decreases the interference from the side lobes to other main beams. The 3D beamforming LTE system has a larger cell maximum radius than the  $4 \times 4$  LTE MIMO system because the 3D beamforming LTE system can have a greater number of antennas in the transmitter.

Techniques on how to overcome variability in SNR of UEs in 3D beamforming is a challenging future topic of research. For the 5G network, our improvement schemes are not only used for the LTE system, but also can be used for the mm-wave transmission. It can improve the performance in 5G communication system in the future.

# **Chapter 5**

## **Optimal Minimum Side lobe Hybrid Beamforming in Millimeter Wave System**



## 5.1 Introduction

In the next-generation 5G system, the 3D beamforming technology is a key component for mm-wave system, which generally has 3 kinds of the beamforming technologies, namely: analogue beamforming, digital beamforming and hybrid beamforming. The complexity to implement an mm-wave Massive MIMO system comes with the difficulty to have a high number of stacked RF chains. Hybrid, analog and digital beamforming systems have then emerged to retain a high number of antennas without as many RF chains in order to keep high beamforming gains.

Hybrid beamforming system can transmit the multiple beams to multiple UEs at same time, but it generates interference between each beam. However, most of researches do not focus on the problem about interference between each beam. This thesis provides a new method to calculate the weighting matrix for hybrid beamforming. The new weighting method then adjusts the values of weighting matrix to direct the main beam in a desired direction and minimize its side lobes in other specific direction. Theoretical analysis shows that the BER from the mm-wave system is lower compared with the BER from the LTE MIMO system by quantifying the average SNR.

In this chapter, the simulation is about applying our ideas in mm-wave system. This simulation is an mm-wave system so the carrier the frequency is 28 GHz and the PL model is given in reference [77]. The mm-wave system usually uses the hybrid beamforming to transmit signals [105] so it has the same problem that there is interference between each beam when they are transmitted at same time. This simulation for mm-wave system still tests that the new weighting method can reduce the interference between each beam and the results are compared with another mm-wave system that used an equal weighting matrix as the weighting method.

The simulation model is used the UML model language to design, which is shown in Appendix B chapter. Moreover, the Matlab R2016b software is used to be simulate the all systems, in which the functions for the programs are shown in Appendix B chapter.

## 5.2 The Analysis of Simulation results

### 5.2.1 Introduction

In this simulation, the 4×4 LTE MIMO system is simulated, which calculates the BER to be compared with the mm-wave system, in order to prove that the new weighting method can reduce the BER. The LTE system usually uses the 4×4 LTE MIMO systems to transmit the signals in 3GPP [39], which is the representational LTE MIMO system.

Figure 5-1 shows the diagrammatic sketch for the simulation system, which consists of  $RF_n$  digital parts (where  $n = 1$  to 4) and the  $W_{x,y}$  analogue parts for this hybrid beamforming mm-wave system. In this mm-wave simulation system, there is the 16×16 rectangular antenna array in a three-dimensional coordinate operating at 28 GHz carrier frequency to transmit the hybrid beamforming as shown in Figure 5-1.

In this thesis, there are two PL models for the hybrid beamforming mm-wave systems, which are from real-world measurements in New York (NY), USA, whose carrier frequencies are at 28GHz and 73GHz [100]. Although the PL equations are different, the characteristic for these two PL models is similar. Therefore, the mm-wave simulation systems show the results for the 28GHz hybrid beamforming mm-wave system to be compared with 4×4 LTE MIMO system.

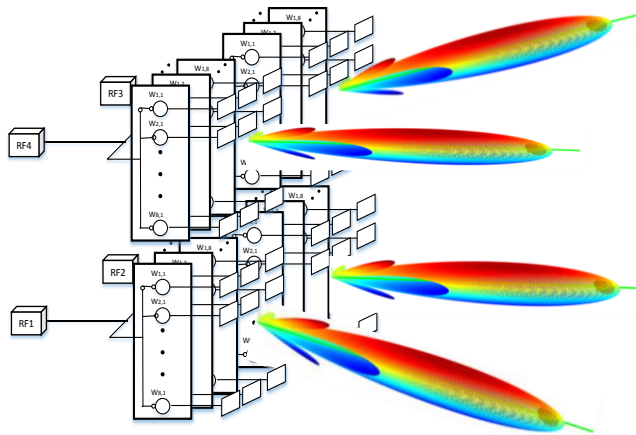


Figure 5- 1: The hybrid beamforming mm-wave system

In Figure 5-1, the hybrid beamforming mm-wave simulation system has 4 data and

4 beams are sent at the same time. The detailed parameters for the simulation system are shown in Table 5-1.

**Table 5- 1: The parameters for running the simulation**

<b>Parameter</b>	<b>Value</b>
Height of the base station(m)	25
Height of the UE(m)	$h_{UT}=3(n_{fl} - 1) + 1.5$ (NOTE 1)
RB size	12 sub-carriers
Sub-carrier spacing(GHz)	1
Mobile terminal	Antenna gain 0dBi, Noise 9dBm
Base station	Antenna gain 0dBi, Noise 5dBm
Transmit power for each antenna element	30 dBm (~1W)
Thermal Noise(dBm/Hz)	-174
The channel model	3GPP TR 36.873 (3D UMa)
The number of time for running simulation	25 times
The number of UEs	4
The size of rectangular antenna arrays	16×16
The size of antenna arrays for each beam	8×8
The min of coverage distance(m)	1
The max of coverage distance(m)	100
The modulation method	R.5 (64-QAM)
The carrier frequency(GHz)	28
The range of SNR for shown(dB)	[0 10 20 30]
The display BER interval (%)	10 to 90
LTE MIMO system size	4×4
LTE MIMO channel Correlation	High

### 5.2.2 The network environment

The network environment for the simulation result in the hybrid beamforming mm-wave system as shown in Figure 5-2. The number of UEs is 4 in this step so there are 4 beams for the 16×16 antenna arrays system.

Network Environment. It has 4 Beams and 4 Users. Time 10 Simulation

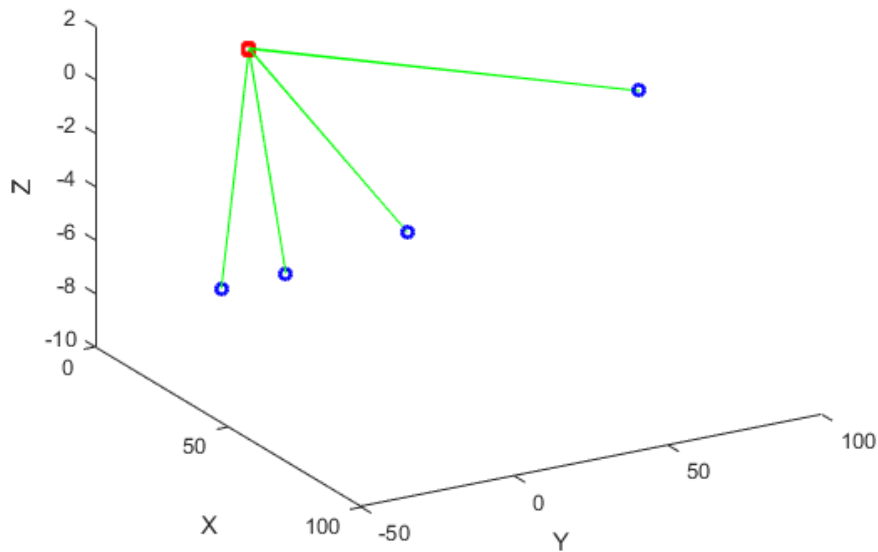


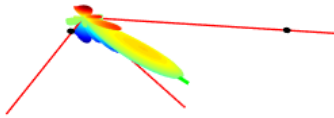
**Figure 5- 2: The simulation result in UMA for16×16 antenna arrays system**

The simulation was run 25 times with different seeds to show the results. In Figure 5-2, the result shows the tenth time for the simulation among these 25 running times, the number of UEs is 4, the number of beams is 4, the modulation is R.5 and the environment is UMA in 16×16 antenna arrays system. In this figure, the green lines represent the direction of the beams and the blue points represent the center point for the clusters of UEs.

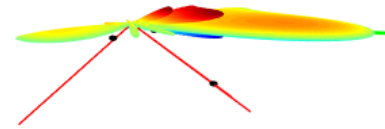
### 5.2.3 The beams

In this part, the environment parameters can be read from the data file. The least squares method is used to calculate the weighting matrix under the maximum SINR. Then the beams are shown in Figure 5-3 for each beam. The beams for the whole cell are shown in Figure 5-4.

The Atten.Rate = -41.9831 -33.7268 -22.0274dB  $\theta=17.5223$   $\phi=-88.8431$



The Atten.Rate = -44.8 -45.0325 -24.2383dB  $\theta=58.4411$   $\phi=89.6398$



The Atten.Rate = -63.7457 -47.8356 -49.616dB  $\theta=69.0094$   $\phi=-54.8056$



The Atten.Rate = -44.0934 -51.8389 -50.96dB  $\theta=82.2693$   $\phi=24.9995$

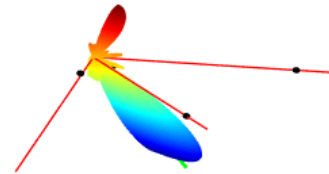


Figure 5- 3: The beams in the 16×16 antenna arrays system with 4 beams

Figure 5-3 shows the 4 beams, respectively, in which each beam covers one UE. The green line is the main beam direction; the red lines are the directions of other beams and the black points are the UEs in Figure 5-3.



**Figure 5- 4: The 3D beam in the 16×16 antenna arrays system with 4 beams**

The beams for the whole cell are shown in Figure 5-4, which are 4 beams for 4 UEs. The main beams are obviously larger than the side lobes.

The simulation has been run 25 times to generate results for the CDF and PDF to be analyzed. The CDFs for the SINR for mm-wave systems are shown in Figure 5-5, and the results from using or not using the new weighting method are compared. The CDFs of the throughput for two mm-wave systems are shown in Figure 5-6.

In Figure 5-5, the CDFs of SINR are from -20 dB to 40 dB for two mm-wave systems. The SINR results obtained using the new weighting method (red line) is always greater than SINR results obtained using the equal weighting method (blue line). For example, if the CDF is 90%, the SINR in the mm-wave system using the new weighting method are larger than 20 dB, but the SINR in the mm-wave system using the equal weighting method are smaller than 20 dB. Therefore, the new weighting method can increase the SINR in the mm-wave system.

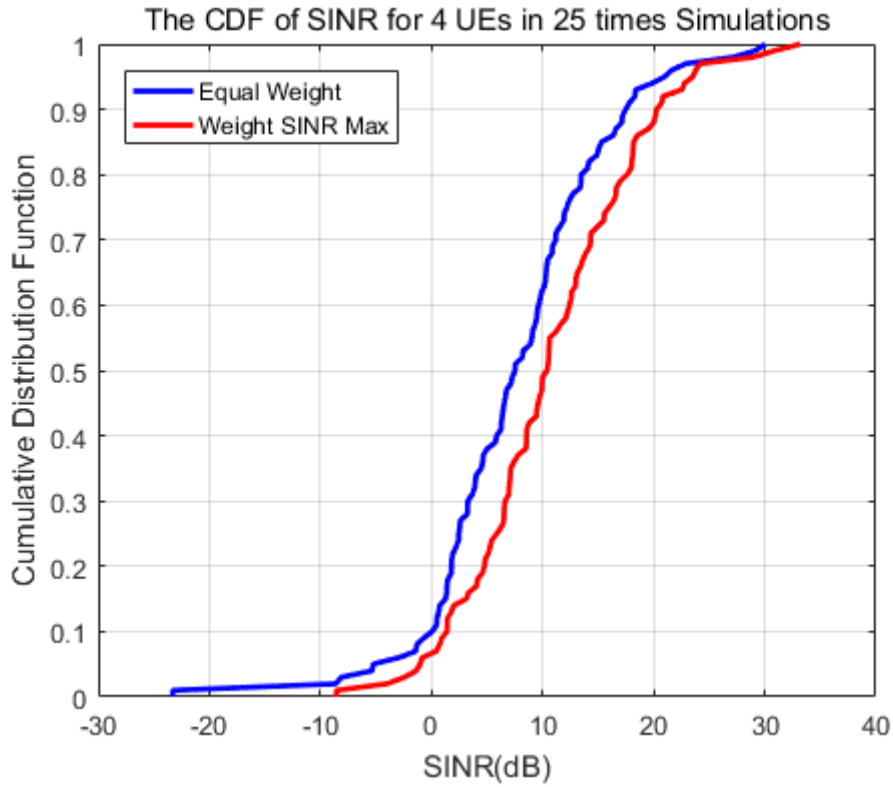


Figure 5- 5: The CDF for the SINR in the two mm-wave systems

In Figure 5-5, the blue line is the SINR in the mm-wave system using equal weighting method; the red line the SINR in the mm-wave system using the new weighting method.

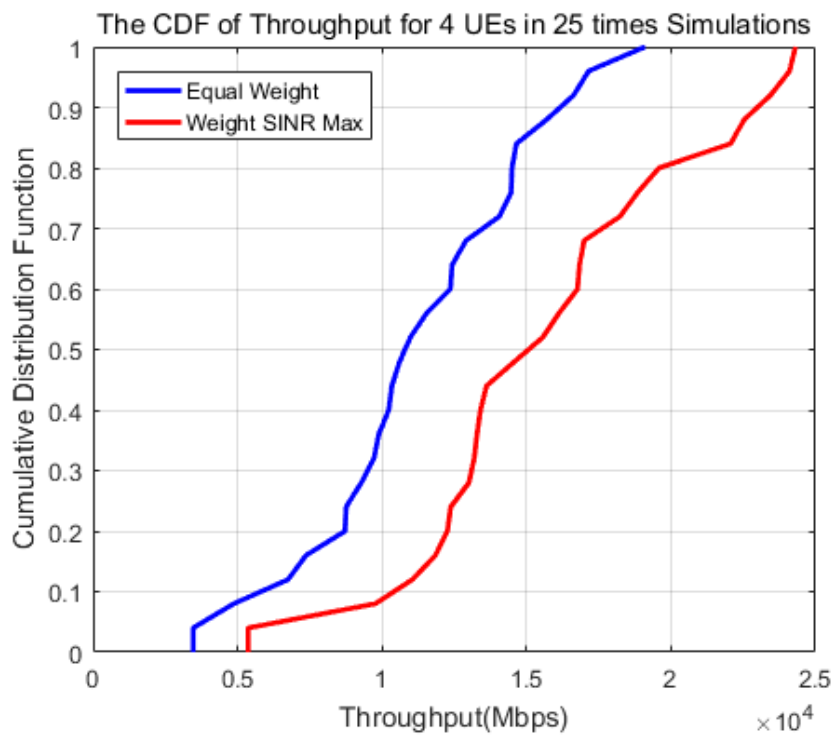


Figure 5- 6: The CDF for the throughput in the two mm-wave systems

In Figure 5-6, the blue line is the throughput for the mm-wave system using equal weighting method; the red line the throughput for the mm-wave system using the new weighting method. The throughput for the mm-wave system using the new weighting method (red line) is larger than the throughput not using (blue line) when the CDF percent are same. The unit for the throughput is megabits per second ( $\times 10^4$ Mbps).

#### **5.2.4 The BER results compared in different mm-wave systems**

This part shows that the BER for two mm-wave systems, in which one is using the equal weighting matrix and the other is using the new weighting matrix for the weighting method. Then the 3D beamforming and 3D Channel model are added into the mm-wave system and then the received signals of the mm-wave system can be obtained. The BER of the transmitted signal and received signal are calculated, which are saved in the BER1 and BER2 data file. The operation parameters for this simulation are set as shown in Table 5-1. The BER is read from the data files to display the BER and the CDF of BER for these two mm-wave systems. If the  $4 \times 4$  LTE MIMO system is chosen in the GUI window, the BER in the  $4 \times 4$  LTE MIMO system can be compared with the BER for one UE in these two mm-wave systems.

The constellation figure of received signals for the UE in the  $4 \times 4$  LTE MIMO system is shown in Figure 5-7 at 30 dB for SNR. The received signal errors in this LTE MIMO system are 51333 bits, which is the largest value in these three systems. Figure 5-8 and Figure 5-9 show the constellation figures of received signals for one UE in these two mm-wave systems. When the SNR is 30 dB, the received signal errors are zero bit errors.



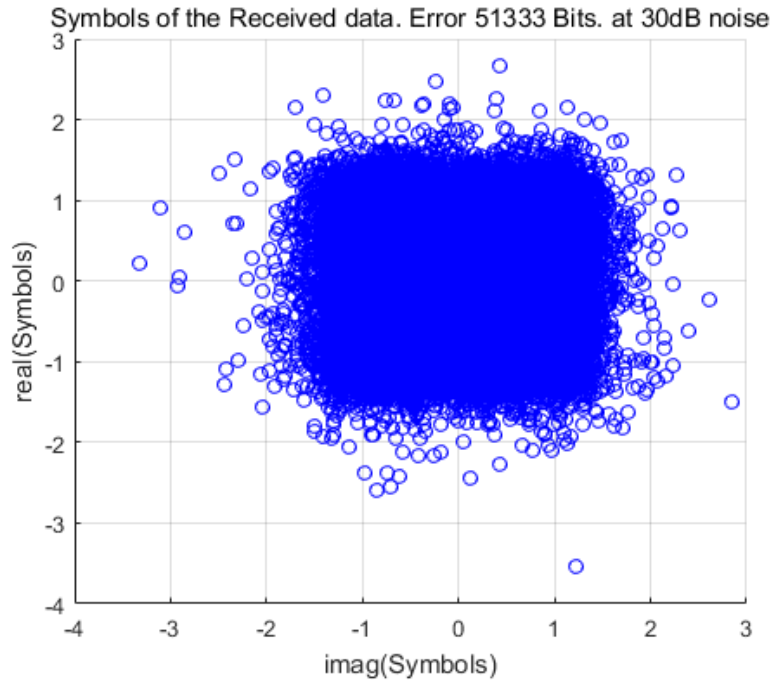


**Figure 5- 7: The constellation figure of the received signals for UE in LTE MIMO system**

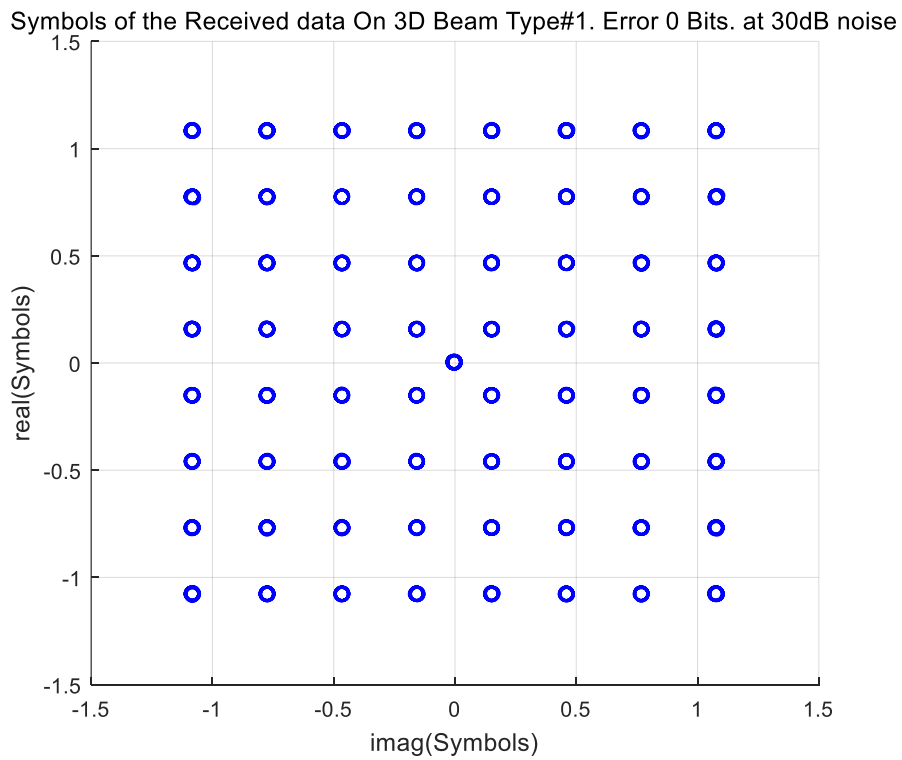


**Figure 5- 8: The constellation figure of the received signals in equal weighting mm-wave system**

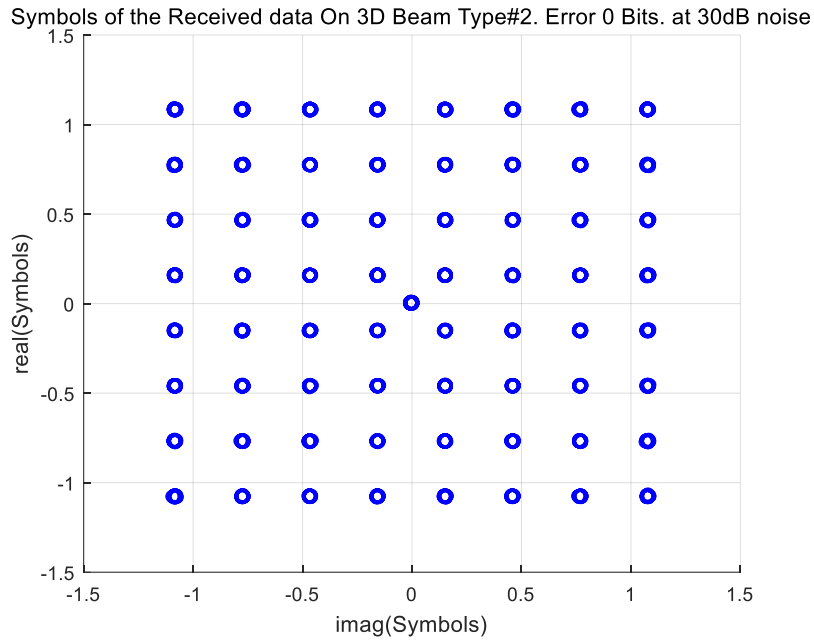


**Figure 5- 9: The constellation figure of the received signals for UE in new weighting mm-wave system**

Figure 5-10 shows the comparison of BER for these three systems. The red line is the BER for one UE in the new weighting mm-wave system; the black line is the BER one UE in the equal weighting mm-wave system; the green line is the BER for the LTE MIMO system when the SNR is from 0 to 30 dB. The BERs in these two mm-wave systems are close to zero, which are smaller than the BER in the LTE MIMO system as shown in green in Figure 5-10.

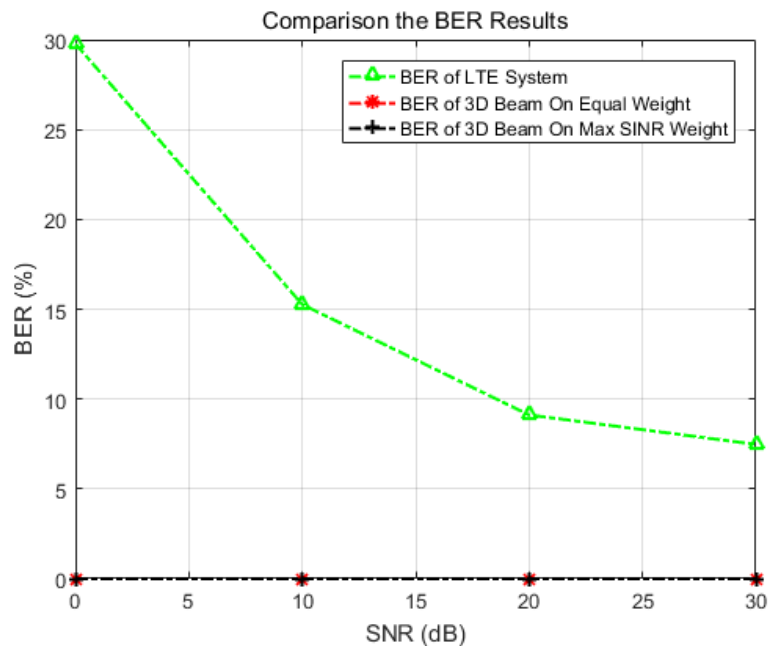


**Figure 5- 10: The comparison of BER for these three systems**

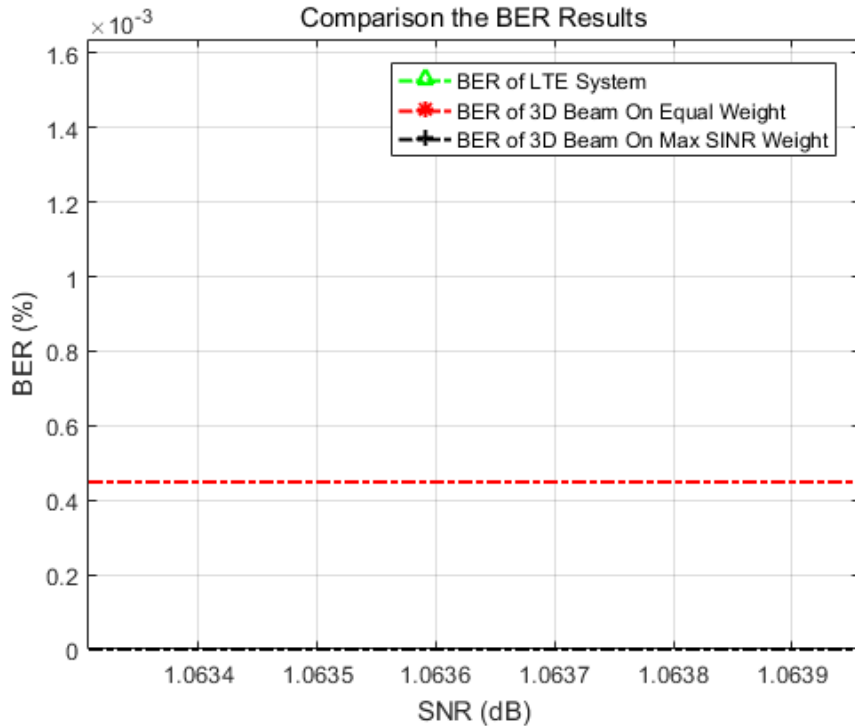
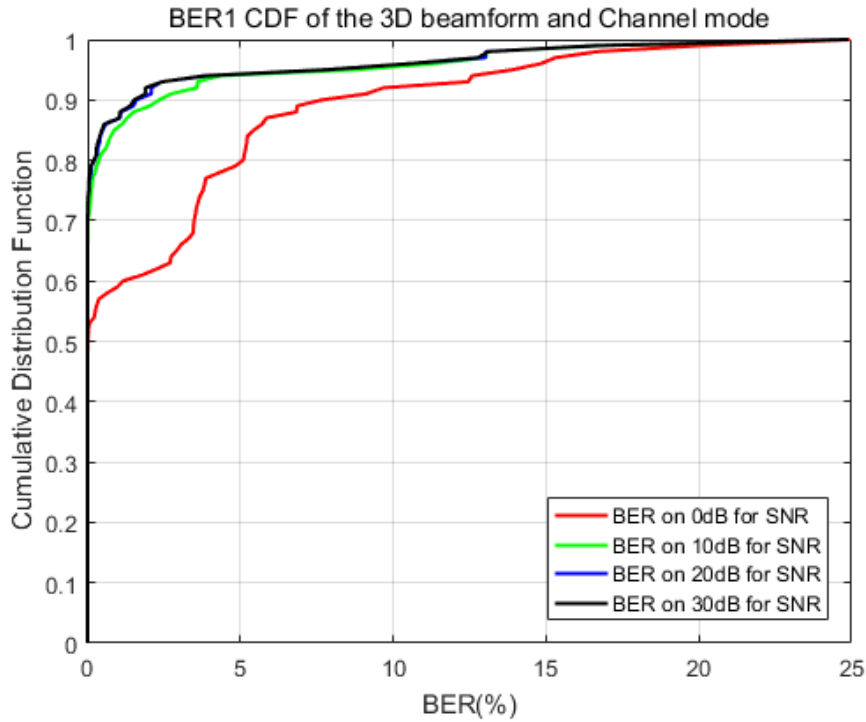


Figure 5- 11: The comparison of BER for two mm-wave systems

Figure 5-11 shows the comparison of BER for these two mm-wave systems. The red line is the BER for one UE in the new weighting mm-wave system; the black line is the BER one UE in the equal weighting mm-wave system. The BER 0.4 % in the equal weighting mm-wave system is larger than the BER 0 % in the new weighting mm-wave system.

Figure 5-12 and Figure 5-13 display the CDFs of BER in the equal weighting mm-wave system and the new weighting mm-wave systems, respectively when the SNR is from 0 to 30 dB. There are a total of 100 data points because there are 4 UEs in one cell and the simulation runs 25 times.

In Figure 5-12 and Figure 5-13, the BER decreases when the SNR increases. The CDF presented in Figure 5-12 shows that 95 % of the data points have a BER of less than 5 % when the SNR is larger than 20 dB in the equal weighting mm-wave system. The CDF presented in Figure 5-13 shows that 95 % of the data points have a BER of 0 % when the SNR is larger than 20 dB in the new weighting mm-wave system. Therefore, BER in the new weighting mm-wave system is smaller than the BER in the equal weighting mm-wave system when the SNR is larger than 20 dB. The new weighting method reduces the BER for mm-wave system.



**Figure 5- 12: The CDF of BER for equal weighting mm-wave system**

In Figure 5-12, the red line is the CDF of BER in 0 dB for SNR; the green line is the CDF of BER in 10 dB for SNR; the blue line is the CDF of BER in 20 dB for SNR and the black line is the CDF of BER in 30 dB for SNR of the equal weighting mm-wave system.

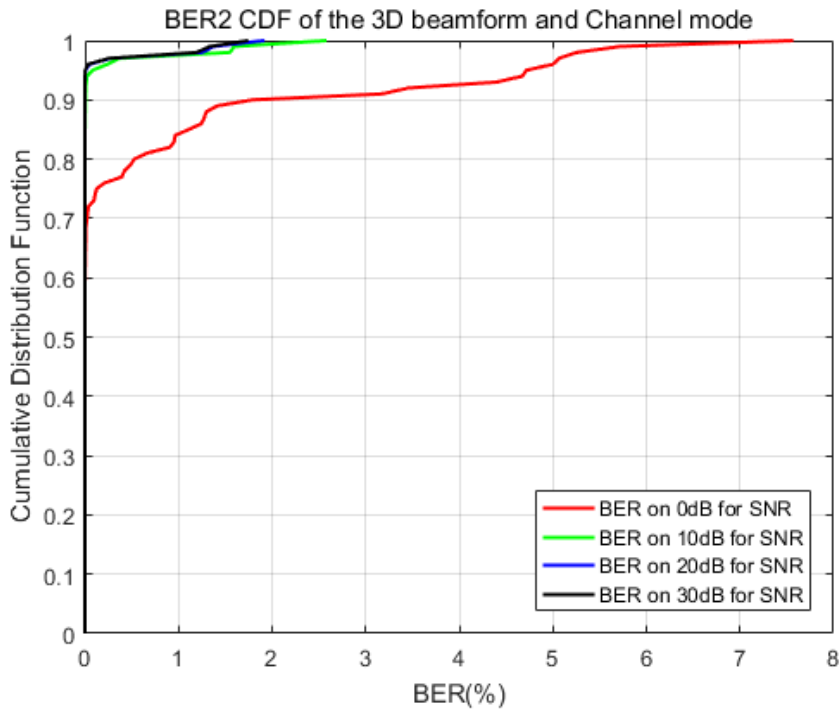


**Figure 5- 13: The CDF of BER for the new weighting mm-wave system**

In Figure 5-13, the red line is the CDF of BER in 0 dB for SNR; the green line is the CDF of BER in 10 dB for SNR; the blue line is the CDF of BER in 20 dB for SNR and the black line is the CDF of BER in 30 dB for SNR of the new weighting mm-wave system.

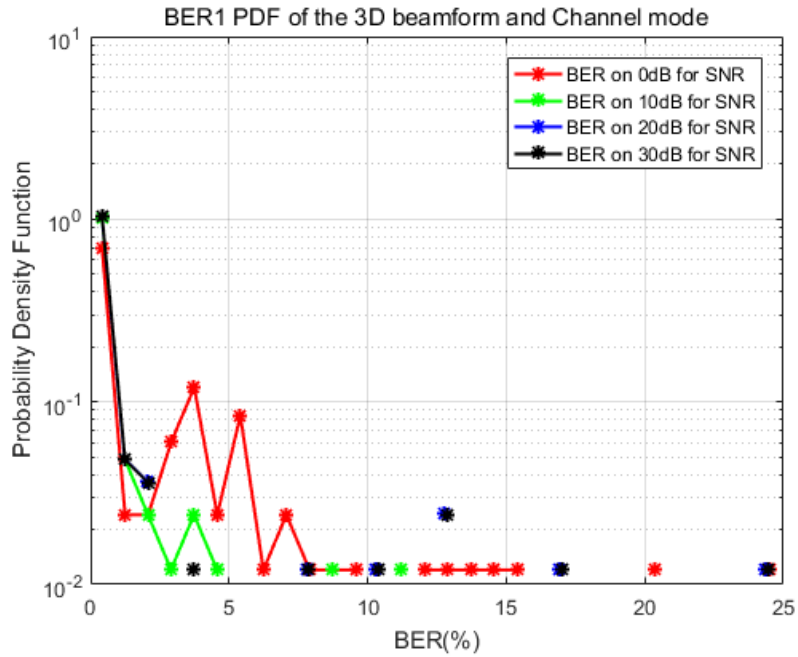
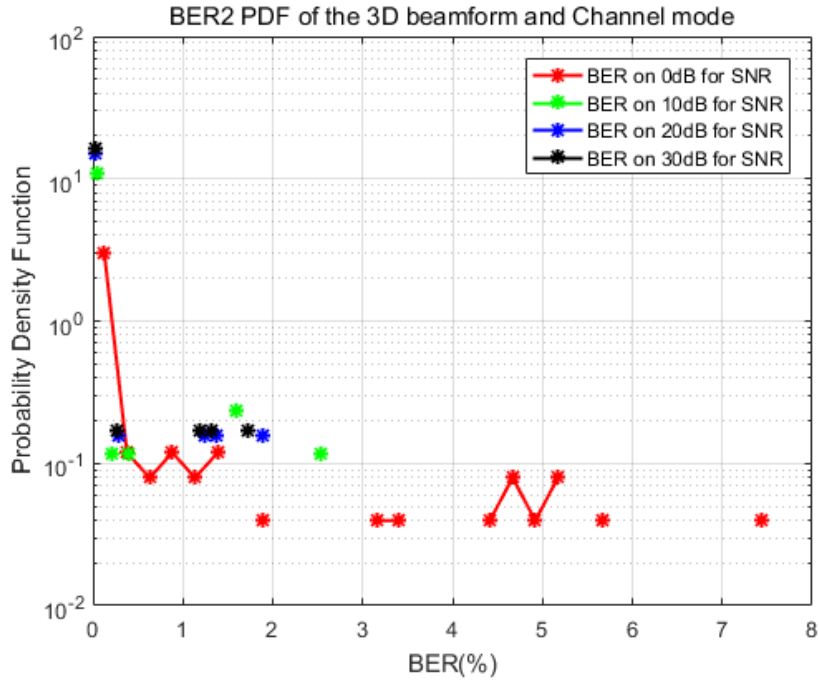


Figure 5- 14: The PDF of BER for equal weighting mm-wave system

In Figure 5-14 the red line is the PDF of BER in 0 dB for SNR; the green line is the PDF of BER in 10 dB for SNR; the blue line is the PDF of BER in 20 dB for SNR and the black line is the PDF of BER in 30 dB for SNR of the equal weighting mm-wave system.



**Figure 5- 15: The PDF of BER for the new weighting mm-wave system**

In Figure 5-15, the red line is the PDF of BER in 0 dB for SNR; the green line is the PDF of BER in 10 dB for SNR; the blue line is the PDF of BER in 20 dB for SNR and the black line is the PDF of BER in 30 dB for SNR of the new weighting mm-wave system.

Moreover, all PDFs of the BER in the equal weighting mm-wave system and the new weighting mm-wave system are recorded, which are respectively shown in Figure 5-14 and Figure 5-15. When the SNR is larger than 20 dB, the BER in the equal weighting mm-wave system has a greater probability to be distrusted in 3 % or less as shown in Figure 5-14, but the BER in the new weighting mm-wave system is distrusted in 0.5 % or less as shown in Figure 5-15. Therefore, the BER in the new weighting mm-wave system are smaller than the BER in the equal weighting mm-wave system when the SNR is larger than 20 dB.

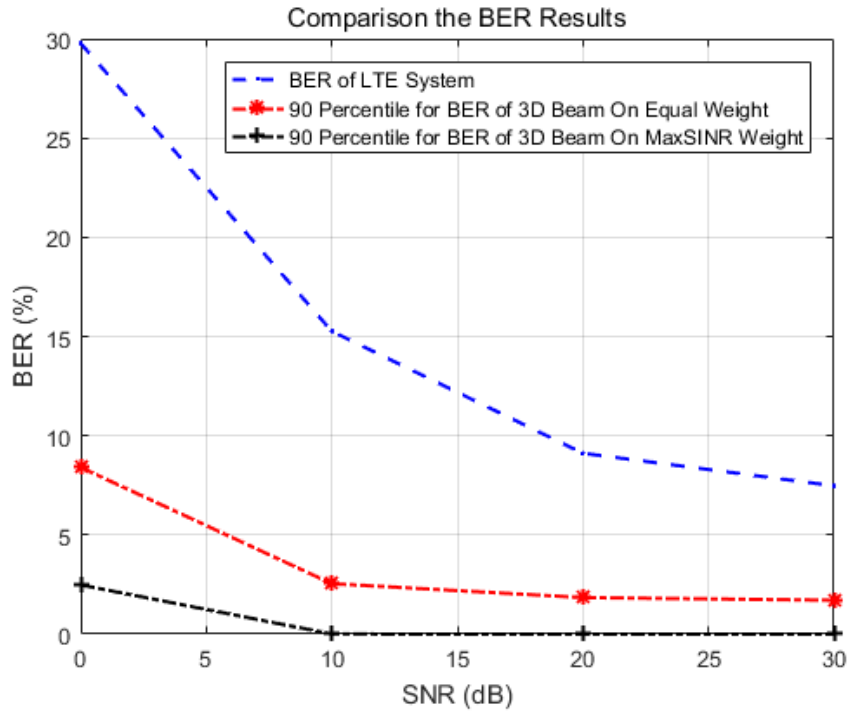


**Figure 5- 16: The comparison of BER for three systems**

In Figure 5-16, the blue line is the BER in the 4×4 LTE MIMO system; the red line is the 90% sample points for BER in the equal weighting mm-wave system; the black line is the 90% sample points for BER in the new weighting mm-wave system when the SNR are 0 dB, 10 dB, 20 dB or 30 dB.

There are 100 sample points for BER in these two mm-wave systems so the maximum values and minimum values are considered as outliers, which are far removed from the mass of data. Then the BER interval value is from 10% to 90%.

All of BERs in these two mm-wave systems are smaller than the BER in the 4×4 LTE MIMO system as shown in Figure 5-16. Therefore, the 3D beamforming mm-wave system has better signal quality over the LTE MIMO system when the modulation method is 64-QAM.

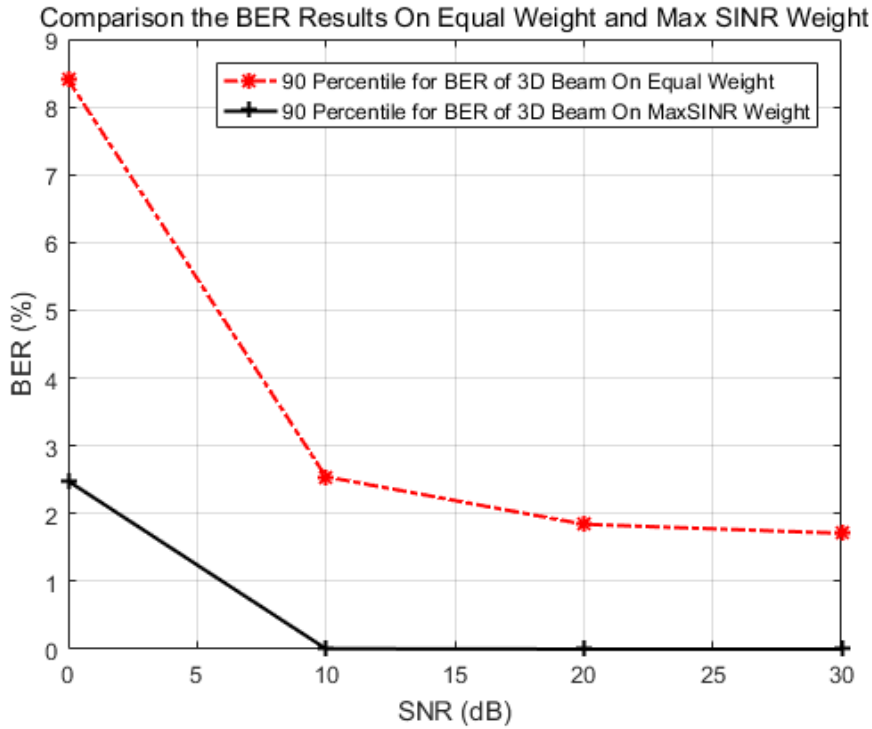


**Figure 5- 17: The comparison of BER for three systems when the SNR have different value**

In Figure 5-17, the red line is the 90% sample points for BER for the equal weighting mm-wave system; the black line is the 90% sample points for BER for the new weighting mm-wave system when the SNR are 0 dB, 10 dB, 20 dB, or 30 dB.

This figure shows that the 90% sample points for BER in the new weighting mm-wave system are smaller than the 90% sample points for BER for the equal weighting mm-wave system. When the SNR is larger than 10 dB, the 90% sample points for BER in the new weighting mm-wave system are close to zero. However, when the SNR is smaller than 10 dB, the 90% sample points for BER in the new weighting mm-wave system is smaller than 2.5%, and the 90% sample points for BER in the equal weighting mm-wave system are larger than 2.5%.

Therefore, the new weighting mm-wave system has the smaller BER than the equal weighting mm-wave system, no matter what is the SNR.

### 5.2.5 CDF of BER in different mm-wave systems

This part shows a comparison about the CDF of BER in the equal weighting mm-wave system and the new weighting mm-wave system, when the SNR is 20 dB.

Figure 5-18 shows that the CDFs of BER are from 0 to 25%, which more clearly



shows the different between these two mm-wave systems. In the 4 beams mm-wave system, the red line is the CDF of BER in the equal weighting mm-wave system; the black line is the CDF of BER in the new weighting mm-wave system. The 0.5% sample points of BER values in the new weighting mm-wave system are not close to zero, whilst the 25 % of BER values in the equal weighting mm-wave system are not close to zero. Therefore, the BER in the new weighting mm-wave system are smaller than the BER in the equal weighting mm-wave system.

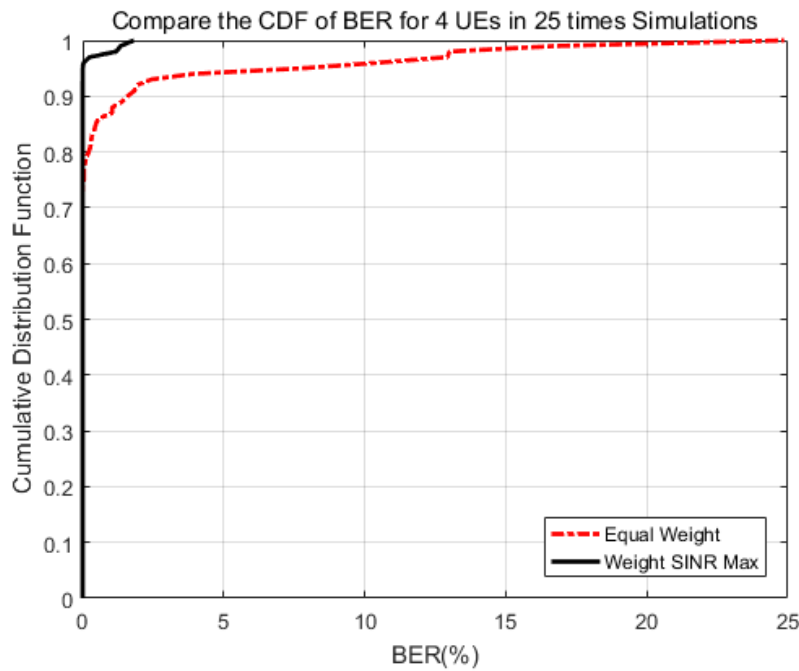


Figure 5- 18: In the 4 beams mm-wave system, the CDF of BER

### 5.3 Compare the different size of antenna arrays and the different numbers of beams

The sizes of the antenna arrays are  $32 \times 32$ ,  $16 \times 16$  and  $8 \times 8$ , which have the effect on the width of the beam pattern. Moreover, the number of beam patterns can impacted the results because there is interference between each beam. In this part, the simulation results used three sizes of the antenna arrays, in which there are different number of UEs. The detailed parameters for the simulation systems are shown in Table 5-2.

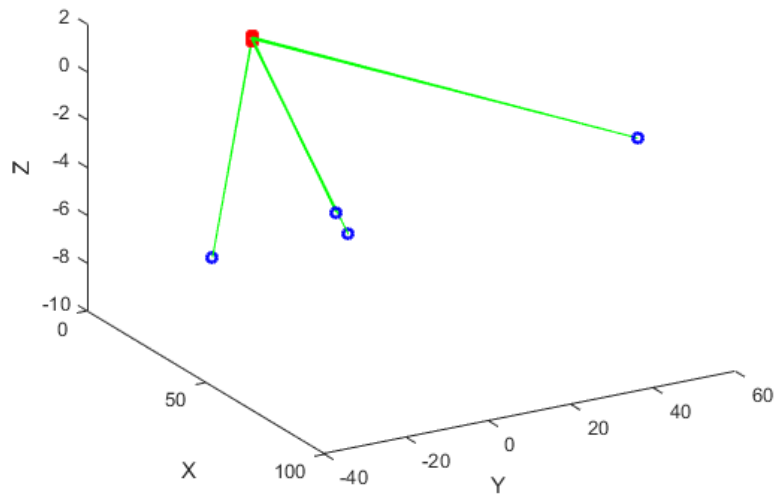
**Table 5- 2: The parameters for running simulation**

<b>Parameter</b>	<b>Value</b>
Height of the base station(m)	25
Height of the UE(m)	$h_{UT}=3(n_{fl} - 1) + 1.5$ (NOTE 1)
RB size	12 sub-carriers
Sub-carrier spacing(GHz)	1
mobile terminal	Antenna gain 0dBi, Noise 9dBm
Base station	Antenna gain 0dBi, Noise 5dBm
Transmit power for each antenna element (dBm)	30(~1W)
Thermal Noise(dBm/Hz)	-174
The channel model	3GPP TR 36.873 (3D UMa)
The number of time for running simulation	25 or 50 or 100 times
The number of UEs	4 or 2 or 1
The size of rectangular antenna arrays	32×32 or 16×16 or 8×8
The size of antenna arrays for each beam	16×16 or 8×8 or 4×4
The min of coverage distance(m)	1
The max of coverage distance(m)	100
The modulation method	R.5 (64-QAM)
The carrier frequency(GHz)	28
The range of SNR for shown(dB)	[0 10 20 30]
The display BER interval (%)	10 to 90
LTE MIMO system size	4×4 or 4×2
LTE MIMO channel Correlation	High

### 5.5.1 32×32 antenna arrays

The simulation was run 25 times with different seeds to show the results. In Figure 5-19, the result shows the tenth time among these 25 running times, the number of UEs is 10, the modulation is R.5 and the environment is UMa in 32×32 antenna arrays system. In this figure, the green lines mean the direction of the beams and the blue points mean the center point for the clusters of UEs.

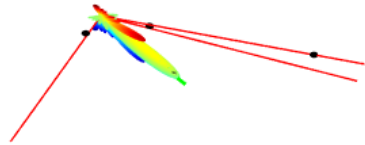
Network Environment. It has 4 Beams and 4 Users. Time 10 Simulation



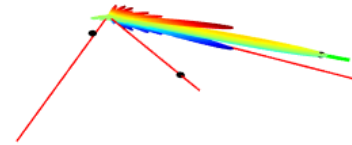
**Figure 5- 19: The simulation result in UMA for 32x32 antenna arrays system**

Figure 5- 20 shows the 4 beams, respectively, in which each beam covers one UE. The green line is the main beam direction; the red lines are the directions of other beams and the black points are the UEs as shown in Figure 5- 20. The beams for the whole cell are shown in Figure 5-21, which are 4 beams for 4 UEs.

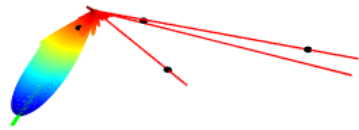
The Atten.Rate = -61.49 -62.4735 -35.0863dB  $\theta=19.2801$   $\phi=-88.4508$



The Atten.Rate = -52.5155 -42.3168 -42.2801dB  $\theta=26.4779$   $\phi=89.3195$



The Atten.Rate = -59.2715 -57.4218 -70.2633dB  $\theta=65.2251$   $\phi=-51.8459$



The Atten.Rate = -55.7077 -53.7014 -83.161dB  $\theta=66.4269$   $\phi=60.4333$

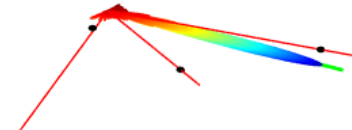
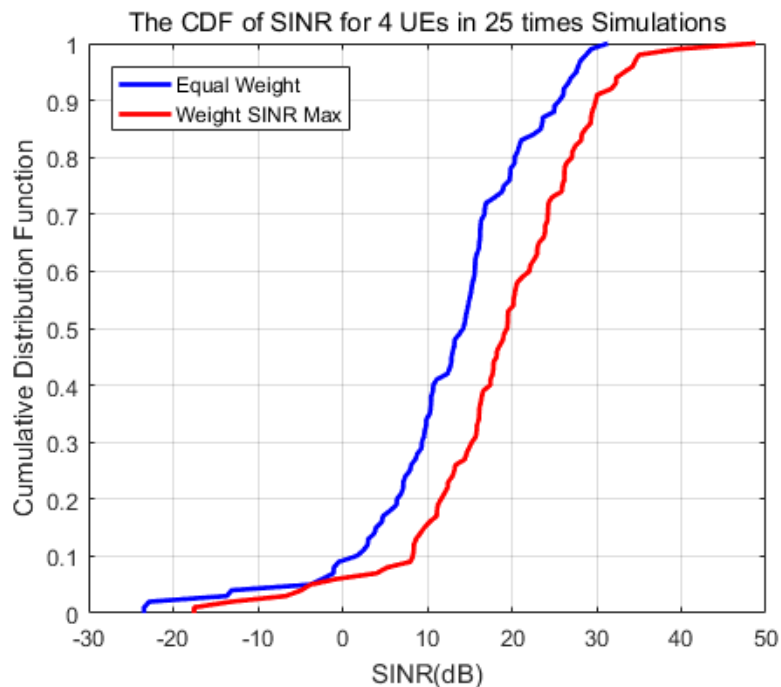


Figure 5- 20: The beams in the 32×32 antenna arrays system with 4 beams



**Figure 5- 21: The 3D beam in the 32×32 antenna arrays system with 4 beams**

The simulation system has been run 25 times to generate results for the CDF and PDF to be analyzed because the number of UEs is decreasing. The CDFs for the SINR for these two mm-wave systems are shown in Figure 5-22, and the blue line is the SINR in the mm-wave system using the equal weighting method, the red line the SINR in the mm-wave system using the new weighting method, where the results are compared when using the new weighting method and when not using it. The CDFs of the throughput for these two mm-wave systems are shown in Figure 5-23.



**Figure 5- 22: The comparison of CDF for the SINR by different methods**

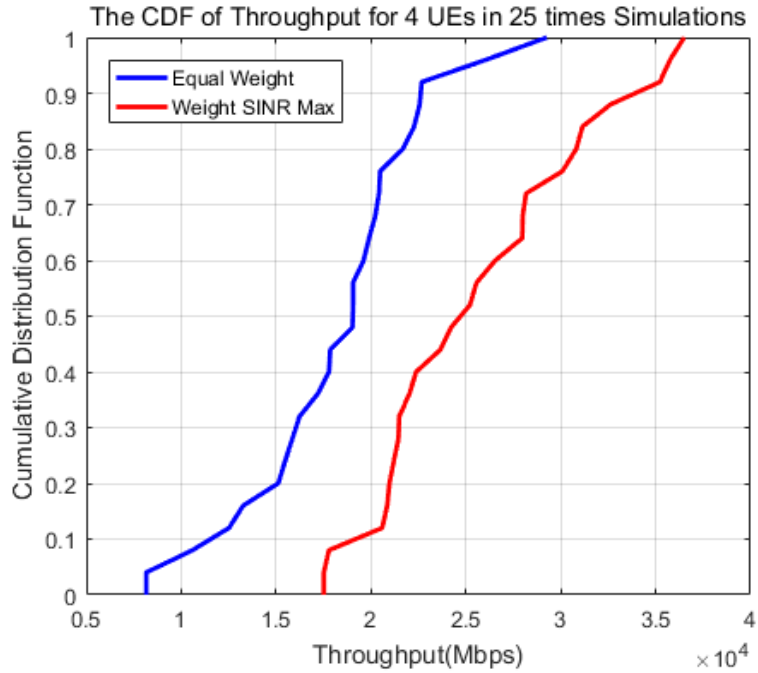


**Figure 5- 23: The comparison of CDF for the throughput by different methods**

In Figure 5-23, the CDFs for the throughput are in these two mm-wave systems; the blue line is the throughput for the mm-wave system using the equal weighting method; the red line the throughput for the mm-wave system using the new weighting method.

In Figure 5-22, the CDFs of SINR are from -30 dB to 50 dB for these two mm-wave systems. The SINR results obtained using the new weighting method (red line) is always greater than SINR results obtained using the equal weighting method (blue line). For example, if the CDF is 90%, the SINR in the mm-wave system using the new weighting method are 30 dB, but the SINR in the mm-wave system using the equal weighting method are 25 dB. Therefore, the new weighting method can increase the SINR in the mm-wave system. Moreover, the maximum value of SINR in this figure is larger than 48 dB, which is bigger than the maximum SINR in the 16×16 antenna arrays mm-wave system with 4 beams.

In Figure 5-23, the throughput for the mm-wave system using the new weighting method (red line) is larger than the throughput not using (blue line). Moreover, the maximum value of throughput is  $3.6 \times 10^4$  Mbps, which is larger than the maximum throughput in the 16×16 antenna arrays system with 4 beams. Moreover, the BERs for three systems are shown in Figure 5-24 when the SNR is from 0 to 30 dB.

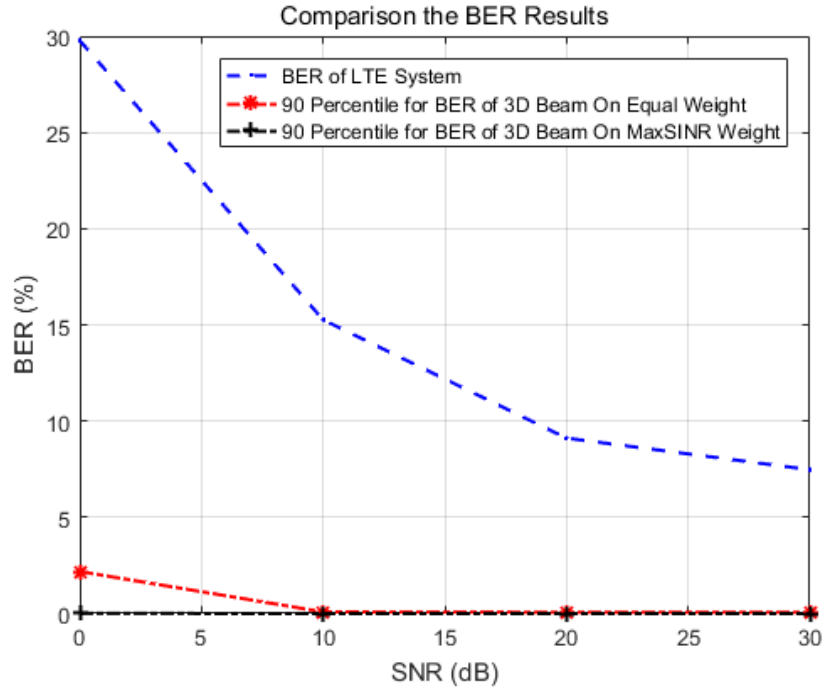


Figure 5- 24: The comparison of BER in three system for different SNR value

In Figure 5-24, the blue line is the BER in the  $4 \times 4$  LTE MIMO system; the red line is the 90% sample points for BER in the equal weighting mm-wave system; the black line is the 90% sample points for BER in the new weighting mm-wave system when the SNR are 0 dB, 10 dB, 20 dB, and 30 dB.

There are 100 sample points for BER in these two mm-wave systems so the maximum values and minimum values are considered as outliers, which are far removed from the mass of data. Then the BER interval value is from 10% to 90%.

All of BERs in these two mm-wave systems are smaller than the BER in the  $4 \times 4$  LTE MIMO system as shown in Figure 5-24. Therefore, the 3D beamforming mm-wave system has better signal quality over the  $4 \times 4$  LTE MIMO system when the modulation method is 64-QAM. The BER in these two mm-wave systems are shown in Figure 5-25.

In Figure 5-25, the red line is the 90% sample points for BER in the equal weighting mm-wave system; the black line is the 90% sample points for BER in the new weighting mm-wave system when the SNR are 0 dB, 10 dB, 20 dB, or 30 dB.

In this figure, when the SNR is larger than 10 dB, the 90% sample points for BER in the new weighting mm-wave system are close to zero, which are smaller than the 90% sample points for BER in the equal weighting mm-wave system. Moreover, the values

in the equal weighting mm-wave system are smaller than 1%, which are close to the values in the new weighting mm-wave system. When the SNR is smaller than 10 dB, the 90% sample points for BER in the equal weighting mm-wave system have a greater spread than the values in the new weighting mm-wave system.

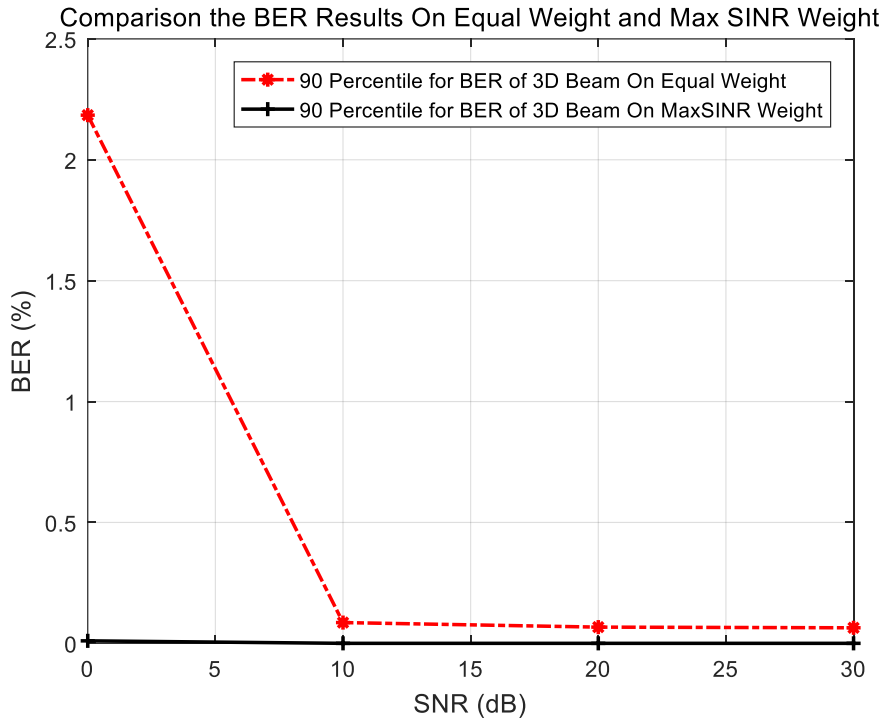


Figure 5- 25: In the 2 beams system, the comparison of BER

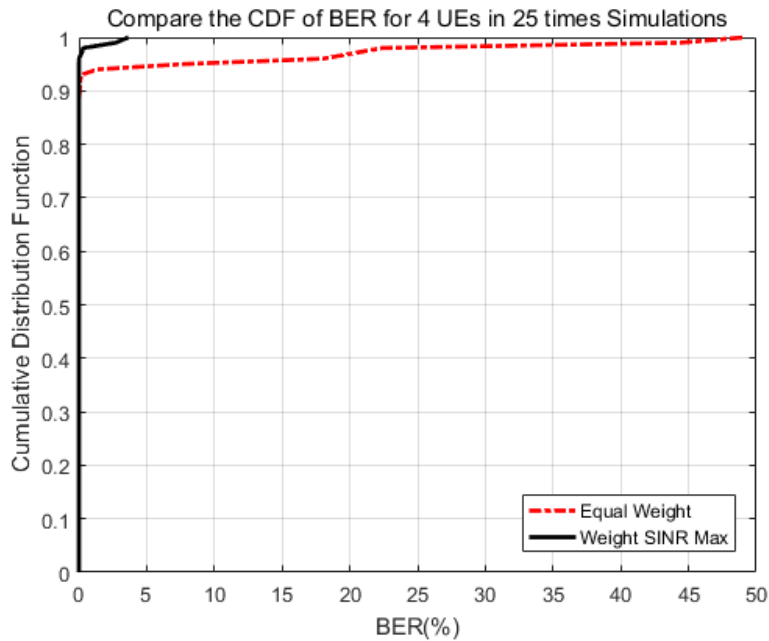


Figure 5- 26: In the 4 beams system, the comparison of BER

Figure 5-26 shows that the red line is the CDF of BER in the equal weighting mm-wave system; the black line is the CDF of BER in the new weighting mm-wave system.



In this figure, the CDFs of BER are from 0 to 25% and there are differences between these two mm-wave systems. Most of BER values in the new weighting mm-wave system are close to zero, but the 4% sample points for BER values in the new weighting mm-wave system are not close zero. Moreover, the 20% sample points for BER values in the equal weighting mm-wave system are not close zero, which are much than the BER values in the new weighting mm-wave system. Therefore, the new weighting mm-wave system has decreased the BER more than the equal weighting mm-wave system.

To sum up, when the size of antenna arrays mm-wave system is increased, the SINR and throughput are increased, whilst the interference and the BER are decreased. In the 32×32 antenna arrays mm-wave system, a larger number of antenna arrays makes the energy from the beams in desired directions be more concentrated in order to the interference be less.

### 5.5.2 16×16 antenna arrays

The simulation was run 50 times with different seeds to show the results. Figure 5-27 shows that the result shows the tenth time among these 50 running times, the number of UEs is 2, the number of beam is 2, the modulation is R.5 and the environment is UMa in 16×16 antenna arrays system.

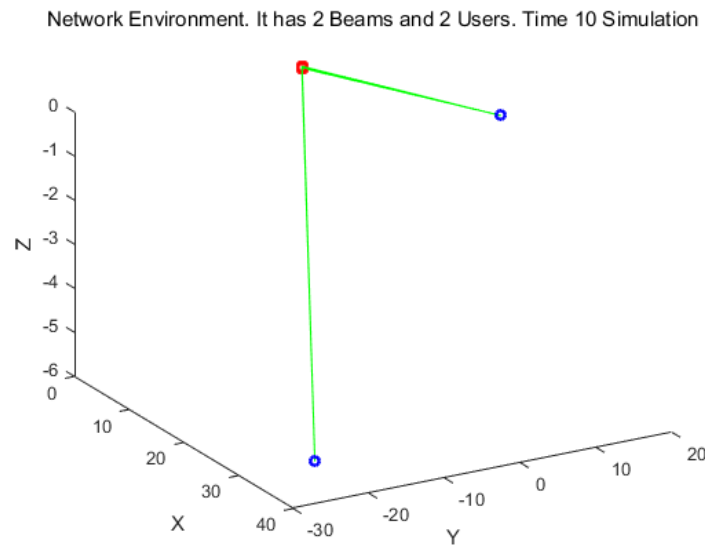


Figure 5- 27: The simulation analysis in UMa for 16×16 antenna arrays system

In this figure, the green lines mean the direction of the beams and the blue points mean the center point for the clusters of UEs.

Figure 5-28 shows the 2 beams, respectively, in which each beam covers one UE. The green line is the main beam direction; the red lines are the directions of other beams and the black points are the UEs as shown in Figure 5-28. The beams for the whole cell are shown in Figure 5-29, which are 2 beams for 2 UEs.



**Figure 5- 28: The beams in the 16×16 antenna arrays system with 2 beams**

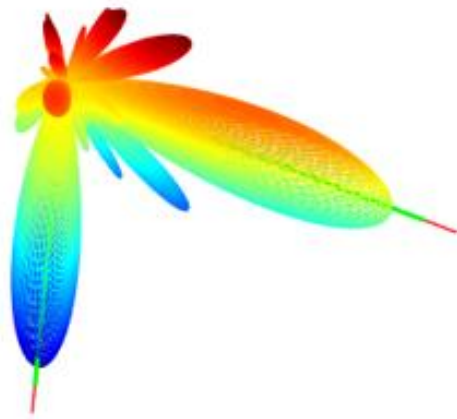


**Figure 5- 29: The 3D beam in the 16×16 antenna arrays system with 2 beams**

The simulation system has been run 50 times to generate results for the CDF and PDF to be analyzed because the number of UEs is decreasing. The CDFs for the SINR for these two mm-wave systems are shown in Figure 5-30, where the results are compared when using the new weighting method and when not using it. The CDFs of the throughput for these two mm-wave systems are shown in Figure 5-31.

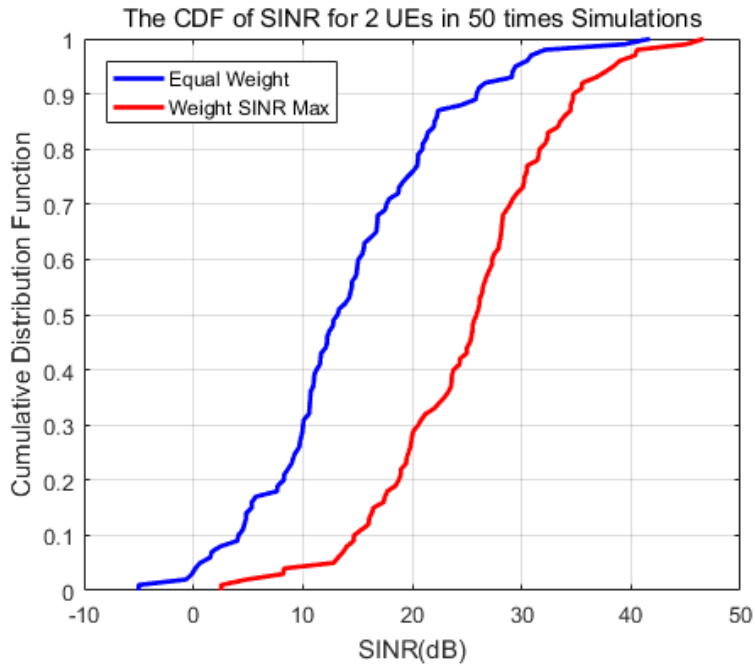


**Figure 5- 30: The CDF for the SINR in mm-wave system obtained by different methods**

In Figure 5-30, the CDFs for the SINR are in these two mm-wave systems; the blue line is the SINR in the equal weighting mm-wave system; the red line the SINR in the new weighting mm-wave system.

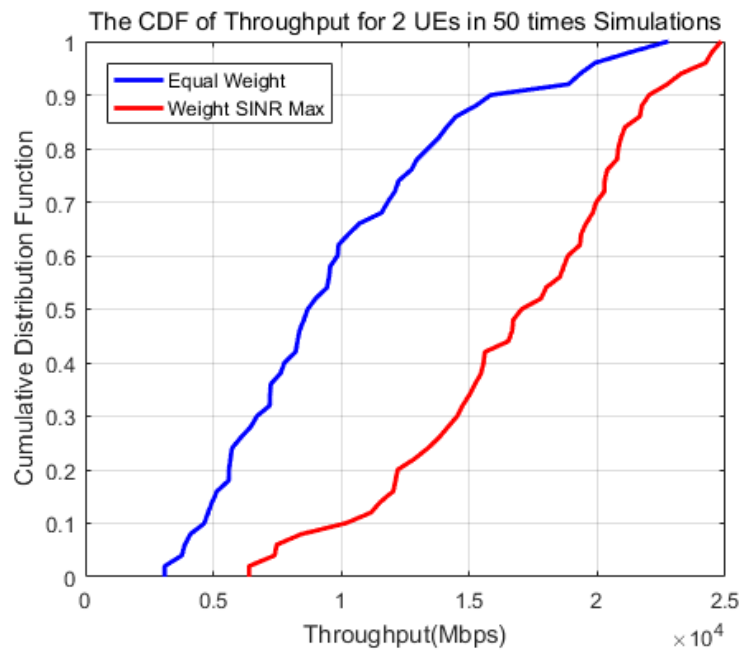


**Figure 5- 31: The CDF for the throughput in mm-wave system obtained by different methods**

Figure 5-31 shows that the CDFs for the throughput are in these two mm-wave systems; the blue line is the throughput for the equal weighting mm-wave system; the red line the throughput for the new weighting mm-wave system.

In Figure 5-30, the CDFs of SINR are from -10 dB to 50 dB for these two mm-wave systems. The SINR results obtained using the new weighting method (red line) is always greater than SINR results obtained using the equal weighting method (blue line). For example, if the CDF is 90%, the SINR in the mm-wave system using the new weighting method are larger than 35 dB, but the SINR in the mm-wave system using the equal weighting method are smaller than 25 dB. Therefore, the new weighting method can increase the SINR in the mm-wave system. Moreover, the maximum value of SINR in this figure is larger than 45 dB, which is bigger than the maximum SINR in the  $16 \times 16$  antenna arrays system with 4 beams.

In Figure 5-31, the throughput for the mm-wave system using the new weighting method (red line) is larger than the throughput not using (blue line). Moreover, the maximum value of throughput is same as the maximum throughput in the  $16 \times 16$  antenna arrays system with 4 beams. When the SNR is from 0 to 30 dB, the BER in three systems are shown in Figure 5-32.

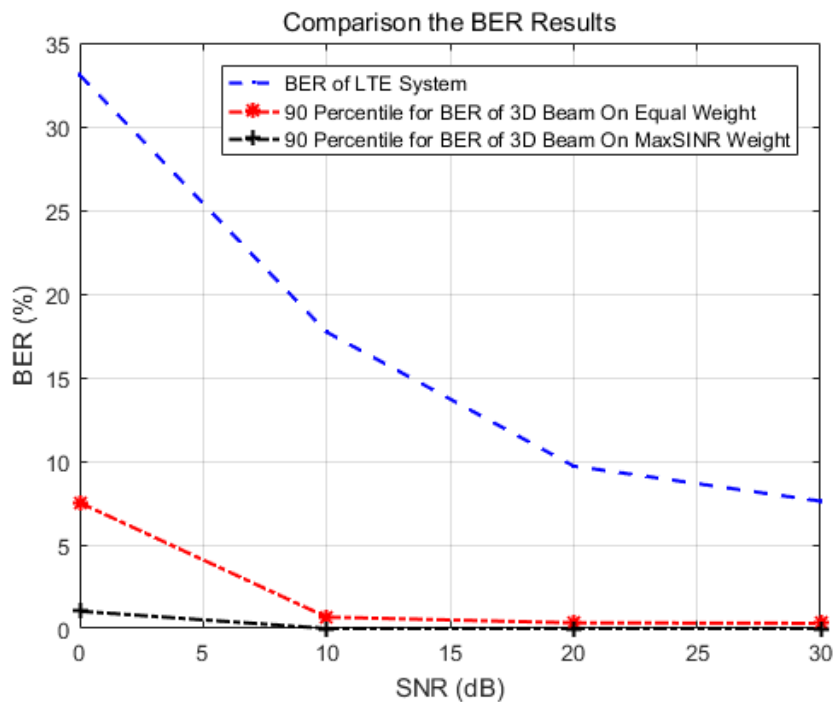


Figure 5- 32: The BER in three systems when the SNR are 0 dB, 10 dB, 20 dB or 30 dB

In Figure 5-32, the blue line is the BER in the  $4 \times 2$  LTE MIMO system; the red line is the 90% sample points for BER in the equal weighting mm-wave system; the black line is the 90% sample points for BER in the new weighting mm-wave system

when the SNR are 0 dB, 10 dB, 20 dB and 30 dB.

There are 100 sample points for BER in these two mm-wave systems so the maximum values and minimum values are considered as outliers, which are far removed from the mass of data. Then the BER interval value is from 10% to 90%.

All of BERs in these two mm-wave systems are smaller than the BER in the  $4 \times 2$  LTE MIMO system as shown in Figure 5-32. Therefore, the 3D beamforming mm-wave system has better signal quality over the  $4 \times 2$  LTE MIMO system when the modulation method is 64-QAM. The BER in these two mm-wave systems are shown in Figure 5-33 when SNR is from 0 to 30 dB.

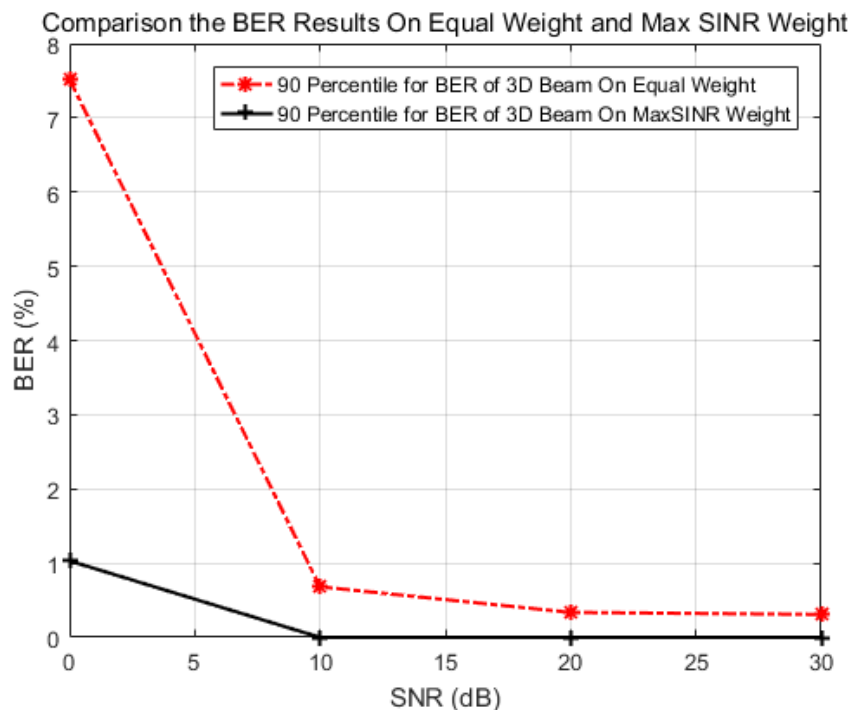


**Figure 5- 33: In the 2 beams system, the BER in two systems for different SNR**

Figure 5-33 shows that the red line is the 90% sample points for BER in the equal weighting mm-wave system; the black line is the 90% sample points for BER in the new weighting mm-wave system when the SNR are 0 dB, 10 dB, 20 dB and 30 dB.

In Figure 5-33, the 90% sample points for BER in the new weighting mm-wave system are close to zero when the SNR is larger than 10 dB, which are smaller than the 90% sample points for BER in the equal weighting mm-wave system. Moreover, the values in the equal weighting mm-wave system are close to the values in the new weighting mm-wave system.

When the SNR is smaller than 10 dB, the 90% sample points for BER in the equal weighting mm-wave system have a greater spread than the values in the new weighting mm-wave system.

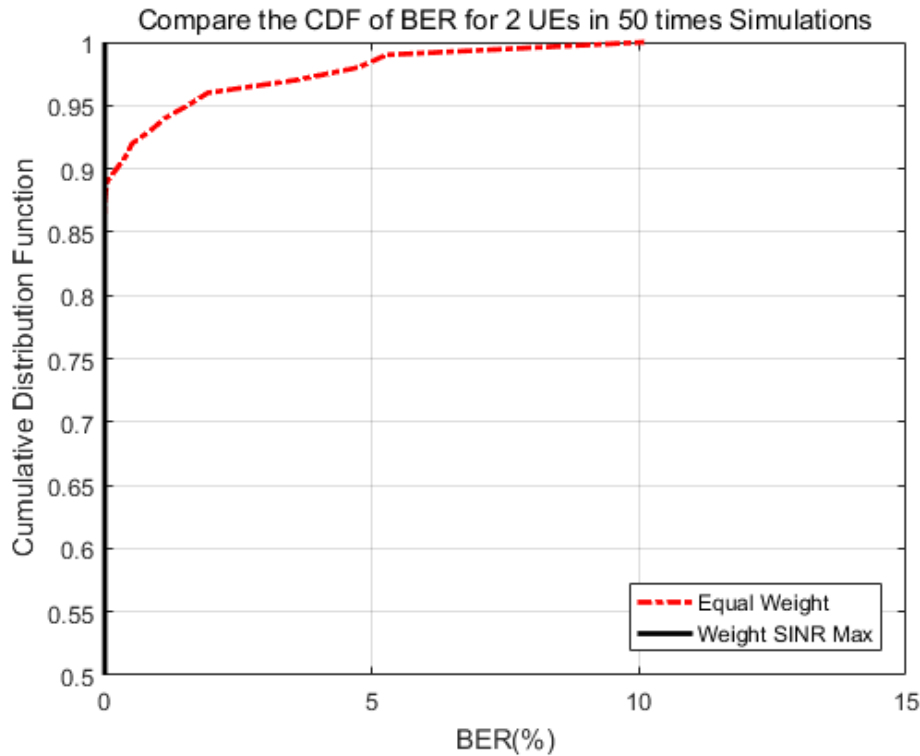


Figure 5- 34: In the 2 beams system, the CDF of BER in two mm-wave systems

Figure 5-34 shows that the red line is the CDF of BER in the equal weighting mm-wave system; the black line is the CDF of BER in the new weighting mm-wave system.

In this figure, the CDFs of BER are from 0 to 15% and there are differences between these two mm-wave systems. All of BER values in the new weighting mm-wave system are close to zero and the 88% sample points for BER values in the equal weighting mm-wave system are close to zero. Therefore, the new weighting mm-wave system has decreased the BER more than the equal weighting mm-wave system.

To sum up, when the number of beams is decreasing in the  $16 \times 16$  antenna arrays mm-wave system, the throughput is not changed, whilst the interference and the BER are decreased.

### 5.5.3 8×8 antenna arrays

#### 5.5.3.1 The 2 beams in the 8×8 antenna arrays mm-wave system

The simulation was run 50 times with different seeds to show the results. Figure 5-35 shows that the result shows the tenth time among these 50 running times, the number of UEs is 2, there are 2 beams, the modulation is R.5 and the environment is UMa in 8×8 antenna arrays system.

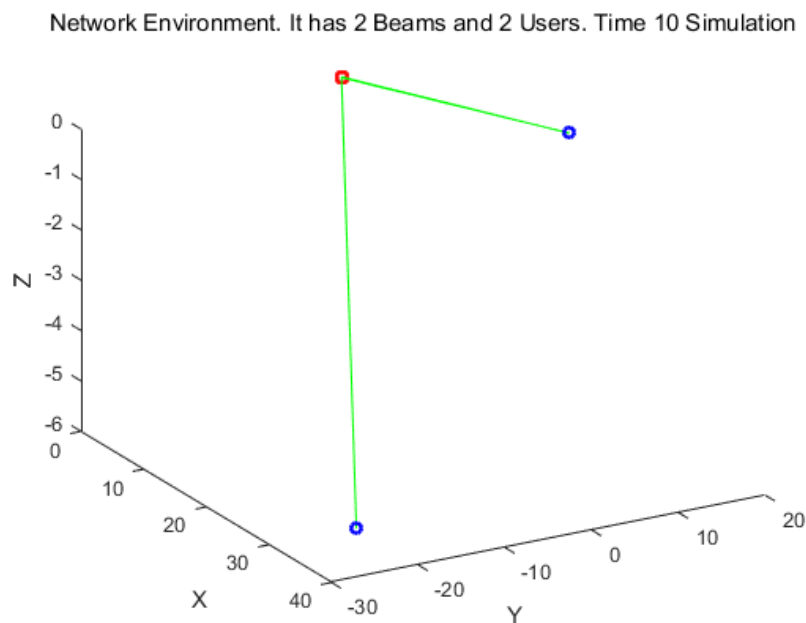


Figure 5- 35: The simulation result in UMa for 8×8 antenna arrays system

In the Figure 5-35, the green lines mean the direction of the beams and the blue points mean the center point for the clusters of UEs.

Figure 5-36 shows the 2 beams, respectively, in which each beam covers one UE. The green line is the main beam direction; the red lines are the directions of other beams and the black points are the UEs as shown in Figure 5-36.

The Atten.Rate = -19.6437dB  $\theta=35.2187$   $\phi=-70.7741$

The Atten.Rate = -19.6402dB  $\theta=46.5161$   $\phi=87.2634$

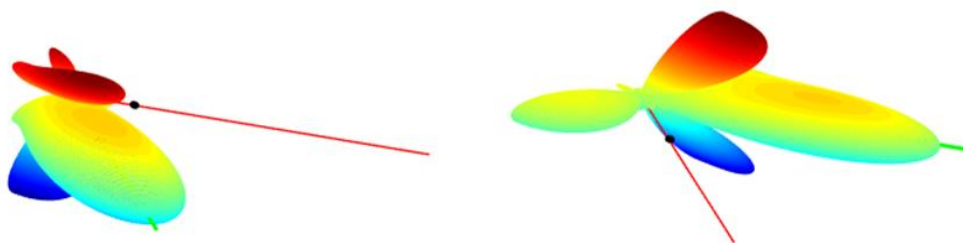
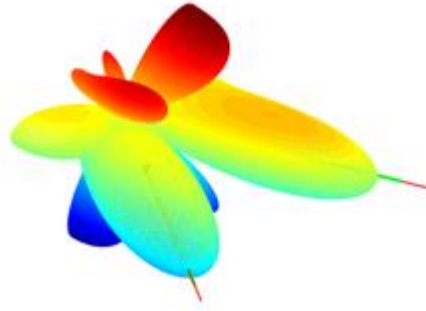


Figure 5- 36: The beams in the 8×8 antenna arrays system with 2 beams



**Figure 5- 37: The 3D beam in the 8×8 antenna arrays system with 2 beams**

The beams for the whole cell are shown in Figure 5-37, which are 2 beams for 2 UEs. In this figure, the main beams are not prominent because the side-lobes are much larger than the side-lobes in the 16×16 antenna arrays system with 2 beams.

The simulation system has been run 50 times to generate results for the CDF and PDF to be analyzed because the number of UEs is decreasing. The CDFs for the SINR for these two mm-wave systems are shown in Figure 5-38, where the results are compared when using the new weighting method and when not using it. The CDFs of the throughput for these two mm-wave systems are shown in Figure 5-39.

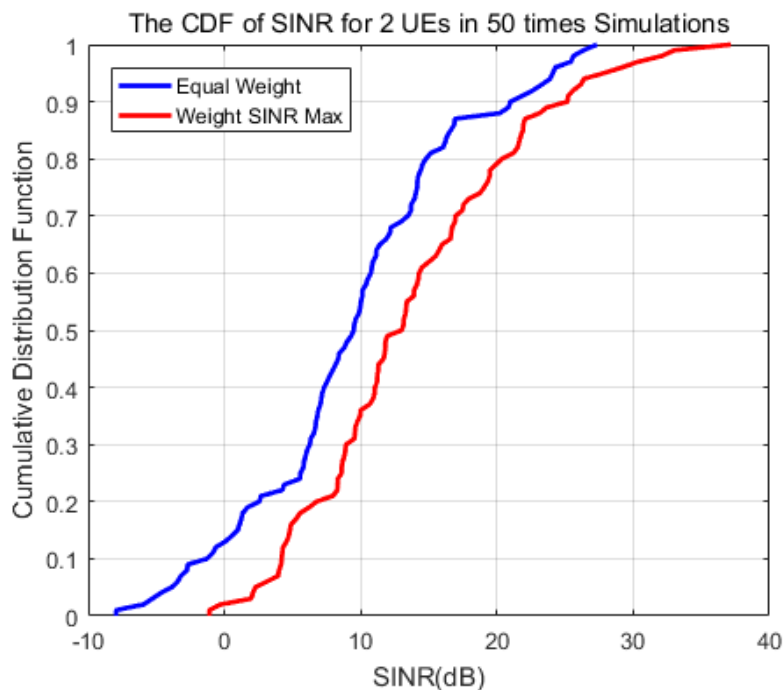


**Figure 5- 38: The CDF for the SINR in two mm-wave systems**

Figure 5-38 shows that the CDFs for the SINR are in these two mm-wave systems; the blue line is the SINR in the equal weighting mm-wave system; the red line the SINR in the new weighting mm-wave system.



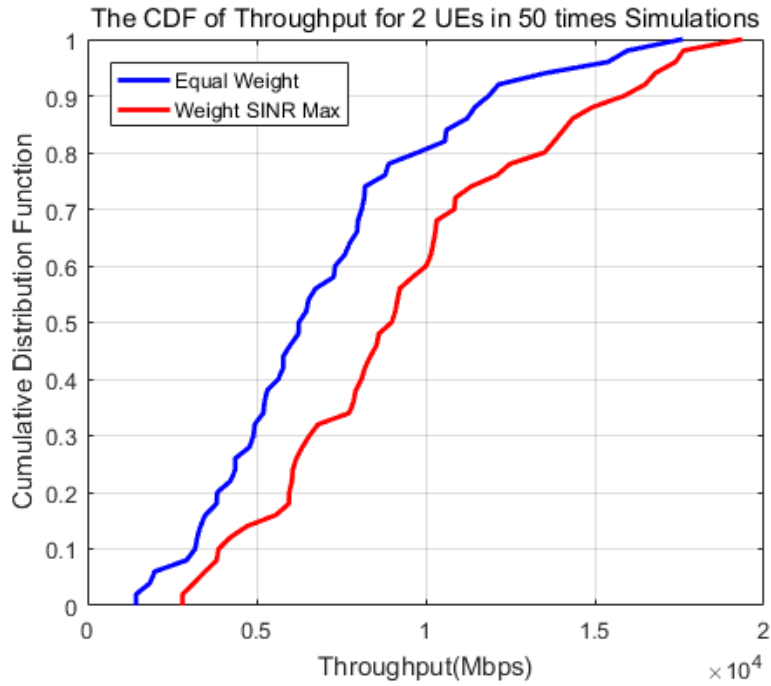


**Figure 5- 39: The CDF for the throughput in two mm-wave systems**

Figure 5-39 shows that the CDFs for the throughput are in these two mm-wave systems; the blue line is the throughput for the equal weighting mm-wave system; the red line the throughput for the new weighting mm-wave system.

In Figure 5-38, the CDFs of SINR are from -10 dB to 40 dB for these two mm-wave systems. The SINR results obtained using the new weighting method (red line) is always greater than SINR results obtained using the equal weighting method (blue line). For example, if the CDF is 90%, the SINR in the mm-wave system using the new weighting method are larger than 23 dB, but the SINR in the mm-wave system using the equal weighting method are smaller than 23 dB. Therefore, the new weighting method can increase the SINR in the mm-wave system. Moreover, the maximum value of SINR in this figure is larger than 36 dB, which is smaller than the maximum SINR in the  $16 \times 16$  antenna arrays system with 2 beams.

In Figure 5-39, the throughput, which is from the mm-wave system using the new weighting method (red line), is larger than the throughput when not using it (blue line) for the same CDF percent points. Moreover, the maximum value of throughput is smaller than the maximum throughput in the  $16 \times 16$  antenna arrays system with 2 beams. Moreover, the BER in three systems are shown in Figure 5-40 when the SNR is from 0 to 30 dB.

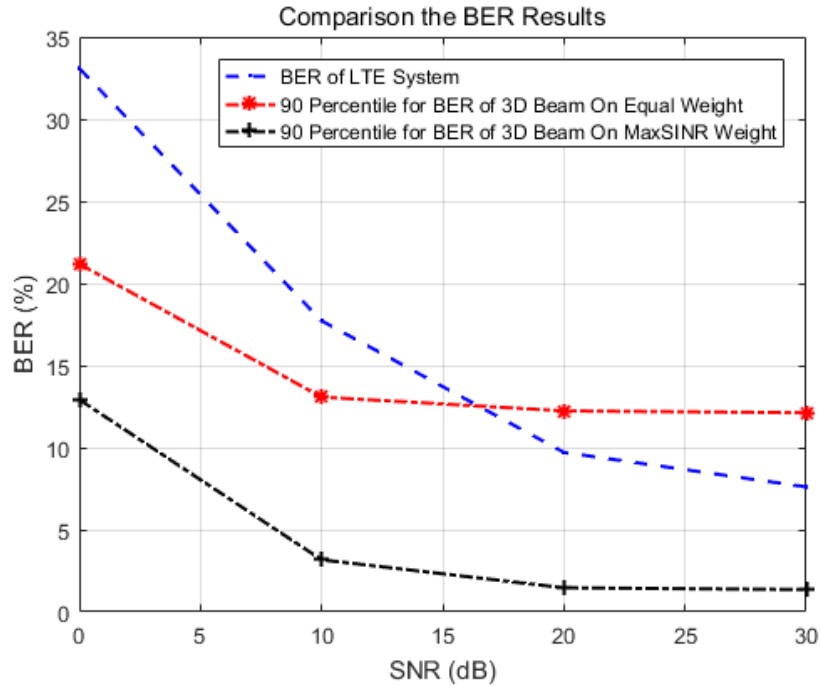


**Figure 5- 40: The BER in three systems when the SNR are 0 dB, 10 dB, 20 dB or 30 dB**

In Figure 5-40, the blue line is the BER in the  $4 \times 2$  LTE MIMO system; the red line is the 90% sample points for BER in the equal weighting mm-wave system; the black line is the 90% sample points for BER in the new weighting mm-wave system when the SNR are 0 dB, 10 dB, 20 dB and 30 dB.

There are 100 sample points for BER in these two mm-wave systems so the maximum values and minimum values are considered as outliers, which are far removed from the mass of data. Then the BER interval value is from 10% to 90%.

All of BER values in the new weighting mm-wave system are smaller than the BER in the  $4 \times 2$  LTE MIMO system as shown in Figure 5-40. However, the BER values in the equal weighting mm-wave system are larger than the BER in the  $4 \times 2$  LTE MIMO system when the SNR is larger than 16 dB. Therefore, when the size of antenna arrays in the mm-wave system is decreased, the BER is larger than BER in the  $4 \times 2$  LTE MIMO system if the mm-wave system is not used the new weighting method. The BER in these two mm-wave systems are shown in Figure 5-41 when the SNR is from 0 to 30 dB.

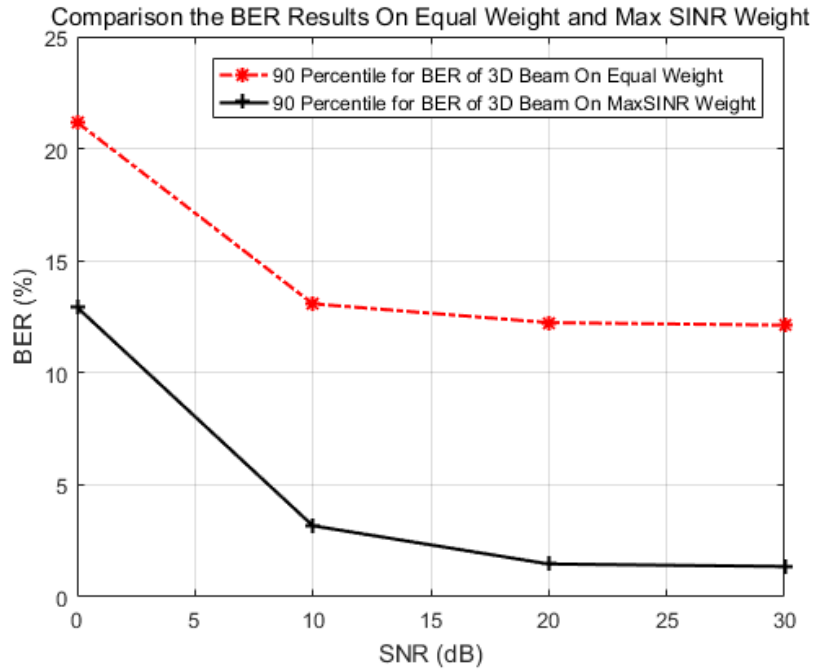


**Figure 5- 41: In the 2 beams system, the 90% sample points for BER in two mm-wave systems**

Figure 5-41 shows that the red line is the 90% sample points for BER in the equal weighting mm-wave system; the black line is the 90% sample points for BER in the new weighting mm-wave system when the SNR are 0 dB, 10 dB, 20 dB and 30 dB.

In Figure 5-41, the 90% sample points for BER in the new weighting mm-wave system are smaller than the 90% sample points for BER in the equal weighting mm-wave system. However, all of the BER values in  $8 \times 8$  antenna arrays mm-wave system are larger than the BER in the  $16 \times 16$  antenna arrays mm-wave system.

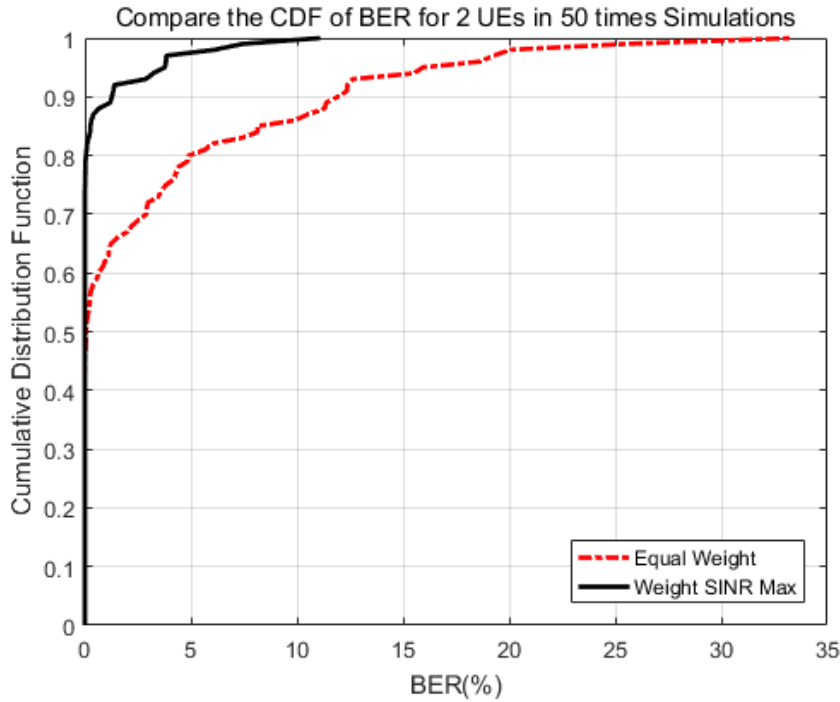


**Figure 5- 42: In the 2 beams system, the CDF of BER in two mm-wave systems**

Figure 5-42 shows that the red line is the CDF of BER in the equal weighting mm-wave system; the black line is the CDF of BER in the new weighting mm-wave system when the SNR is 0 dB to 15 dB.

This figure shows that the CDF of BER are from 0 to 35% and there are difference between these two mm-wave systems. The 80% sample points for BER values in the new weighting mm-wave system are close to zero. Moreover, the 50% sample points for BER values in the equal weighting mm-wave system are larger than zero. Therefore, the new weighting  $8 \times 8$  antenna arrays mm-wave system has decreased the BER more than the equal weighting  $8 \times 8$  antenna arrays mm-wave system. However, the BER in this  $8 \times 8$  antenna arrays mm-wave system are larger than the BER in new weighting  $16 \times 16$  antenna arrays mm-wave system.

To sum up, when the size of antenna arrays mm-wave system is decreased, the throughput and SINR is decreased, whilst the interference and the BER are increased.

### 5.5.3.2 The 1 beam in the $8 \times 8$ antenna arrays mm-wave system

The simulation was run 100 times with different seeds to show the results. Figure 5-43 shows that the result shows the tenth time among these 100 running times, the

number of UEs is 1 and there is 1 beam, the modulation is R.5 and the environment is UMa in the  $8 \times 8$  antenna arrays system with 1 beam.

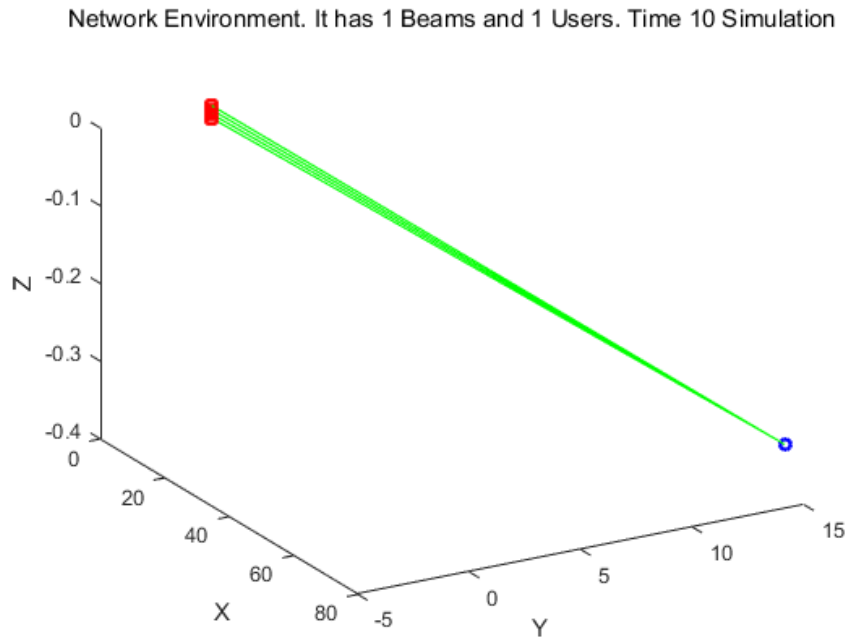


**Figure 5- 43: The simulation result in UMa for the  $8 \times 8$  antenna arrays system with 1 beam**

In Figure 5-43, the green line means the direction of the beams and the blue point means UE.

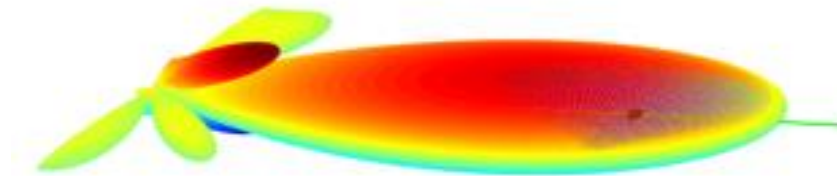


**Figure 5- 44: The 3D beam in the  $8 \times 8$  antenna arrays system with 1 beam**

Figure 5-44 shows the 1 beam covers one UE, in which the green line is the main beam direction, the red lines are the directions of other beams and the black points are the UEs.

The simulation system has been run 100 times to generate results for the CDF and PDF to be analyzed because the number of UE is 1. The CDF for the SINR for the mm-wave system is shown in Figure 5-45, where the results are compared when using the new weighting method and when not using it. Moreover, the CDFs of the throughput for these mm-wave systems are shown in Figure 5-46.

In Figure 5-45, the CDFs of SINR are from 20 dB to 55 dB for the mm-wave systems, which are larger than the values of SINR in the  $16 \times 16$  antenna arrays mm-wave system. The SINR results obtained using the new weighting method (red line) is always greater than SINR results obtained using the equal weighting method (blue line). For example, if the CDF is 90%, the SINR in the mm-wave system using the new weighting method are larger than 48 dB, but the SINR in the mm-wave system using the equal weighting method are smaller than 48 dB. However, the curves for these two mm-wave systems are close to each other. The effect of our new weighting method on the mm-wave system is smaller than hybrid beamforming system because there is one beam in analog beamforming system.

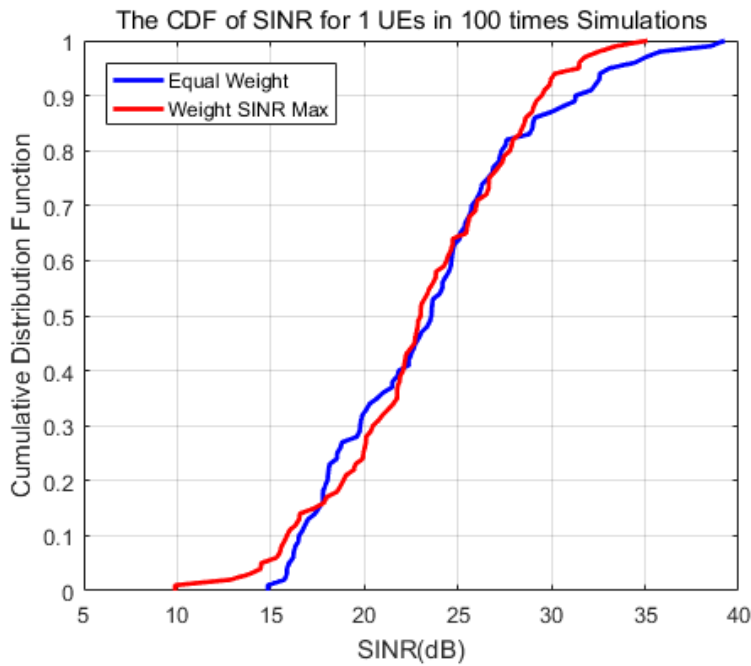


**Figure 5- 45: The CDF for the SINR in two mm-wave systems**

In Figure 5-45, the CDFs for the SINR are in these two mm-wave systems; the blue line is the SINR in the equal weighting mm-wave system; the red line the SINR in the new weighting mm-wave system.

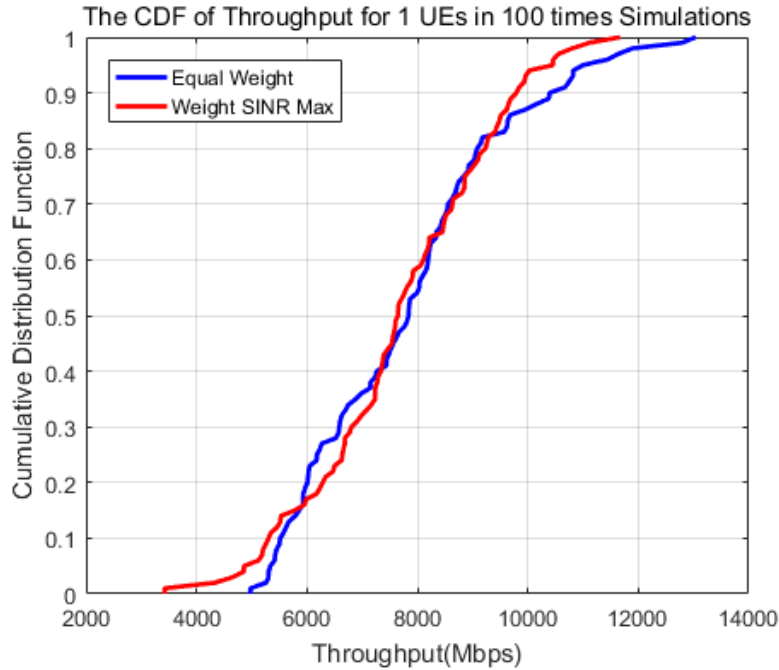


**Figure 5- 46: The CDF for the throughput in two mm-wave systems**

In Figure 5-46, the CDFs for the throughput are in the two mm-wave systems; the blue line is the throughput for the equal weighting mm-wave system; the red line is the throughput for the new weighting mm-wave system.

In Figure 5-46, the throughput, which is from the mm-wave system using the new weighting method (red line) are close to the throughput when not using it (blue line) for the same CDF percent points. Moreover, the maximum value of throughput in this system is smaller than the maximum throughput in the  $16 \times 16$  antenna arrays system. Moreover, the BER in three systems are shown in Figure 5-47 when the SNR is from 0 to 30 dB.

In Figure 5-47, the blue line is the BER in the LTE SISO system; the red line is the 90% sample points for BER in the equal weighting mm-wave system; the black line is the 90% sample points for BER in the new weighting mm-wave system when the SNR are 10 dB, 20 dB, 30 dB and 40 dB.

The 90% sample points for BER values in these two mm-wave systems are smaller than the BER in the LTE SISO system as shown in Figure 5-47 so the analog beamforming mm-wave system has better signal quality over the LTE SISO system. However, the new weighting matrix can be replaced by the equal weighting matrix because the BER values in these two systems are similar in the analog beamforming

mm-wave system. Therefore, the new weighting method is not the necessary, which cannot make the BER values be less than the BER values from the equal weighting method in the analog beamforming mm-wave system.

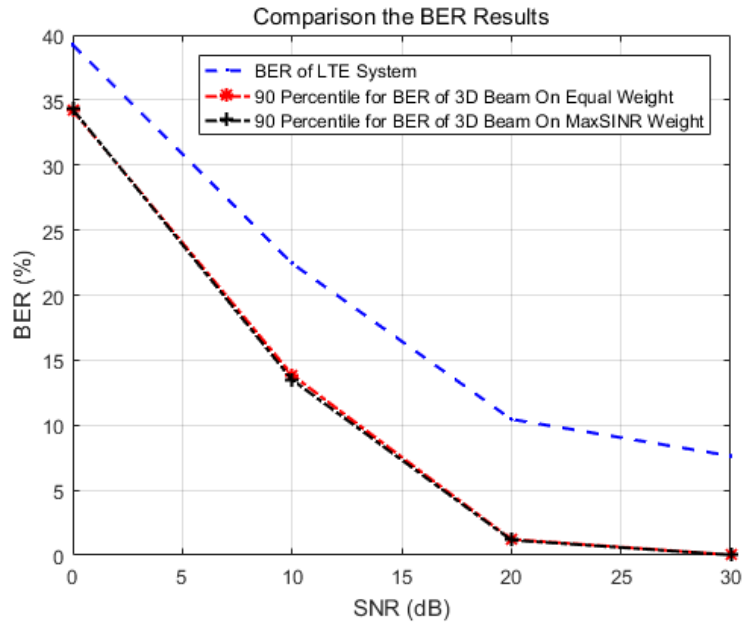


Figure 5- 47: The BER in three systems when the SNR are 10 dB, 20 dB, 30 dB or 40 dB

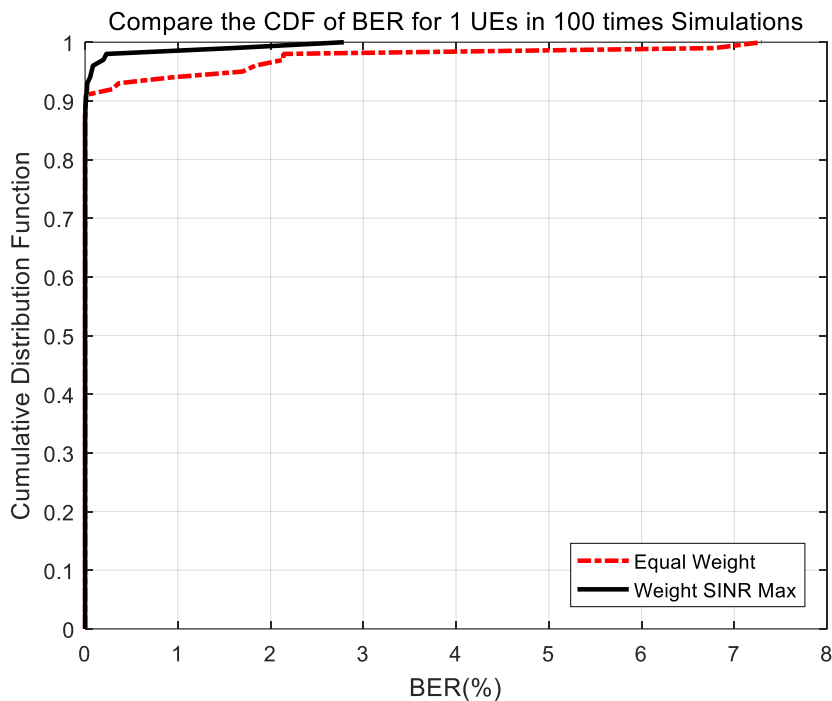


Figure 5- 48: The CDF of BER in two mm-wave systems when the SNR is 0 dB to 15 dB

In Figure 5-48, the red line is the CDF of BER in the equal weighting mm-wave system; the black line is the CDF of BER in the new weighting mm-wave system when the SNR is 0 dB to 15 dB.



In this figure, the 90% sample points for BER in the new weighting mm-wave system are same as the equal weighting mm-wave system, which are close to zero. Therefore, the new weighting methods are not taking effect on this mm-wave system. In the analog beamforming system, the new weighting method cannot have a contribution to improve the performance of the mm-wave system.

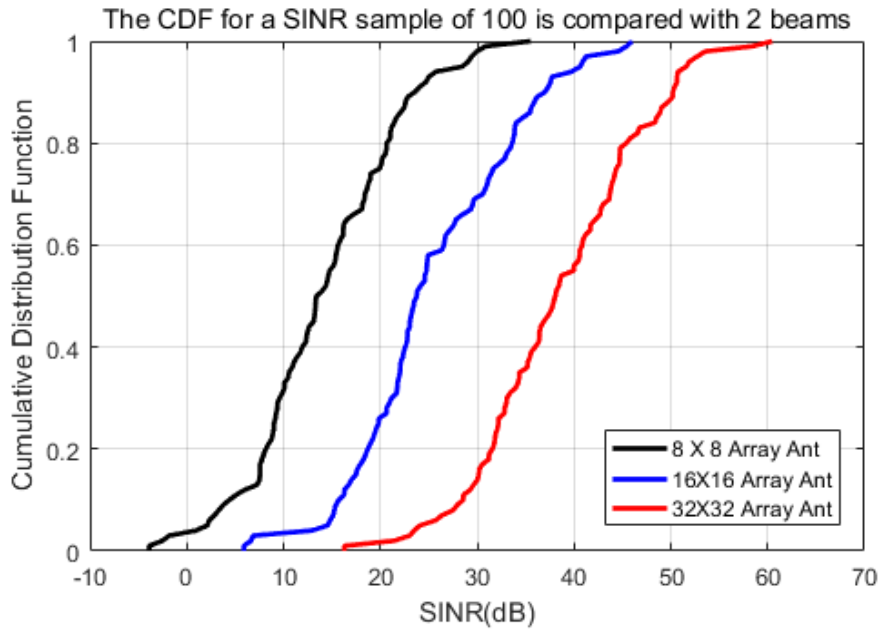
#### 5.5.4 Comparison of the results

This part shows that the results for different sizes of antenna arrays that transmits a different number of beams, in which the SINR for these three systems are compared. Moreover, in Chapter 5.5, the simulation system BER results have shown when the SNR is from 0 to 30 dB so the CDFs of BER for these three systems are compared in this chapter when the SNR is 10 dB. The types of systems that are compared using simulation are shown in Table 5-3.

**Table 5- 3: The parameters for comparison systems**

<b>The size of antenna array</b>	<b>The number of beams</b>	<b>SNR</b>
32×32	2	10 dB
	4	
16×16	2	10 dB
	4	
8×8	2	10 dB
	4	

When there are 2 beams in these three new weightingmm-wave systems, the CDFs for the SINR are shown in Figure 5-49. Moreover, when there are 4 beams in these three new weightingmm-wave systems, the CDFs for the SINR are shown in Figure 5-50.



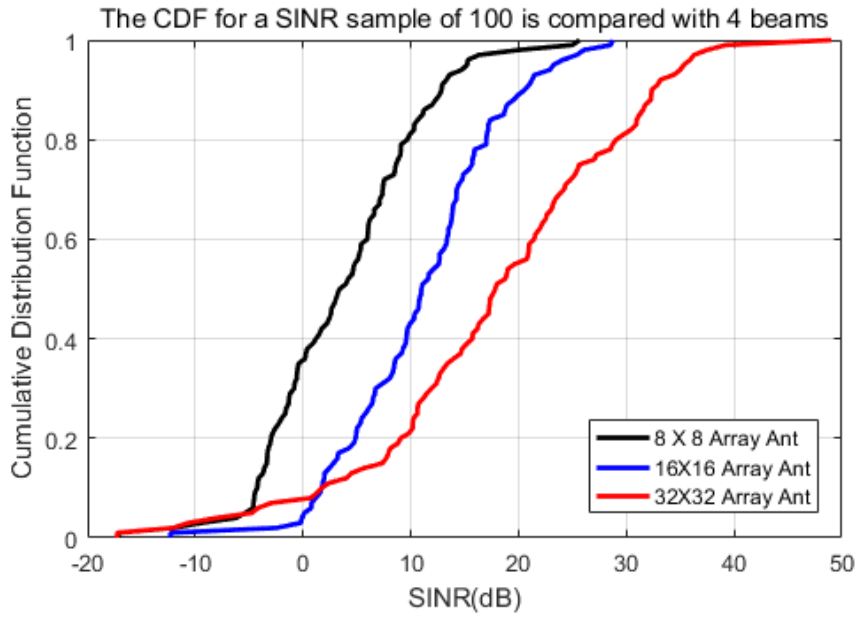
**Figure 5- 49: The CDF for the SINR in 2 beams mm-wave system**

Figure 5-49 shows that the CDFs for the SINR are in these 2 beams mm-wave systems, in which the black line is the SINR in the 8×8 antenna array mm-wave system; the blue line is the SINR in the 16×16 antenna array mm-wave system; the red line is the SINR in the 32×32 antenna array mm-wave system.

In Figure 5-49, the detailed SINR results for these three new weighting mm-wave systems are shown in Table 5-4. The SINR values in the 32×32 antenna array mm-wave system are largest among these three new weighting mm-wave systems when the number of beams is 2.

**Table 5- 4: The detailed SINR for the simulation results in Figure 5-50**

<b>CDF (%)</b>	<b>SINR(dB)8×8 antenna array</b>	<b>SINR(dB)16×16 antenna array</b>	<b>SINR(dB)32×32 antenna array</b>
10	4.392201	15.71406	28.5464
20	8.191428	18.71568	31.55939
30	9.604234	21.18126	33.08332
40	11.91541	22.55713	35.99212
50	13.40112	23.76783	38.07711
60	15.63784	26.57336	40.84994
70	18.41256	30.57251	43.69442
80	20.65056	33.63216	45.39749
90	23.54791	36.97355	50.20683
100	35.52434	45.98612	60.47485



**Figure 5- 50: The CDF for the SINR in 4 beams mm-wave system**

Figure 5-50 shows that the CDFs for the SINR are in these 4 beams mm-wave systems, in which the black line is the SINR in the  $8 \times 8$  antenna array mm-wave system; the blue line is the SINR in the  $16 \times 16$  antenna array mm-wave system; the red line is the SINR in the  $32 \times 32$  antenna array mm-wave system.

In Figure 5-50, the detailed SINR results for these three new weighting mm-wave systems are shown in Table 5-5. When the CDF is smaller than 10%, then some of SINR values in the  $32 \times 32$  antenna array mm-wave system are smaller than the SINR values in the  $16 \times 16$  and  $8 \times 8$  antenna array mm-wave systems, but all of SINR values in the  $32 \times 32$  antenna array mm-wave system are largest when the CDF is larger than 10%.

**Table 5- 5: The detailed SINR for results in Figure 5-50**

<b>CDF (%)</b>	<b>SINR(dB)<math>8 \times 8</math> antenna array</b>	<b>SINR(dB)<math>16 \times 16</math> antenna array</b>	<b>SINR(dB)<math>32 \times 32</math> antenna array</b>
10	-4.249709059	1.7311902	1.713184133
20	-2.969022699	4.880672146	9.047170867
30	-0.817302774	6.719007524	11.92066011
40	1.195894795	9.581131144	15.7166165
50	3.379609134	10.97562081	17.83741877
60	5.957372165	13.35009429	21.44949531
70	7.39089879	14.24991103	24.22052124
80	9.680346872	17.00770967	29.05055278
90	12.85155952	20.57011291	32.35393035
100	25.67378694	28.72804062	49.00789586

When there are 2 beams in these three new weighting mm-wave systems, the CDFs for the BER are shown in Figure 5-51. When there are 4 beams in these three new weighting mm-wave systems, the CDFs for the BER are shown in Figure 5-52.

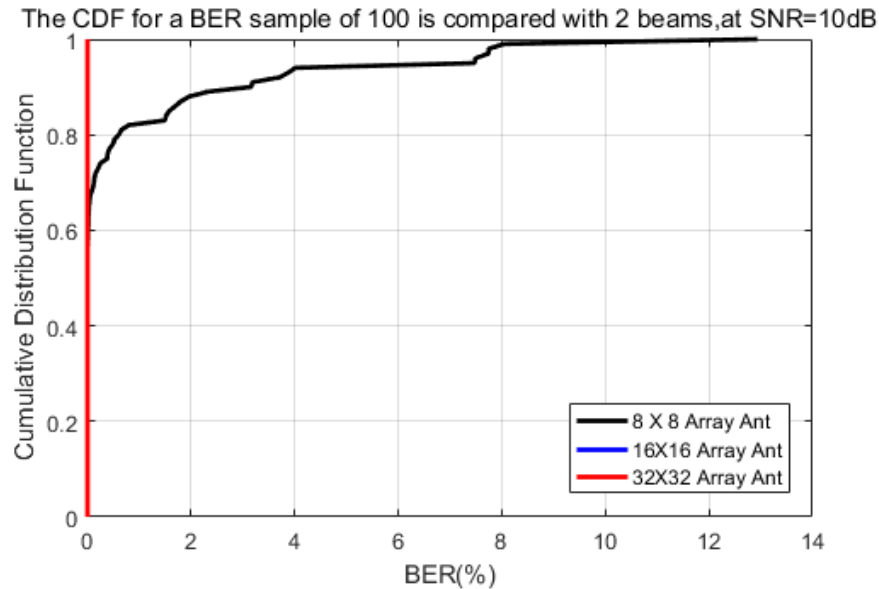


Figure 5- 51: The CDF for the BER in 2 beams mm-wave system

Figure 5-51 shows that the CDFs for the BER are in these 2 beams mm-wave systems, in which the black line is the SINR in the 8×8 antenna array mm-wave system; the blue line is the SINR in the 16×16 antenna array mm-wave system; the red line is the SINR in the 32×32 antenna array mm-wave system.

In Figure 5-51, the detailed CDFs for BER are in these three new weighting mm-wave systems when the number of beams is 2, which are shown in Table 5-6. The 90% of BER values in the 16×16 antenna array mm-wave systems are zero. All of the BER values in the 32×32 antenna array mm-wave systems are zero. However, the BER values in the 8×8 antenna array mm-wave system are not zero when the CDF is larger than 50%.

Table 5- 6: The detailed CDF for BER in Figure 5- 51

CDF (%)	BER(%)8×8 antenna array	BER(%)16×16 antenna array	BER(%)32×32 antenna array
10	0	0	0
20	0	0	0
30	0	0	0
40	0	0	0
50	0	0	0

60	0.011051	0	0
70	0.125075	0	0
80	0.603777	0	0
90	3.159032	0	0
100	12.93651	0.002512	0

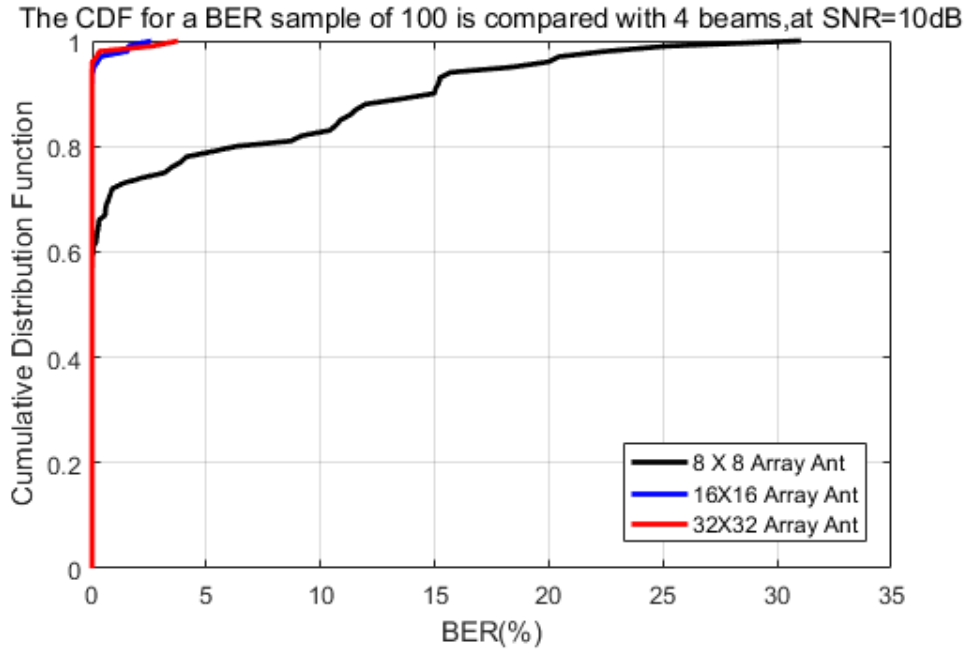


Figure 5- 52: The CDF for the BER in 4 beams mm-wave system

Figure 5-52 shows the CDFs for the BER are in these 4 beams mm-wave systems, in which the black line is the SINR in the  $8 \times 8$  antenna array mm-wave system; the blue line is the SINR in the  $16 \times 16$  antenna array mm-wave system; the red line is the SINR in the  $32 \times 32$  antenna array mm-wave system

In Figure 5-52, the detailed CDFs for BER are in these three new weighting mm-wave systems when the number of beams is 4, which are shown in Table 5-7. The 80% of BER values in the  $16 \times 16$  antenna array mm-wave systems are zero. And the 90% of the BER values in the  $32 \times 32$  antenna array mm-wave systems are zero. However, the BER values in the  $8 \times 8$  antenna array mm-wave system are not zero when the CDF is larger than 50%.

**Table 5- 7: The detailed CDF for BER in Figure 5-52**

<b>CDF (%)</b>	<b>BER(%)8×8 antenna array</b>	<b>BER(%)16×16 antenna array</b>	<b>BER(%)32×32 antenna array</b>
10	0	0	0
20	0	0	0
30	0	0	0
40	0	0	0
50	0.001005	0	0
60	0.049226	0	0
70	0.727346	0	0
80	6.327607	0	0
90	14.9789	0.005525	0
100	31.03627	2.581877	3.762307

To sum up, the size of antenna array has an effect on the new weighting mm-wave systems, which should be as large as possible. In the results,  $32 \times 32$  antenna array mm-wave systems have the best performance in SINR and BER. Moreover, the size of antenna array should not be smaller than  $8 \times 8$  because the beam patterns are much too wide, which makes the interference between each beam much bigger. When the number of beams is increased, the BER for these three mm-wave systems are increased. Therefore, the size of antenna array should be more than  $32 \times 32$  (such as  $128 \times 128$ ) in mm-wave system when the massive number of beams need to be transmitted.

## **5.6 Conclusion**

The simulation systems show that our ideas can improve the mm-wave system performance, when the carrier the frequency is 28 GHz and the PL model, given in reference [100], is used. The simulation for mm-wave system shows that the new weighting method can reduce the interference between each beam. In order to illustrate that the new method with the weighting is more advanced, the comparison of the simulation results with another mm-wave system that used an equal weighting matrix as the weighting method was performed. The result shows that the BER from the mm-wave system is lower compared with the BER from the LTE MIMO system by quantifying the average SNR. These simulation systems are achieved by obtaining:

1. The 3D network environment for the mm-wave new weighting simulation system;
2. The beam patterns for the mm-wave new weighting simulation system;
3. The constellation figure of the received signals in these two mm-wave systems;
4. The CDF of the SINR in these two mm-wave systems;
5. The CDF of the throughput in these two mm-wave systems;
6. The BER of these two mm-wave simulation systems, which are compared with the LTE MIMO system or the LTE SISO system;
7. The comparison of the CDFs and PDFs of BER in these two mm-wave systems with using the new weighting method or not using;
8. The comparison of the CDF of SINR in the different size of antenna arrays transmit the different number of beams for the new weighting mm-wave system;
9. The comparison of the CDF of BER in the different size of transmitting antenna arrays, the different number of beams for the new weighting mm-wave system.

The results show the mm-wave system has already obtained a definite improvement for signal quality over the 4G LTE system. Moreover, the new weighting method has a greater contribution to reduce interference. However, the size of antenna array should be as large as possible because the beam pattern are narrower when the size of antenna array are larger, which can make the side lobes much smaller to decrease the interference.

# **Chapter 6**

## **Discussion, Conclusions and Future Work**



## 6.1 Discussion

Chapter 4 and Chapter 5 have shown the simulation system results for the 3D beamforming LTE system and the mm-wave system. The constellation figures show that the received signals in these two systems are better than the received signals in the LTE system so these two mm-wave systems have better signal quality over the LTE system.

In the 3D beamforming LTE simulation system, the network environment figure shows that the system can use the less number of beams than the number of UEs to cover each UE with using the K-mean clustering algorithm. The number of UEs is an influential parameter for BER in the same environment so decreasing the number of UEs with using the K-mean clustering algorithm is necessary when the multiple UEs need be transmitted.

The 3D beamforming LTE system has a larger cell maximum radius than the 4×4 LTE MIMO system because the 3D beamforming LTE system can have more number of antennas in transmitter and the energy from the antenna array can focus in one direction. However, the distance of propagation in the mm-wave system is the shortest value in the 4×4 LTE MIMO system, the 3D beamforming LTE system and the mm-wave system.

The challenge in the mm-wave system is that the carrier frequency is the highest (such as 28GHz) value, which makes the signal attenuation are very much larger. In other words, the signal cannot be transmitted farther away even there is a huge value of transmitting power. Therefore, the mm-wave technology is usually used to the indoor transmission or the short-range outdoor transmission, which cannot penetrate any obstacles. If there are buildings as the obstacles in the outdoor transmission, the 3D beamforming LTE system can be applied to transmit signal because its carrier frequency is about 6GHz to 10GHz, which can be used to the remote transmission.

The BER in the 3D beamforming LTE simulation system and the hybrid beamforming mm-wave simulation system are smaller than the BER in the LTE simulation system. Therefore, the new weighting method has a contribution to improve

the performance of these two systems. Moreover, the Chapter 5.5 shows that the larger size of antenna array can make the energy be more focused in one desired direction. The interference from the side lobes are less than the other smaller size of antenna array systems when the number of beams are same. Therefore, when the number of UEs is increasing, the size of antenna array should be as large as possible because the beam patterns should be kept narrow, which can make the energy from the antenna array focused in the desired direction and the signal quality not be reduced.

The K-mean clustering algorithm and the new weighting method can be used for a wide range of applications in the 5G beamforming system. For example, the massive MIMO system, the satellite communication, the digital video broadcasting baseline terrestrial system, the mobile communication and wireless network. The most of communication systems, which need the beamforming technology to transmit the signal into multiple UEs, can be used them.

## **6.2 Conclusions**

In this research, the improvements of 3D beamforming technology in the antenna array using in the Full Dimension Multiple-Input Multiple-Output (FD-MIMO) system and Millimeter-wave (mm-wave) system have been proposed, which are the improved K-means clustering algorithm and the maximum SINR weighting method. Moreover, both of them can enhance the performance for 3D beamforming systems, which is approved by the simulation results. In Chapter 2, some of relevant literatures about the key technologies in 5G communication system have been introduced in detail in this chapter. The main technology, which was chosen from them to be researched and improved in this thesis, is the 3D beamforming technology. The first reason for using the 3D beamforming technology as the key researching focus among these technologies is that it can make the energy from the antenna array focus in one direction, which means that they can be transmitted farther away. The second reason is that the 3D beamforming technology allows the antenna to use the higher carrier frequencies (such as 10GHz, 28GH and 73GH).In the communication system, the bandwidth is limited

so the carrier frequency needs be increased in order for broader bandwidths to be available, but the signals experience severe PL and rain fading when the carrier frequency is increased. Therefore, the signal cannot be transmitted too far when the carrier frequency is higher (such as higher than 20GHz) if the communication system does not use the 3D beamforming technology.

The Chapter 3 shows the contribution to minimize the side lobes in beamforming system. To overcome the challenges from 3D beamforming technology, the K-means algorithm clustering and the new weighting method have been used. Even when multiple UEs need to be covered with multiple beams, the K-means algorithm has the optimal grouping to cluster the UEs. The minimum number of beams can cover all of UEs if our calculation method is used, in order to the narrow beam can cover multiple UEs. However, there is more interference between these beams from their side lobes when the multiple beams are transmitted by same antenna array. For overcoming this problem, we proposed a new method to construct the weighting matrix, which can make the main beam have the maximum value in the desired direction and its side lobes have the minimum values in other undesired directions. This new weighting matrix is combined by the horizontal direction weighting vector and the vertical direction weighting vector. The calculation methods for two weighting vectors are described in this chapter, which can be determined by the least-squares solution of the matrix. Afterward, the received signal for the system how to be obtained by the new weighting matrix are shown, which can be used in simulation systems.

In order to test our proposed methods, the simulation is finished applying our ideas in the 3D beamforming LTE system and the mm-wave system respectively. The results show not only the 3D beamforming LTE system but also the mm-wave system has already obtained a definite improvement for signal quality over the 4G LTE system.

In Chapter 4, when the beamforming technology transmits the different signals at the same time with using the same bandwidth, there are two problems. The first problem of the 3D beamforming technology is that how to use the beams to cover multiple UEs in different directions. The second problem is that there is interference between each beam when they are transmitted at the same time. In order to solve these problems an

enhanced dynamic beamforming algorithm is proposed, where the beamforming vector can be obtained according to both the UEs' horizontal and vertical directions. The new weighting method not only adjusts the values of the weighting matrix to direct the main beam in a desired direction but also minimise its side lobes in other specific directions.

In Chapter 5, the 3D beamforming technology is a key technology for mm-wave system in the 5G system. Analog beamforming restricts the size of antenna array and number of beams whereas Hybrid Beamforming and Digital Beamforming allows the effective increase in antenna array and number of beams, which in turn improves the SINR and BER performance. However, there are two challenges in the 3D hybrid beamforming for mm-wave system. The first challenge is how to use the beams to cover multiple UEs in different directions. The second is the interference between each beam when they are transmitted simultaneously. This thesis provides a new method to calculate the weighting matrix for the hybrid beamforming system. The new weighting method then adjusts the values of weighting matrix to direct the main beam in a desired direction and minimize its side lobes in other specific directions. The weighting method prefers to be used in the hybrid beamforming system because it is not practically functional in the analog beamforming system. In the future, the new weighting method not only is used in the mm-wave system, but also is applied in the long-distance communication because it can reduce the interference between the each beam when the energy is focused on the main beam direction.

To sum up, the main aim of the thesis is providing the improvement schemes to be applied the 3D beamforming system. Moreover, the 3D beamforming system and the mm-wave systems are simulated to test and verify the methods can be operated in the 5G communication system. The aims and contributions of this research have provided improvements to improve the performance of the next communication system.

### **6.3 Future Work**

After having completed the research into this investigated subject, a lot of relevant further researches could be started as the future work. The following provides some

potential research issues, but obviously these further investigations are not limited to these topics:

1. Coordinated multipoint transmission and reception techniques in LTE system has been proved to bring significant gains to system performance since it can mitigate the inter-cell interference to increase the received power especially for cell-edge UEs. How to use our proposed methods in the coordinated multipoint transmission and reception techniques is needed to be investigated.
2. The hybrid beamforming mm-wave simulation system results express that the BER values can be smaller if size of antenna array is larger in Chapter 5.5. Moreover, the values of BER in R.0 (16-QAM) system are smaller than the values of BER in R.5 (64-QAM) system in the 3D beamforming LTE simulation system. Therefore, when the power of Quadrature Amplitude Modulation is increased such as 256-QAM, the values of BER are increased so the size of antenna array should be increased such as  $128 \times 128$ . In the future, the 256-QAM can be extensive used in the 5G communication system. Therefore, the  $128 \times 128$  antenna array system is one of the most important research subjects.
3. Our mm-wave simulation system is based on the PL formula, which is derived by real-world measurements at 28 and 73 GHz in New York, NY, USA [Chapter2 Ref.100]. In the future, the 3GPP organization can provide the IMT-2020 (5G) standardization, which is based on being used to improve our mm-wave simulation system.

# References:

- [1] Hamzeh Beyranvand, Martin Lévesque, Martin Maier, et al., “Toward 5G: FiWi Enhanced LTE-A HetNets With Reliable Low-Latency Fiber Backhaul Sharing and WiFi Offloading”, *IEEE/ACM Transactions on Networking*, vol. 25, pp. 690-707, 2017.
- [2] Jeffrey G. Andrews, Stefano Buzzi, Wan Choi, et al., “What Will 5G Be?”, *IEEE Journal on Selected Areas in Communication*, vol. 32, pp. 1065-1082, 2014.
- [3] Stefano Buzzi, Carmen D’Andrea. “Massive MIMO 5G Cellular Networks: mm-Wave vs.  $\mu$ -Wave Frequencies”, *ZTE Communications*, vol. 15, pp. 41-49, 2017.
- [4] Federico Boccardi, Vodafone Robert W. Heath Jr., Angel Lozano. “Five Disruptive Technology Directions for 5G”, *IEEE Communications Magazine*, vol. 52, pp. 74-80, 2014.
- [5] Theodore S. Rappaport, Shu Sun, Rimma Mayzus, et al., “Millimeter wave mobile communications for 5G cellular: It will work!”, *IEEE Access*, vol. 1, pp. 335-349, 2013.
- [6] S Kutty, D Sen, “Beamforming for Millimeter Wave Communications: An Inclusive Survey”, *IEEE Communications Surveys & Tutorials*, vol. 18, pp. 949-973, 2016.
- [7] Jean-Marc Kelif, Marceau Coupechoux, Mathieu Mansanarez, “A 3D beamforming analytical model for 5G wireless networks”, *14th International Symposium on Modeling and Optimization in Mobile, Ad Hoc, and Wireless Networks*, pp. 1-8, 2016.
- [8] Chao He, Richard D. Gitlin, “System Performance of Cooperative Massive MIMO Downlink 5G Systems”, *Wireless and Microwave Technology*

- Conference, IEEE 17th Annual, Conference Location: Clearwater, FL, USA, pp. 11-13, 2016.
- [9] Xiang Cheng, Bo Yu, Liuqing Yang, et al., “Communicating In The Real World: 3D MiMO”, IEEE Wireless Communications, vol. 21, pp.136-144, 2014.
- [10] 3GPP TR 36.873, “Study on 3D channel model for LTE”, 2015.
- [11] J. Koppborg, H. Halbauer, S. Saur and C. Hoek, “3D Beamforming Trials with an Active Antenna Array”, International ITG Workshop on Smart Antennas, pp. 110-114, 2012.
- [12] Manh-Tuan Dao, Viet-Anh Nguyen, Yun-Taek Im, et al., “3D polarized channel modeling and performance comparison of mimo antenna configurations with different polarizations”, IEEE Transactions on Antennas and Propagation, vol. 59, pp. 2672-2682, 2011.
- [13] Zhengzheng Xiang, Meixia Tao, Xiaodong Wang, “Coordinated Multicast Beamforming in Multicell Networks”, IEEE Transactions on Wireless Communications, vol. 12, pp. 12-21, 2013.
- [14] Tin-Yu Wu, Tse Chang, “Interference Reduction by Millimeter Wave Technology for 5G-Based Green Communications”, IEEE Access, vol. 4, pp. 10228–10234, 2016.
- [15] J. Foutz, A. Spanias, S. Bellofiore, C. A. Balanis, “Adaptive eigen-projection beamforming algorithms for 1D and 2D antenna arrays”, IEEE Antennas and Wireless Propagation Letters, vol. 2, pp. 62-65, 2003.
- [16] Yan Li, Xiaodong Ji, Dong Liang, Yuan Li, “Dynamic Beamforming for Three-Dimensional MIMO Technique in LTE-Advanced Networks”, International Journal of Antennas and Propagation, vol. 2013, pp. 1-8, 2013.
- [17] Yiyan Zhang, Pinyi Ren, Li Sun, et al., “Antenna Tilt Assignment for Three-Dimensional Beamforming in Multiuser Systems”, IEEE Global Communications Conference, pp. 6-10, 2015.

- [18] Yuan Yuan, Ying Wang, Weidong Zhang, Fei Peng. “Separate Horizontal & Vertical Codebook Based 3D MIMO Beamforming Scheme in LTE-A Networks”, IEEE 78th Vehicular Technology Conference, pp. 1-5,2013.
- [19] Elpiniki P. Tsakalaki, Luis A’ngel Maestro Ruiz de Temiñõ, Tomi Haapala, et al., “Deterministic Beamforming for Enhanced Vertical Sectorization and Array Pattern Compensation”, 6th European Conference on Antennas and Propagation, pp. 2789-2793, 2012.
- [20] Wonil Roh, Ji-Yun Seol, Jeongho Park, et al., “Millimeter-Wave Beamforming as an Enabling Technology for 5G Cellular Communications: Theoretical Feasibility and Prototype Results”, IEEE Communications Magazine, vol. 52, pp. 106-113, 2014.
- [21] Foad Sohrabi, Wei Yu, “Hybrid Digital and Analog Beamforming Design for Large-Scale Antenna Arrays”, IEEE Journal of Selected Topics In Signal Processing, vol. 10, pp. 501-513, 2016.
- [22] Zheda Li, Shengqian Han, Andreas F. Molisch, “Optimizing Channel-Statistics-Based Analog Beamforming for Millimeter-Wave Multi-User Massive MIMO Downlink”, IEEE Transactions on Wireless Communications, vol. 16, pp. 4288-4303, 2017.
- [23] Jing-xiang Yin, “Directional Constant Beamwidth Beamforming by Second Order Cone Programming Constraints”, 5th International Conference on BioMedical Engineering and Informatics, pp. 1443-1445, 2012.
- [24] Xin Song, Jinkuan Wang, Bin Wang. “Robust blind adaptive beamforming under double constraints”, Neural Computing & Application, vol. 22, pp. 295 – 302,2013.
- [25] Haohai Sun, Shefeng Yan, U. Peter Svensson. “Robust Minimum Sidelobe Beamforming for Spherical Microphone Arrays” IEEE Transactions on Audio, Speech, and Language Processing, vol. 19, pp.1045-1051, 2011.
- [26] Haohai Sun, Shefeng Yan, U. Peter Svensson, Hao-Feng Sun. “Spherical Harmonics Based Optimal Minimum Sidelobe Beamforming for Spherical



- Sensor Arrays”, International ITG workshop on smart antennas, pp. 286-291 2010.
- [27]Qurrat-Ul-Ain Nadeem, Abla Kammoun, Mérouane Debbah, Mohamed-Slim Alouini, “Design of 5G Full Dimension Massive MIMO Systems”, IEEE Transactions on Communications, vol. 66, pp.726-740, 2018.
- [28]Erik Dahlman Stefan ParkvallJohan Skold. “4G, LTE-Advanced Pro and The Road to 5G”, Academic Press, 2016.
- [29]3GPP TR 36.814, “Evolved Universal Terrestrial Radio Access (E-UTRA); Further advancements for E-UTRA physical layer aspects”, 2010.
- [30]3GPP Release 11, “Understanding the Standards for HSPA+ and LTE\_Advanced Enhancements”, 2014.
- [31]3GPP TS 36.213, “Evolved Universal Terrestrial Radio Access (E-UTRA); Physical layerprocedures”, 2009.
- [32]Chang R. W., “Synthesis of Band-Limited Orthogonal Signals for Multichannel Data Transission”, Bell Labs Technical Journal, vol.45, pp.1775 – 1796, 1966.
- [33]Weinstein S. B. , P. M. Ebert, “Data Transmission of Frequency Division .Multiplexing Using the Discrete Frequency Transform”, IEEE Transactions on Communications, vol.19, pp.623-634, 1971.
- [34]Peled A., A.Ruiz, “Frequency Domain Data Transmission Using Reduced Computational Complexity Algorithms”, IEEE International Conference on Acoustics, Speech and Signal Processing , pp.964-967, 1980.
- [35]A.J.Paulraj T. Kailat, “Increasing Capacity in Wireless Broadcast Systems Using Distributed Transmission Directional Reception”, U.S, Patent, 1994.
- [36]I.E. Telattar, “Capacity of Multi-Antenna Gaussian Channels”, European Transactions On Telecommunications, vol.6, pp.311-335, 1998.

- [37]G.J. Foschini, “Layered Space-Time Architecture for Wireless Communication in a Fading Environment When Using Multi-Element Antenna”, Bell Labs Technical Journal, pp.41-59, 1996.
- [38]JunhongYe, Ying Jun Angela Zhang, “Low- complexity downlink MMSE beamforming in massive MIMO systems, IEEE International Conference on Ubiquitous Wireless Broadband”, pp. 1 – 4, 2016.
- [39]3GPP Technical Specification TS 36.101, “User Equipment (UE) radio transmission and reception”, 2016.
- [40]Yuefeng Peng, Wei Yang, Yuan Zhu, Xiaogang Chen, “Transmission Scheme for 2D Antenna Array MIMO Systems with Limited Feedback”, Wireless Personal Communications, vol. 75, pp. 759–774, 2014.
- [41]Nasim Ebrahimi, Abbas Pirhadi, Majid Karimipour, “Optimum Design of Shaped Beam Cylindrical Array Antenna with Electronically Scan Radiation Pattern”, Advanced Computational Techniques in Electromagnetics, vol. 2013, pp. 1–11, 2013.
- [42]Yan Li, Xiaodong Ji, Mugen Peng, et al., “An Enhanced Beamforming Algorithm for Three Dimensional MIMO in LTE-Advanced Networks”, International Conference on Wireless Communications & Signal Processing, pp. 24-26, 2013.
- [43]Jianquan Huang, Feng Qiu, Wei Lin, et al., “A New Compactand High Gain Circularly-Polarized Slot Antenna Array for Ku-Band Mobile Satellite TV Reception”, IEEE Access, vol. 5, pp. 6707- 6714, 2017.
- [44]Younsun Kim, Hyoungju Ji, Juho Lee, et al., “Full dimension MIMO (FD-MIMO): The next evolution of MIMO in LTE systems”, IEEE Wireless Communications, vol. 21, pp. 92-100, 2014.
- [45]Frank B. Gross, “Smart Antennas for Wireless Communications with Matlab”, The McGraw-Hill Companies, 2005.
- [46]Chang-Shen Lee, Ming-Chun Lee, Chung-Jung Huang, Ta-Sung Lee, “Sectorization with Beam Pattern Design Using 3D Beamforming Techniques”,

- Signal and Information Processing Association Annual Summit and Conference, pp.1-5, 2015.
- [47]Rui Xu, Donald Wunsch II, “Survey of Clustering Algorithms”, IEEE Transactions On Neural Networks, vol. 16, pp. 645-678, 2005.
- [48]Sokal, Sneath, “Principles of Numerical Taxonomy”, San Francisco, W.H. Freeman and Company, 1963.
- [49]Hartigan, “A K-Means Clustering Algorithm”, Applied Statistics, vol. 28, pp.100-108, 1979.
- [50]Nisha, Puneet Jai Kaur, “A Survey of Clustering Techniques and Algorithms”, 2nd International Conference on Computing for Sustainable Global Development, pp. 304-307, 2015.
- [51]Aastha Joshi, Rajneet Kaur, “A Review: Comparative Study of Various Clustering Techniques in Data Mining”, International Journal of Advanced Research in Computer Science and Software , vol.3, pp.55-57, 2013.
- [52]SakshiPatel, ShivaniSihmar, AmanJatain, “A Study of Hierarchical Clustering Algorithm”, 2nd International Conference on Computing for Sustainable Global Development. pp.537-541, 2015.
- [53]Rezende , H. R, Esmín , A.A.A ,“Proposed Application of Data Mining Techniques for Clustering Software Project”, INFOCOMP – Special Edition, Brazil, pp.43-48, 2010.
- [54]Zhongxiang, FanSun Yan, “Clustering of College Students Based on Improved K-means Algorithm”, International Computer Symposium, pp. 676-679, 2016.
- [55]Soumi Ghosh,Sanjay Kumar Dubey, “Comparative Analysis of K-Means and Fuzzy C-Means Algorithms”, International Journal of Advanced Computer Science and Applications, vol. 4, pp. 35-39, 2013.
- [56]Purnawansyah, Haviluddin, “K-Means Clustering Implementation in Network Traffic Activities”, International Conference on Computational Intelligence and Cybernetics, pp.51-54, 2016.

- [57] Baolin Yi, Haiquan Qiao, Fan Yang, Chenwei Xu, “An Improved Initialization Center Algorithm for K-Means Clustering”, International Conference on Computational Intelligence and Software Engineering, pp.1-4, 2010.
- [58] Tapas Kanungo, David M. Mount, Nathan S. Netanyahu, et al., “An Efficient k-Means Clustering Algorithm: Analysis and Implementation”, IEEE Transactions on Pattern Analysis and Machine Intelligence, vol. 24, pp. 881-892, 2002.
- [59] Anindita Ray, Debashis De, “Energy Efficient Clustering Protocol Based on K-Means (EECPK-means)-Midpoint Algorithm for Enhanced Network Lifetime in Wireless Sensor Network”, IET Wireless Sensor Systems, pp. 181-191, 2016.
- [60] D T Pham, S S Dimov, C D Nguyen. “Selection of K in K-means clustering”, Part C: J. Mechanical Engineering Science, vol. 219, pp. 103-119, 2004.
- [61] E. Ezhilarasan M.Dinakaran. “A Review on mobile technologies: 3G, 4G and 5G”, Second International Conference on Recent Trends and Challenges in Computational Models, pp.369-373, 2017.
- [62] Long Bao Le1, Vincent Lau, Eduard Jorswieck, “Enabling 5G mobile wireless technologies”, EURASIP Journal on Wireless Communications and Networking, vol. 2015, pp.1-14, 2015.
- [63] Guangyi Liu and Dajie Jiang, “5G: Vision and Requirements for Mobile Communication System towards Year 2020”, Chinese Journal of Engineering, vol. 2016, pp.1-14, 2016.
- [64] Brahmī, Nadia, “METIS: Mobile communications for 2020 and beyond”, Proceedings: ITG-Fb. 242: Mobilkommunikation, 2013.
- [65] Rachid EI Hattachi, “NGMN 5G White Paper”, NGMN Alliance, 2015.
- [66] Yahia Medjahdi, Sylvain Traverso, Robin Gerzaguet, et al, “On the Road to 5G: Comparative Study of Physical Layer in MTC Context”, IEEE Access, vol. 5, pp. 26556 - 26581, 2017.

- [67]Hamidreza Shariatmadari, Ruifeng Duan, Sassan Iraj, “Resource Allocations for Ultra-Reliable Low-Latency Communications”, *International Journal of Wireless Information Networks* , vol. 24, pp.317–327, 2017.
- [68]Asvin Gohil, Hardik Modi, Shobhit K Patel, “5G technology of mobile communication: A survey”, *International Conference on Intelligent Systems and Signal Processing*, pp.288–292, 2013.
- [69]Wang C X, Haider F, Gao X Q, et al, “Cellular architecture and key technologies for 5G wireless communication networks”, *IEEE Communications Magazine*, vol. 52, pp. 122–130, 2014.
- [70]Taro Eichler, Corbett Rowell, “The 5G Technology Ecosystem”, ROHDE&SCHWARZ, 2016.
- [71]Doug Brake, “5G and Next Generation Wireless: Implications for Policy and Competition”, *Information Technology and Innovation Foundation*, vol.1, pp.1–22, July 2016.
- [72]“A Horizon 2020 Work Programme 2016–2017”, *Information and Communication Technologies*, European Commission Decision C (2016)4614 of 25, July 2016.
- [73]Alrabadi O N, Tsakalaki E, Huang H, et al, “Beamforming via large and Dense Antenna Arrays Above a Clutter”, *IEEE Journal on Selected Areas in Communications*, vol.31, pp.314-325, 2013.
- [74]Mohammed S K, Larsson E G, “Per-antenna constant envelope precoding for large multi-user MIMO systems”, *IEEE Transactions on Communications*, vol. 61, pp.1059–1071, 2013.
- [75]W Roh, J-Y Seol, J Park, et al, “Millimeter-wave beamforming as an enabling technology for 5G cellular communications: theoretical feasibility and prototype results”, *IEEE Transactions on Communications*, vol. 52, pp.106 – 113, 2014.

- [76] Yuan Zhou, Shaozhen Guo, “PSO-based Vertical Beamforming for 3D Massive MIMO Systems in 5G”, 10th International Conference on Communications and Networking, pp.819-823, 2015.
- [77] T. Rappaport, F. Gutierrez, E. Ben-Dor, et al, “Broadband millimeter-wave propagation measurements and models using adaptive-beam antennas for outdoor urban cellular communications”, IEEE Transactions Antennas Propag, vol. 61, pp.1850–1859, 2013.
- [78] Hongwei Kong, Zhu Wen, Ya Jing, Michael Yau “A compact millimeter wave (mmWave) mid-field over the air (OTA) RF performance test system for 5G massive MIMO devices”, 2018 IEEE MTT-S International Wireless Symposium , pp. 1– 4, 2018.
- [79] Chan-Byoung Chae, Insoo Hwang, Robert W. Heath, Jr., Vahid Tarokh, “Interference Aware-Coordinated Beamforming in a Multi-Cell System”, IEEE Transactions on Wireless Communications, vol. 11, pp. 3692-370. 2012.
- [80] T. Zhou, M. Peng, W. Wang, and H. Chen, “Low-complexity coordinated beamforming for downlink multi-cell SDMA/OFDM system”, IEEE Transactions on Vehicular Technology, vol. 62, pp. 247 - 255, 2013.
- [81] Zehua Wei, Ying Wang, Wenxuan Lin, “Optimization of Downtilts Adjustment Combining Joint Transmission and 3D Beamforming in 3D MIMO”, IEEE 2014 Symposium on Wireless Communication Systems, pp. 728-732, 2014.
- [82] Yaying Wu, Xiaohui Li, Yongqiang Hei, “Downtilts adjustment and power allocation algorithm based on PSO for 3D MIMO systems”, IET international conference on information and communications technologies, pp. 27-29, 2013.
- [83] John D. Kraus, Ronald J. Marhefka, “Antennas for All Application, Third Edition”, The McGraw-Hill Companies, 2008.
- [84] Hyoungju Ji, Younsun Kim, Juho Lee, et al, “Overview of Full-Dimension MIMO in LTE-Advanced Pro”, IEEE Communications Magazine, vol. 55, pp. 176 – 184, 2017.

- [85] Gary Xu, Yang Li, Jin Yuan, et al, “Full Dimension MIMO (FD-MIMO): Demonstrating Commercial Feasibility”, *IEEE Journal on Selected Areas in Communications*, vol. 35, pp.1876 – 1886, 2017.
- [86] Yiyang Zhang, Pinyi Ren, Li Sun, et al, “Antenna Tilt Assignment for Three-Dimensional Beamforming in Multiuser Systems”, *IEEE Global Communications Conference*, pp.1-6, 2015.
- [87] Shuai Li, Xiaopeng Yang, Liyue Ning, et al, “Broadband Constant Beamwidth Beamforming for Suppressing Mainlobe and Sidelobe Interferences”, *IEEE Radar Conference*, pp.1041-1045, 2017.
- [88] Haohai Sun, Shefeng Yan, U. Peter Svensson, “Robust Minimum Sidelobe Beamforming for Spherical Microphone Arrays”, *IEEE Transactions On Audio, Speech, And Language Processing*, vol.19, pp.1041-1045, 2011.
- [89] Xianghao Yu, Jun Zhang, K. B. Letaief. “Coverage analysis for dense millimeter wave cellular networks: The impact of array size”, *IEEE Wireless Communications and Networking Conference*, pp.1-6, 2016.
- [90] Foad Sahrabi, Wei Yu, “Hybrid Digital and Analog Beamforming Design for Large-Scale Antenna Arrays”, *IEEE Journal Of Selected Topics In Signal Processing*, vol. 10, pp. 501-513, 2016.
- [91] Nelson Jorge G. Fonseca, Ahmed Ali, Hervé Aubert, “Cancellation of Beam Squint with Frequency in Serial Beamforming Network-Fed Linear Array Antennas”, *IEEE Antennas and Propagation Magazine*, vol. 54, pp.32-39, 2012.
- [92] A. Alkhateeb, J. Mo, N. González-Prelcic, Heath, Robert W. Jr, “MIMO Precoding and Combining Solutions for Millimeter-Wave Systems”, *IEEE Communications Magazine*, vol. 52, pp. 122 – 131, 2014.
- [93] M. Reil, G. Lloyd, “Millimeter-Wave Beamforming: Antenna Array Design Choices & Characterization”, White Paper, ROHDE & SCHWARZ, 2016.
- [94] Zheda Li, Shengqian Han, Andreas F. Molisch. “Optimizing Channel-Statistics-Based Analog Beamforming for Millimeter-Wave Multi-User

- Massive MIMO Downlink”, IEEE Transactions on Wireless Communications, vol. 16, pp. 4288 - 4303, 2017.
- [95] Yaniv Azar, George N. Wong, Kevin Wang, et al., “28 GHz propagation measurements for outdoor cellular communications using steerable beam antennas in New York City”, IEEE International Conference on Communications , pp. 5143–5147, 2013.
- [96] Foad Sohrabi, Wei Yu .“Hybrid Digital and Analog Beamforming Design for Large-Scale Antenna Arrays”, IEEE Journal of Selected Topics In Signal Processing, vol.10, pp. 501-513, 2016.
- [97] Yaning Zou, Wolfgang Rave, Gerhard Fettweis,“Analog Beamsteering for Flexible Hybrid Beamforming Design in Mmwave Communications”, 2016 European Conference on Networks and Communications , 2016.
- [98] W Roh , JY Seol , J Park , B Lee, “Millimeter-Wave Beamforming as an Enabling Technology for 5G Cellular Communications: Theoretical Feasibility and Prototype Results”, IEEE Communications Magazine, vol. 52, pp. 106-113, 2014.
- [99] William E. McKinzie, Per Iversen, Edward Szpindor, et al., “60 GHz reference chip antenna for gain verification of millimeter wave test chambers”, AMTA 2016 Proceedings, January 2017.
- [100] George R. MacCartney, Junhong Zhang, Shuai Nie, Theodore S. Rappaport, “Path loss models for 5G millimeter wave propagation channels in urban microcells”, 2013 IEEE Global Communications Conference , 2014.
- [101] Federico Boccardi, Vodafone, Robert W. Heath Jr., et.al., “Five Disruptive Technology Directions for 5G”, IEEE Communications Magazine, pp.74-80,2014.
- [102] Kok-Lim Alvin Yau, Junaid Qadir, Celimuge Wu, et.al., “Cognition-inspired 5G cellular networks: a review and the road ahead”, IEEE Access, vol.2, pp.1–22, 2018.



- [103]Weidong Zhang, Ying Wang, Fei Peng, Yuan Yuan, “Interference Coordination with Vertical Beamforming in 3D MIMO-OFDMA Networks”, IEEE Communications Letters, vol. 18, pp. 34 – 37, 2014.
- [104]Yuwen Pan, Qinglin Luo, Guodong Li, et al., “Performance Evaluation of 3D MIMO LTE-Advanced System”, IEEE 78th Vehicular Technology Conference, pp. 1-5, 2013.
- [105]Mustafa Riza Akdeniz, Yuanpeng Liu, Mathew K. Samimi, et.al., “Millimeter Wave Channel Modeling and Cellular Capacity Evaluation”, IEEE Journal on Selected Areas in Communications, vol. 32, pp. 1164–1179, 2014.

**Appendices:  
Programs**

**Simulation**

# Appendix A: Simulation Design for Minimal Side Lobe 3D Beamforming LTE System towards a Group of User Equipment

The **main.m** is the main function for the simulation, which has 7 sub-systems including **SimStart\_Callback**, **ReadStart\_Callback**, **BeamStart\_Callback**, **CBERStart\_Callback**, **ReadBERStart\_Callback**, **BERCellUEsStart\_Callback** and **Plot3DStart\_Callback** as Figure A-1 shown.

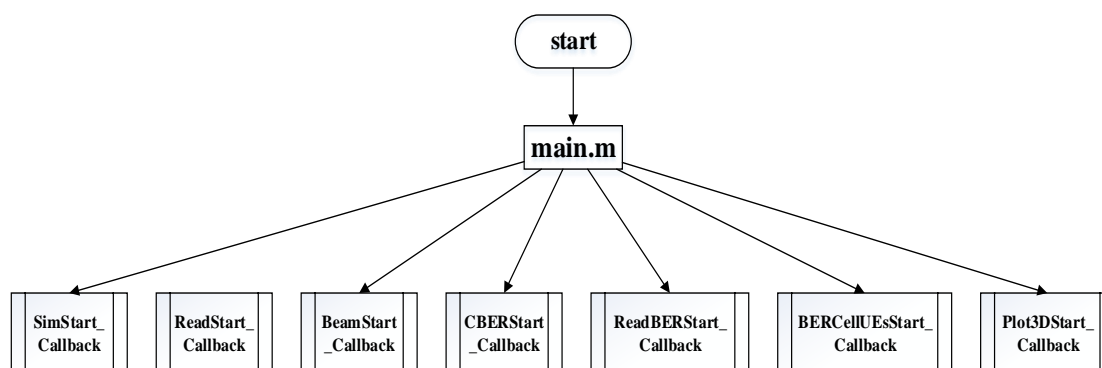


Figure A- 1: The main function for the simulation

## A.1 UML Modeling for Simulation System

### A.1.1 Introduction

The simulation should implement these functions so there needs to be 7 UML use-cases. UML is a general-purpose, developmental, modelling language in the field of software engineering, which is intended to provide a standard way to visualise the design of software systems. UML diagrams represent two different views of a system model:

- Static model: emphasises the static structure of the system using objects, attributes, operations and relationships. It includes class diagrams and composite structure diagrams.
- Dynamic model: emphasizes the dynamic behaviour of the system by showing collaboration among objects and changes to the internal states of objects. This view includes sequence diagrams, activity diagrams and state machine diagrams.

In this thesis, class diagrams, composite structure diagrams, sequence diagrams and activity diagrams were used to represent the 4 simulation use-cases (**SimStart**, **BeamStart**, **CBERStart**, **BERCellUEsStart**) and 3 present data use-cases (**ReadStart**, **ReadBERStart**, **Plot3DStart**).

The UML use-cases model is shown in Figure A-2. There is one actor who is the analyzer and 7 use-cases, namely: **SimStart**, **ReadStart**, **BeamStart**, **CBERStart**, **ReadBERStart**, **BERCellUEsStart** and **Plot3DStart**.

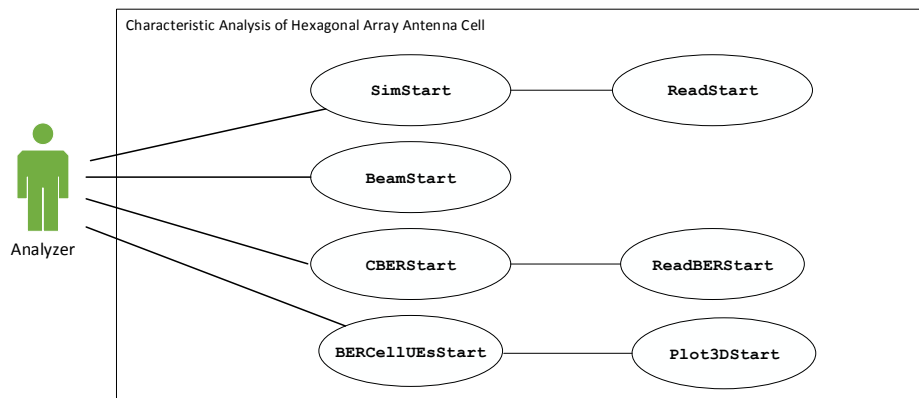


**Figure A-2: UML use-cases model**

Since the simulation takes a long time, we need to divide the program into four sub-systems and provide a further program to read the results of the two most important sub-systems in the simulation as shown in Figure A-2. The use-case **SimStart** sets up the simulation communication environment according to the simulation parameters from the environment data file; the use-case **BeamStart** generates the beams, which having the weighting matrix makes the SINR to be a maximum value; the use-case **CBERStart** calculates the BER for the LTE SISO system and LTE 3D beamforming system in the 3D channel model; the use-case **BERCellUEsStart** tests the impact on the LTE 3D beamforming system of the different environments and the different

modulation methods. At **SimStart** use-case interim results can be read and displayed using **ReadStart**, at **CBERStart** use-case interim results can be read and displayed using **ReadBERStart** and at **BERCellUEsStart** use-case interim results can be read and displayed using **Plot3DStart**.

### A.1.2 SimStart Use-case

Table A-1 shows the UML use-case description for “**SimStart**” and Figure A-3 is the activity diagram for this use-case.

**Table A- 1: The UML use-case description for “SimStart”**

<p><b>Name of Use Case:</b> <b>SimStart</b></p> <p><b>Introduction:</b> Setting up 3D channel environment according to the parameters.</p> <p><b>Participator:</b> Analyzer</p> <p><b>Preconditions:</b> Set up the simulation parameters, the running simulation times, the number of UEs, the antenna array, the base station coverage, the radius of cell, the scenario of simulation and the carrier frequency.</p> <p><b>Main sequence (as Figure A-3 shown):</b></p> <ol style="list-style-type: none"> <li>1. Start the analyzer.</li> <li>2. Generate the 3D channel model according to the 3GPP TR36.873.</li> <li>3. Set the cell has 6 faces and each face is an antenna array. The each antenna array has 4 sub-array so there are 24 areas for the cell.</li> <li>4. The UEs is random distributed in one cell, which has 24 areas. If the number of UEs is larger than 2 in one area, the K-means algorithm will be used to cluster the UEs. Then the coordinates of the center for clustering can be determined.</li> <li>5. Transfer the local coordinate of UEs and antenna array to the global coordinates.</li> <li>6. Create the environment data file.</li> <li>7. Read the environment data file.</li> <li>8. Displays the communication environment according to the selected simulation time.</li> </ol> <p><b>Alternative sequence:</b></p> <p>None.</p> <p><b>Post-condition:</b></p> <p>The system displays the communication environment.</p>
---

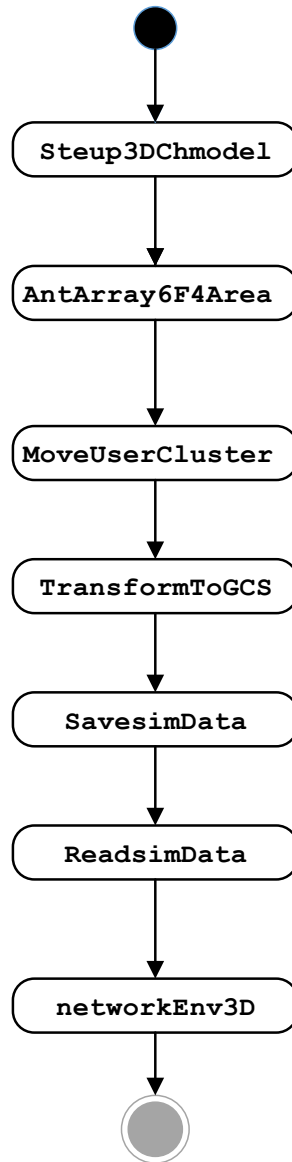
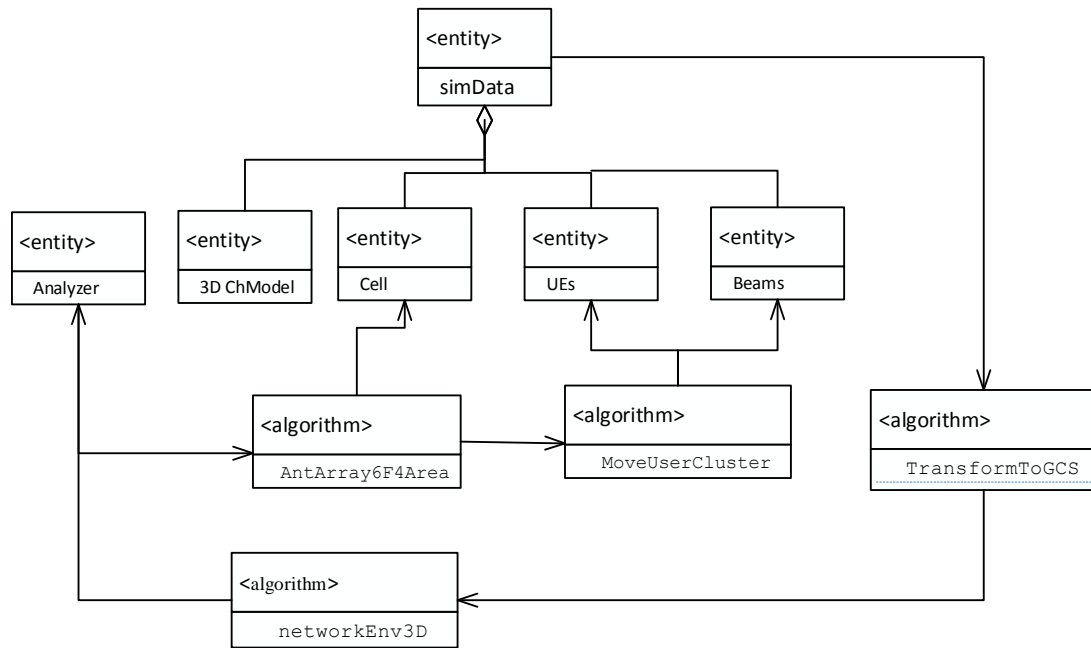
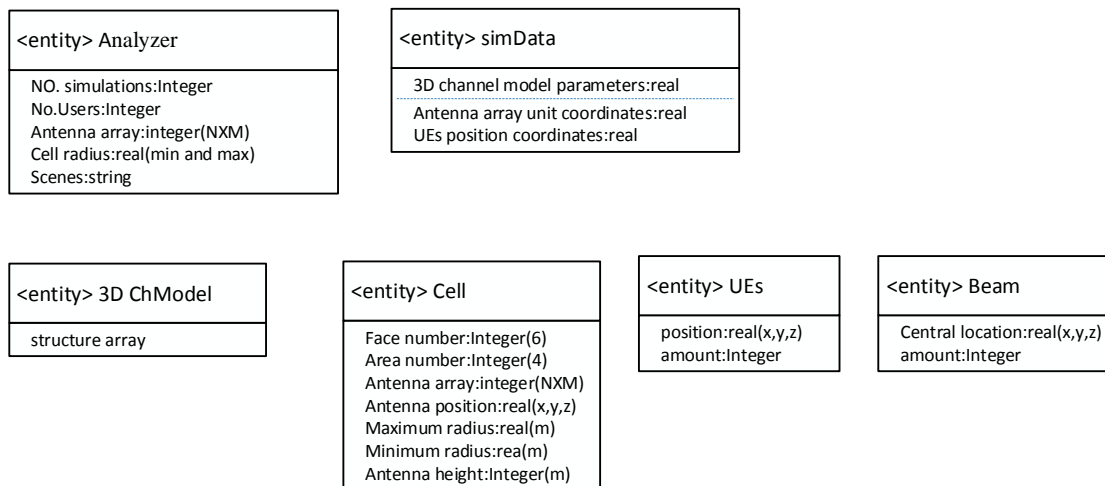


Figure A-3: Activity diagram for UML this use-case

The static model of the use-case **SimStart** is shown in Figure A-3, which has four categories, entity class, aggregate class, algorithm class and output class. The entity class includes the “<entity>:Analyzer” and “<entity>:simData”. Moreover, the description of the entity class is shown in Figure A-4. The aggregate class is in “<entity>:simData”, which includes the “<entity>:3D ChModel”, “<entity>:Cell”, “<entity>:UEs” and “<entity>:Beams”. The algorithm class includes the “<algorithm>:AntArray6F4Area”, “<algorithm>:MoveUserCluster”, “<algorithm>:TransformToGCS” and “<algorithm>:networkEnv3D”.



**Figure A-4: The static model of the use-case SimStart**



**Figure A-5: The description of the entity class**

The “<user interaction>:Analyzer Interaction” should be created because entity class “<entity>:Analyzer” has to interact with external users as shown in Figure A-5. In Figure A-6, the entity class “<entity>:simData” is aggregated into the “<data>:simData”.

Create 3D communication environment use case SimStart

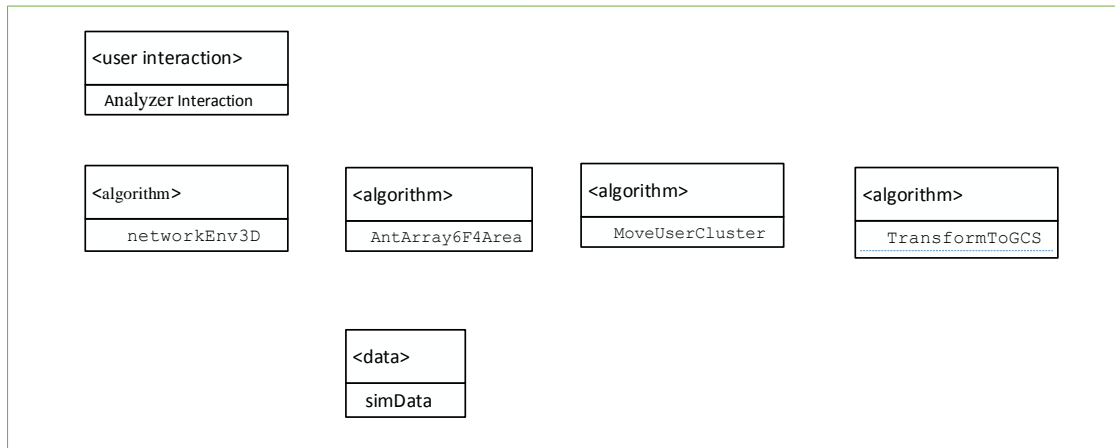


**Figure A-6: Interaction between the entity class “<entity>:Analyzer” and external UEs**

The dynamic model of the use-case **SimStart** is shown in Figure A-7 and the message description is in Table A-2.

**Table A- 2: The message description of the dynamic model of the use-case SimStart**

<p><b>E1:</b> The “Analyzer” sends the start to “&lt;user interaction&gt;:Analyzer Interaction”.</p> <p><b>E2:</b> The “&lt;user interaction&gt;: Analyzer Interaction” send the simulation parameters to the “&lt;algorithm&gt;:AntArray6F4Area”.</p> <p><b>E3.1:</b> The “&lt;algorithm&gt;:AntArray6F4Area” send the areas information, there are 24 areas in the cell, to “&lt;algorithm&gt;:MoveUserCluster”.</p> <p><b>E3.2:</b> The “&lt;algorithm&gt;:AntArray6F4Area” send the coordinates of each antenna array unit to “&lt;algorithm&gt;:TransformToGCS”.</p> <p><b>E4:</b> The “&lt;algorithm&gt;:MoveUserCluster” send the coordinates of each UE and beam to “&lt;algorithm&gt;:TransformToGCS”.</p> <p><b>E5:</b> The “&lt;algorithm&gt;:TransformToGCS” send the global coordinates of each antenna array unit, UE and beam to “&lt;data&gt;:simData”, which is the data file for the communication environment.</p> <p><b>E6:</b> The “&lt;algorithm&gt;:networkEnv3D” read the global coordinates of each antenna array unit, UE and beam from “&lt;data&gt;:simData”</p> <p><b>E7:</b> The “&lt;algorithm&gt;:networkEnv3D” is displayed the communication environment by “&lt;user interaction&gt;: Analyzer Interaction”.</p>
---



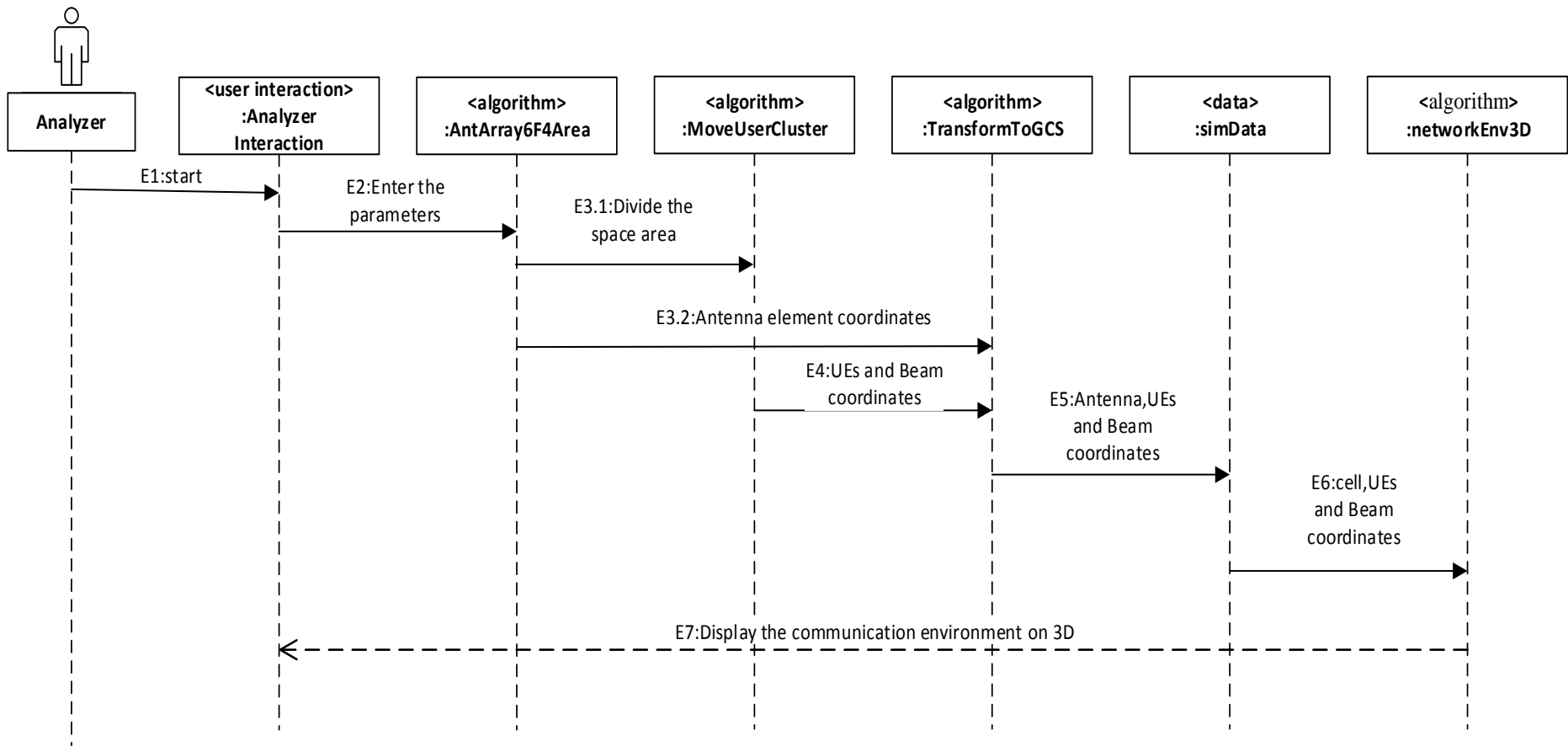


Figure A-7: The dynamic model of the use-case SimStart

### A.1.3 ReadStart Use-case

Table A-3 shows the read and present data use-cases description for “**ReadStart**” and Figure A-8 is the activity diagram for this use-case.

**Table A- 3: The read and present data use-cases description for “ReadStart”**

<p><b>Name of Use Case:</b> ReadStart</p> <p><b>Introduction:</b> Read simulation data and show the communication environment for system.</p> <p><b>Participator:</b> Analyzer</p> <p><b>Preconditions:</b> Set up the running simulation times.</p> <p><b>Main sequence (as FigureA-8 shown):</b></p> <ol style="list-style-type: none"><li>1. Start the analyzer.</li><li>2. Read the environment data file.</li><li>3. Displays the communication environment according to the selected simulation time.</li></ol> <p><b>Alternative sequence:</b></p> <p>None.</p> <p><b>Post-condition:</b></p> <p>The system displays the communication environment.</p>
--

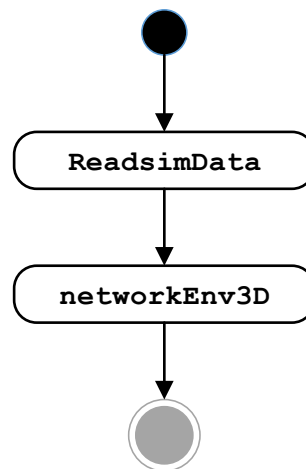


**Figure A-8: The activity diagram for use-case**

The static model of the use-case **ReadStart** is shown in Figure A-9, which has two categories, entity class and algorithm class. The entity class includes the “<entity>:Analyzer” and “<entity>:simData”. Moreover, the description of the entity class is shown in Figure A-10. The algorithm class is “<algorithm>:networkEnv3D”.

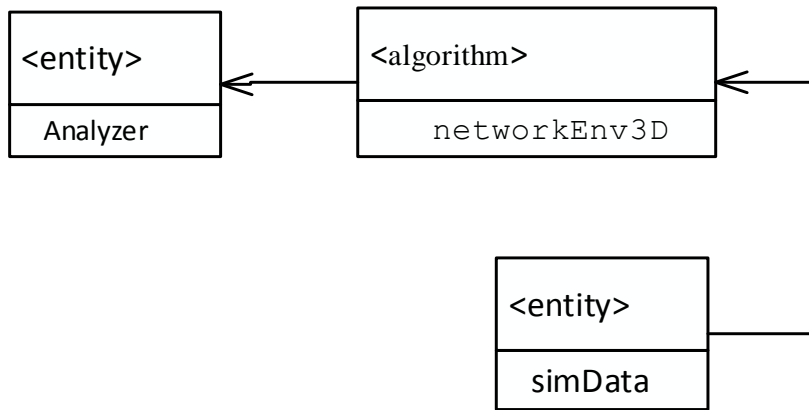


**Figure A-9: The static model of the use-case ReadStart**

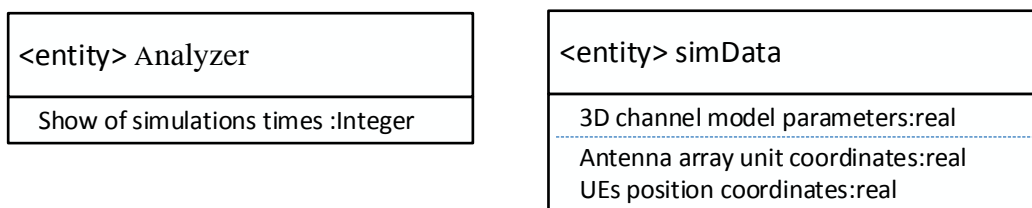


**Figure A-10: The description of the entity class**

The “<user interaction>:Analyzer Interaction” should be created because entity class “<entity>:Analyzer” has to interact with external users as shown in Figure A-11. In Figure A-11, the entity class “<entity>:simData” is changed to the “<data>simData”.

**Show 3D communication environment use case ReadStart**

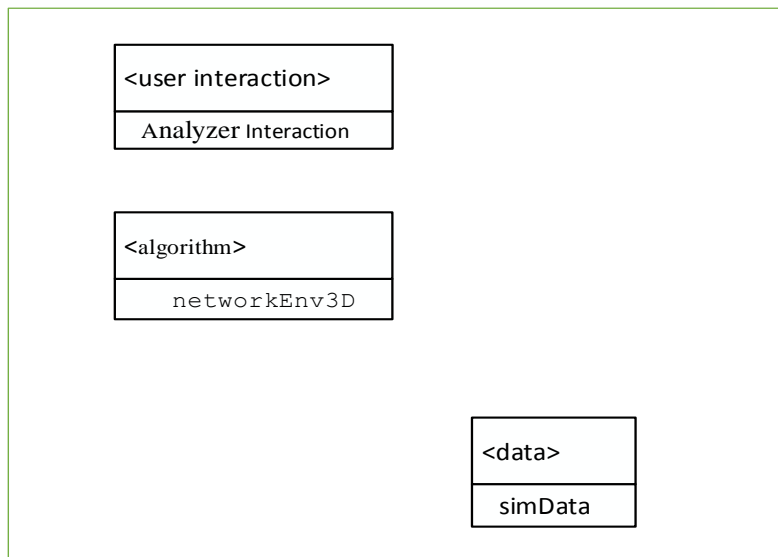


**Figure A-11: The interaction between entity class “<entity>:Analyzer” and external UEs**

The dynamic model of the use-case **ReadStart** is shown in Figure A-12 and the message description is in Table A-4.

**Table A- 4: The message description of the use-case ReadStart**

<p><b>R1:</b> The “Analyzer” sends the start to “&lt;user interaction&gt;: Analyzer Interaction”.</p> <p><b>R2:</b> The “&lt;user interaction&gt;: Analyzer Interaction” selects the designated data, the number of UEs, the modulation type and the scene of simulation, or current parameters. After that the “&lt;algorithm&gt;:networkEnv3D” will be started.</p> <p><b>R3:</b> The “&lt;algorithm&gt;:networkEnv3D” send the read data request to “&lt;data&gt;simData”.</p> <p><b>R4:</b> The “&lt;data&gt;simData” send the data to “&lt;algorithm&gt;:networkEnv3D”.</p> <p><b>R5:</b> The “&lt;algorithm&gt;:networkEnv3D” is shown the 3D beamforming communication environment to “Analyzer” by the “&lt;user interaction&gt;: Analyzer Interaction”.</p>
--

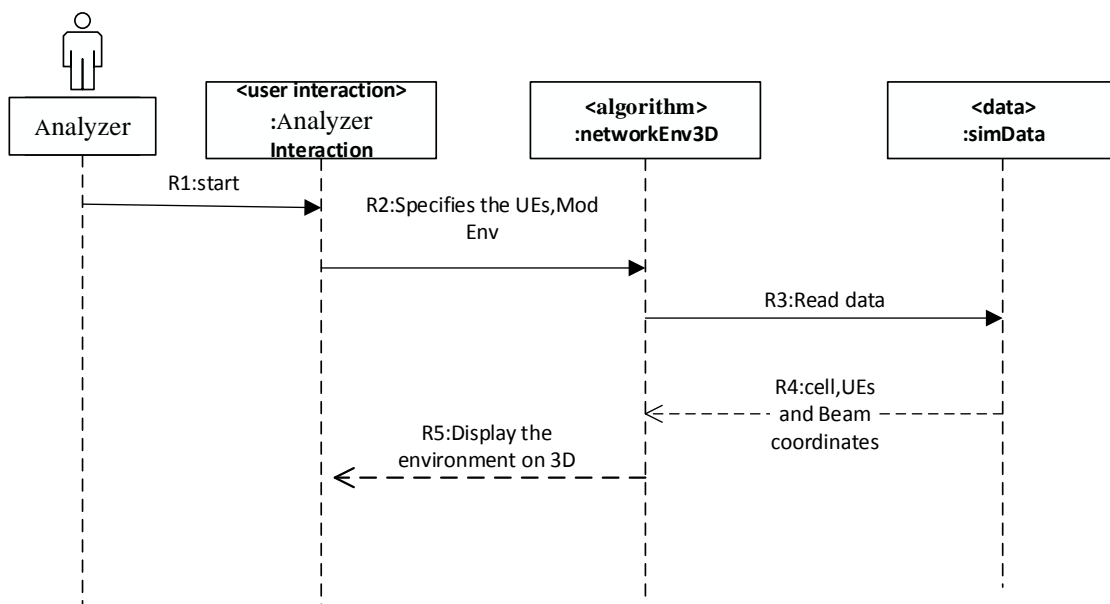


**Figure A-12: The dynamic model of the use-case ReadStart**

### A.1.4 BeamStart Use-case

Table A-5 shows the UML use-case description for “**BeamStart**” and Figure A-13 is the activity diagram for this use-case.

**Table A- 5: The UML use-case description for “BeamStart”**

**Name of Use Case: BeamStart**

**Introduction:** The communication environment data is read, and then the weighting matrix for the beamforming will be calculated, under the maximum SINR. The CDF and PDF of the SINR and throughput are calculated and shown.

**Participator:** Analyzer

**Preconditions:** Select the time of running simulation and the face of cell.

**Main sequence (as FigureA-13 shown):**

1. Start the analyzer.
2. Read the environment data file.
3. The least square method is used to calculate the weighting matrix under the maximum SINR.
4. Create the weighting matrix data file.
5. Display the beams by the selected face.
6. Display the beams for whole cell by selected the time of running simulation.
7. Calculate the SINR and throughput and then the data will be saved.
8. Calculate and Display the CDF and PDF of SINR and throughput.

**Alternative sequence:**

None.

**Post-condition:** The system shows the beams by the selected face, the beams for whole cell and the CDF and PDF of SINR and throughput.

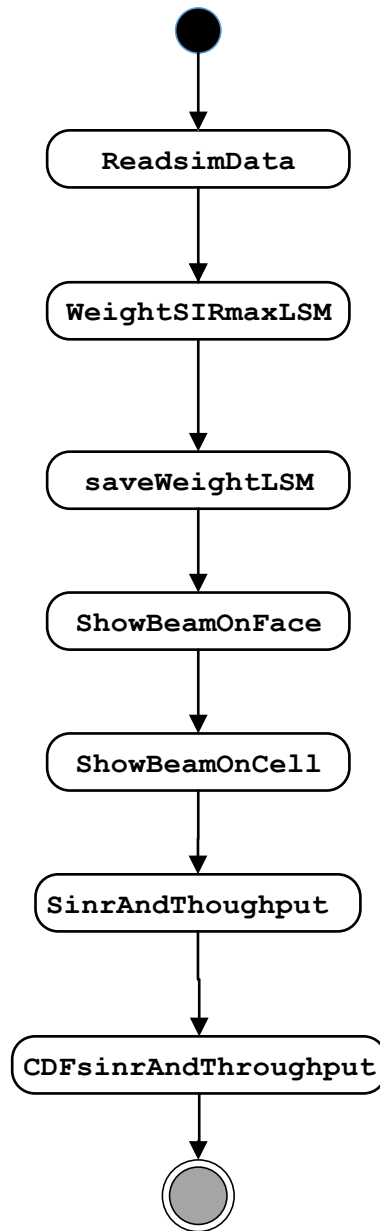
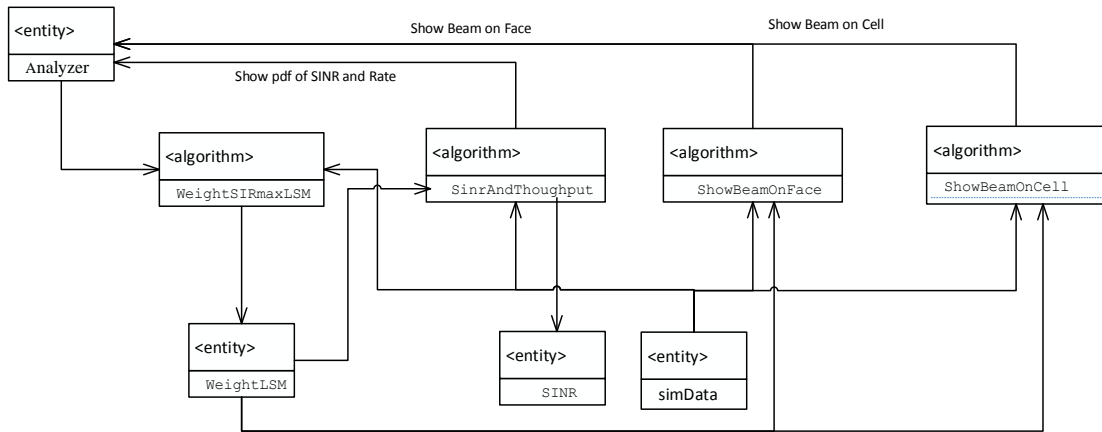
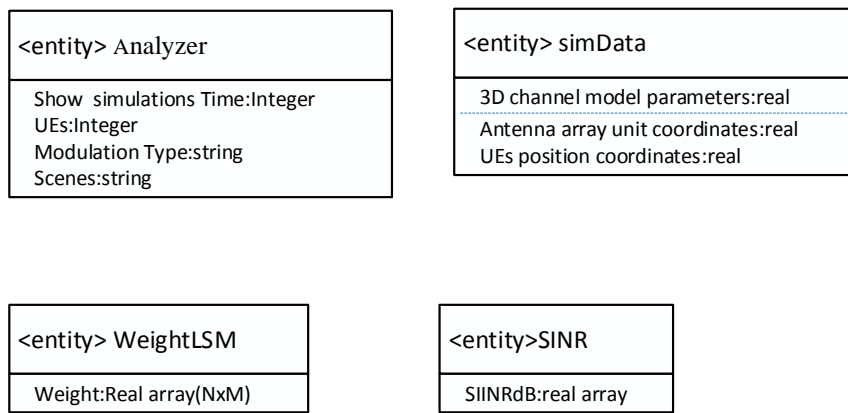


Figure A-13: The activity diagram for use-case

The static model of the use-case **BeamStart** is shown in Figure A-14, which has two categories, entity class and algorithm class. The entity class includes the “<entity>:Analyzer”, “<entity>:WeightLSM”, “<entity>:SINR” and “<entity>:simData”. The description of the entity class is shown in Figure A-15. The algorithm class includes the “<algorithm>:WeightSIRmaxLSM”, “<algorithm>:SinrAndThroughput”, “<algorithm>:ShowBeamOnFace” and “<algorithm>:ShowBeamOnCell”.



**Figure A-14: The static model of the use-case BeamStart**



**Figure A-15: The description of the entity class**

The “<user interaction>:Analyzer Interaction” should be created because entity class “<entity>:Analyzer” has to interact with external users as shown in Figure A-16. In Figure A-16, the output data has the “<data>:simData”, “<data>:WeightLSM” and “<data>:SINR”

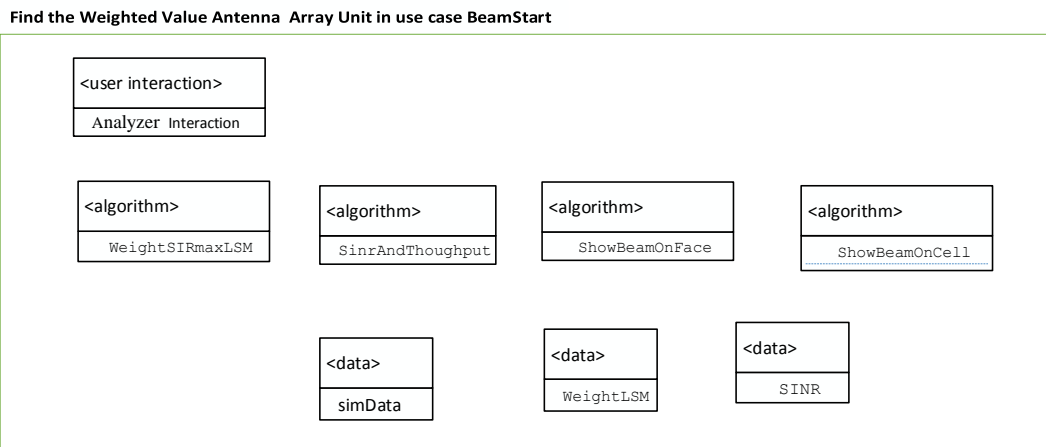


**Figure A-16: The interaction between entity class “<entity>:Analyzer” and external UEs**

The dynamic model of the use-case **BeamStart** is shown in Figure A-17 and the message description is in Table A-6.

**Table A- 6: The message description of the use-case BeamStart**

<p><b>B1:</b> The “Analyzer” sends the start to “&lt;user interaction&gt;: Analyzer Interaction”.</p> <p><b>B2:</b> The “&lt;user interaction&gt;: Analyzer Interaction” sends the start the calculation to the “&lt;algorithm&gt;:WeightSIRmaxLSM”.</p> <p><b>B3.1:</b> The “WeightSIRmaxLSM” reads the simulation environment data from the “&lt;data&gt;:simData”.</p> <p><b>B3.2:</b> The “&lt;algorithm&gt;:WeightSIRmaxLSM” reads the weighting data from the “&lt;data&gt;:WeightLSM”.</p> <p><b>B4.1:</b> The “&lt;algorithm&gt;:SinrAndThroughput” reads the simulation environment data from the “&lt;data&gt;:simData”.</p> <p><b>B4.2:</b> The “&lt;algorithm&gt;:SinrAndThroughput” reads the weighting data from the “&lt;data&gt;:WeightLSM”.</p> <p><b>B4.3:</b> The “&lt;algorithm&gt;:SinrAndThroughput” creates the SINR data file to the “&lt;data&gt;:SINR”.</p> <p><b>B4.4:</b> The “&lt;algorithm&gt;:SinrAndThroughput” displays the CDF of SINR and throughput by the “&lt;user interaction&gt;:Analysts Interaction”.</p> <p><b>B5.1:</b> The “&lt;algorithm&gt;:ShowBeamOnFace” reads the simulation environment data from the “&lt;data&gt;:simData”.</p> <p><b>B5.2:</b> The “&lt;algorithm&gt;:ShowBeamOnFace” reads the weighting data from the “&lt;data&gt;:WeightLSM”.</p> <p><b>B5.3:</b> The “&lt;algorithm&gt;:ShowBeamOnFace” displays the beams for one face by the “&lt;user interaction&gt;:Analysts Interaction”.</p> <p><b>B6.1:</b> The “ShowBeamOnCell” reads the simulation environment data from the “&lt;data&gt;:simData”.</p> <p><b>B6.2:</b> The “&lt;algorithm&gt;:ShowBeamOnCell” reads the weighting data from the “&lt;data&gt;:WeightLSM”.</p> <p><b>B6.3:</b> The “&lt;algorithm&gt;:ShowBeamOnCell” displays the beams for whole cell by the “&lt;user interaction&gt;: Analyzer Interaction”.</p>
--



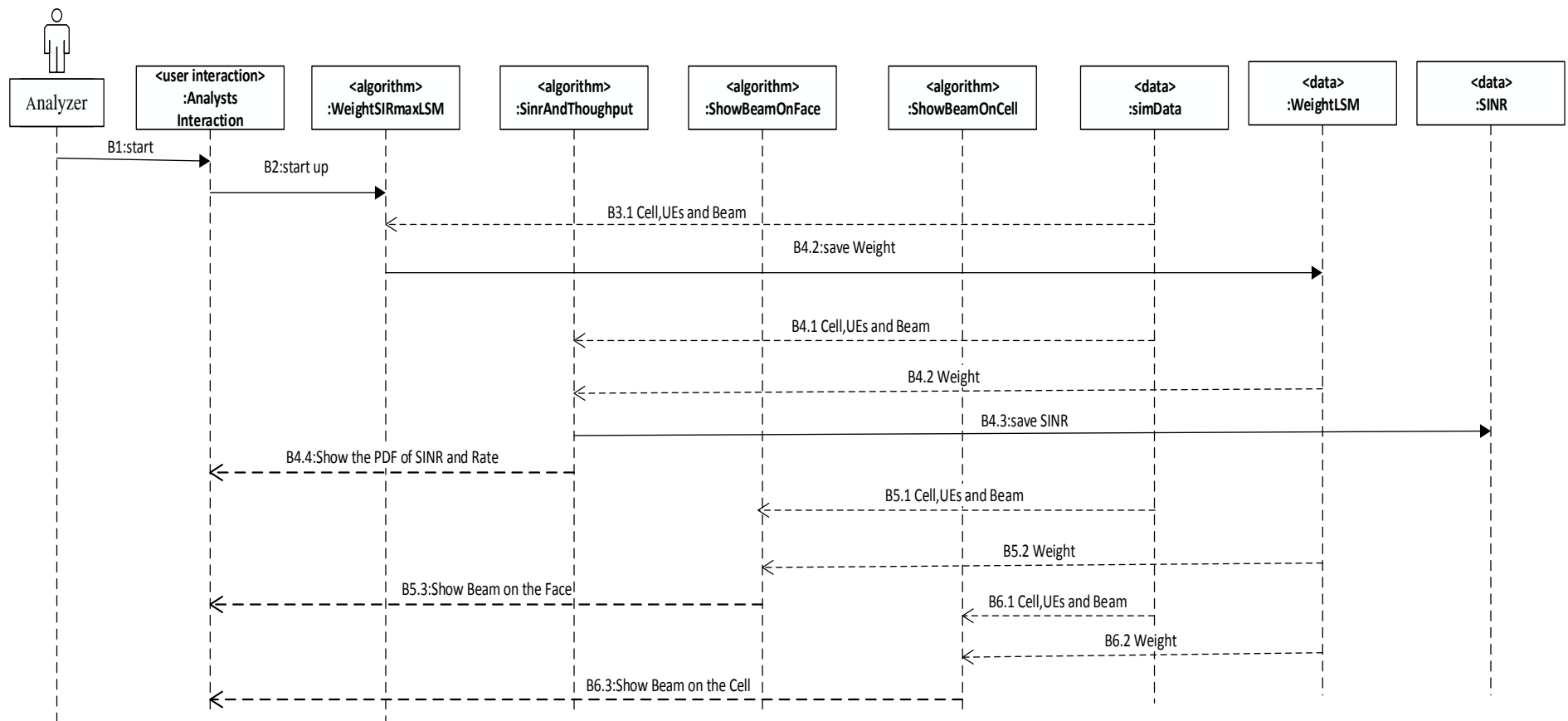


Figure A-17: The dynamic model of the use-case BeamStart

## A.1.5 CBERStart Use-case

Table A-7 shows the UML use-case description for “**CBERStart**”, Figure A-18 is the activity diagram for this use-case.

**Table A- 7: The UML use-case description for “CBERStart”**

<p><b>Name of Use Case:</b> CBERStart</p> <p><b>Introduction:</b> The 3D beamforming and 3D Channel model are added into the transmitting terminals and receiving terminals of the LTE system. Moreover, the received signals of 3D beamforming system are obtained. The BER of the transmitted signal and received signal is calculated, which is saved in the BER data file.</p> <p><b>Participator:</b> Analyzer</p> <p><b>Preconditions:</b> Set up the modulation method and SNR.</p> <p><b>Main sequence (as Figure A-18 shown):</b></p> <ol style="list-style-type: none"><li>1. Start the analyzer.</li><li>2. Read the SINR data file.</li><li>3. Generate the transmitting signals for every beam.</li><li>4. According to the 3GPP TR36.873, the impulse response function of 3D channel model is generated.</li><li>5. For obtaining the received signal, the beam signal, which is formed by the weighting matrix and LTE transmitting signal, is in convolution with the impulse response function of the 3D channel model.</li><li>6. The noise and the interference between the beams are added into the received signal.</li><li>7. Calculate the BER.</li><li>8. Create the BER data files for all simulation UEs.</li></ol> <p><b>Alternative sequence:</b></p> <p>None.</p> <p><b>Post-condition:</b></p> <p>The system displays the BER for comparison.</p>
--

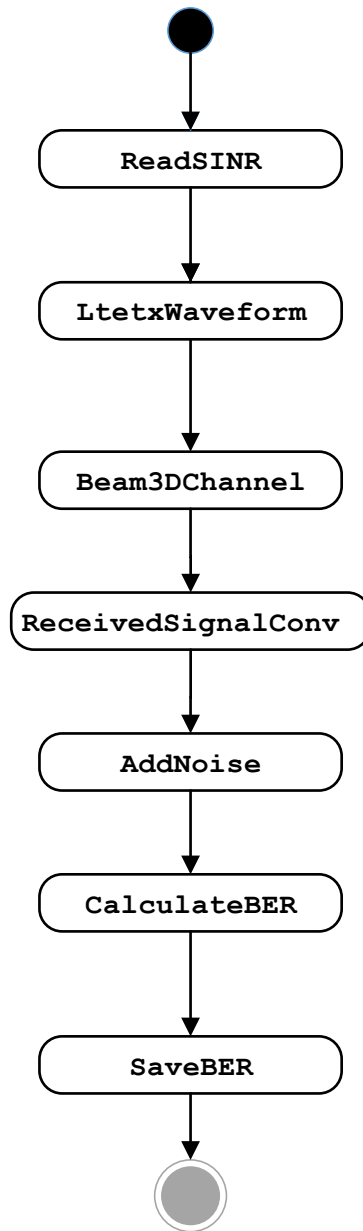


Figure A-18: The activity diagram for use-case

The static model of the use-case **CBERStart** is shown in Figure A-19, which has two categories, entity class and algorithm class. The entity class includes the “<entity>:Analyzer”, “<entity>:simData”, “<entity>:WeightLSM”, “<entity>:SINR” and “<entity>:BER”. The description of the entity class is shown in Figure A-20. The algorithm class includes the “<algorithm>:LTE System”, “<algorithm>:Beam3DChannel”, “<algorithm>:receivedSignalConv”, “<algorithm>:AddNoise” and “<algorithm>:calculateBER”.

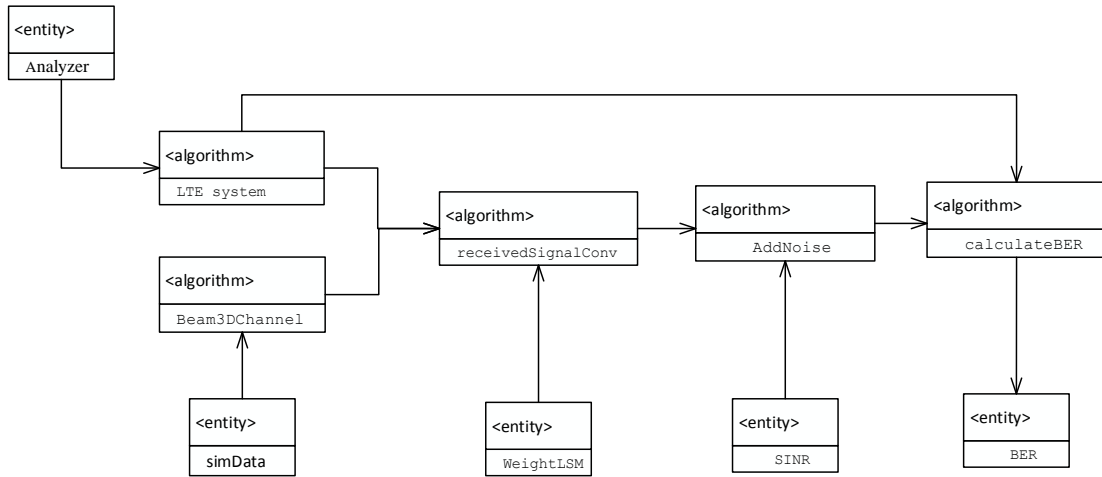


Figure A-19: The static model of the use-case CBERStart

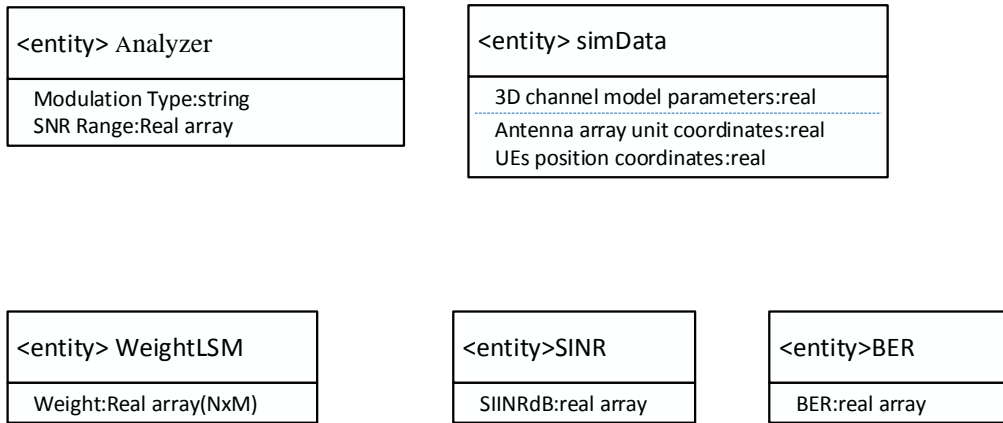


Figure A-20: The description of the entity class

The “<user interaction>:Analyzer Interaction” should be created because entity class “<entity>:Analyzer” has to interact with external users as shown in Figure A-21. In Figure A-21, the output data has the “<data>:simData”, “<data>:WeightLSM”, “<data>:SINR” and “<data>:BER”.

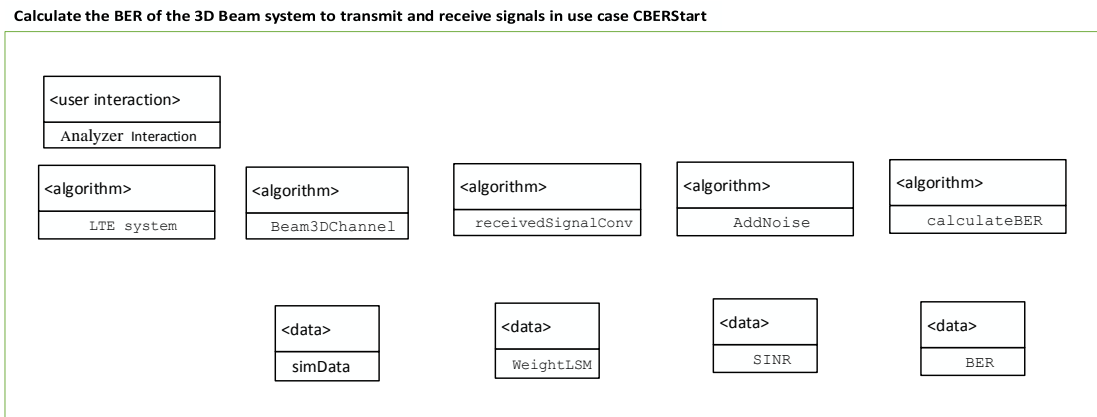


Figure A-21: The interaction between entity class “<entity>:Analyzer” and external UEs

The dynamic model of the use-case **CBERStart** is shown in Figure A-22 and the message description is in Table A-8.

**Table A- 8: The message description of the use-case CBERStart**

<p><b>C1:</b> The “Analyzer” sends the start to “&lt;user interaction&gt;:Analyzer Interaction”.</p> <p><b>C2:</b> The “&lt;user interaction&gt;:Analyzer Interaction” sends information about the modulation types and the SNR range to the “&lt;algorithm&gt;:LTE System”, and then start the calculation.</p> <p><b>C3.1:</b> The “&lt;algorithm&gt;:LTE System” send the transmitting signals to the “&lt;algorithm&gt;:receivedSignalConv”.</p> <p><b>C3.2:</b> The “&lt;algorithm&gt;:LTE System” send the transmitting signals to the “&lt;algorithm&gt;:calculateBER”.</p> <p><b>C4.1:</b> The “&lt;algorithm&gt;:Beam3DChannel” reads the simulation parameters (such as channel model and environment data) from the “&lt;data&gt;:simData”.</p> <p><b>C4.2:</b> The “&lt;algorithm&gt;:Beam3DChannel” send the impulse response function to the “&lt;algorithm&gt;:receivedSignalConv”.</p> <p><b>C5.1:</b> The “&lt;algorithm&gt;:receivedSignalConv” reads the weighting data from the “&lt;data&gt;:WeightLSM”.</p> <p><b>C5.2:</b> The “&lt;algorithm&gt;:receivedSignalConv” send the received signals to the “&lt;algorithm&gt;:AddNoise”.</p> <p><b>C6.1:</b> The “&lt;algorithm&gt;:AddNoise” reads the SINR data from the “&lt;data&gt;:SINR”.</p> <p><b>C6.2:</b> The “&lt;algorithm&gt;:AddNoise” send the received signals, which are after the calculation, to the “&lt;algorithm&gt;:calculateBER”.</p> <p><b>C7:</b> The “&lt;algorithm&gt;:calculateBER” creates the BER data file in the “&lt;data&gt;:BER”.</p>
--

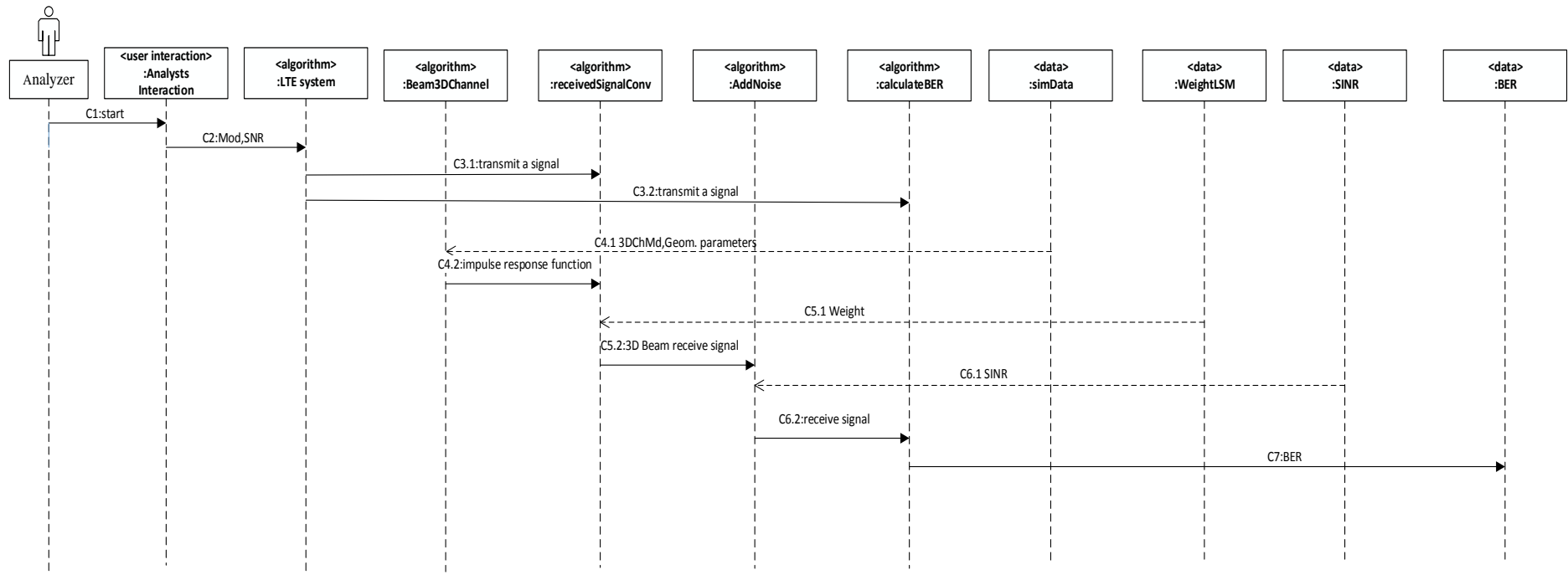


Figure A-22: The dynamic model of the use-case CBERStart

## A.1.6 ReadBERStart Use-case

Table A-9 shows the read and present data use-cases description for “ReadBERStart” and Figure A-23 is the activity diagram for this use-case.

**Table A- 9: The description for “ReadBERStart”**

<p><b>Name of Use Case: ReadBERStart</b></p> <p><b>Introduction:</b> Read the BER data file to calculate the BER by the statistical boundary. The BER of LTE SISO or LTE MIMO system is compared.</p> <p><b>Participant:</b> Analyzer</p> <p><b>Preconditions:</b> Set up the statistical boundary and select the system such as SISO or MIMO.</p> <p><b>Main sequence (as FigureA-23 shown):</b></p> <ol style="list-style-type: none"><li>1. Start the analyzer.</li><li>2. In the LTE system, the received signal is displayed in the constellation diagram and the BER is calculated.</li><li>3. The beam and UEs in this beam are randomly selected. In the 3D beamforming system, the received signal is displayed in the constellation diagram and the BER is calculated.</li><li>4. Read the BER data file.</li><li>5. Calculate the BER by the statistical boundary.</li><li>6. Displays the BER for 3D beamforming system and LTE system in same figure, and then compare them.</li></ol> <p><b>Alternative sequence:</b></p> <p>None.</p> <p><b>Post-condition:</b></p> <p>The system displays the BER.</p>
--

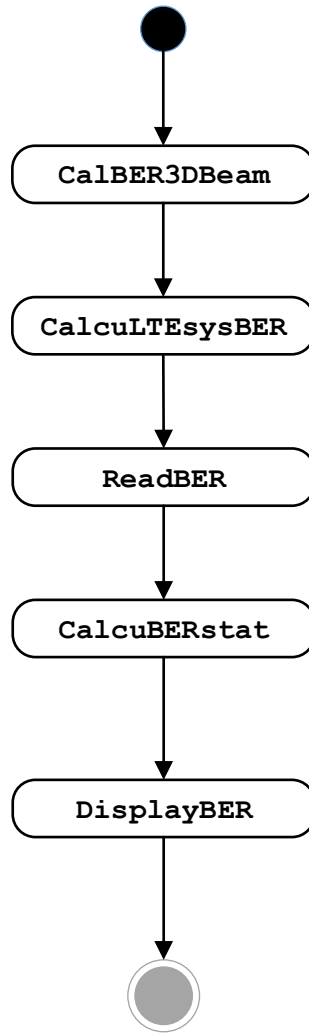


**Figure A-23: The activity diagram for this use-case**

The static model of the use-case **ReadBERStart** is shown in Figure A-24, which has three categories, entity class, output class and algorithm class. The entity class includes the “<entity>:Analyzer” and “<entity>:BER”. Moreover, the description of the entity class is shown in Figure A-25. The output class includes the “<output>:scatter” and “<output>:plot”. The algorithm class includes the “<algorithm>:calBER3DBeam”, “<algorithm>:calBERLteSystem” and “<algorithm>:readBER”.



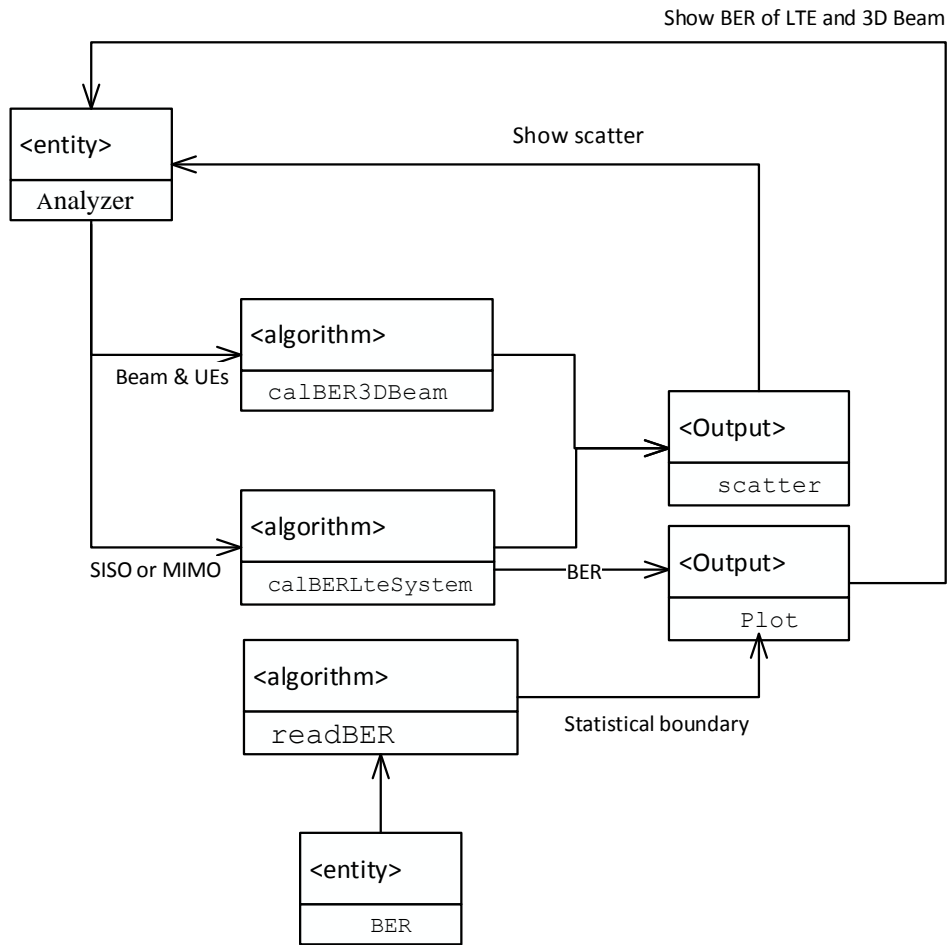


Figure A-24: The static model of the use-case ReadBERStart

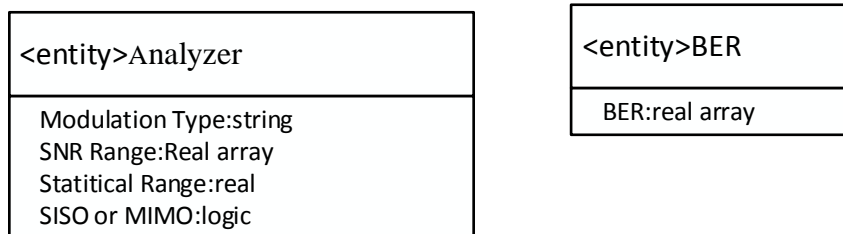


Figure A-25: The description of the entity class

The “<user interaction>:Analyzer Interaction” should be created because entity class “<entity>:Analyzer” has to interact with external users as shown in Figure A-26. In Figure A-26, the entity class “<entity>:BER” is changed into the “<data>:BER”.

Compare the BER of 3D Beam and LTE system in use case ReadBERStart

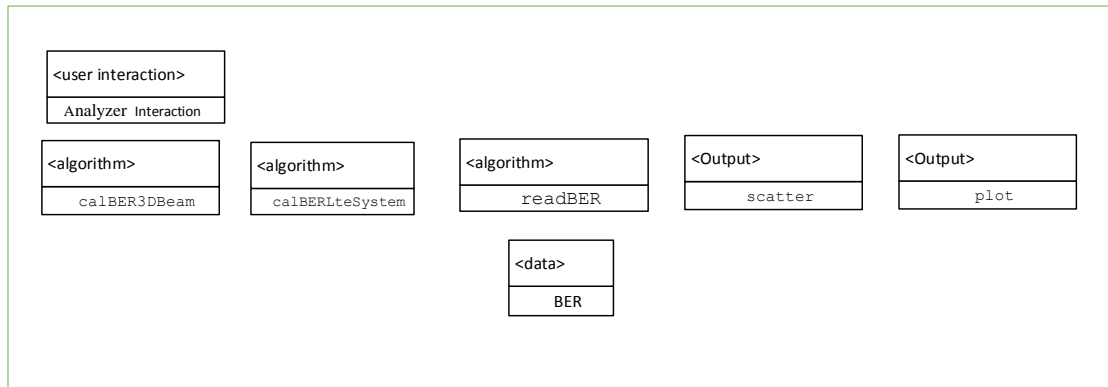


Figure A-26: The interaction between entity class “<entity>:Analyzer” and external UEs

The dynamic model of the use-case **ReadBERStart** is shown in Figure A-27 and the message description is in Table A-10.

Table A- 10: The message description of the use-case ReadBERStart

<p><b>D1:</b> The “Analyzer” sends the start to “&lt;user interaction&gt;: Analyzer Interaction”.</p> <p><b>D2.1:</b> The “&lt;user interaction&gt;: Analyzer Interaction” sends information about the modulation types, type of system (LTE SISO or MIMO) and the SNR range to the “&lt;algorithm&gt;:calBERLteSystem”, and then start the calculation.</p> <p><b>D2.2:</b> The “&lt;algorithm&gt;:calBERLteSystem” outputs the BER to “&lt;output&gt;:plot”.</p> <p><b>D2.3:</b> The “&lt;algorithm&gt;:calBERLteSystem” sends the transmitting signals to the “&lt;output&gt;:scatter”.</p> <p><b>D3.1:</b> The “&lt;user interaction&gt;:Analyzer Interaction” send the information, chose the beams and UEs on random selection, to “&lt;algorithm&gt;:calBER3DBeam”.</p> <p><b>D3.2:</b> The “&lt;algorithm&gt;:calBER3DBeam” send the received signals to “&lt;output&gt;:scatter”.</p> <p><b>D4.1:</b> The “&lt;algorithm&gt;:readBER” reads the BER from the “&lt;data&gt;:BER”.</p> <p><b>D4.2:</b> The “&lt;algorithm&gt;:readBER” outputs the Statistical Boundary of BER to the “&lt;output&gt;:plot”.</p> <p><b>D5:</b> The “&lt;output&gt;:scatter” shows the scatter for Received signal in the “&lt;user interaction&gt;:Analysts Interaction”.</p> <p><b>D6:</b> The “&lt;output&gt;:plot” shows the plot of the BER in the “&lt;user interaction&gt;: Analyzer Interaction”.</p>
---

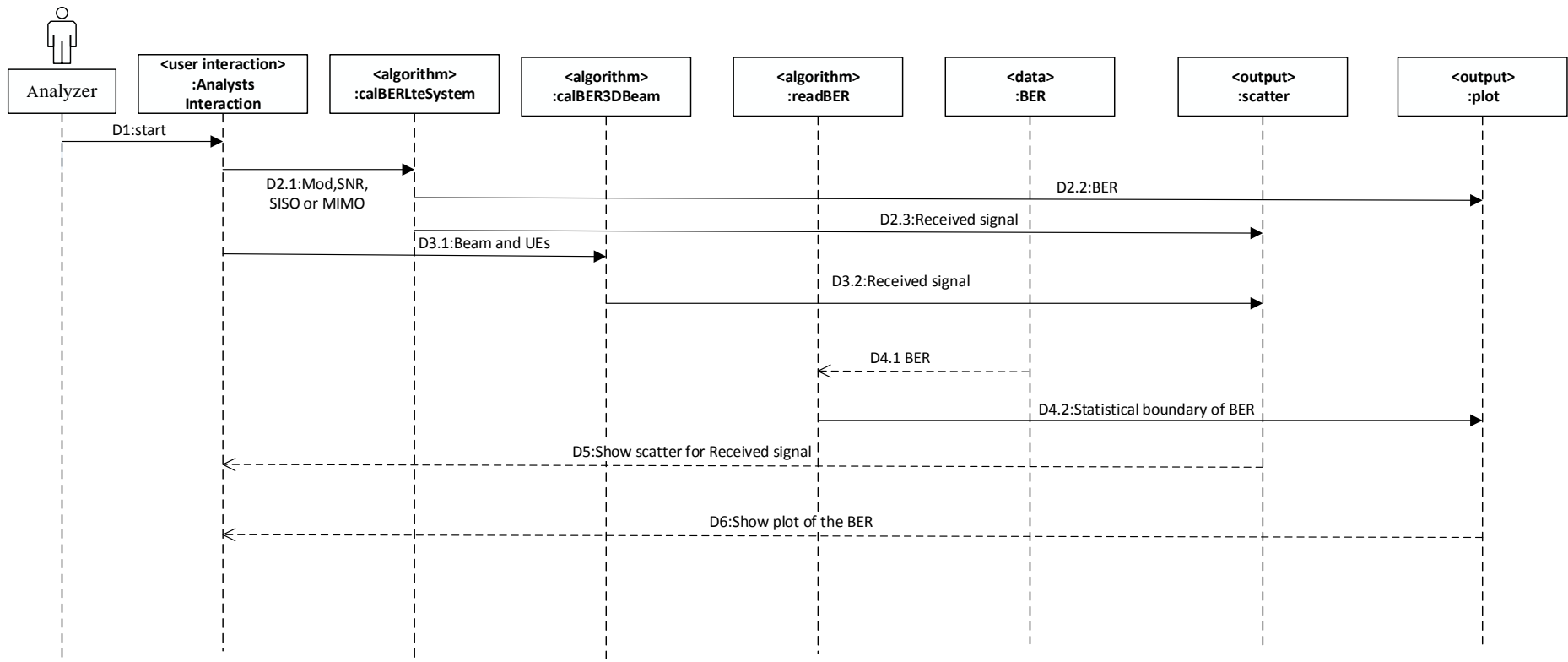


Figure A-27: The dynamic model of the use-case ReadBERStart

### A.1.7 BERCellUEsStart Use-case

Table A-11 shows the UML use-case for “**BERCellUEsStart**” and Figure A-28 is the sequence for this use-case.

**Table A- 11: The UML use-case for “BERCellUEsStart”**

<p><b>Name of Use Case:</b> BERCellUEsStart</p> <p><b>Introduction:</b> Calculate the BER under the different number of UEs, cell environments and modulation types.</p> <p><b>Participator:</b> Analyzer</p> <p><b>Preconditions:</b> Set up the SNR for analysis.</p> <p><b>Main sequence (as Figure A-28 shown):</b></p> <ol style="list-style-type: none"><li>1. Start the analyzer.</li><li>2. Set up the number of UEs.</li><li>3. Set up the base station scenes.</li><li>4. Set up the modulation type.</li><li>5. Establish the communication environment.</li><li>6. Display the communication environment.</li><li>7. The weighting matrix under maximum SINR is calculated by the least square method.</li><li>8. Calculates the BER in the 3D beamforming system.</li><li>9. Create the BER data file.</li></ol> <p><b>Alternative sequence:</b></p> <p>None</p> <p><b>Post-condition:</b></p> <p>Create a data file“&lt;entity&gt;:xxxxxxBER” (e.g. 2UMaR0BER).</p>
---

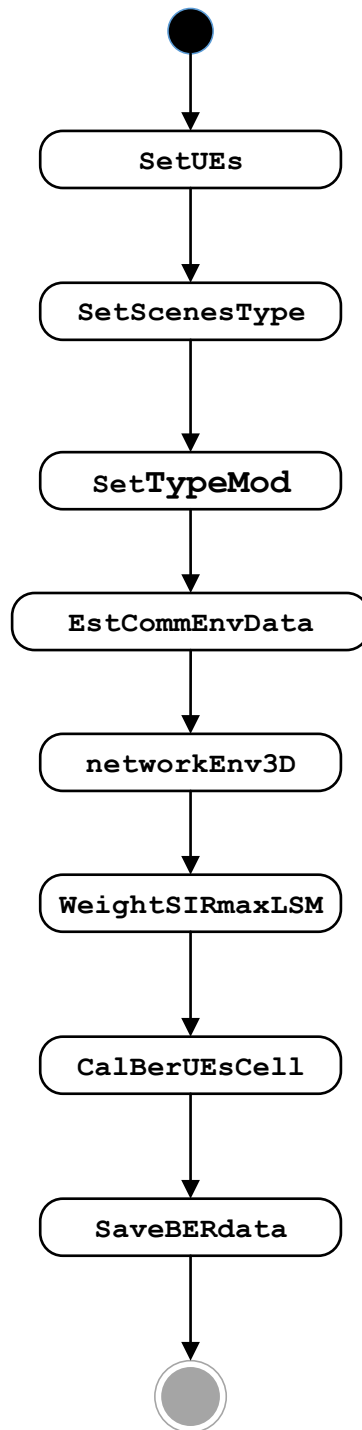


**Figure A-28: The sequence for this use-case**

The static model of the use-case **BERCellUEsStart** is shown in Figure A-29, which has three categories, entity class, algorithm class and output class. The entity class includes the “<entity>:Analyzer”, “<entity>:simData”, “<entity>:WeightLSM”, “<entity>:SINR” and “<entity>:xxxxxxxBER”. Moreover, the description of the entity class is shown in Figure A-30. The algorithm class includes the

“<algorithm>:EstCommEnvDataBER”, “<algorithm>:networkEnv3D”,  
 “<algorithm>:WeightSIRmaxLSM” and “<algorithm>:CalBerUEsCell”.

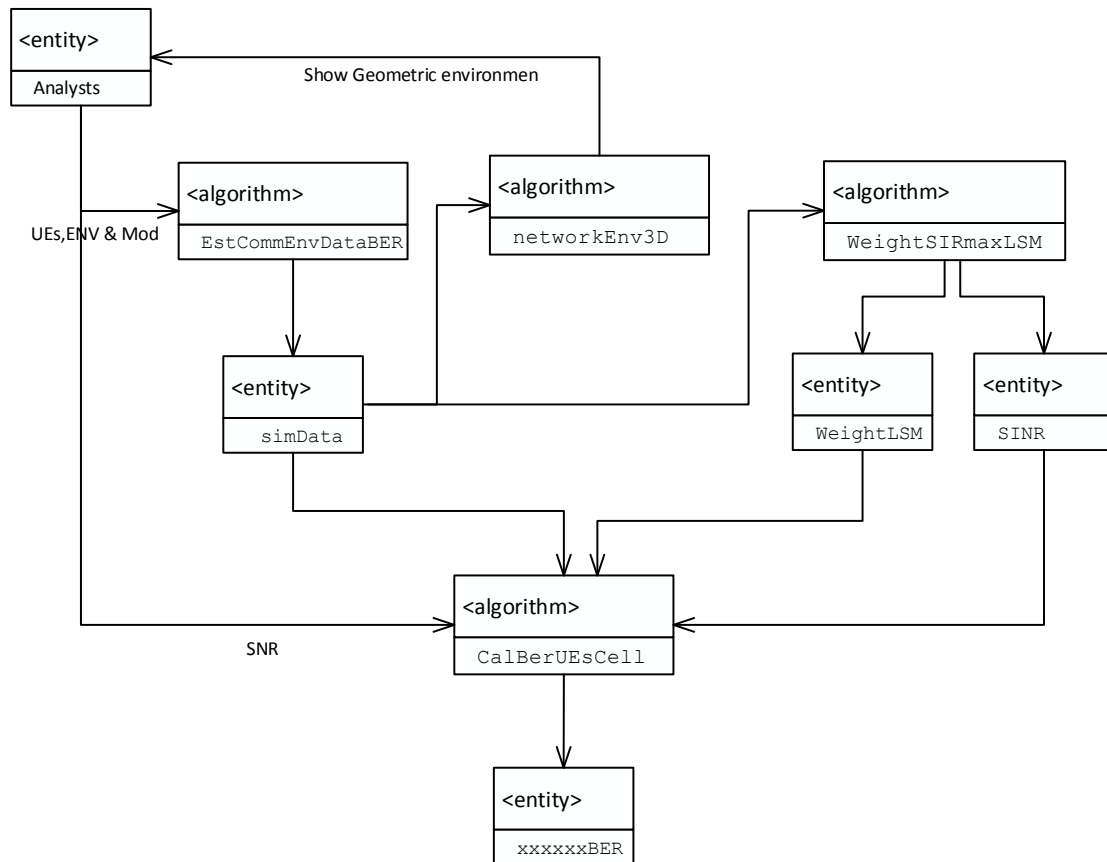


Figure A-29: The static model of the use-case BERCellUEsStart

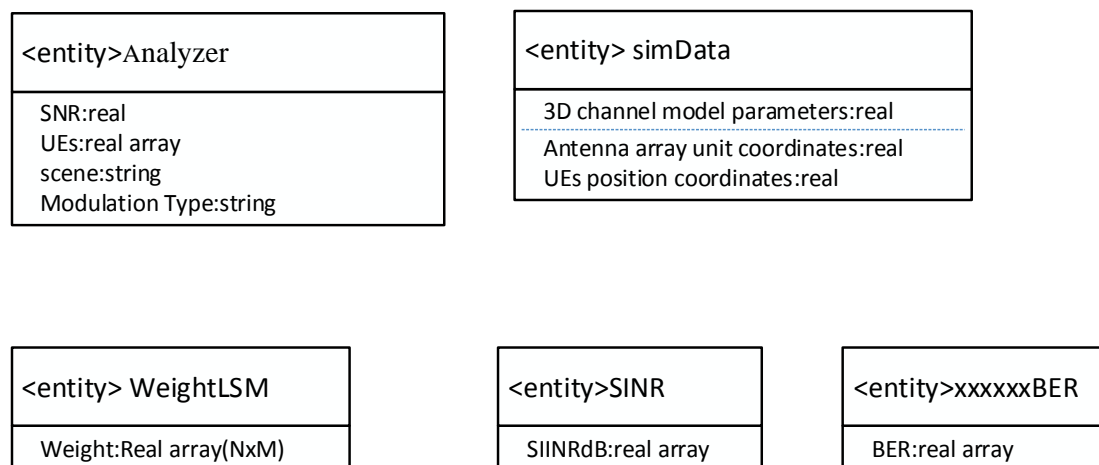
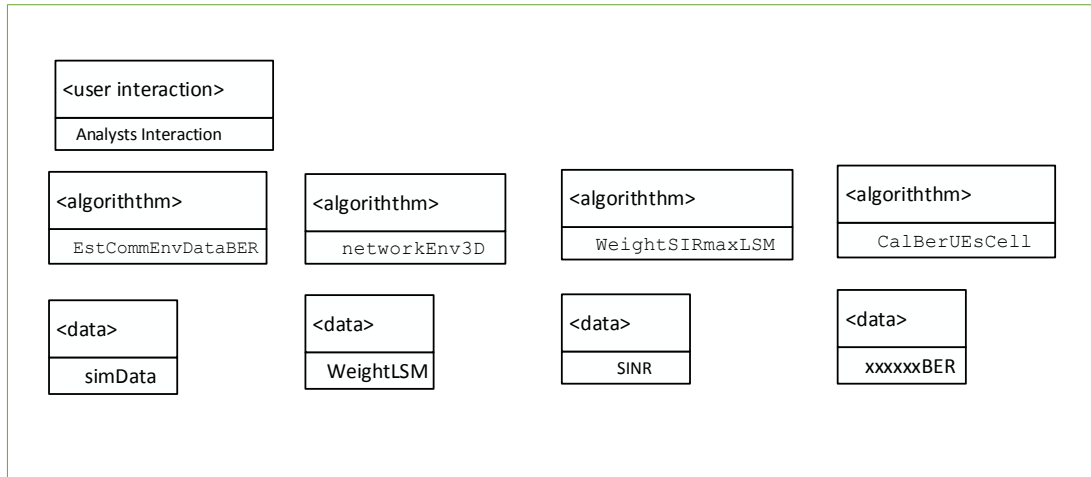


Figure A-30: The description of the entity class

The “<user interaction>:Analyzer Interaction” should be created because entity class “<entity>:Analyzer” has to interact with external users as shown in Figure A-31. In Figure A-31, the output data have the “<data>:simData”, “<data>:WeightLSM”, “<data>:SINR” and “<data>:xxxxxxBER”.

Calculate the BER for different environments in use case BERCellUEs



**Figure A-31: The interaction between entity class “<entity>:Analyzer” and external UEs**

The dynamic model of the use-case **BERCellUEsStart** is shown in Figure A-32 and the message description is in Table A-12.

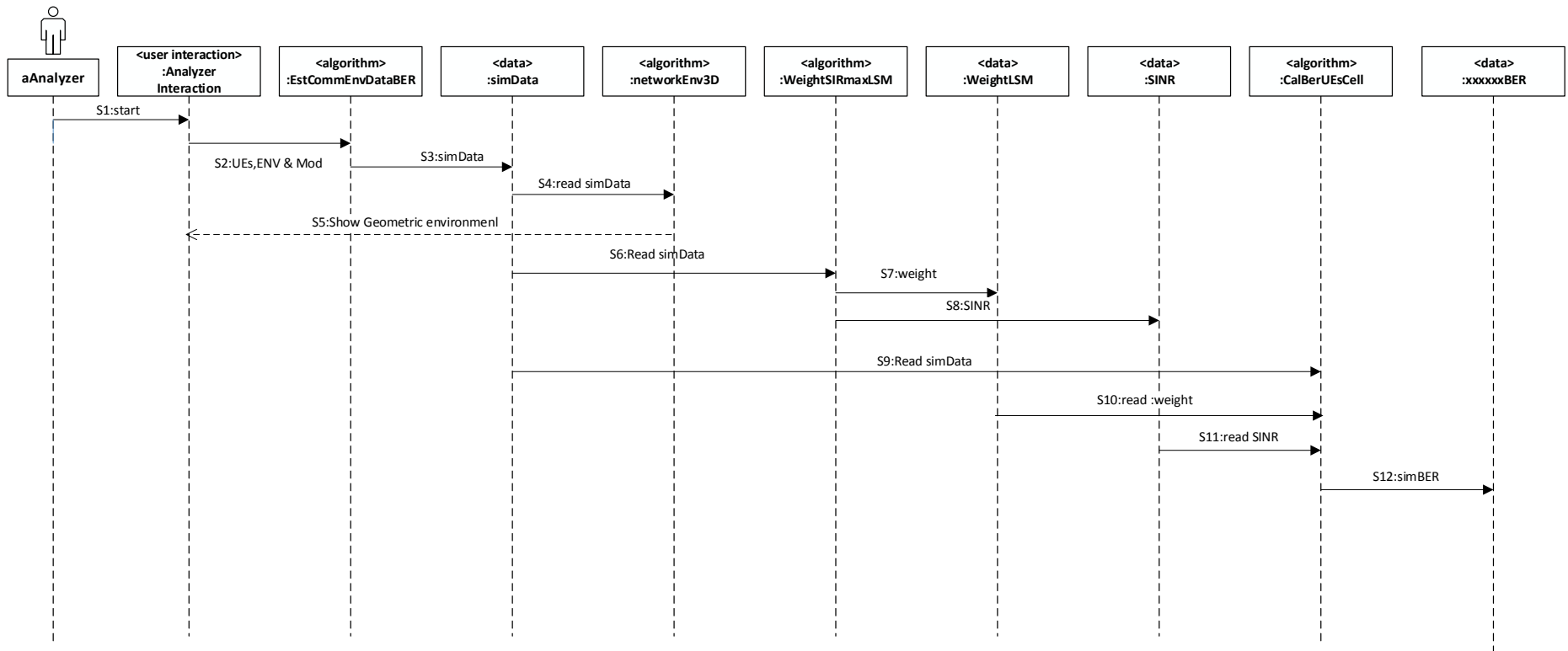


Figure A-32: The dynamic model of the use-case BERCellUEsStart



**Table A- 12: The message description of the use-case BERCellUEsStart**

<p><b>S1</b> : The “Analyzer” sends the start to “&lt;user interaction&gt;: Analyzer Interaction”.</p> <p><b>S2</b>: The “&lt;user interaction&gt;: Analyzer Interaction” sends the information, the number of UEs, the environment and modulation types, to the “&lt;algorithm&gt;:EstCommEnvDataBER”, and then start the calculation.</p> <p><b>S3</b> : The “&lt;algorithm&gt;:EstCommEnvDataBER” sends the simulation environment data to the “&lt;data&gt;simData”.</p> <p><b>S4</b> : The “&lt;algorithm&gt;:networkEnv3D” reads the simulation environment data from the “&lt;data&gt;:simData”.</p> <p><b>S5</b> : The “&lt;algorithm&gt;:networkEnv3D” displays the network figure in the “&lt;user interaction&gt;:Analyzer Interaction”.</p> <p><b>S6</b> : The “&lt;algorithm&gt;:WeightSIRmaxLSM” reads the simulation environment data from the “&lt;data&gt;:simData”.</p> <p><b>S7</b> : The “&lt;algorithm&gt;:WeightSIRmaxLSM” creates the weighting data file in the “&lt;data&gt;:WeightLSM”.</p> <p><b>S8</b> : The “&lt;algorithm&gt;:WeightSIRmaxLSM” creates the SINR data file in the “&lt;data&gt;:SINR”.</p> <p><b>S9</b> : The “&lt;algorithm&gt;:CalBerUEsCell” reads the simulation environment data from the “&lt;data&gt;:simData”.</p> <p><b>S10</b> : The “&lt;algorithm&gt;:CalBerUEsCell” reads the weighting data file in the “&lt;data&gt;:WeightLSM”.</p> <p><b>S11</b> : The “&lt;algorithm&gt;:CalBerUEsCell” reads the SINR data file to the “&lt;data&gt;:SINR”.</p> <p><b>S12</b> : The “&lt;algorithm&gt;:CalBerUEsCell” creates the BER data file in the “&lt;data&gt;:xxxxxxBER”.</p>
--

## A.1.8 Plot3DStart Use-case

Table A-13 shows the read and present data use-cases description for “**Plot3DStart**” and Figure A-33 is the activity diagram for this use-case.

**Table A- 13: The description for “Plot3DStart”**

<p><b>Name of Use Case: Plot3DStart</b></p> <p><b>Introduction:</b> Read the BER data under the different number of UEs, cell environments and modulation types and display.</p> <p><b>Participator:</b> Analyzer</p> <p><b>Preconditions:</b> The “&lt;data&gt;:xxxxxxBER” data files have been created.</p> <p><b>Main sequence (as FigureA-33 shown):</b></p> <ol style="list-style-type: none"><li>1. Start the analyzer.</li><li>2. Read the “&lt;data&gt;:xxxxxxBER” data file.</li><li>3. Displays the BER under the different number of UEs, environment and modulation types.</li></ol> <p><b>Alternative sequence:</b></p> <p>None.</p> <p><b>Post-condition:</b></p> <p>The system displays the BER under the different number of UEs, cell environments and modulation types.</p>
---

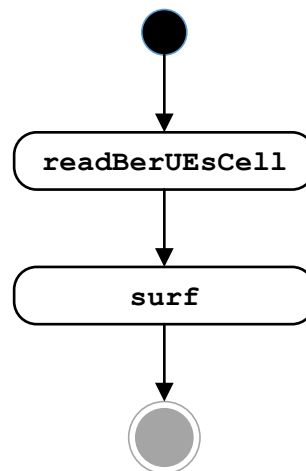


**Figure A-33: The activity diagram for use-case**

The static model of the use-case **Plot3DStart** is shown in Figure A-34, which has three categories, entity class, algorithm class and output class. The entity class includes the “<entity>:Analyzer” and “<entity>:xxxxxxBER”. Moreover, the description of the entity class is shown in Figure A-35. The output class is “<output>:surf”. The algorithm

class is “readBerUEsCell”.

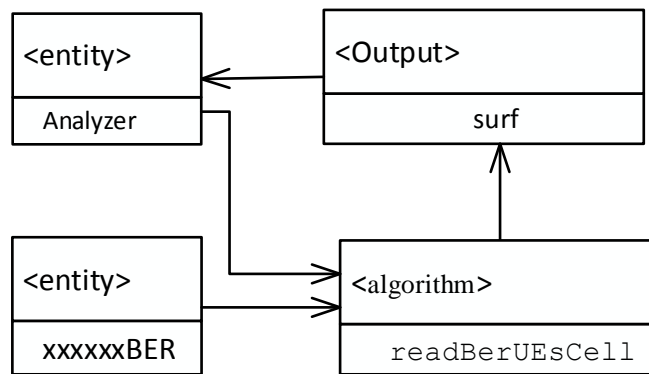


Figure A-34: The static model of the use-case Plot3DStart

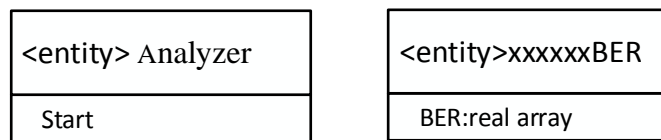


Figure A-35: The description of the entity class

The “<user interaction>:Analyzer Interaction” should be created because entity class “<entity>:Analyzer” has to interact with external users as shown in Figure A-36. In Figure A-36, the entity class “<entity>:xxxxxxBER” is changed to the “<data>:xxxxxxBER”.

Read and displays the BER under the different number of UEs, environment and modulation types use case Plot3DStart

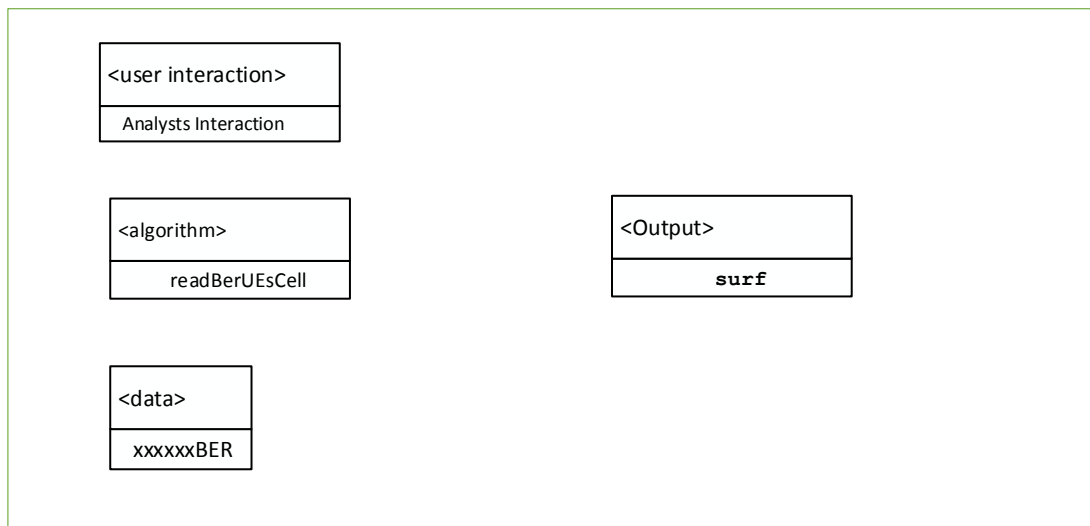
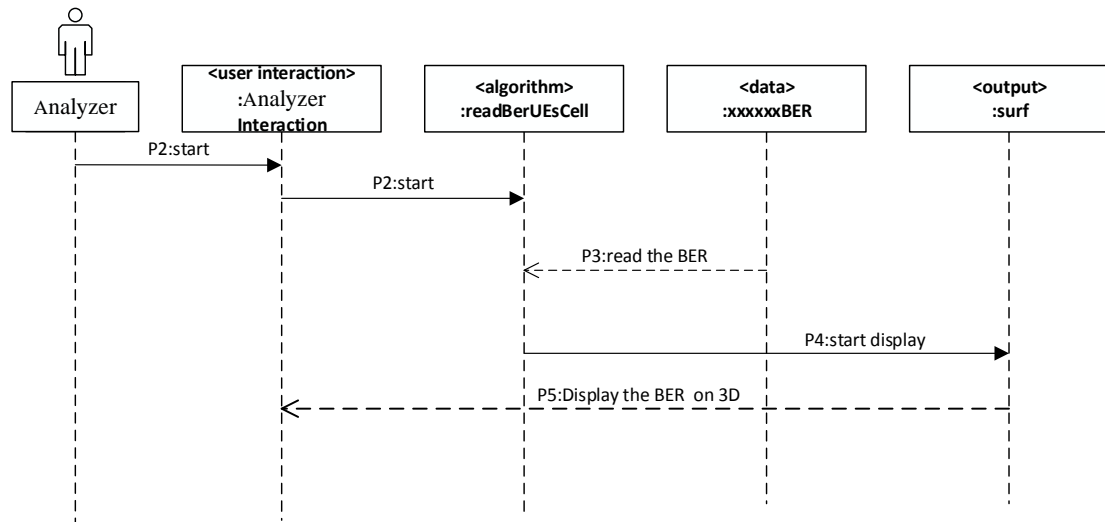


Figure A-36: The interaction between entity class “<entity>:Analyzer” and external UEs

The dynamic model of the use-case **Plot3DStart** is shown in Figure A-37 and the message description is in Table A-14.

**Table A- 14: The message description of the use-case Plot 3D Start**

<p><b>P1:</b> The “Analyzer” sends the start to “&lt;user interaction&gt;: Analyzer Interaction”.</p> <p><b>P2:</b> The “&lt;user interaction&gt;: Analyzer Interaction” sends the start to the “&lt;algorithm&gt;:readBerUEsCell”.</p> <p><b>P3:</b> The “&lt;algorithm&gt;:readBerUEsCell” reads the data from the “&lt;data&gt;:xxxxxxxBER”.</p> <p><b>P4:</b> The “&lt;algorithm&gt;:readBerUEsCell” sends the data to the “&lt;output&gt;:surf”.</p> <p><b>P5:</b> The “&lt;output&gt;:surf” displays the BER under the different number of UEs, environment and modulation types in the “&lt;user interaction&gt;: Analyzer Interaction”.</p>
---



**Figure A-37: The dynamic model of the use-case Plot3DStart**

## A.2 The Simulation System design

All simulation system designs are under the environment of the Matlab R2016b software.

### A.2.1 Data Class

In these 7 UML use-cases, there are 5 classes, which are shown in Figure A-38. In the Matlab R2016b program, they are all structure variables, which are used in different functions.

data classes in 7 use cases

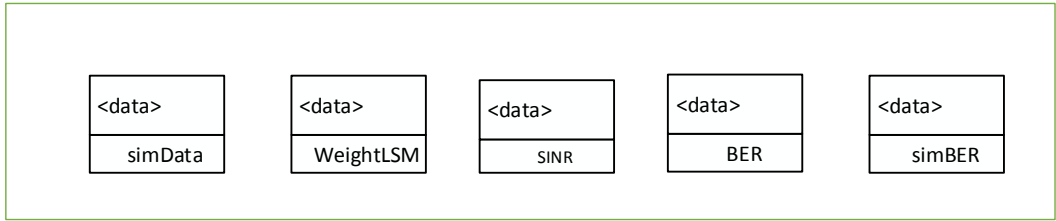


Figure A-38: Data classes in 7 UML use-cases

### A.2.2 Output Class

In these 7 UML use-cases, there are 3 classes, which are shown in Figure A-39. In the Matlab program, they are all corresponding functions.

output classes in 7 use cases

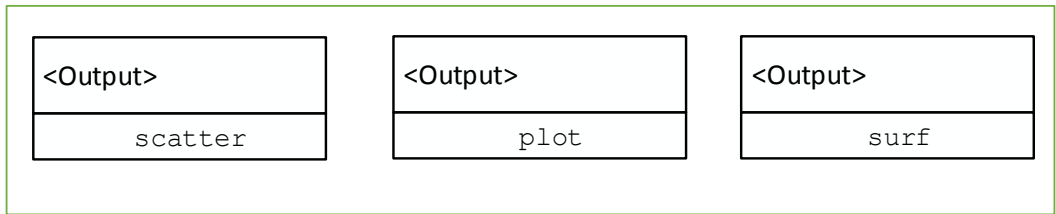


Figure A-39: Output classes in 7 UML use-cases

### A.2.3 Interactive Interface

In these 7 UML use-case, there are 7 interactive interfaces, which have different input parameters as shown in Figure A-40.

user interaction classe

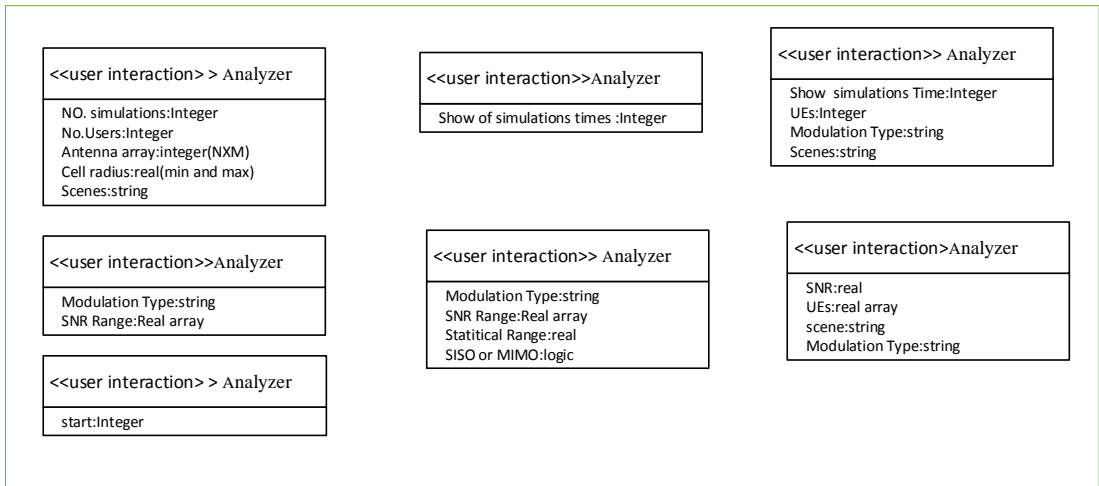
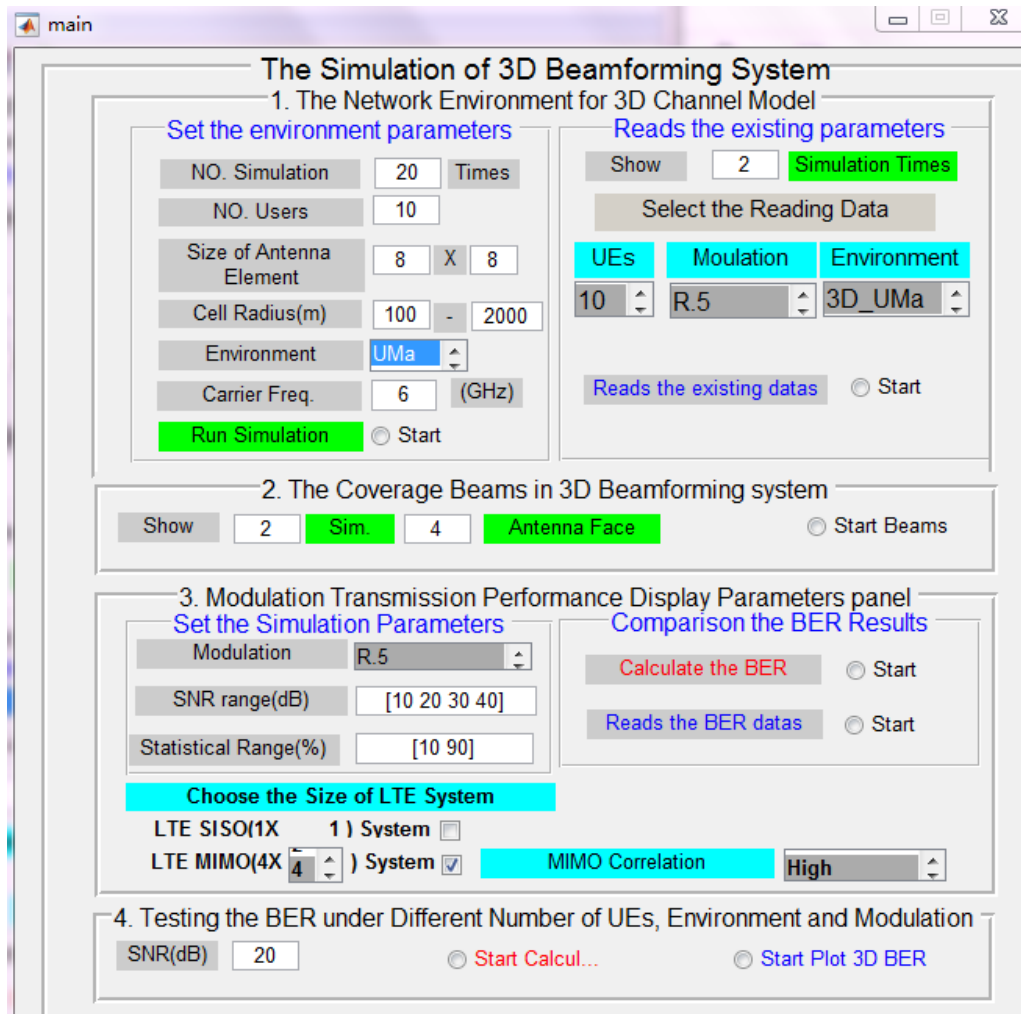


Figure A-40: 7 UML use-case interactive interfaces

The Matlab R2016b software was used to create a GUI function for the interactive

interface as shown in Figure A-41, which is named **main.m**.



**Figure A-41: GUI function for the interactive interface**

In this program, all options and parameters are built in **main.fig**, namely the Simulation of 3D Beamforming System. This function presents the “Set the environment parameters” (related to **SimStart\_Callback**) in the “Network Environment for 3D Channel Model” and asks the user to set the simulation parameters such as number of UEs etc. Since 24 areas may be covered and 20 or more simulation runs may be used and it is impractical for all these to be presented, the user needs to choose which simulation run and which coverage area to display. This processing is done in the “Coverage Beams in 3D Beamforming system” (related to **BeamStart\_Callback**).

“Modulation Transmission Performance Display Parameters panel” (related to **CBERStart\_Callback**) allows the user to set the modulation type for the 3D

beamforming system and the MIMO type, size and correlation for the comparison LTE system. It also allows the user to define what SNR range to display and the BER confidence interval to plot for the 3D beamforming system.

“Testing the BER under Different Number of UEs, Environment and Modulation” (related to **BERCellUEsStart\_Callback**), which displays a figure to compare how the BER is affected by the number of UEs, the types of channel environment and modulation at a particular SNR denied by the user. According to the location of UEs, the K-means algorithm can cluster them into different clusters in a hexagonal antenna arrays cell.

### A.3 Function SimStart\_Callback (hObject, eventdata, handles)

Call the function “**SimStart\_Callback**” in **main.m**, which is a radio button in **main.fig**. In here, the program can finish the first step for simulation and set the parameters form the 3D network environment. The parameter “hObject” represents the handling for function, “eventdata” is reserved to be defined in a future version of MATLAB and “handles” is structured the handles and input data. The flow chart of functions is shown in Figure A-42.



Figure A-42: The flow chart of functions

#### A.3.1 Function EstCommEnv

- **Function [simData] = EstCommEnv( NumSim, NumUser, Nz, Ny, N\_AntUE, typeScenario, FreqCarrier, d2Dmax, d2Dmin, h\_UTmax, h\_UTmin )**

Call the function **EstCommEnv.m** from the function “**SimStart\_Callback**”,

which is built the 3D network environment. Save the setting parameters form the options in **main.fig** in the file 'data\data0'. The flow chart of functions is shown in Figure A-43. In this function, the parameters are same as the parameters in **RunSim.m** and it can run the simulation for NumSim (e.g:NumSim=20) times.

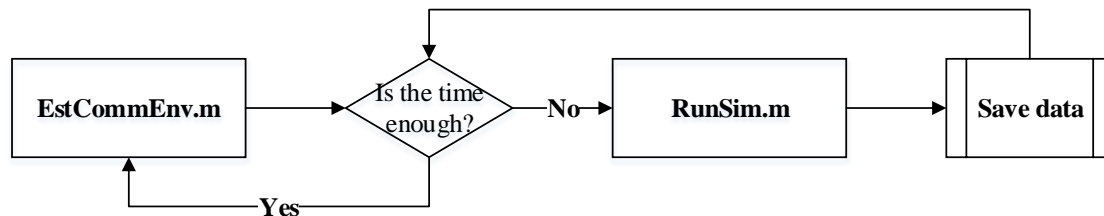


Figure A-43: The flow chart of functions of EstCommEnv

According to the number of time for simulation 'NumSim', the function **RunSim.m** is run to simulation and the results can be respectively stored in 'data\SimData1.mat' to 'data\SimData20.mat'. The parameter “NumSim” represents the time of running simulation and other parameters are shown in next function.

### A.3.1.1 Function RunSim

- Function [simData] = RunSim (NumUser, Nz, Ny, N\_AntUE, typeScenario, FreqCarrier, d2Dmax, d2Dmin, h\_UTmax, h\_UTmin)

Call the function **RunSim.m** from the function **EstCommEnv.m**. In this function, the parameters in the “3GPP TR36.873” are saved in function **fixparset.m**, which are about the channel. The parameters in the “3GPP TR36.873” are stored in **ScenParTables.m**, which are about the environment 3D-UMi and 3D-UMa in order to generate the structure variable parameters **Envpar** for the network environment. Then a structure variable **simData** can be generated, which includes **Envpar**, **antArray** and **UserPosit**. They are the network environment parameters, the antenna array parameters and the location parameters of users. The parameters are explained in the Table A-15.



**Table A- 15: Parameters about the channel**

<b>Parameters</b>	<b>Meaning</b>
simData	The simulation results as the output data
NumUser	The number of UEs
Nz	The number of antenna array in y-z-plane for transmitter
Ny	The number of antenna array in x-y-plane for transmitter
N_AntUE	The number of antenna in receiver
typeScenario	The scenarios for system
FreqCarrier	The carrier frequency
d2Dmax	The maximum value of 2D distance in 3D Channel Model
d2Dmin	The minimum value of 2D distance in 3D Channel Model
h_UTmax	The maximum value of height of UE in 3D Channel Model
h_UTmin	The minimum value of height of UE in 3D Channel Model

In this function, all local coordinates from other subroutines are changed to global coordinates for the cell. The flow chart of functions is shown in Figure A-44.

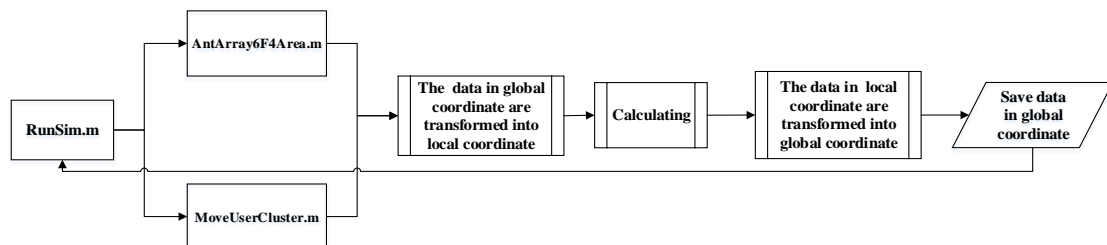


**Figure A-44: The flow chart of functions of RunSim**

### A.3.1.1.1 Function AntArray6F4Area

- **Function antArray = AntArray6F4Area (lambda, Nz, Ny, hBS, NUMFace, NUMArea)**

Call the function **AntArray6F4Area.m** from the function **RunSim.m**. The antenna array is generated. In one cell, there are 6 faces and each face can be separate to 4 areas. The origin coordinates for each area are changed to global coordinates for the cell. The parameters of antenna array and the coordinate's data are record in the structure variable **antArray**. The parameters are explained in the Table A-16. The flow chart of functions is shown in Figure A-45.

**Table A- 16: parameters of antenna array and the coordinate's data**

<b>Parameters</b>	<b>Meaning</b>
antArray	The antenna array information as the output data
lambda	The $\lambda$
Nz	The number of antenna array in y-z-plane for transmitter
Ny	The number of antenna array in x-y-plane for transmitter
hBS	The height of the base station
NUMFace	The number of faces
NUMArea	The number of areas

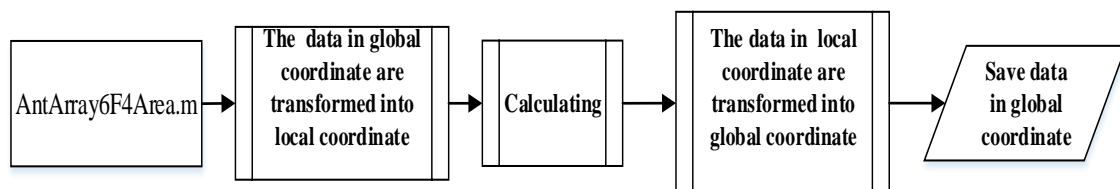


**Figure A-45: The flow chart of functions of AntArray6F4Area.m**

### A.3.1.1.1.1 Function MoveUserCluster

Uses Sub Functions:

1. Function MoveUser
2. Function UserInFaceArea

- **Function UserPosit = MoveUserCluster(NUMFace, NUMArea, NumUser, antArray, simData)**

Call the function **MoveUserCluster.m** from the function **RunSim.m**. In this function, the multiple UEs are generated in the cell, in which the UEs in same area is as one cluster and the center coordinates of the cluster are recorded, which is the basis of the direction of the 3D beamforming. The parameters are explained in the Table A-17. The flow chart of functions is shown in Figure A-46.

**Table A- 17: The parameters in the function MoveUserCluster.m**

<b>Parameters</b>	<b>Meaning</b>
UserPosit	The location of UEs as the output data
NUMFace	The number of faces
NUMArea	The number of areas
NumUser	The number of UEs
antArray	The antenna array information
simData	The simulation channel information

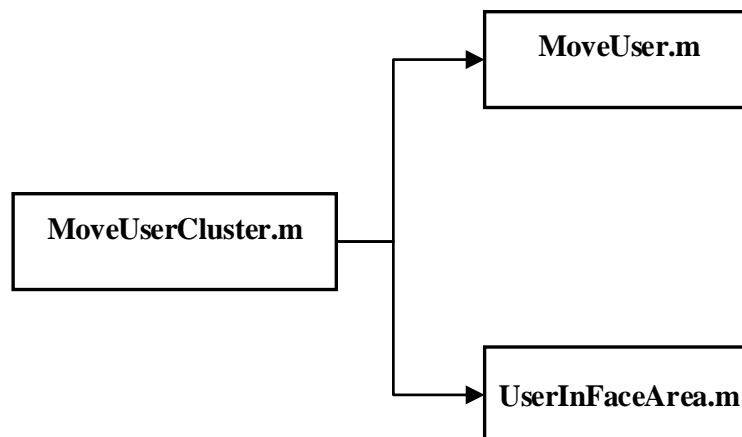


**Figure A-46: The flow chart of function MoveUserCluster**

- **Function [X,Y,Z] = MoveUser (NumUser, simData)**

In this function, generate the location coordinates of users, which is random distribution in the cell. The parameter “NumUser” represents the number of UEs and X, Y, Z are is global coordinates of each UEs.

- **Function UserPosit = UserInFaceArea(NUMFace, NUMArea, NumUser, X, Y, Z, antArray)**

In this function, the UEs in different areas are made the users be covered in different 3D beamforming, which are saved in the structure variable **UserPosit**. Moreover, the global coordinates of users are changed to the local coordinates for the cell. The parameters are explained in the Table A-18.

**Table A- 18: The parameters in function UserPosit**

<b>Parameters</b>	<b>Meaning</b>
UserPosit	The location of UEs as the output data
NUMFace	The number of faces
NUMArea	The number of areas
NumUser	The number of UEs
X	The data in x-axis
Y	The data in y-axis
Z	The data in z-axis
antArray	The antenna array information

### **A.3.2 Function networkEnv3D**

- **Function [NumSim, NumUser, Nz, Ny, d2Dmin, d2Dmax, Type] = networkEnv3D (umSim0)**

Call the function **networkEnv3D.m** from the function “**SimStart\_Callback**”. Load the setting data from the file 'data\data0'. Then choose one time of the simulation

and load the data from the file 'data\SimDataX.mat'(X=1 to 20). The function **networkEnv3D.m** can draw the network environment for the cell as Figure A-47 shown.

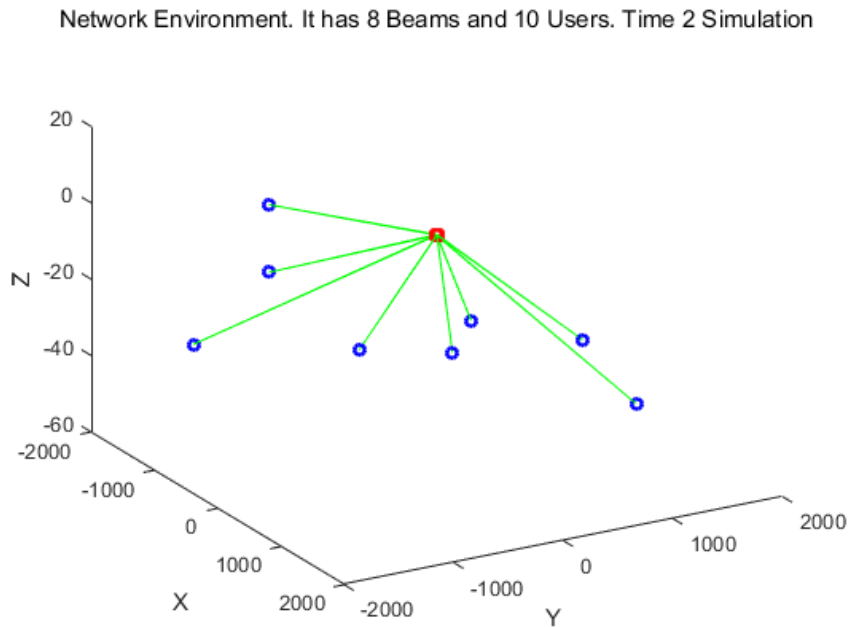


**Figure A-47: The network environment for the cell**

The parameters are explained in the Table A-19. The flow chart of functions is shown in Figure A-48.

**Table A- 19: The parameters of function networkEnv3D**

Parameters	Meaning
NumSim	The time of running simulation
NumUser	The number of UEs
Nz	The number of antenna array in y-z-plane for transmitter
Ny	The number of antenna array in x-y-plane for transmitter
d2Dmax	The maximum value of 2D distance in

	3D Channel Model
d2Dmin	The minimum value of 2D distance in 3D Channel Model
Type	The type of the 3D Channel Model
umSim0	Which time for running simulation

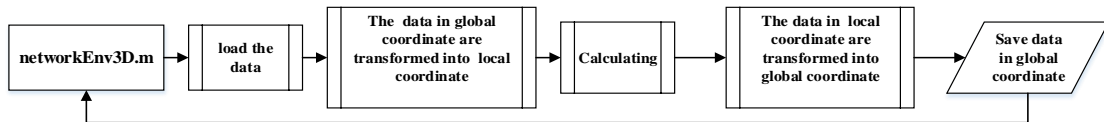


Figure A-48: The flow chart of function networkEnv3D

#### A.4 Function ReadStart\_Callback (hObject, eventdata, handles)

Call the function “**ReadStart\_Callback**” in **main.m**, which is a radio button in **main.fig**. In this function, the program reads the data of the channel model from the file 'data' and show the results in the figures. The flow chart of functions are shown in Figure A-49.

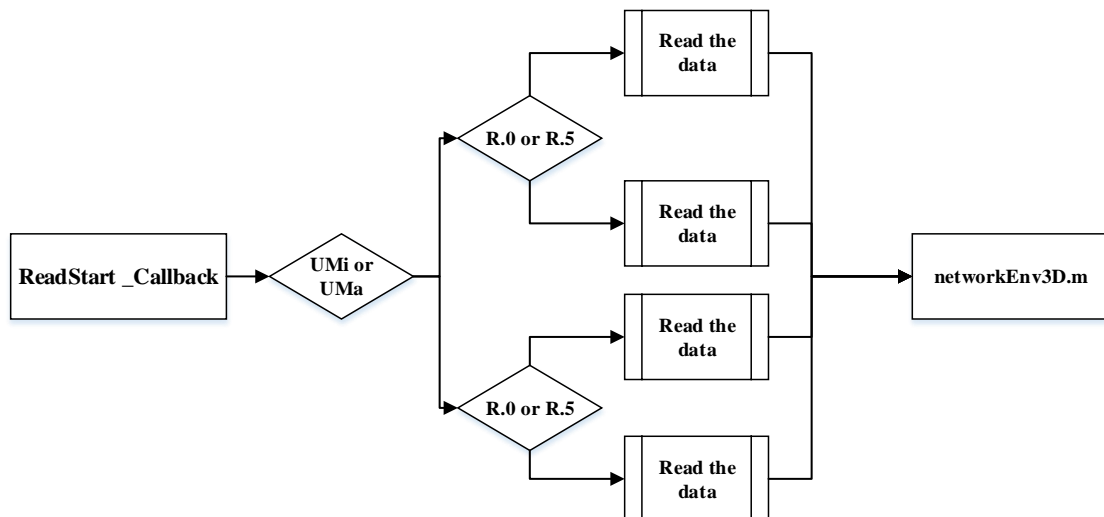


Figure A-49: The flow chart of function ReadStart\_Callback

## A.5 Function BeamStart\_Callback ( hObject, eventdata, handles)

Call the function “**BeamStart\_Callback**” in **main.m**, which is a radio button in **main.fig**. If we choose this button, the program can draw all beam patterns for the cell and show the face by the chosen. The parameter “ hObject” represents the handling for function, “ eventdata” is reserved to be defined in a future version of MATLAB and “ handles” is structured the handles and input data. The flow chart of functions are shown in Figure A-50.

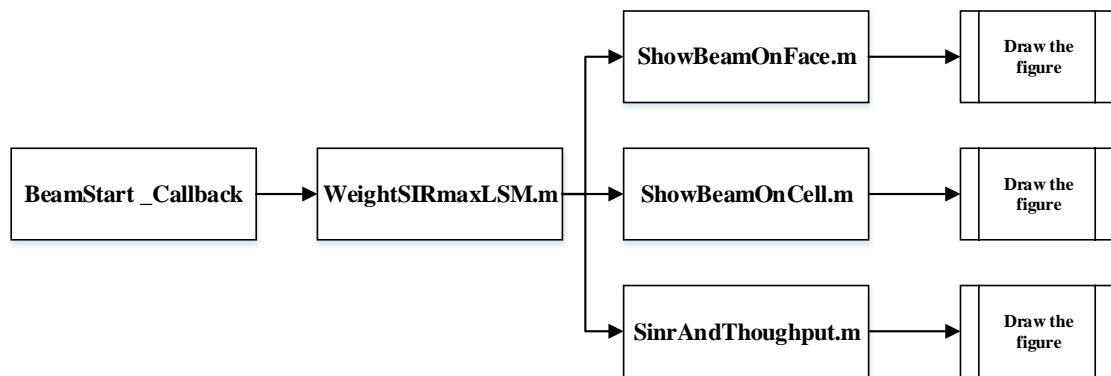


Figure A-50: The flow chart of function **BeamStart\_Callback**

### A.5.1 Function **WeightSIRmaxLSM**

- **Function [WeightLSM] = WeightSIRmaxLSM**

Call the function **WeightSIRmaxLSM.m** from the function “**BeamStart\_Callback**”, which is calculating the weighting of the antenna array for the maximum values of SIR. According to the number of time for simulation 'NumSim', the function can calculate the weighting for different time of simulation and the data weighting, angle theta( $\theta$ ) and angle phi( $\varphi$ ) are saved in the structure variable **WeightLSM**. After calculating, all results are stored in the file 'data\ WeightwA.mat'. The parameter “WeightLSM” represents the weighting matrix for the beam. The flow chart of functions is shown in Figure A-51.

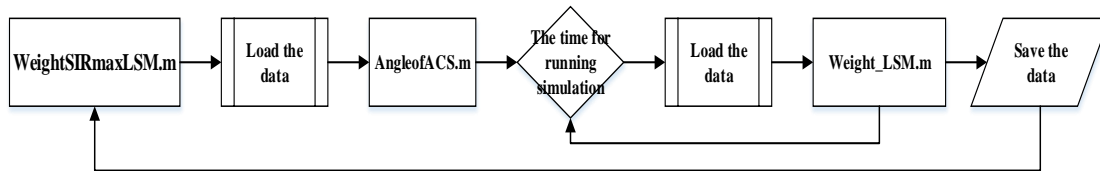


Figure A-51: The flow chart of function WeightSIRmaxLSM

### A.5.1.1 Function AngleofACS

- **Function**  $[Angle] = \text{AngleofACS}(\text{NUMFace}, \text{NUMArea})$

Call the function **AngleofACS.m** from the function **WeightSIRmaxLSM.m**. In this function, the center point **coordinates** for the beam are obtained, in which the angle theta and the angle phi for main beam and other users are calculated. Then they and weighting data are read by the file 'data\SimDataX.mat'. Moreover, the data can be changed to global coordinates and they are saved in structure variable **Angle**. The parameter “Angle” represents the direction angle of beams, “NUMFace” represents the number of faces and “NUMArea” represents the number of areas. The flow chart of functions is shown in Figure A-52.

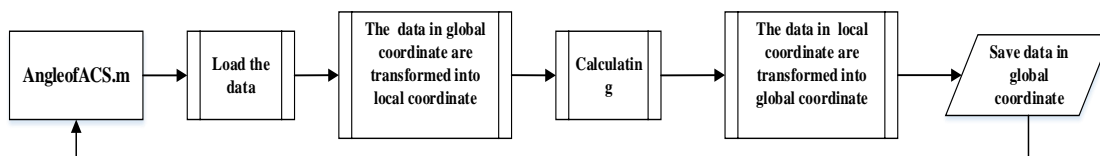


Figure A-52: The flow chart of function AngleofACS

### A.5.1.2 Function Weight\_LSM

- **Function**  $[w] = \text{Weight\_LSM}(\text{theta}, \text{phi}, L, N, M, Xs0, dx, Ys0, dy, K)$

Call the function **Weight\_LSM.m** from the function **WeightSIRmaxLSM.m**. In this function, the weighting matrix for one face are calculated. In this method, the main beam for one cluster is maximum, however, the side-lobes for other users have been closed to zero. The parameters are explained in the Table A-20.

Table A- 20: The parameters in the function Weight\_LSM



Parameters	Meaning
w	The weighting matrix as the output
theta	The angle $\theta$
phi	The angle $\varphi$
L	The number of beams
N	The number of antenna element in x-direction
M	The number of antenna element in y-direction
Xs0	The initial value for x
dx	The distance between each antenna element in x-direction
Ys0	The initial value for y
dy	The distance between each antenna element in y-direction
K	An constant value

The function is the calculation for the equation in the section:

$$\begin{aligned}
 AF_x &= \sum_{m=1}^M a_m e^{j(m-1)(kd_x \sin \theta \cos \varphi + \beta_x)} \\
 &= \begin{bmatrix} 1 & e^{j(kd_x \sin \theta \cos \varphi + \beta_x)} & \dots & e^{j(M-1)(kd_x \sin \theta \cos \varphi + \beta_x)} \end{bmatrix} \begin{bmatrix} a_1 \\ a_2 \\ \dots \\ a_M \end{bmatrix} \quad (A-1)
 \end{aligned}$$

$$\begin{aligned}
 AF_y &= \sum_{n=1}^M b_n e^{j(n-1)(kd_y \sin \theta \cos \varphi + \beta_y)} \\
 &= \begin{bmatrix} 1 & e^{j(kd_y \sin \theta \cos \varphi + \beta_y)} & \dots & e^{j(n-1)(kd_y \sin \theta \cos \varphi + \beta_y)} \end{bmatrix} \begin{bmatrix} b_1 \\ b_2 \\ \dots \\ b_N \end{bmatrix} \quad (A-2)
 \end{aligned}$$

### A.5.2 Function ShowBeamOnFace

- **Function [status] = ShowBeamOnFace( NSim, nFace )**

Call the function **ShowBeamOnFace.m** from the function “**BeamStart\_Callback**”, which is drawing the beam patterns for users and showing one face in the figures. According to read the structure variable **WeightLSM** from the file 'data\WeightwA.mat', the field strength is calculated by the equation (A-1) and (A-2), which is the beam pattern for clusters. The parameter “status” is a counter, “NSim” represents the time for running simulation and “nFace” represents the number of the faces. The flow chart of functions is shown in Figure A-53.

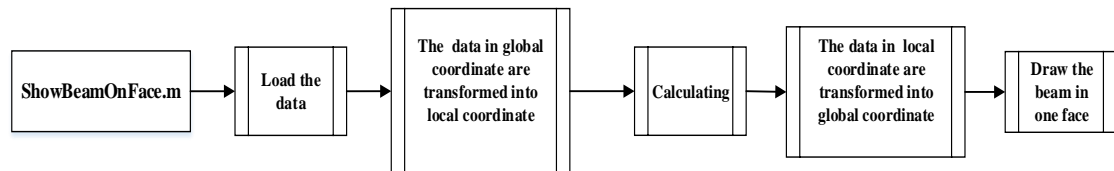


Figure A-53: The flow chart of function ShowBeamOnFace

### A.5.3 Function ShowBeamOnCell

- **Function [status] = ShowBeamOnCell( NSim )**

Call the function **ShowBeamOnCell.m** from the function “**BeamStart\_Callback**”, which is drawing the beam patterns for all users in one cell. The function reads the structure variable **WeightLSM** from the file 'data\WeightwA.mat' for calculating, which is as same as the calculation method in over function. The parameter “status” is a counter and the “NSim” represents the time for running simulation. The flow chart of functions is shown in Figure A-54.

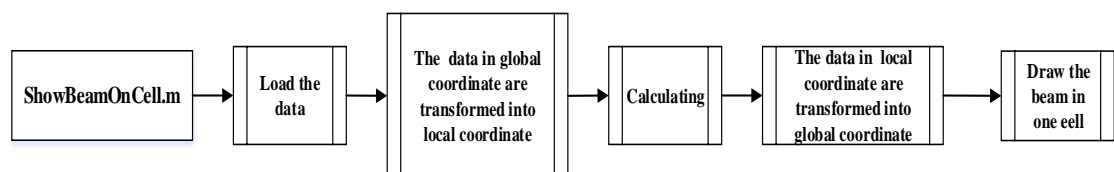


Figure A-54: The flow chart of function ShowBeamOnCell

## A.5.4 Function SinrAndThroughput

- **Function [status] = SinrAndThroughput**

Call the function **SinrAndThroughput.m** from the function “**BeamStart\_Callback**”, which is calculating the SINR and the theoretical maximum values of throughput for all users in one cell. The function reads the structure variable **WeightLSM** from the file 'data\ WeightwA.mat' and the structure variable **simData** from the file 'data\SimDataX.mat' for calculating. The parameter “status” is a counter. The flow chart of functions is shown in Figure A-55.

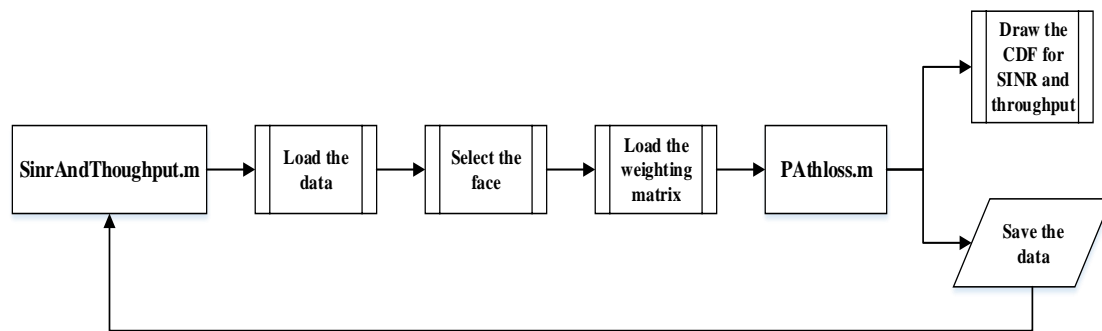


Figure A-55: The flow chart of function Sinr And Throughput

### A.5.4.1 Function pathloss

- **Function [PL, SF] = pathloss(Envpar, d3D, d2D, hUT, hBS, TypeCluster)**

Call the function **pathloss.m** from the function **SinrAndThroughput.m**, which is calculating the PL for the channel. The parameters in the equation for PL are based on the “3GPP TR36.873”. The parameters are explained in the Table A-21.

Table A- 21: The parameters in the function pathloss

Parameters	Meaning
PL	Path loss as output
SF	Shadow fading as output
Envpar	The parameters for the network environment
d3D	The 3D distance in 3D Channel Model

d2D	The 2D distance in 3D Channel Model
h_UT	The height of UE in 3D Channel Model
h_BS	The height of BS in 3D Channel Model
TypeCluster	The type of the path : NLOS or LOS

## A.6 Function CBERStart\_Callback (hObject, eventdata, handles)

Call the function “**CBERStart\_Callback**” in **main.m**, which is a radio button in **main.fig**. In this function, the program can calculate the impulse response function of channel and the BER for each user. The parameter “hObject” represents the handling for function, “eventdata” is reserved to be defined in a future version of MATLAB and “handles” is structured the handles and input data. The flow chart of functions is shown in Figure A-56.

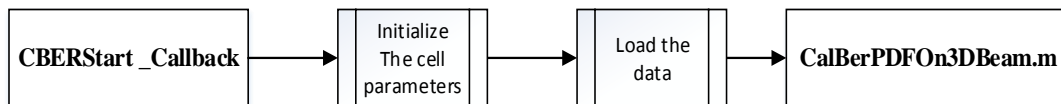


Figure A-56: The flow chart of function CBERStart\_Callback

### A.6.1 Function CalBerPDFOn3DBeam

- **Function [simBER] = CalBerPDFOn3DBeam(SNRIn, SINRdB, enb)**

Call the function **CalBerPDFOn3DBeam.m** from the function “**CBERStart\_Callback**”, which is based on the example in the Matlab 2016b how to measure the Physical Downlink Shared Channel (PDSCH) throughput performance using the LTE System Toolbox(TM). The BER is calculated for PDF and CDF shown in the figures, which is saved in the file 'data\BER.mat'. The parameters are explained in the Table A-22. The flow chart of functions is shown in Figure A-57.

Table A- 22: The parameters in function CalBerPDFOn3DBeam

Parameters	Meaning
simBER	The BER of simulation as output
SNRIn	The initializing values of SNR
SINRdB	The SINR from the calculation

enb	The structure variable from the RMC R.0-9 in Matlab 2016b
-----	--

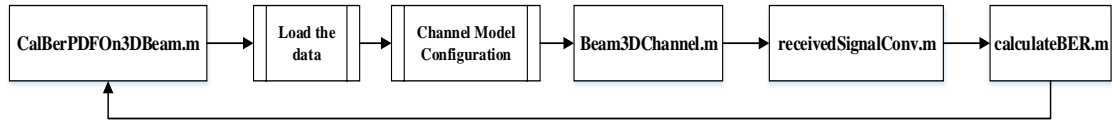


Figure A-57: The flow chart of function CalBerPDFOn3DBeam

## A.6.2 Function Beam3DChannel

- **Function [ht, Weight, Nif, d3D] = Beam3DChannel (Nsim, Nface, Nbeam, nUser, info, NPoffset)**

Call the function **Beam3DChannel.m** from the function **CalBerPDFOn3DBeam.m**. In this function, 3D Channel Impulse Response Function for each beamforming has been built, which is the variable **ht**. The parameters are explained in the Table A-23. The flow chart of functions is shown in Figure A-58.

Table A- 23: The parameters in function Beam3DChannel

Parameters	Meaning
ht	The transfer function of channel model as output
Weight	An equal weighting matrix as output
Nif	The non-equal-spaced fast Fourier transform
d3D	The 3D distance in 3D Channel Model
Nsim	The time of running simulation
Nface	The number of faces
Nbeam	The number of beams
nUser	The number of UEs
info	The information for OFDM
NPoffset	The offset

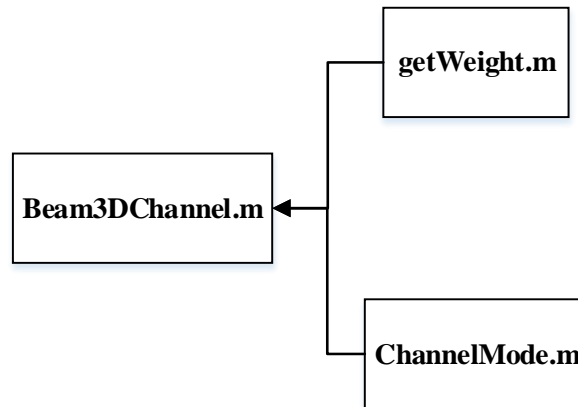


Figure A-58: The flow chart of function Beam3DChannel

### A.6.2.1 Function getWeight

- **Function [Weight, Num,xyzUE, Center] = getWeight (Nsim, nFace, nArea)**

Call the function **getWeight.m** from the function **Beam3DChannel.m**. The weighting matrix for antenna array is read from the structure variable **WeightLSM** from the file 'data\WeightwA.mat'. The parameters are explained in the Table A-24.

Table A- 24: The parameters in function getWeight

Parameters	Meaning
Weight	An all one matrix as output
Num	The size of antenna array as output
xyzUE	The location of UEs as output
Center	The center of cluster for the beam as output
Nsim	The time of running simulation
Nbeam	The number of beams
nFace	The number of faces
nArea	The number of areas

### A.6.2.2 Function ChannelMode

- **Function** `[h] = ChannelMode( Nsim, nFace, nBeam, nUser, NIRF, L, N, M, Time)`

Call the function **ChannelMode.m** from the function **Beam3DChannel.m**. The channel impulse response function is generated. The transfer function is determined. The parameters are explained in the Table A-25. The flow chart of functions is shown in Figure A-59.

**Table A- 25: The parameters in the function ChannelMode**

<b>Parameters</b>	<b>Meaning</b>
h	The transfer function for channel model as the output
Nsim	The time of running simulation
nface	The number of faces
nbeam	The number of beams
nUser	The number of UEs
NIRF	The non-equal-spaced fast Fourier transform
L	The number of beams
N	The number of antenna element in x-direction
M	The number of antenna element in y-direction
Time	The time delay

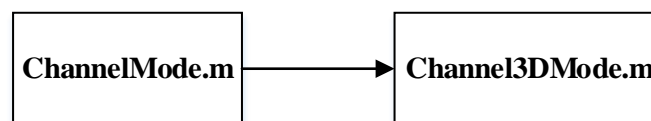


**Figure A-59: The flow chart of the function ChannelMode**

### A.6.2.2.1 Function Channel3DMode

- **Function [Channel,Nz,Ny,N\_AntUE] = Channel3DMode (Nsim, nFace, nArea, nUser, Tnsec )**

Call the function **Channel3DMode.m** from the function **ChannelMode.m**. In this function, according to “3GPP TR 36.873”, the two angles of departure from the transmitter and two angle of arrival from the receiver has been calculated, which are in the channels. The output data is changed to global coordinates, which is saved in the structure variable **Envpar**. The parameters are explained in the Table A-26. The flow chart of functions is shown in Figure A-60.

**Table A- 26: The parameters in the function Channel 3D Mode**

<b>Parameters</b>	<b>Meaning</b>
Channel	Size of antenna array as output
Nz	The number of antenna array in y-z-plane for transmitter as output
Ny	The number of antenna array in x-y-plane for transmitter as output
N_AntUE	The size of antenna for UEs as output
Nsim	The time of running simulation
nFace	The number of faces
nArea	The number of areas
nUser	The number of UEs
Tnsec	The delay offset

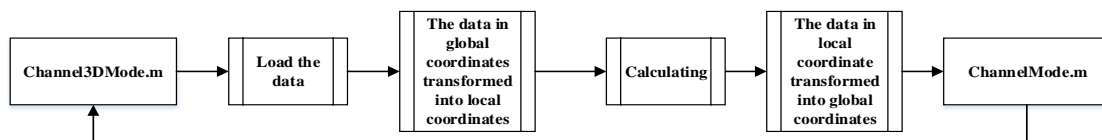


**Figure A-60: The flow chart of the function Channel 3D Mode**



### A.6.2.2.1.1 Function ChannelModel

Uses Sub Functions:

1. Function ArrDepangle
2. Function fieldPattern
3. Function explambda
4. Function xpr
5. Function ChannelLoS

5.1. Function fieldPatternLoS

5.2. Function xpr

5.3. Function explambdaLoS

- **Function [Hus,angleAD] = ChannelModel(parset, fixpar, Envpar, Tnsec)**

Call the function **ChannelModel.m** from the function **Channel3DMode.m**. In this function, according to “3GPP TR 36.873”, there are two kinds of channel coefficients for paths, which are calculated by the next equations. The parameters are explained in the Table A-27.

**Table A- 27: The parameters in the function Channel Model**

<b>Parameters</b>	<b>Meaning</b>
Hus	The channel coefficient as output
angleAD	The arrived and departure angle for both azimuth and elevation as output
parset	A structure variable for saving the parameter which is from “3GPP TR 36.873 Table 7.3-1”
fixpar	A structure variable for saving the parameter which is from “3GPP TR 36.873 Table 7.3-1”
Envpar	The parameters for the network environment

Tnsec	The delay offset
-------	------------------

The channel coefficient for the NLOS is :

$$\begin{aligned}
 H_{u,s,n}(t) = & \sqrt{P_n/M} \sum_{m=1}^M \left[ \begin{array}{c} F_{rx,u,\theta}(\theta_{n,m}, ZOA, \varphi_{n,m}, AOA) \\ F_{rx,u,\varphi}(\theta_{n,m}, ZOA, \varphi_{n,m}, AOA) \end{array} \right]^T \\
 & \left[ \begin{array}{cc} \exp(j\Phi_{n,m}^{\theta\theta}) & \sqrt{\kappa_{n,m}^{-1}} \exp(j\Phi_{n,m}^{\theta\varphi}) \\ \sqrt{\kappa_{n,m}^{-1}} \exp(j\Phi_{n,m}^{\varphi\theta}) & \exp(j\Phi_{n,m}^{\varphi\varphi}) \end{array} \right] \\
 & \left[ \begin{array}{c} F_{tx,s,\theta}(\theta_{n,m}, ZOD, \varphi_{n,m}, AOD) \\ F_{tx,s,\varphi}(\theta_{n,m}, ZOD, \varphi_{n,m}, AOD) \end{array} \right] \exp \left( j2\pi\lambda_0^{-1} \left( \hat{r}_{rx,n,m}^T \cdot \bar{d}_{rx,u} \right) \right) \\
 & \bullet \exp \left( j2\pi\lambda_0^{-1} \left( \hat{r}_{tx,n,m}^T \cdot \bar{d}_{tx,s} \right) \right) \exp(j2\pi\nu_{n,m}t)
 \end{aligned} \tag{A-3}$$

The channel coefficient for the LOS is :

$$\begin{aligned}
 H_{u,s,n}(t) = & \sqrt{\frac{I}{K_R + I}} H'_{u,s,n}(t) \\
 & + \delta(n-1) \sqrt{\frac{K_R}{K_R + I}} \left[ \begin{array}{c} F_{rx,u,\theta}(\theta_{LOS}, ZOA, \varphi_{LOS}, AOA) \\ F_{rx,u,\varphi}(\theta_{LOS}, ZOA, \varphi_{LOS}, AOA) \end{array} \right]^T \\
 & \left[ \begin{array}{cc} \exp(j\Phi_{LOS}) & 0 \\ 0 & -\exp(j\Phi_{LOS}) \end{array} \right] \\
 & \left[ \begin{array}{c} F_{tx,s,\theta}(\theta_{LOS}, ZOD, \varphi_{LOS}, AOD) \\ F_{tx,s,\varphi}(\theta_{LOS}, ZOD, \varphi_{LOS}, AOD) \end{array} \right] \exp \left( j2\pi\lambda_0^{-1} \left( \hat{r}_{rx,LOS}^T \cdot \bar{d}_{rx,u} \right) \right) \\
 & \bullet \exp \left( j2\pi\lambda_0^{-1} \left( \hat{r}_{tx,LOS}^T \cdot \bar{d}_{tx,s} \right) \right) \exp(j2\pi\nu_{LOS}t)
 \end{aligned} \tag{A-4}$$

where the **H<sub>us</sub>** as the final channel coefficient for all paths are saved, which is the probability for each path selected. The flow chart of functions is shown in Figure A-61.

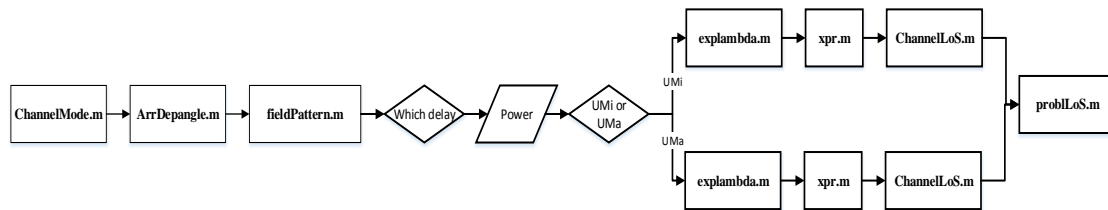


Figure A-61: The flow chart of the function ChannelModel

- **Function [angleAD] = ArrDepangle(parset, fixpar, Envpar)**

Call the function **ArrDepangle.m** from the function **ChannelModel.m**. In this function, the arrived and departure angles are generated in horizontal and vertical direction when the environments are UMa and UMi, which depends on different clusters. The data is saved in the structure variable **angleAD**. The parameters are same as the last function. The flow chart of functions is shown in Figure A-62.

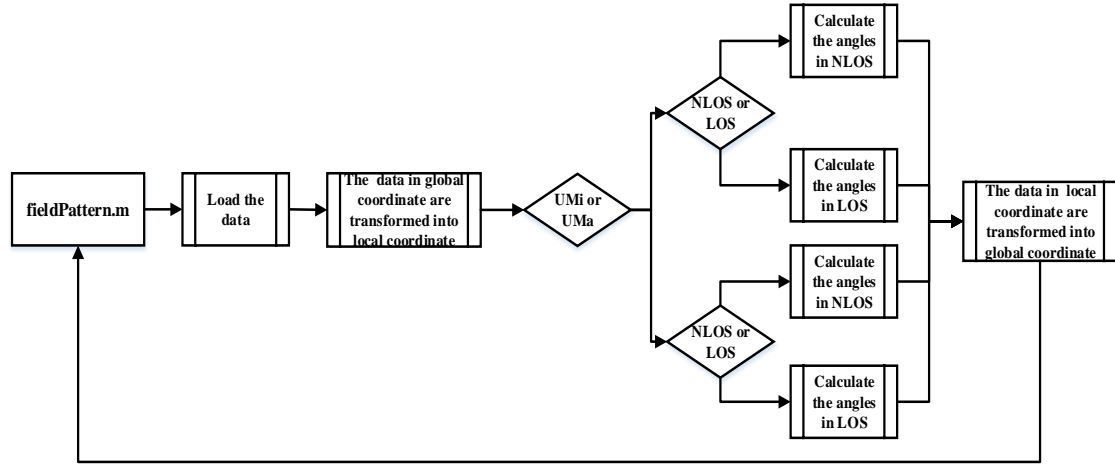


Figure A-62: The flow chart of function ArrDepangle

- **Function [FieldData] = fieldPattern(Envpar, angleAD)**

Call the function **fieldPattern.m** from the function **ChannelModel.m**. This function is for NOLS, according to the equation (A-5) and (A-6), the electric field strength for BS are obtained as next shown:

$$EFS_{tx} = \begin{bmatrix} F_{tx,s,\theta} \left( \theta_{n,m}, ZOD, \varphi_{n,m}, AOD \right) \\ F_{tx,s,\varphi} \left( \theta_{n,m}, ZOD, \varphi_{n,m}, AOD \right) \end{bmatrix} \quad (A-5)$$

and the electric field strength for UE obtained as next shown:

$$EFS_{rx} = \begin{bmatrix} F_{rx,u,\theta} \left( \theta_{n,m}, ZOA, \varphi_{n,m}, AOA \right) \\ F_{rx,u,\varphi} \left( \theta_{n,m}, ZOA, \varphi_{n,m}, AOA \right) \end{bmatrix} \quad (A-6)$$

The all data are saved in the structure variable **FieldData**. The parameters “FieldData” is the electric field strength, “Envpar” is the parameters for the network environment and “angleAD” is the arrived and departure angle for both azimuth and elevation. The flow chart of functions is shown in Figure A-63.

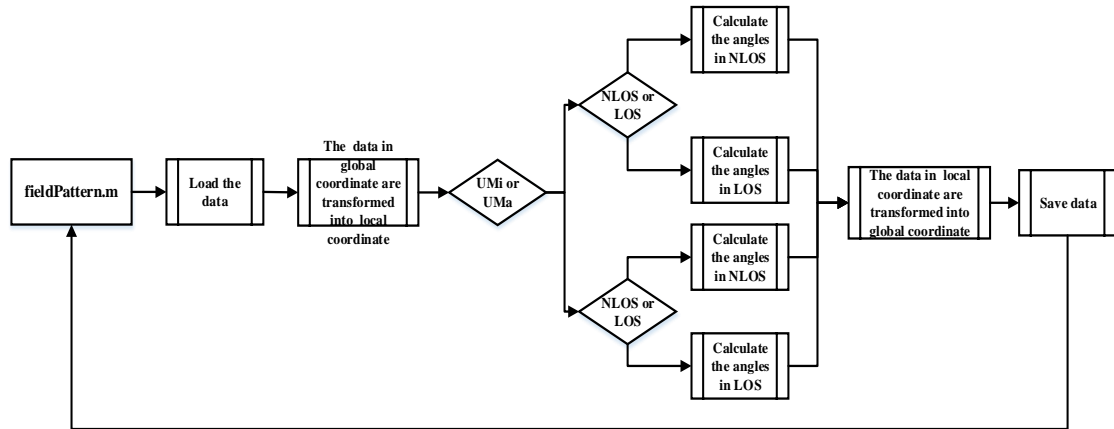


Figure A-63: The flow chart of the function fieldPattern

- **Function [ExpLambda\_NLoS, ExpLambda\_LoS] = explambda(typescen, Envpar, angleAD)**

Call the function **explambda.m** from the function **ChannelModel.m**. In this function, the electric field strength are obtained as next shown:

$$\begin{aligned}
 ExpNLoS &= \exp \left( j2\pi\lambda_0^{-1} \left( \hat{r}_{rx,n,m}^T \cdot \bar{d}_{rx,u} \right) \right) \\
 \bullet \exp \left( j2\pi\lambda_0^{-1} \left( \hat{r}_{tx,n,m}^T \cdot \bar{d}_{tx,s} \right) \right) &\exp \left( j2\pi\nu_{n,m} t \right)
 \end{aligned} \tag{A-7}$$

The data is saved in the two variables **ExpLambda\_NLoS** and **ExpLambda\_LoS**. The channel coefficient for NLOS is saved in **HusNLoS**. The parameters are explained in the Table A-28. The flow chart of functions is shown in Figure A-64.

Table A- 28: The parameters in the function explambda

Parameters	Meaning
ExpLambda_NLoS	The exp for NLOS as output
ExpLambda_LoS	The exp for LOS as output
typescen	The environment : UMi or UMa
Envpar	The parameters for the network environment
angleAD	The arrived and departure angle for both azimuth and elevation

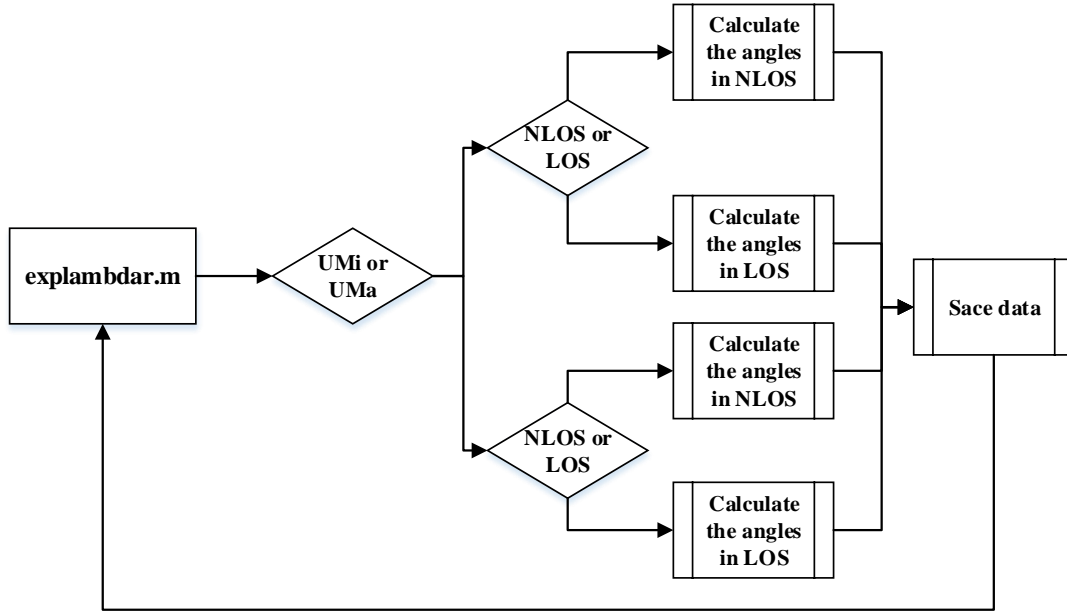


Figure A-64: The flow chart of the function explambda

- **Function [Exp] = xpr(typescen, typepath, fixpar)**

Call the function **xpr.m** from the function **ChannelModel.m**. In this function, according to the equation (A-8), the exponential function are obtained as next shown:

$$xpr = \begin{bmatrix} \exp(j\Phi_{n,m}^{\theta\theta}) & \sqrt{\kappa_{n,m}^{-1}} \exp(j\Phi_{n,m}^{\theta\phi}) \\ \sqrt{\kappa_{n,m}^{-1}} \exp(j\Phi_{n,m}^{\phi\theta}) & \exp(j\Phi_{n,m}^{\phi\phi}) \end{bmatrix} \quad (\text{A-8})$$

The data is saved in the variable **Exp**. The parameter “Exp” is the matrix as shown, “typescen” is the environment UMi or UMa, “typepath” is the path NLOS or LOS and “fixpar” is a structure variable for saving the parameter which is from “3GPP TR 36.873 Table 7.3-1”. The flow chart of functions is shown in Figure A-65.

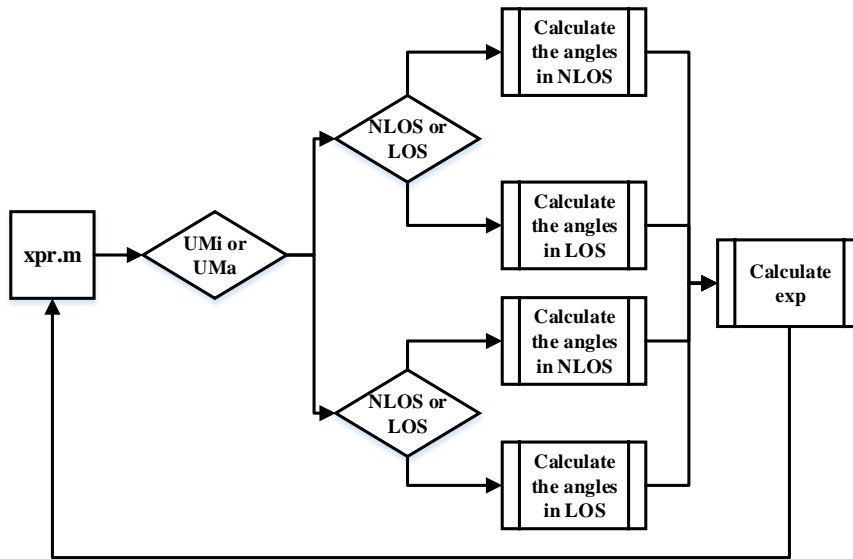


Figure A-65: The flow chart of the function xpr

- **Function [HusLoS] = ChannelLoS(TypeScen, TypePath, fixpar, Envpar, angleAD )**

Call the function **ChannelLoS.m** from the function **ChannelModel.m**. This function is about channel coefficient for the LOSas equation (A-4) shown. The data is saved in the variable **HusLoS**. The parameters are explained in the Table A-29. The flow chart of functions is shown in Figure A-66.

Table A- 29: The parameters in the function ChannelLoS

Parameters	Meaning
HusLoS	The $H'_{u, s, n}(t)$ as output
TypeScen	The environment : UMi or UMa
TypePath	The type of path: NLOS or LOS
fixpar	A structure variable for saving the parameter which is from “3GPP TR 36.873 Table 7.3-1”
Envpar	The parameters for the network environment
angleAD	The arrived and departure angle for both azimuth and elevation

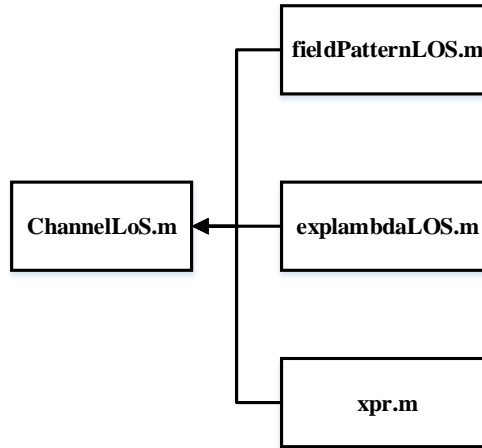


Figure A-66: The flow chart of the function ChannelLoS

- **Function [FieldTxLoS, FieldRxLoS] = fieldPatternLoS(Envpar, angleAD)**

Call the function **fieldPatternLoS.m** from the function **ChannelLoS.m**. In this function, according to the equation (A-7) and (A-8), the electric field strength for BS are obtained as next shown:

$$EFS_{txLoS} = \begin{bmatrix} F_{tx,s,\theta}(\theta_{LOS,ZOD}, \varphi_{LOS,AOD}) \\ F_{tx,s,\varphi}(\theta_{LOS,ZOD}, \varphi_{LOS,AOD}) \end{bmatrix} \quad (A-9)$$

and the electric field strength for UE obtained as next shown:

$$EFS_{rxLoS} = \begin{bmatrix} F_{rx,u,\theta}(\theta_{LOS,ZOA}, \varphi_{LOS,AOA}) \\ F_{rx,u,\varphi}(\theta_{LOS,ZOA}, \varphi_{LOS,AOA}) \end{bmatrix} \quad (A-10)$$

The all data are saved in the two variables **FieldTxLoS** and **FieldRxLoS**. The parameter “Envpar” express the network environment and “angleAD” are arrived and departure angle for both azimuth and elevation. The flow chart of functions is shown in Figure A-67.

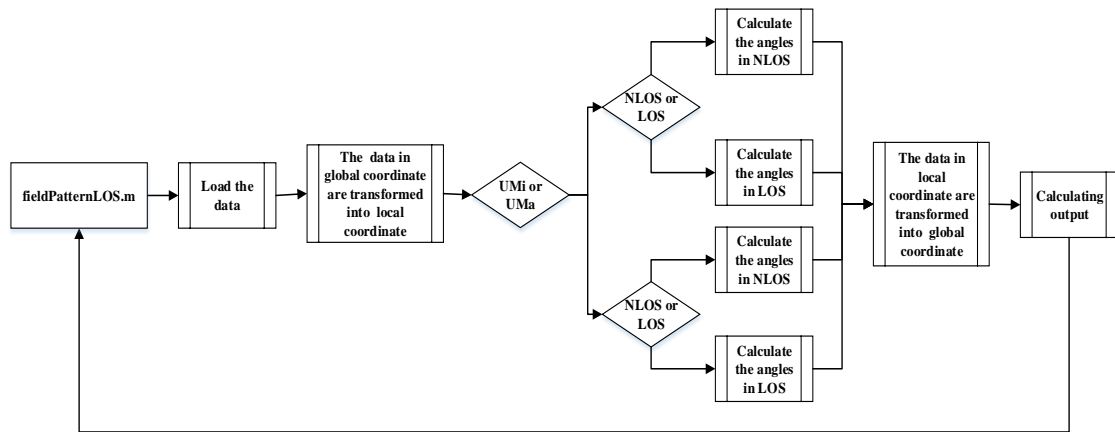


Figure A-67: The flow chart of the function fieldPatternLoS

- **Function [Exp] = xpr(typescen, typepath, fixpar)**

Call the function **xpr.m** from the function **ChannelLoS.m**. In this function, according to the equation (A-10), the exponential function are obtained as next shown:

$$xprLoS = \begin{bmatrix} \exp(j\Phi_{LOS}) & 0 \\ 0 & -\exp(j\Phi_{LOS}) \end{bmatrix} \quad (A-11)$$

The data is saved in the variable **Exp**.

- **Function explambdaLoS**

Call the function **explambdaLoS.m** from the function **ChannelLoS.m**. In this function, the electric field strength are obtained as next shown:

$$ExpLoS = \exp(j2\pi\lambda_0^{-1}(\hat{r}_{rx,LOS}^T \cdot \bar{d}_{rx,u})) \exp(j2\pi\lambda_0^{-1}(\hat{r}_{tx,LOS}^T \cdot \bar{d}_{tx,s})) \exp(j2\pi\nu_{LOS}t) \quad (A-12)$$

The data is saved in the variable **ExpLambdaLoS**.

### A.6.3 Function receivedSignalConv

- **Function [Rxx,W] = receivedSignalConv( ht, Weight, txSignal, Nfft )**

Call the function **receivedSignalConv.m** from the function **CalBerPDFOn3DBeam.m**. This function distributes the signals into the antenna array, which is based on the weighting matrix in order to generate the weighting signals (**WeightSignal**). Then it convolutes the 3D channel impulse response function (**ht**) to determine received signals, which is saved in the variable **rxWaveform**. The parameters are explained in the Table A-30. The flow chart of functions is shown in



Figure A-68.

Table A- 30: The parameters in the function receivedSignalConv

Parameters	Meaning
Rxx	The received signal as output
W	The weighting matrix as output
ht	The transfer function of channel model
Weight	An all one matrix
txSignal	The transmit signal
Nfft	The non-equal-spaced fast Fourier transform

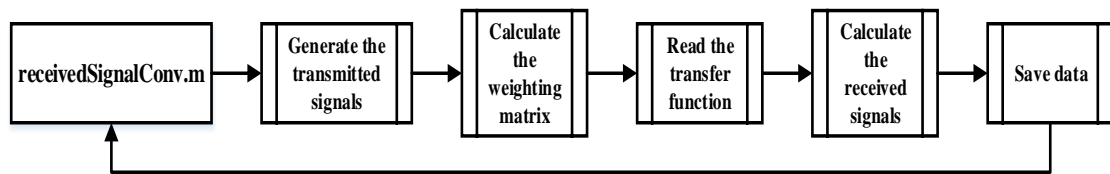


Figure A-68: The flow chart of the function receivedSignalConv

#### A.6.4 Function calculateBER

- **Function** [nErrors, numData] = calculateBER(refData, rxData, nErrors, numData, new)

Call the function **calculateBER.m** from the function **CalBerPDFOn3DBeam.m**. It is the calculation of BER function for the transmitting signals and the received signals, the BER for all users is determined, in which the BER are saved in the variable **nErrors** and the number of errors are saved in the variable **numBits**. The parameters are explained in the Table A-31.

Table A- 31: The parameters in the function calculateBER

Parameters	Meaning
nErrors	The BER as output
numData	The number of error data as output

refData	The transmit data
rxData	The receive data
nErrors	The initializing BER
numData	The initializing error data
ncw	The switch parameter

## A.7 Function ReadBERStart\_Callback ( hObject, eventdata, handles)

Call the function “**ReadBERStart\_Callback**” in **main.m**, which is a radio button in **main.fig**. In this function, the program reads the data of the BER for each user from the file 'data\BER.mat' and show the results in the figures. The flow chart of functions is shown in Figure A-69.

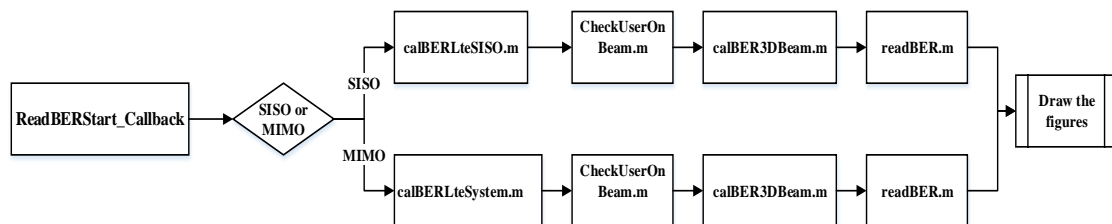


Figure A-69: The flow chart of function ReadBERStart\_Callback

### A.7.1 Function calBERLteSystem

- Function [simBER] = calBERLteSystem(enb, SNRIn, NRxAnt, MIMOCorr )

Call the function **calBERLteSystem.m** from the function “**ReadBERStart\_Callback**”, which generates the LTE MIMO system and calculates the BER for the system. Moreover, it shows the results in the figures, which draws the constellation figure for receiver and the mean of BER for LTE system. The parameters are explained in the Table A-32. The flow chart of functions is shown in Figure A-70.

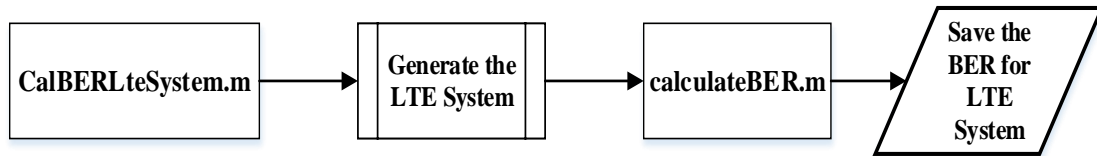


Figure A-70: The flow chart of function calBERLteSystem

### A.7.2 Function calBERLteSISO

- **Function [ simBER ] = calBERLteSISO( enb, SNRIn )**

Call the function **calBERLteSISO.m** from the function “**ReadBERStart\_Callback**”, which is based on the example in Matlab how to measure the Physical Downlink Shared Channel (PDSCH) throughput performance using the LTE System Toolbox(TM). The function simulates the LTE SISO system, then it calculates BER and shows the results in the figures. Moreover, it draws the constellation figure for receiver. The parameters “enb” is the structure variable from the RMC R.0-9 in Matlab 2016band “SNRIn” is the setting SNR from GUI. The flow chart of functions is shown in Figure A-71.

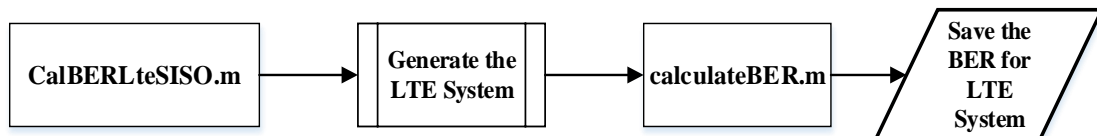


Figure A-71: The flow chart of the function calBERLteSISO

### A.7.3 Function CheckUserOnBeam

- **Function [ N1, N2, N3, N4 ] = CheckUserOnBeam(Nsim1, Nuser)**

Call the function **CheckUserOnBeam.m** from the function “**ReadBERStart\_Callback**”. In this function, one UE, which is in an appointed beam, can be selected and checked it whether is covered by beam. The function reads the information data for UEs. The parameters are explained in the Table A-32.

**Table A- 32: The parameters in the function CheckUserOnBeam**

<b>Parameters</b>	<b>Meaning</b>
N1	The order time for running simulation as output
N2	The order number of face as output
N3	The order number of beam as output
N4	The order numberof UEs as output
Nsim1	The number of time for running simulation
Nuser	The number of UEs

#### **A.7.4 Function calBER3DBeam**

- **Function [simBER] = calBER3DBeam(enb, SNRIn, SINRdB, Nsim, Nface, Nbeam, nUser,W12)**

Call the function **calBER3DBeam.m** from the function “**ReadBERStart\_Callback**”. The function calculates the BER for 3D beamforming system, which is similar to **CalBerPDFOn3DBeam.m**. In this function, the constellation figure and the figure of BER for 3D beamforming system has been shown. The parameters are explained in the Table A-33.The flow chart of functions is shown in Figure A-72.

**Table A- 33: The parameters in the function calBER3DBeam**

<b>Parameters</b>	<b>Meaning</b>
simBER	The BER for 3D beamforming system as output
enb	The structure variable from the RMC R.0-9 in Matlab 2016b
SNRIn	The setting SNR from GUI
SINRdB	The loading SINR from the files
Nsim	The time of running simulation

Nface	The number of faces
Nbeam	The number of beams
nUser	The number of UEs
W12	The chosen of the weighting matrix

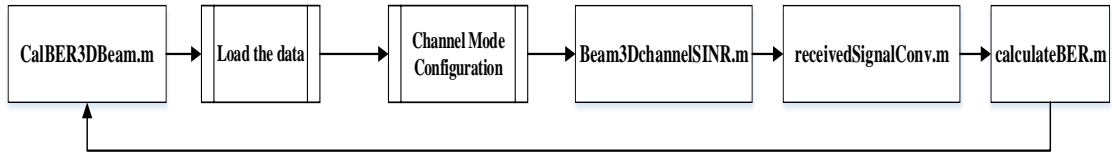


Figure A-72: The flow chart of the function calBER3DBeam

### A.7.5 Function readBER

- **Function [medianBER, p5BER, p95BER] = readBER(SNRdB, Prc, W12)**

Call the function `readBER.m` from the function “`ReadBERStart_Callback`”. The function reads the BER data from the file 'data\ BER.mat'. The structure variable `simBER` has been read to show the CDF and PDF figures of BER for each user, which is based on the chosen percentile value. The parameters are explained in the Table A-34.

Table A- 34: The parameters in the function readBER

Parameters	Meaning
medianBER	The BER in median values of percentile value for UE as output
p5BER	The BER in minimum values of percentile value for UE as output
p95BER	The BER in maximum values of percentile for UE as output
SNRdB	The SNR for calculation
Prc	The interval values of percentile
W12	The chosen of the weighting matrix

## A.8 Function BERCellUEsStart\_Callback (hObject, eventdata, handles)

Call the function “**BERCellUEsStart\_Callback**” in **main.m**, which is a radio button in **main.fig**. In this function, the parameters are set which is running the simulation to test whether the different users have effect on the BER in different environments. Repeat above steps and use the functions, **EstCommEnv.m**, **networkEnv3D.m** and **WeighSIRmaxLSM.m**, in order to obtain the beamforming for each users. The parameter “hObject” represents the handling for function, “eventdata” is reserved to be defined in a future version of MATLAB and “handles” is structured the handles and input data. The flow chart of functions is shown in Figure A-73.

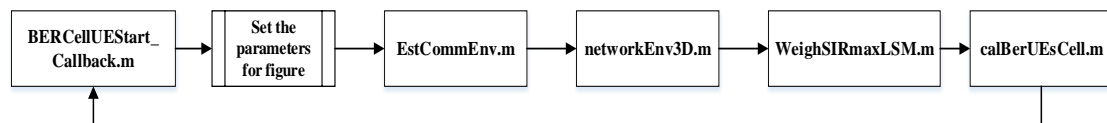


Figure A-73: The flow chart of the function BERCellUEsStart\_Callback

### A.8.1 Function CalBerUEsCell

- **Function [simBER] = CalBerUEsCell(SNRIn, SINRdB, enb, ScenesType, RMC, UEsStr)**

Call the function **CalBerUEsCell.m** from the function “**BERCellUEsStart\_Callback**”. The function can calculate the BERs which depends on different SNR for each users when the different users are in different environments. The data is saved in the file 'dataBER\UEsStr\ScenesType\RMC\BER'. The all results are shown in the figure. The parameters are explained in the Table A-35. The flow chart of functions is shown in Figure A-74.

**Table A- 35: The parameters in the function CalBerUEsCell**

<b>Parameters</b>	<b>Meaning</b>
simBER	The simulation BER as the output
SNRIn	The setting SNR
SINRdB	The loading SINR from the files
enb	The structure variable from the RMC R.0-9 in Matlab 2016b
ScenesType	The scenarios for system
RMC	The types of the modulation
UEsStr	The number of UEs

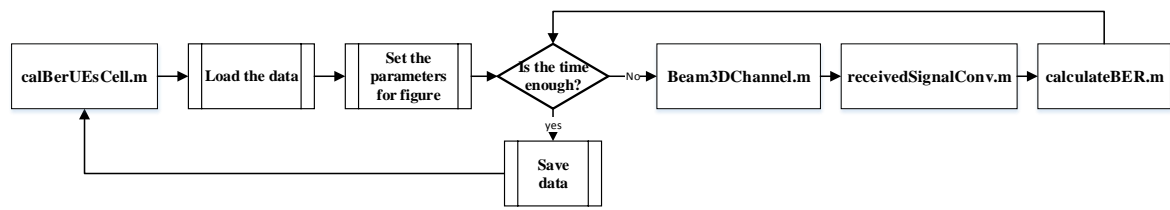


**Figure A-74: The flow chart of the function CalBerUEsCell**

## A.9 Function Plot3DStart\_Callback (hObject, eventdata, handles)

Call the function “**Plot3DStart\_Callback**” in **main.m**, which is a radio button in **main.fig**. This function drawing the figure is based on the reading data from the function **CalBerUEsCell.m**. The flow chart of functions is shown in Figure A-75.



**Figure A-75: The flow chart of the function Plot3DStart\_Callback**

### A.9.1 Function readBerUEsCell

- **Function [simBER] = readBerUEsCell( ScenesType, RMC, UEsStr )**

Call the function **readBerUEsCell.m** from the function “**Plot3DStart**

**\_Callback**". The function reads the data from the function **CalBerUEsCell.m**, which is in the file 'dataBER\UEsStr ScenesType RMC BER'. The parameters are same as the parameters in **CalBerUEsCell.m**.



# Appendix B: Simulation Design for Optimal Minimum Side lobe Hybrid Beamforming of Millimeter Wave System

The **main.m** is the main program for the simulation, which has 7 sub-systems including **SimStart\_Callback**, **ReadStart\_Callback**, **BeamStart\_Callback**, **mmCBERStart\_Callback**, **ReadBERStart\_Callback**, **CompBERStart\_Callback** and **ReadCompBER\_Callback** as Figure B-1 shown. In next parts, the functions in these 7 sub-systems are illustrated. Moreover, the parameters in the function are explained the meaning.

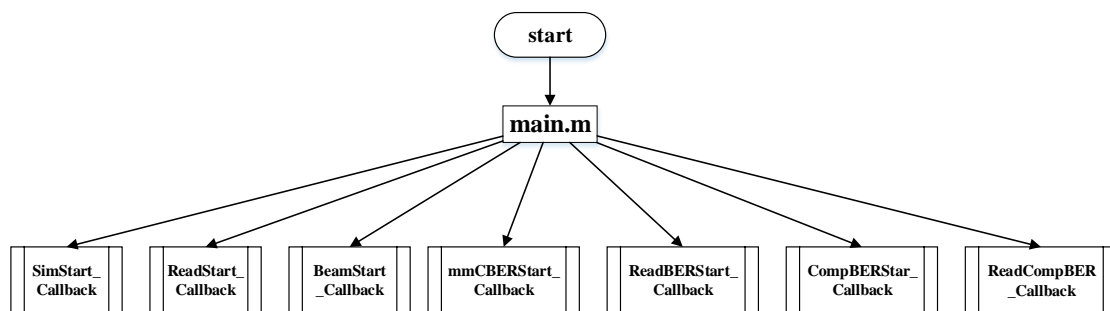


Figure B- 1: The main program for the simulation

The sub-systems **SimStart\_Callback**, **ReadStart\_Callback** and **BeamStart\_Callback** are same as the sub-systems with the same name in cluster user program. Therefore, the next parts can explain the meaning of function for **mmCBERStart\_Callback**, **ReadBERStart\_Callback**, **CompBERStart\_Callback** and **ReadCompBER\_Callback**.

## B.1 UML Modeling for mm-wave antenna arrays system

### B.1.1 Introduction

The simulation is of the mm-wave antenna arrays system, which uses the hybrid beamforming to transmit the signal. One mm-wave system is transmitting the beams by the new weighting method, which can decrease the overall BER. Another mm-wave system is transmitting the beams by the equal weighting matrix. Moreover, the results from the simulation show the comparison of the BER for these two systems, in order to show that the new weighting design is a more advanced system with an improved BER. The simulation should implement these functions so there needs be 7 UML use-cases.

In this thesis, class diagrams, composite structure diagrams, sequence diagrams and activity diagrams were used to represent the 4 simulation use-cases (**SimStart**, **BeamStart**, **mmCBERStart** and **mmReadBERStart**) and 3 present data use-cases (**ReadStart**, **mmReadBERStart** and **ReadCompBER**).

The UML use-cases model is shown in Figure B-2. There is one actor who is the analyzer and 7 use-cases such as **SimStart**, **ReadStart**, **BeamStart**, **mmCBERStart**, **mmReadBERStart**, **CompBERStart** and **ReadCompBER**.

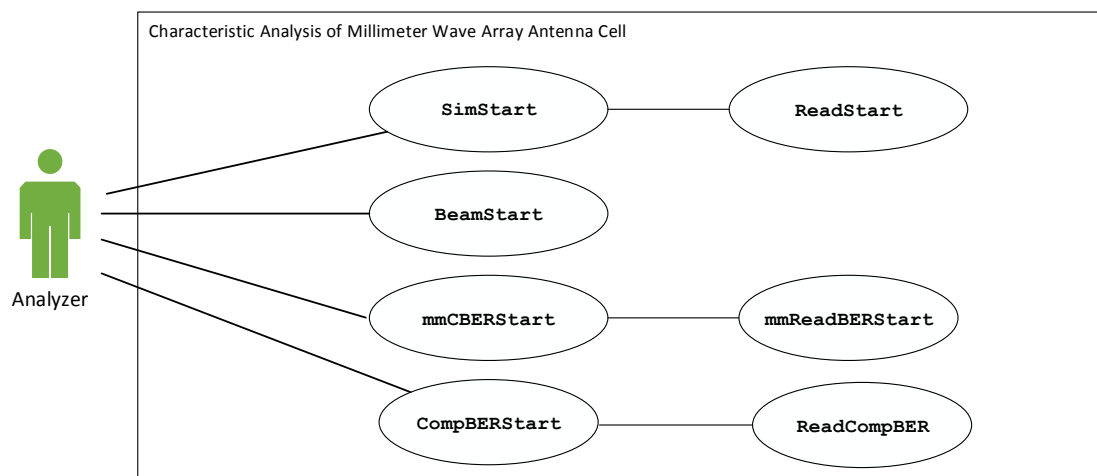


Figure B- 2: The UML use-cases model

Since the simulation takes a long time, we need to divide the program into four sub-systems and provide further program to read the results of the two most important sub-systems in the simulation as shown in Figure B-2. The use-case **SimStart** sets up

the simulation communication environment according to the simulation parameters from the environment data file; the use-case **BeamStart** generates the beams, which having the weighting matrix makes the SINR to be a maximum value; the use-case **mmCBERStart** calculates the BER for two mm-wave systems in different weighting and save the BER in the data file; the use-case **CompBERStart** calculates the CDF of the BER for these two mm-wave systems. At **SimStart** use-case interim results can be read and displayed using **ReadStart**, at **mmCBERStart** use-case interim results can be read and displayed using **mmReadBERStart** and at **CompBERStart** use-case interim results can be read and displayed using **ReadCompBER**.

### **B.1.2 Same use-case as the simulation of a hexagonal antenna arrays cell in last Section**

The use-case **SimStart**, **ReadStart** and **BeamStart** are same as the use-case with the same name in Chapter 4 simulation system “3D Beamforming LTE System towards a Group of User Equipment”, which is called cluster UE program. However, the number of faces and area are different, which set the antenna arrays has 4 sub-arrays in one cell so there are 4 beams for the transmitter. Moreover, the coverage area of angle range for each beam is changed  $(-90^{\circ}, 0^{\circ}, +90^{\circ})$ . Therefore, the static model and the dynamic model are same as the use-case with the same name in cluster UE program.

### **B.1.3 mmCBERStart Use-case**

The use case **mmCBERStart** is different with the use-case **CBERStart** in cluster UE program. Table B-1 shows the UML use-case description for “**mmCBERStart**” and Figure B-3 is the activity diagram for this use-case.

**Table B- 1: The UML use-case description for “mmCBERStart”**

<p><b>Name of Use Case:</b> mmCBERStart</p> <p><b>Introduction:</b> The 3D Channel model are generated for the new weighting and the equal weighting in the mm-Wave system. Moreover, the received signals of mm-Wave system are obtained. The BER of these two mm-Wave systems are calculated, which are saved in the BER1 and BER2 data file.</p> <p><b>Participator:</b> Analyzer</p> <p><b>Preconditions:</b> None.</p> <p><b>Main sequence (as Figure5-2 shown):</b></p> <ol style="list-style-type: none"><li>9. Analyzer start up.</li><li>10. Read the SINR data file.</li><li>11. Generate the transmitting signals for every beam.</li><li>12. According to the millimeter wave characteristics revise the 3GPP TR36.873 channel model, the impulse response function of 3D channel model is generated.</li><li>13. The hybrid beamforming transmitting signals are generated by the transmitting signals with the new weighting matrix or the equal weighting matrix, which are in convolution with the impulse response function of the 3D channel model.</li><li>14. The noise and the SINR between the beams are added into the received signal.</li><li>15. Calculate the BER1 for the equal weighing and BER2 for the new weighting.</li><li>16. Create the BER1 andBER2 data files for all simulation UEs.</li></ol> <p><b>Alternative sequence:</b></p> <p>None.</p> <p><b>Post-condition:</b></p> <p>The system displays the BER1 and BER2 for comparison.</p>
---

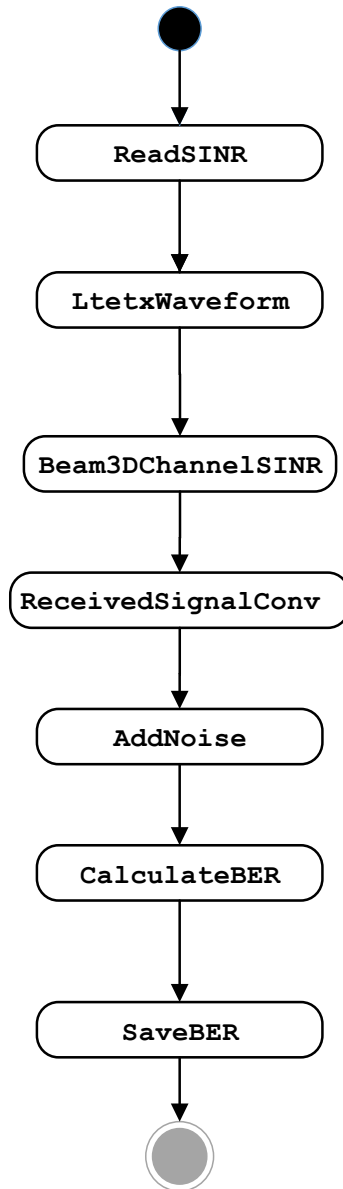


**Figure B- 3: The activity diagram for this use-case mmCBERStart**

The static model of the use-case **mmCBERStart** is shown in Figure B-4, which has two categories, entity class and algorithm class. The entity class includes the “<entity>:Analyzer”, “<entity>:simData”, “<entity>:WeightLSM”, “<entity>:SINR” , “<entity>:BER1” and “<entity>:BER2”. Moreover, the description of the entity class is shown in Figure B-5. The algorithm class includes the “<algorithm>:LTESystem”, “<algorithm>:Beam3DChannel”, “<algorithm>:receivedSignalConv”, “<algorithm>:AddNoise” and “<algorithm>:calculateBER”.

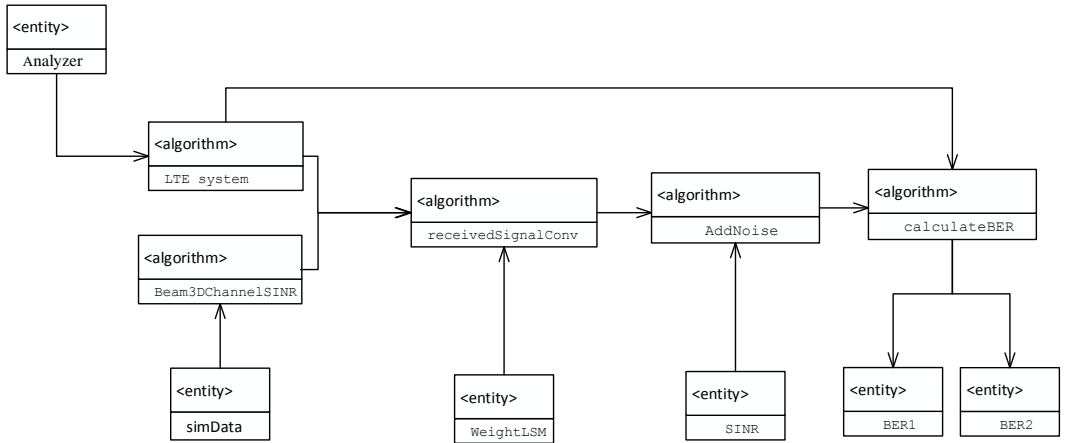


Figure B- 4: The static model of the use-case mmCBERStart

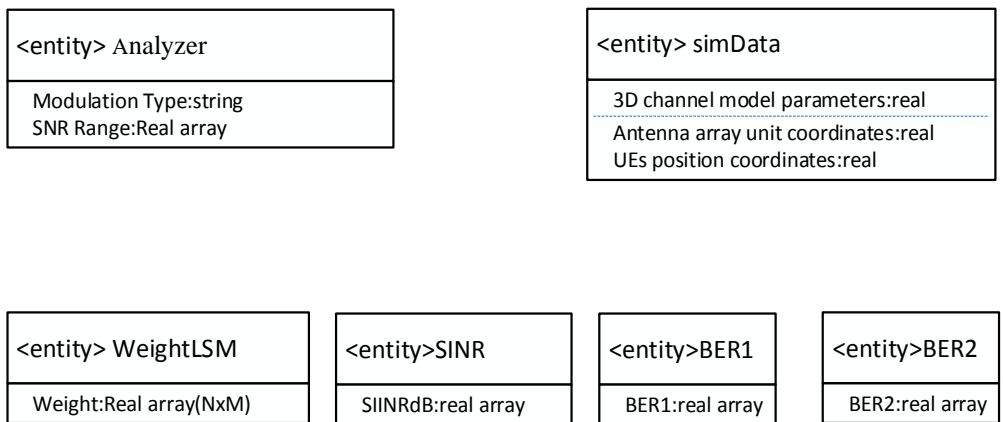


Figure B- 5: The entity class of the use-case mmCBERStart

The “<user interaction>:Analyzer Interaction” should be created because entity class “<entity>:Analyzer” has to interact with external users as shown in Figure B-6. In Figure B-6, the output data has the “<data>:simData”, “<data>:WeightLSM” “<data>:SINR”, “<data>:BER1” and “<data>:BER2”.

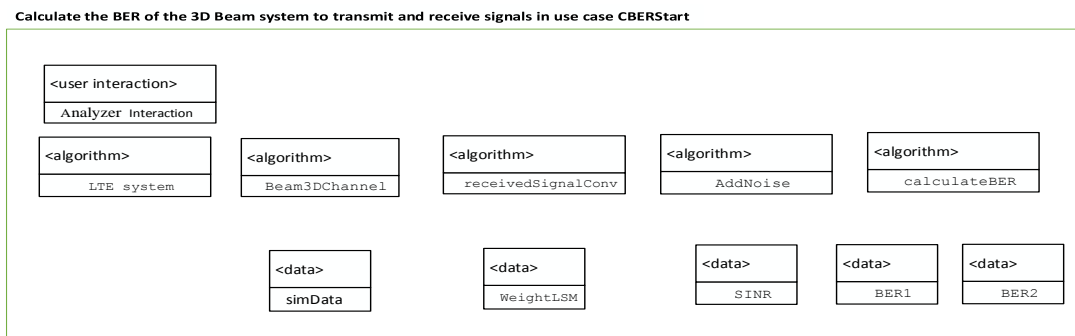


Figure B- 6: The class chart of the use-case mmCBERStart

The dynamic model of the use-case **mmCBERStart** is shown in Figure B-7 and the message description is in Table B-2.

**Table B- 2: The message description**

- C1:** The “Analyzer” sends the start to “<user interaction>:Analyzer Interaction”.
- C2:** The “<user interaction>:Analyzer Interaction” sends information about the modulation types and the noise range to the “<algorithm>:LTE System”, and then start the calculation.
- C3.1:** The “<algorithm>:LTE System” send the transmitting signals to the “<algorithm>:receivedSignalConv”.
- C3.2:** The “<algorithm>:LTE System” send the transmitting signals to the “<algorithm>:calculateBER”.
- C4.1:** The “<algorithm>:Beam3DChannelSINR” reads the simulation parameters (such as channel model and environment data) from the “<data>:simData”.
- C4.2:** The “<algorithm>:Beam3DChannelSINR” send the impulse response function to the “<algorithm>:receivedSignalConv”.
- C5.1:** The “<algorithm>:receivedSignalConv” reads the weighting data from the “<data>:WeightLSM”.
- C5.2:** The “<algorithm>:receivedSignalConv” send the received signals of two weighting to the “<algorithm>:AddNoise”.
- C6.1:** The “<algorithm>:AddNoise” reads theSINR data from the “<data>:SINR”.
- C6.2:** The “<algorithm>:AddNoise” send the received signals of two weighting , which are after the calculation, to the “<algorithm>:calculateBER”.
- C7:** The “<algorithm>:calculateBER” creates the BER1 data file in the “<data>:BER1”.
- C8:** The “<algorithm>:calculateBER” creates the BER2 data file in the “<data>:BER2”.

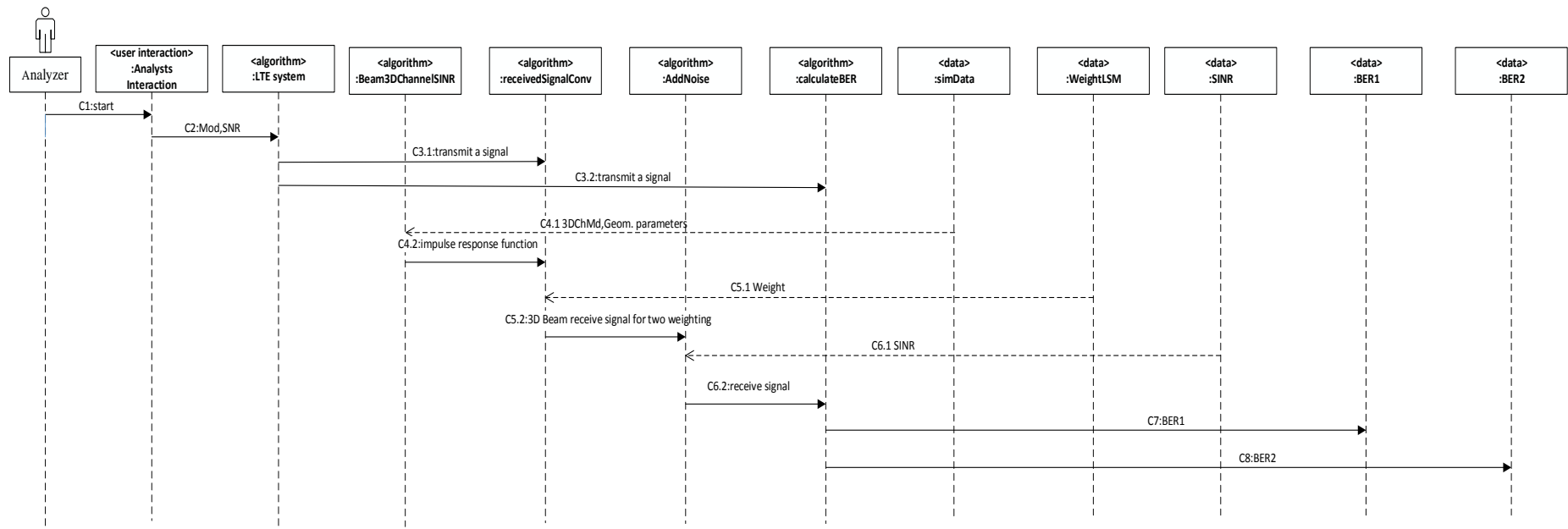


Figure B- 7: The dynamic model of the use-case mmCBERStart



### B.1.4 mmReadBERStart Use-case

The use-case **mmReadBERStart** is different with the use-case **ReadBERStart** in cluster UE program. Table B-3 shows the read and present data use-cases description for “**mmReadBERStart**” and Figure B-8 is the activity diagram for this use-case.

**Table B- 3: The read and present data use-cases description**

<p><b>Name of Use Case: mmReadBERStart</b></p> <p><b>Introduction:</b> Read the BER1 and BER2 data file to calculate the BER by the statistical boundary.</p> <p><b>Participator:</b> Analyzer</p> <p><b>Preconditions:</b> None</p> <p><b>Main sequence (as FigureB-8 shown):</b></p> <ol style="list-style-type: none"><li>7. Analyzer start up.</li><li>8. The beam and UEs in this beam are randomly selected. In these two mm-Wave systems, the received signals are displayed in the constellation diagram and the BER1 and BER2 are calculated.</li><li>9. In the LTE system, the received signal is displayed in the constellation diagram and the BER is calculated.</li><li>10. Read the BER1 and BER2 data file.</li><li>11. Calculate the BER1 and BER2 by the statistical boundary.</li><li>12. Displays the BER for two mm-Wave systems in same figure, and then compare them.</li></ol> <p><b>Alternative sequence:</b></p> <p>None.</p> <p><b>Post-condition:</b></p> <p>The system displays the BER for two mm-Wave systems.</p>
---

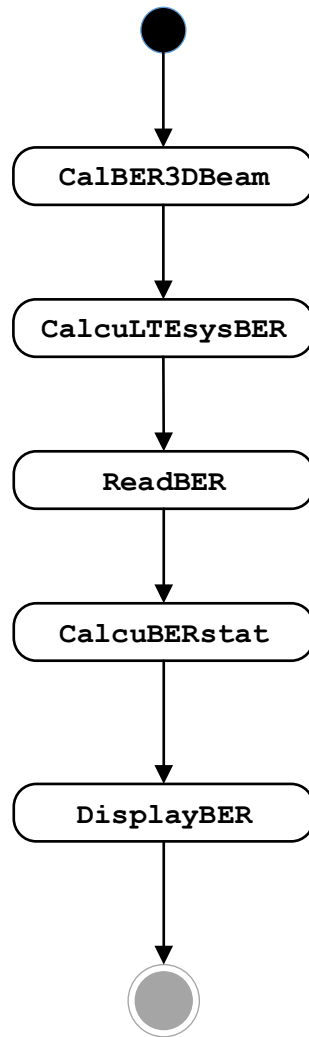


**Figure B- 8: The activity diagram for this use-case mmReadBERStart**

The static model of the use-case **mmReadBERStart** is shown in Figure B-9, which has three categories, entity class, output class and algorithm class. The entity class includes the “<entity>:Analyzer” ,“<entity>:BER1”and “<entity>:BER2”. Moreover, the description of the entity class is shown in Figure B-10. The output class includes the “<output>:scatter” and “<output>:plot”. The algorithm class includes the “<algorithm>:calBER3DBeam”, “<algorithm>:calBERLteSystem” and “<algorithm>:readBER”.

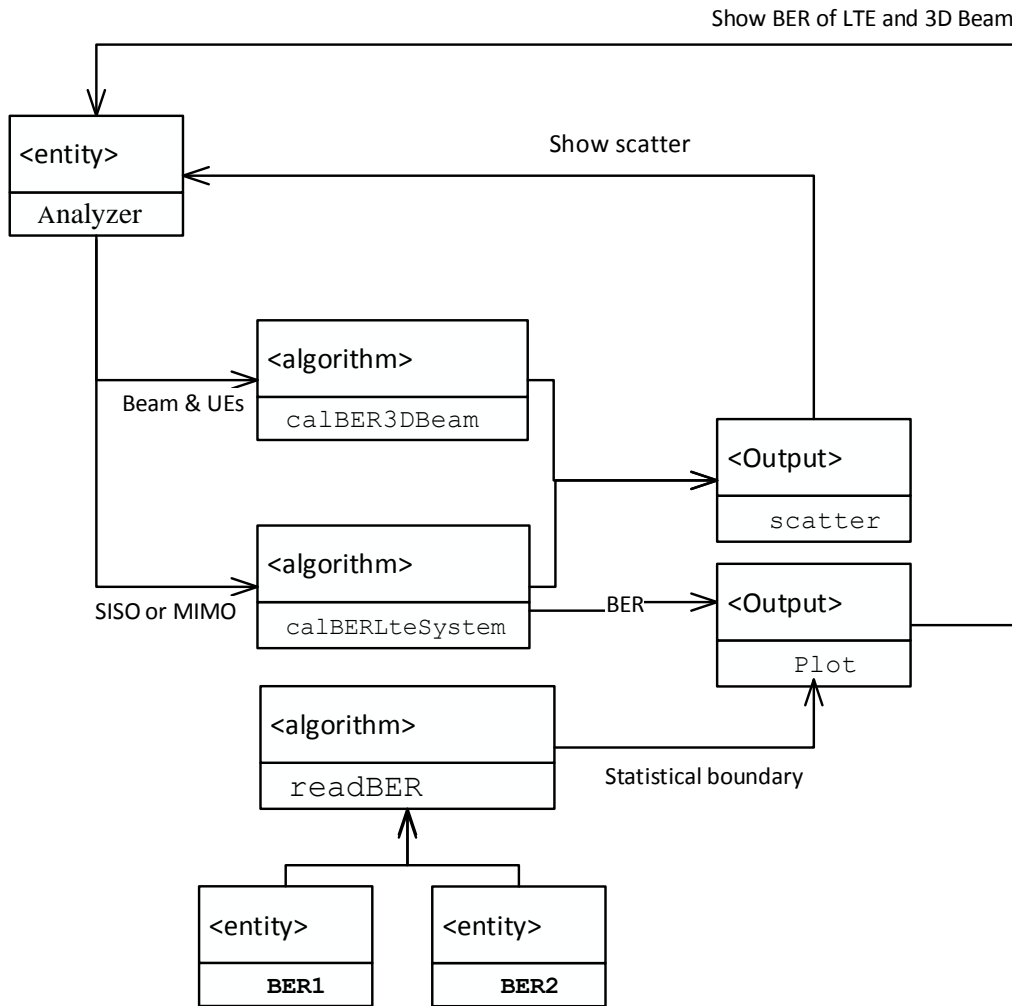


Figure B- 9: The static model of the use-case mmReadBERStart

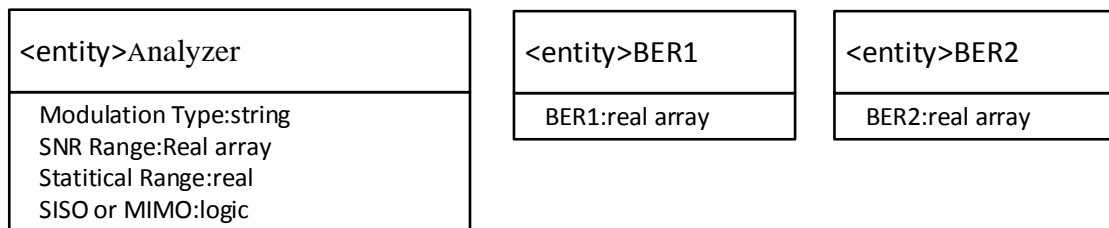


Figure B- 10: The entity class of the use-case mmReadBERStart

The “<user interaction>:Analyzer Interaction” should be created because entity class “<entity>:Analyzer” has to interact with external users as shown in Figure B-11. In Figure B-11, the entity class “<entity>:BER1” and “<entity>:BER2” is changed into the “<data>:BER1” and “<data>:BER2”.

Compare the BER of 3D Beam and LTE system in use case ReadBERStart

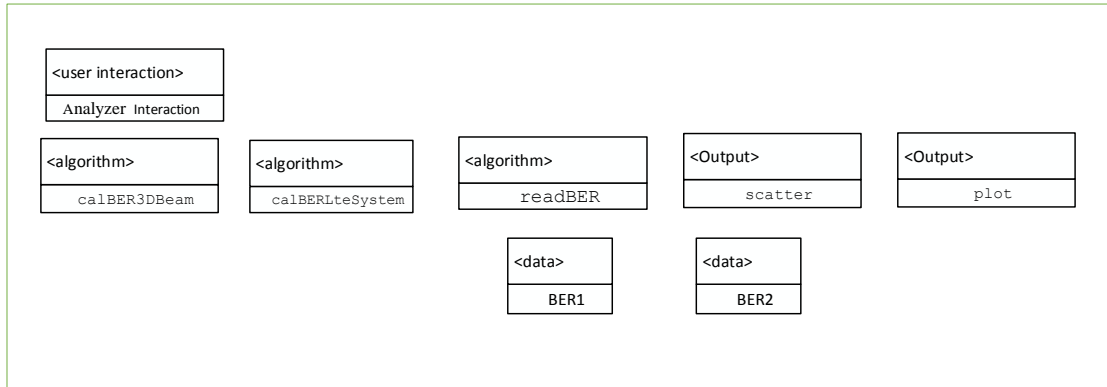


Figure B- 11: The class chart of the use-case mmReadBERStart

The dynamic model of the use-case **mmReadBERStart** is shown in Figure B-12 and the message description is in Table B-4.

Table B- 4: The message description

<p><b>D1:</b> The “Analyzer” sends the start to “&lt;user interaction&gt;: Analyzer Interaction”.</p> <p><b>D2.1:</b> The “&lt;user interaction&gt;: Analyzer Interaction” sends information about the modulation types, type of system (SISO or MIMO) and the noise range to the “&lt;algorithm&gt;:calBERLteSystem”, and then start the calculation.</p> <p><b>D2.2:</b> The “&lt;algorithm&gt;:calBERLteSystem” outputs the BER to “&lt;output&gt;:plot”.</p> <p><b>D2.3:</b> The “&lt;algorithm&gt;:calBERLteSystem” sends the transmitting signals to the “&lt;output&gt;:scatter”.</p> <p><b>D3.1:</b> The “&lt;user interaction&gt;:Analyzer Interaction” send the information, chose the beams and UEs on random selection, to “&lt;algorithm&gt;:calBER3DBeam”.</p> <p><b>D3.2:</b> The “&lt;algorithm&gt;:calBER3DBeam” sends the two received signals from two different weighting methods to the “&lt;output&gt;:scatter”.</p> <p><b>D4.1:</b> The “&lt;algorithm&gt;:readBER” reads the BER from the “&lt;data&gt;:BER1”.</p> <p><b>D4.2:</b> The “&lt;algorithm&gt;:readBER” outputs the Statistical Boundary of BER1 to the “&lt;output&gt;:plot”.</p> <p><b>D4.3:</b> The “&lt;algorithm&gt;:readBER” reads the BER from the “&lt;data&gt;:BER2”.</p> <p><b>D4.4:</b> The “&lt;algorithm&gt;:readBER” outputs the Statistical Boundary of BER2 to the “&lt;output&gt;:plot”.</p> <p><b>D5:</b> The “&lt;output&gt;:scatter” shows the scatter for Received signal in the “&lt;user interaction&gt;:Analysts Interaction”.</p> <p><b>D6:</b> The “&lt;output&gt;:plot” shows the plot of the BER in the “&lt;user interaction&gt;: Analyzer Interaction”.</p>
--

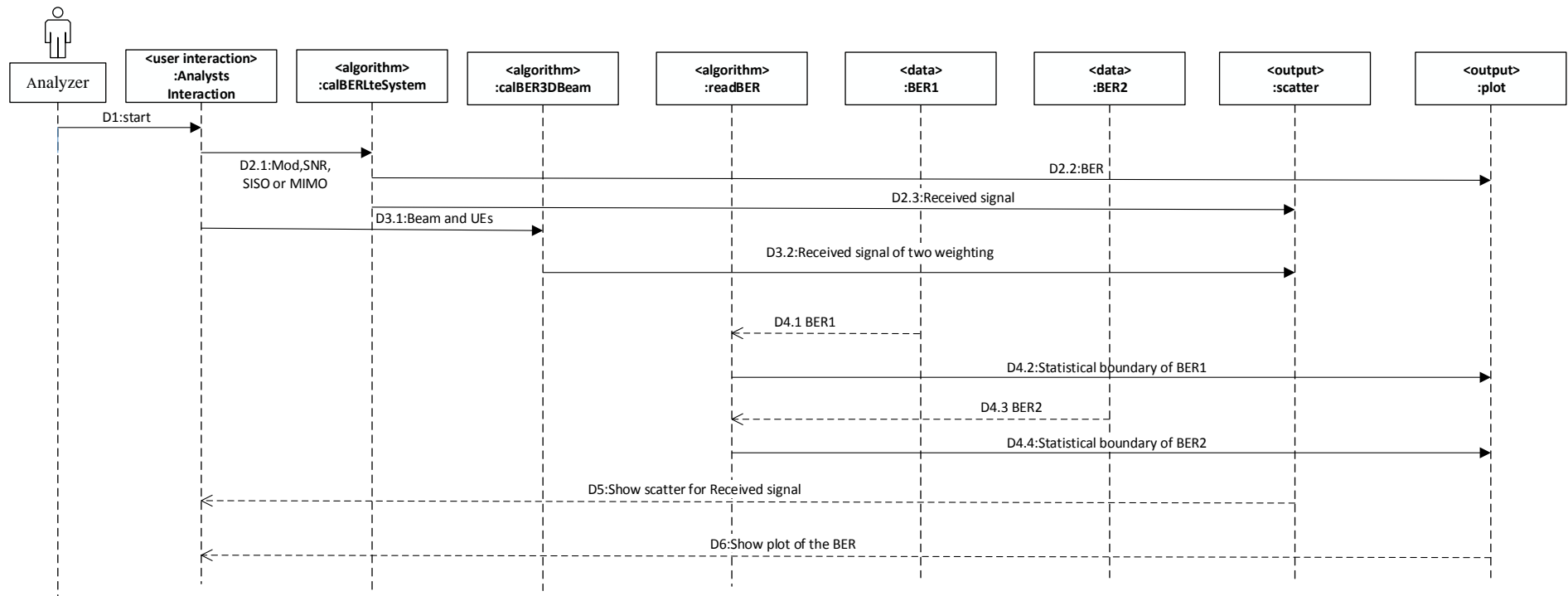


Figure B- 12: The dynamic model of the use-case mmReadBERStart

## B.1.5 CompBERStart Use-case

The use-case **CompBERStart** is different with the use-case **BERCellUEsStart** in cluster UE program. Table B-5 shows the UML use-case description for “**CompBERStart**” and Figure B-13 is the activity diagram for this use-case.

**Table B- 5: The UML use-case description for “CompBERStart”**

<p><b>Name of Use Case:</b> <b>CompBERStart</b></p> <p><b>Introduction:</b> Calculate the BER under the two weighting methods and save them in two data files such as simBER1 and simBER2; and then the CDF of BER will be displayed.</p> <p><b>Participator:</b> Analyzer</p> <p><b>Preconditions:</b> The Simulation data, base station, weighting matrices, SINR data are presented.</p> <p><b>Main sequence (as FigureB-13 shown):</b></p> <ol style="list-style-type: none"><li>10. Analyzer start up.</li><li>11. Calculate the BER1 for the equal weighting.</li><li>12. Calculate the BER2 for the new weighting.</li><li>13. Generate the data files, simBER1 and simBER2, to save the BER1 and BER2.</li><li>14. Calculate the CDF for BER1 and BER2.</li><li>15. Display the CDF of BER1 and BER2.</li></ol> <p><b>Alternative sequence:</b></p> <p>None</p> <p><b>Post-condition:</b></p> <p>Display the CDF of BER1 and BER2.</p>
--

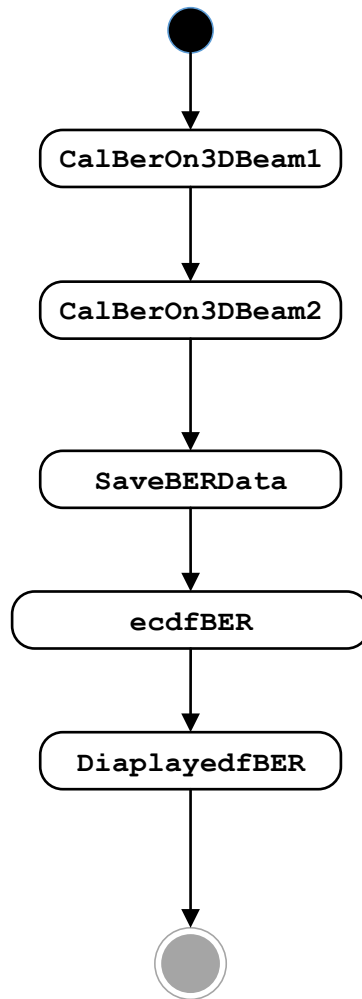


**Figure B- 13: The activity diagram for this use-case CompBERStart**

The static model of the use-case **CompBERStart** is shown in Figure B-14 which has three categories, entity class, algorithm class and output class. The entity class includes the “<entity>:Analyzer”, “<entity>:simData”, “<entity>:WeightLSM”, “<entity>:SINR” , “<entity>:simBER1”and “<entity>:simBER2”. Moreover, the description of the entity class is shown in Figure B-15. The algorithm class includes the “<algorithm>:CalBerOn3DBeam”, and “<algorithm>:ecdf”.The output class is "<output>:plot".

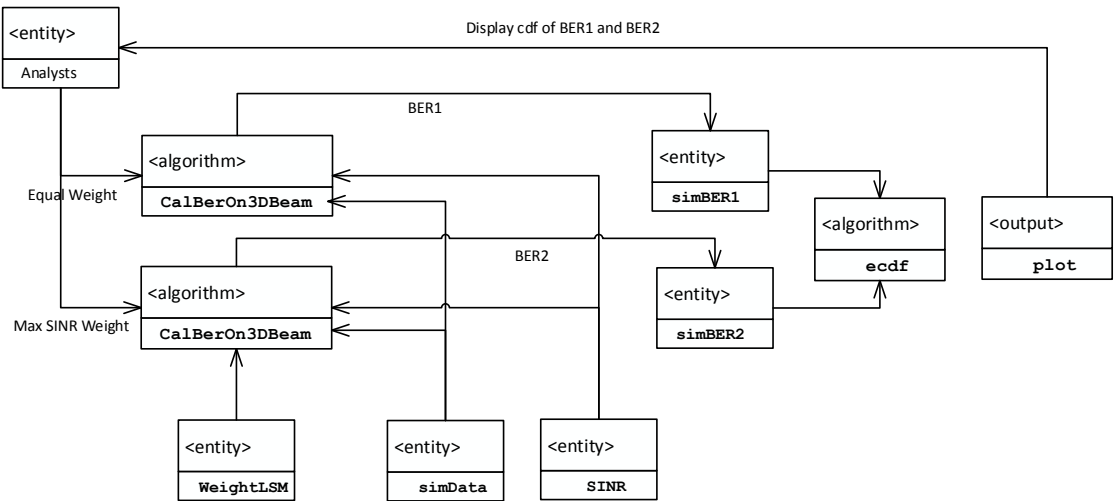


Figure B- 14: The static model of the use-case CompBERStart

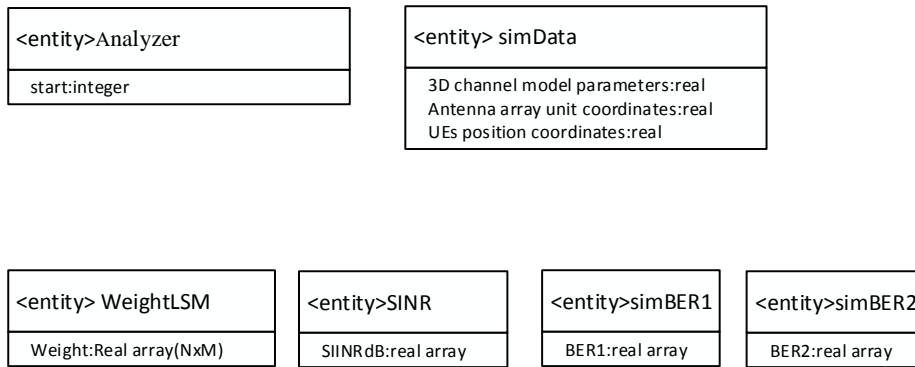


Figure B- 15: The entity class CompBERStart

The “<user interaction>:Analyst Interaction” should be created because the entity class “<entity>:Analyzer” has to interact with external users as shown in Figure B-16. In Figure B-16, the output data have the “<data>:simData”, “<data>:WeightLSM”, “<data>:SINR”, “<data>:simBER1” and “<data>:simBER2”.

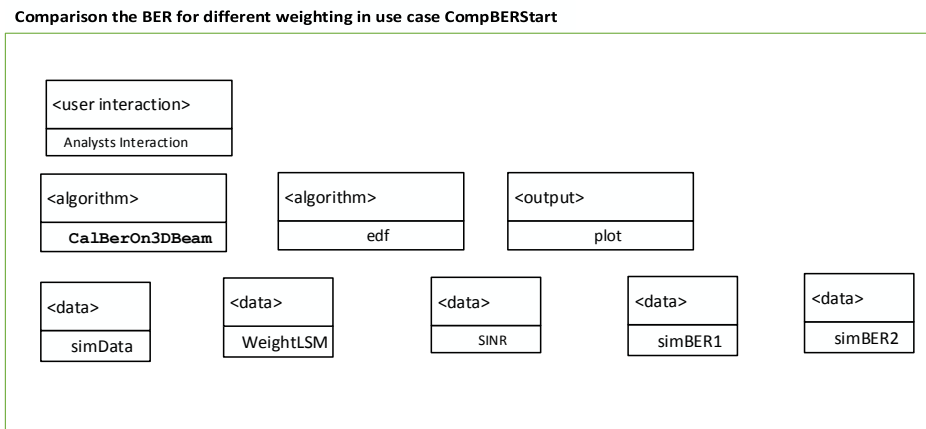


Figure B- 16: The class chart of the use-case CompBERStart



The dynamic model of the use-case **CompBERStart** is shown in Figure B-17 and the message description is in Table B-6.

**Table B- 6: The message description for use-case CompBERStart**

- |  |
|--|
| <p><b>C1:</b> The “Analyzer” sends the start to “&lt;user interaction&gt;: Analyzer Interaction”.</p> <p><b>C2:</b> The “&lt;user interaction&gt;: Analyzer Interaction” sends the information, the equal weighting or new weighting, to the “&lt;algorithm&gt;: CalBerOn3DBeam”, and then start the calculation.</p> <p><b>C3:</b> The “&lt;algorithm&gt;:CalBerOn3DBeam” reads the simulation environment data from the “&lt;data&gt;:simData”.</p> <p><b>C4:</b> The “&lt;algorithm&gt;:CalBerOn3DBeam” reads the weighting data file from the “&lt;data&gt;:WeightLSM”.</p> <p><b>C5:</b> The “&lt;algorithm&gt;:CalBerOn3DBeam” reads the SINR data file from the “&lt;data&gt;:SINR”.</p> <p><b>C6:</b> The “&lt;algorithm&gt;:CalBerOn3DBeam” creates the BER1 data file in the “&lt;data&gt;:BER1”.</p> <p><b>C7:</b> The “&lt;algorithm&gt;:CalBerOn3DBeam” creates the BER2 data file in the “&lt;data&gt;:BER2”.</p> <p><b>C8:</b> The “&lt;algorithm&gt;:ecdf” reads the BER1 data from the “&lt;data&gt;:simBER1”.</p> <p><b>C9:</b> The “&lt;algorithm&gt;:ecdf” reads the BER2 data from the “&lt;data&gt;:simBER2”.</p> <p><b>C10:</b> The “&lt;algorithm&gt;:ecdf” sends the CDF of the BER1 and BER2 to “&lt;output&gt;:plot”.</p> <p><b>C11:</b> The “&lt;output&gt;:plot” display the CDF in the “&lt;user interaction&gt;: Analyzer Interaction”.</p> |
|--|

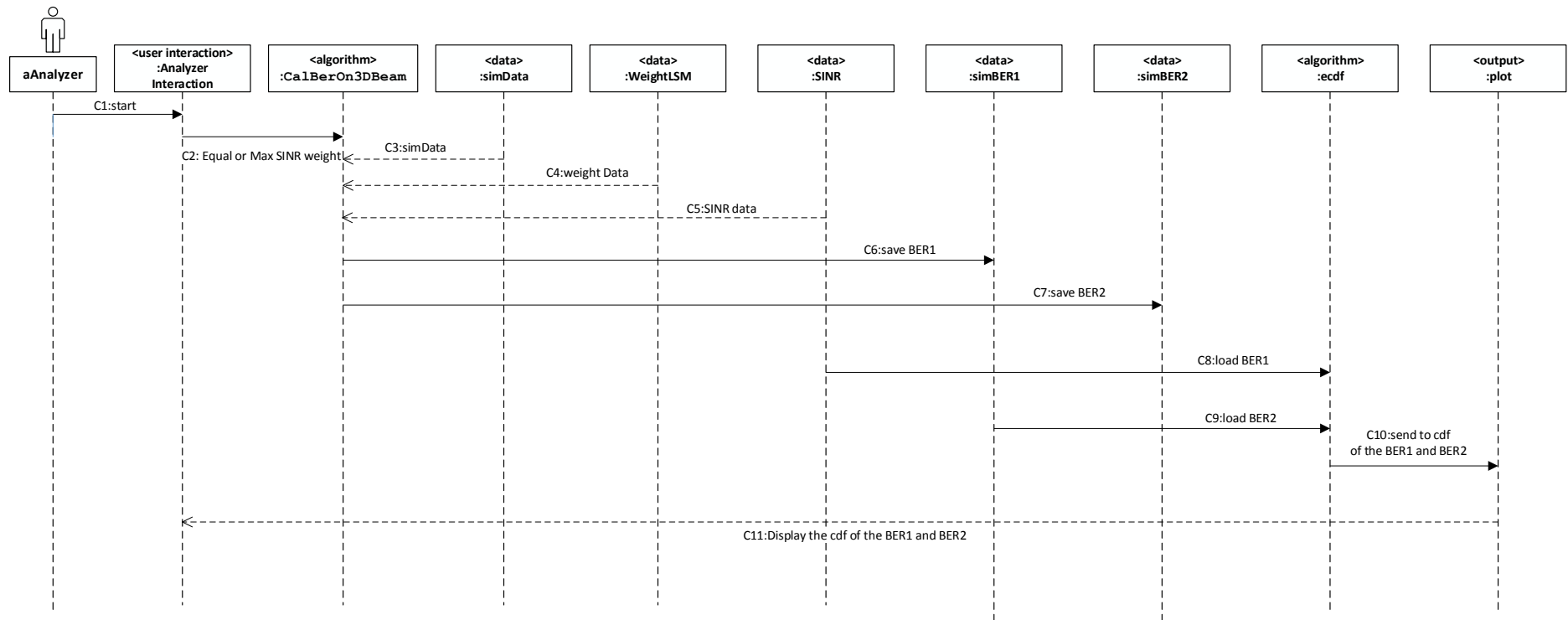


Figure B- 17: The dynamic model of the use-case CompBERStart

## B.1.6 ReadCompBER Use-case

The use-case **ReadCompBER** is different with the use-case **Plot3DStart** in cluster UE program. Table B-7 shows the read and present data use-cases description for “**ReadCompBER**” and Figure B-18 is the activity diagram for this use-case.

**Table B- 7: The read and present data use-cases description for “ReadCompBER”**

<p><b>Name of Use Case: ReadCompBER</b></p> <p><b>Introduction:</b> Read the BER data under the different weightings and display them.</p> <p><b>Participator:</b> Analyzer</p> <p><b>Preconditions:</b> The data files “&lt;data&gt;:simBER1” and “&lt;data&gt;:simBER2” have been created.</p> <p><b>Main sequence (as FigureB-18 shown):</b></p> <ol style="list-style-type: none"><li>1. Analyzer start up.</li><li>2. Read the BER data for the “&lt;data&gt;:simBER1” and “&lt;data&gt;:simBER1”.</li><li>3. Calculate the CDF for BER1 and BER2.</li><li>4. Displays the CDF of BER1 and BER2 under the different weightings.</li></ol> <p><b>Alternative sequence:</b></p> <p>None.</p> <p><b>Post-condition:</b></p> <p>The system displays the the CDF of BER1 and BER2 under the different weighting.</p>
--

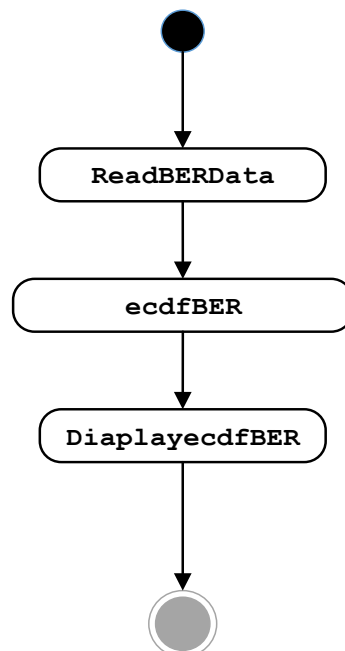


**Figure B- 18: The activity diagram for this use-case ReadCompBER**

The static model of the use-case **ReadCompBER** is shown in Figure B-19, which has three categories, entity class, algorithm class and output class. The entity class includes the “<entity>:Analyzer”, “<entity>:simBER1” and “<entity>:simBER2”. Moreover, the description of the entity class is shown in Figure B-20. The output class is “<output>:plot”. The algorithm class is “<algorithm>:ecdf”.

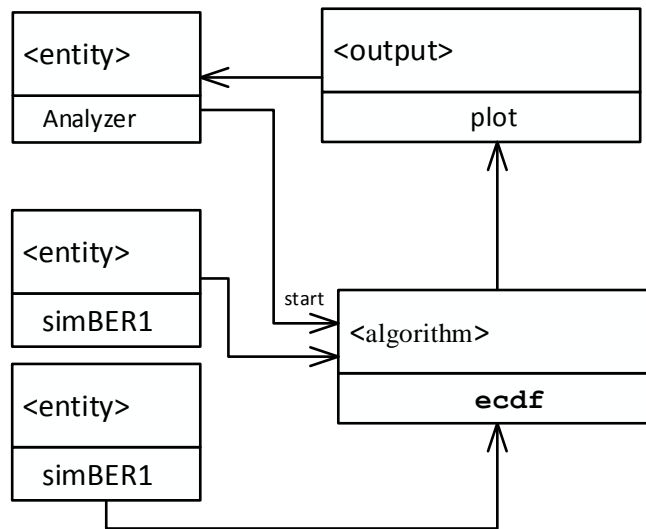


Figure B- 19: The static model of the use-case ReadCompBER

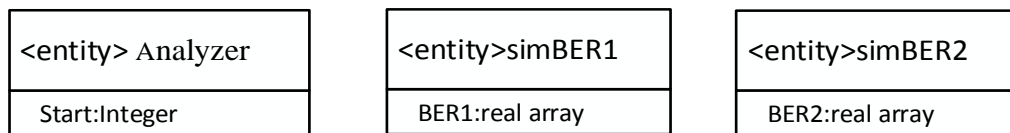


Figure B- 20: The entity class of the use-case ReadCompBER

The “<user interaction>:Analyzer Interaction” should be created because entity class “<entity>:Analyzer” has to interact with external users as shown in Figure B-21. In Figure B-21, the entity class “<entity>:simBER1” and “<entity>:simBER2” is changed to the “<data>simBER1” and “<data>simBER2”.

Displays the CDF of BER1 and BER2 under the different weighting in use case ReadCompBER

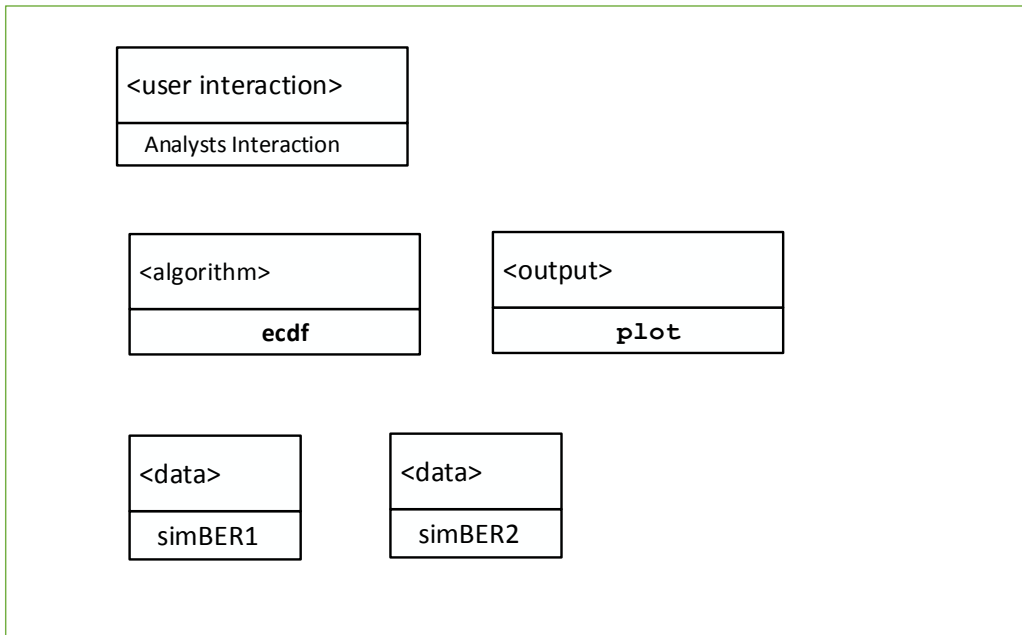


Figure B- 21: The class chart of the use-case ReadCompBER

The dynamic model of the use-case **ReadCompBER** is shown in Figure B-22 and the message description is in Table B-8.

Table B- 8: The message description of use-case ReadCompBER

<p><b>P1:</b> The “Analyzer” sends the start to “&lt;user interaction&gt;: Analyzer Interaction”.</p> <p><b>P2:</b> The “&lt;user interaction&gt;: Analyzer Interaction” sends the start to “&lt;algorithm&gt;:ecdf”.</p> <p><b>P3:</b> The “&lt;algorithm&gt;:ecdf” reads the BER data from “&lt;data&gt;simBER1”.</p> <p><b>P4:</b> The “&lt;algorithm&gt;:ecdf” reads the BER data from “&lt;data&gt;simBER2”.</p> <p><b>P5:</b> The “&lt;algorithm&gt;:ecdf” sends the CDF data to “&lt;output&gt;:plot” and start to it.</p> <p><b>P6:</b> The “&lt;output&gt;:plot” displays the CDF of the BER1 and BER2 under the different weightings in the “&lt;user interaction&gt;: Analyzer Interaction”.</p>
---

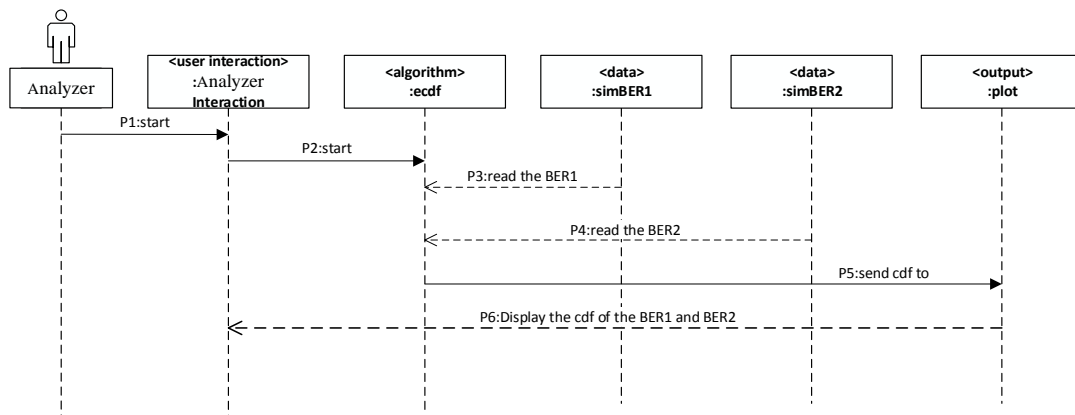


Figure B- 22: The dynamic model of the use-case ReadCompBER

## B.2 The Simulation System design

All the simulation system designs are performed under the Matlab R2016b software environment.

### B.2.1 Data Class

In these 7 UML use-cases, there are 5 classes, which are shown in Figure B-23. In the Matlab R2016b program, they are all structure variables, which are used in different functions.

data classes in 7 use cases

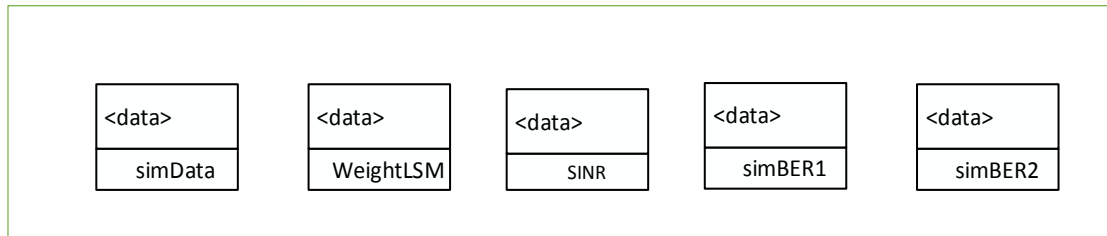


Figure B- 23: Data classes for 7 UML use-cases

### B.2.2 Output Class

In these 7 UML use-cases, there are 2 classes, which are shown in Figure B-24. In the Matlab R2016b program, they are all corresponding functions.

output classes in 7 use cases

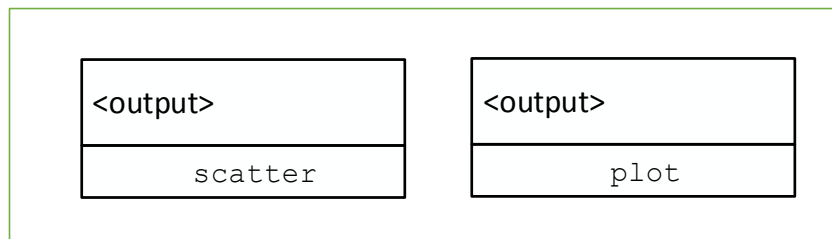
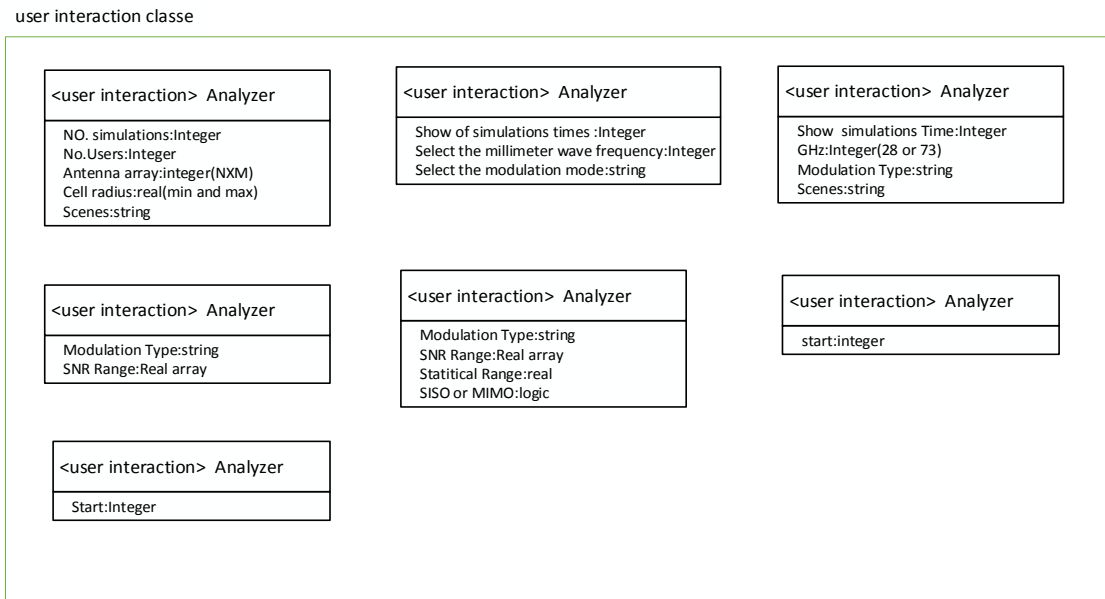


Figure B- 24: Output classes for 7 UML use-cases

### B.2.3 Interactive Interface

In these 7 UML use-cases, there are 7 interactive interfaces, which have different

input parameters as shown in Figure B-25.



**Figure B- 25: Interactive interfaces in7 UML use-cases**

The Matlab R2016b software was used to create a GUI function for the interactive interface as shown in Figure B-26, which is named **main.m**.

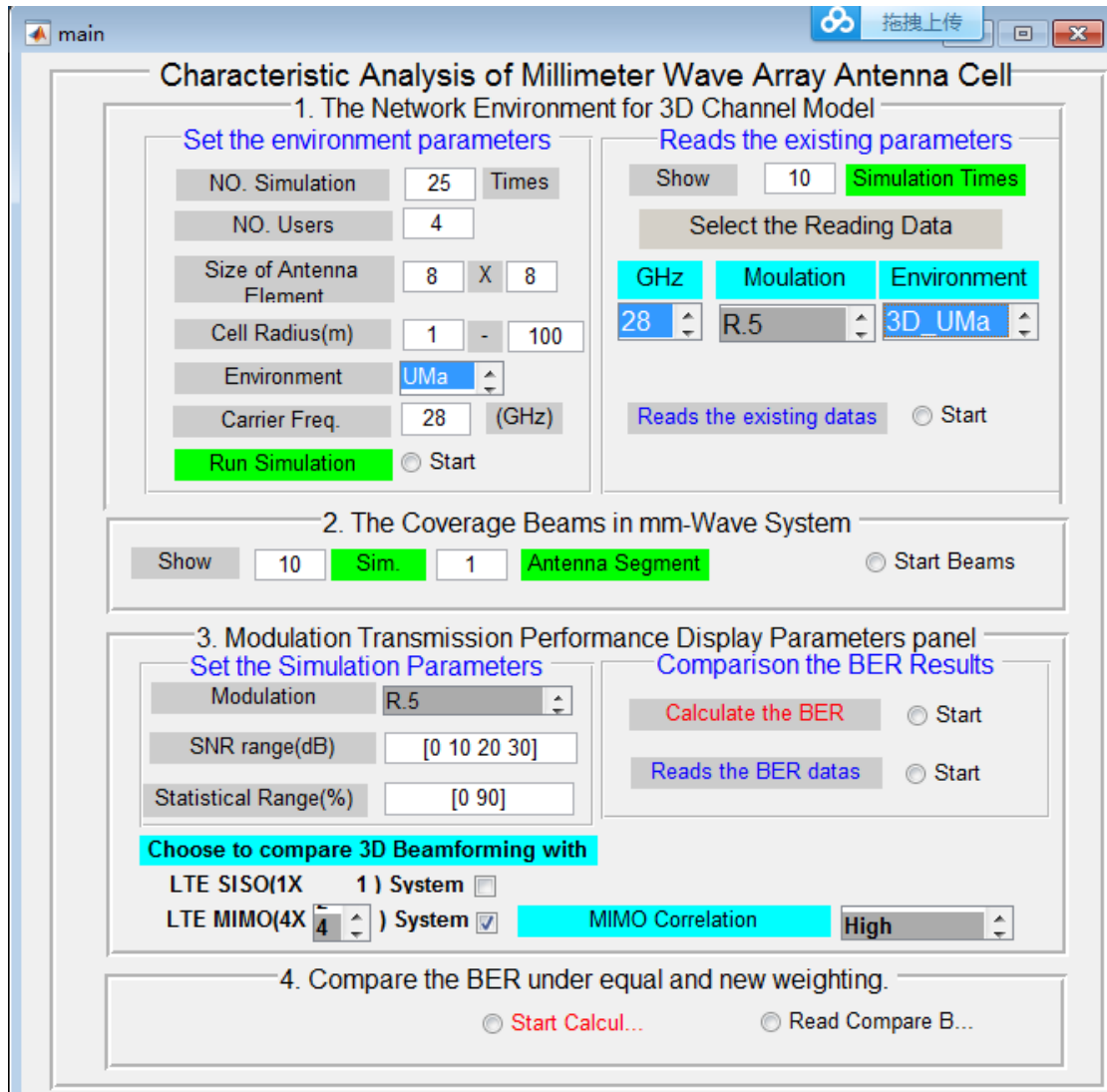


Figure B- 26: A GUI function for the interactive interface

In this program, all options and parameters are built in **main.fig**, namely the “Characteristic Analysis of Millimeter Wave Antenna Arrays Cell”. This function presents “Set the environment parameters” (related to **SimStart\_Callback**) in the “Network Environment for 3D Channel Model” and asks the user to set the simulation parameters such as number of UEs etc. Since 4 areas may be covered and 20 or more simulation runs may be used and it is impractical for all these to be presented, the user needs to choose which simulation run and which coverage area to display. This processing is performed in the “Coverage Beams in mm-wave system” (related to **BeamStart\_Callback**).

“Modulation Transmission Performance Display Parameters panel” (related to **mmCBERStart\_Callback**) allows the user to set the modulation type for the mm-



wave system; and the type, size and correlation for the comparison LTE MIMO system. It also allows the user to define what SNR range to display and the BER confidence interval to plot in mm-wave system.

“Comparison of the BER under equal and new weighting” (related to **CompBERStart\_Callback**) displays a figure to compare how the BER in different systems, which use the equal weighting matrix and the new weighting matrix in two mm-wave systems. The CDF of BER for both of them are shown in one figure for comparison.

### B.2.4 The simulation systems

The **main.m** is the main program for the simulation system, which has 7 sub-systems including **SimStart\_Callback**, **ReadStart\_Callback**, **BeamStart\_Callback**, **mmCBERStart\_Callback**, **ReadBERStart\_Callback**, **CompBERStart\_Callback** and **ReadCompBER\_Callback** as shown in Figure B-27.

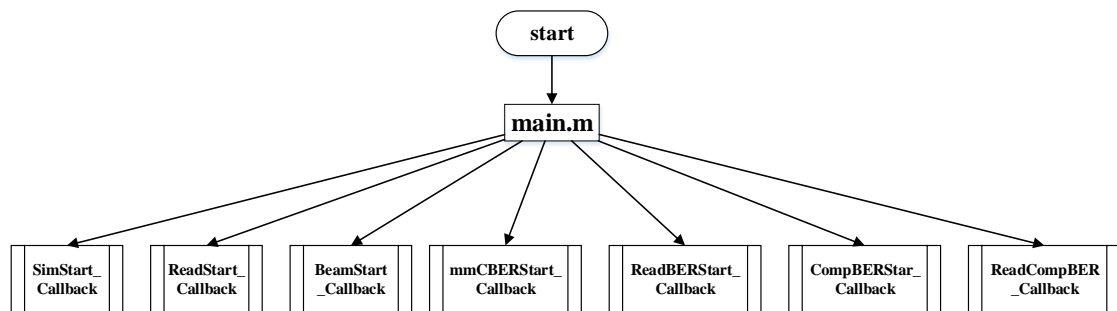


Figure B- 27: sub-systems in the main.m

In Appendix B, the sub-systems **SimStart\_Callback**, **ReadStart\_Callback** and **BeamStart\_Callback** are same as the sub-systems with the same name in Chapter 4 simulation system. Therefore, Appendix B explained the significance of function for **mmCBERStart\_Callback**, **ReadBERStart\_Callback**, **CompBERStart\_Callback** and **ReadCompBER\_Callback**.

### B.3 Function mmCBERStart\_Callback (hObject, eventdata, handles)

Call the function “**mmCBERStart\_Callback**” in **main.m**, which is a radio button in **main.fig**. In this function, the 3D Channel model are regenerated by the new weighting or the equal weighting in the mm-wave system and the received signals of mm-wave system are obtained. Moreover, The BER for each UE in these two mm-wave systems are calculated, which are saved in the BER1 and BER2 data file. The parameter “hObject” represents the handling for function, “eventdata” is reserved to be defined in a future version of MATLAB and “handles” is structured the handles and input data. The flow chart of functions is shown in Figure B-28.

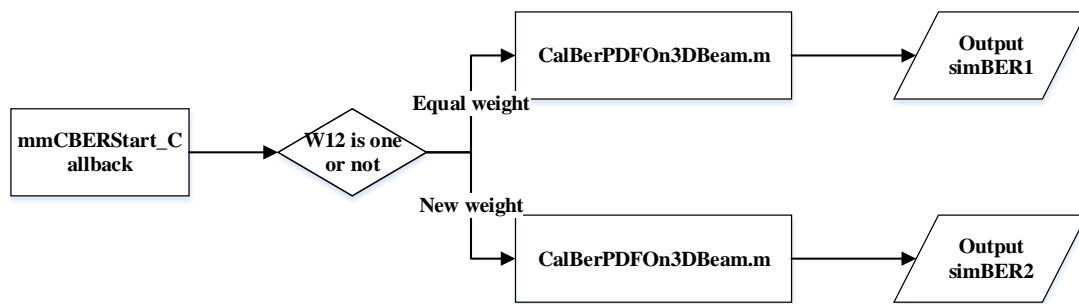


Figure B- 28: The flow chart of the function mmCBERStart\_Callback

#### B.3.1 Function CalBerPDFOn3DBeam

- **Function [simBER] = CalBerPDFOn3DBeam(SNRIn, SINRdB, enb, W12)**

Call the function **CalBerPDFOn3DBeam.m** from the function “**CBERStart\_Callback**”, in which the equal weighting matrix or the new weighting matrix could be chosen to calculate the BER as the weighting method (W12 is 1, then the equal weighting matrix could be chosen to calculate the BER, others using the new weighting matrix). The BER are calculated for PDF and CDF shown in the figures, which are saved in the files 'data\ BER1.mat' and 'data\ BER2.mat'. The parameters are explained in the Table B-9. The flow chart of functions is shown in Figure B-29.

Table B- 9: The parameters in the function CalBerPDFOn3DBeam

Parameters	Meaning
simBER	The BER of simulation as output
SNRIn	The setting SNR from GUI
SINRdB	The loading SINR from the files
enb	The structurevariable from the RMC R.0-9
W12	The chosen of the weighting matrix

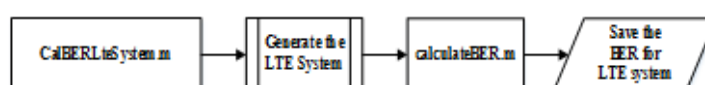


Figure B- 29: The flow chart of the function CalBerPDFOn3DBeam

### B.3.1.1 Function Beam3DChannelSINR

- Function [ht, Weight, Nif, d3D] = Beam3DChannelSINR( Nsim, Nface, Nbeam, nUser, info, Npoffset, Weight\_Ones)

Call the function **Beam3DChannelSINR.m** from the function **CalBerPDFOn3DBeam.m**. In this function, 3D Channel Impulse Response Function for each beamforming has been built, which is the variable **ht**. The parameters are explained in the Table B-10. The flow chart of functions is shown in Figure B-30.

Table B- 10: The parameters in the function Beam3DChannelSINR

Parameters	Meaning
ht	The transfer function of channel model as output
Weight	The weighting matrix as output
Nif	The non-equal-spaced fast Fourier transform
d3D	The 3D distance in 3D Channel Model
Nsim	The time of running simulation

Nface	The number of faces
Nbeam	The number of beams
nUser	The number of UEs
info	The information for OFDM
NPoffset	The offset
Weight_Ones	The chosen of the weighting matrix

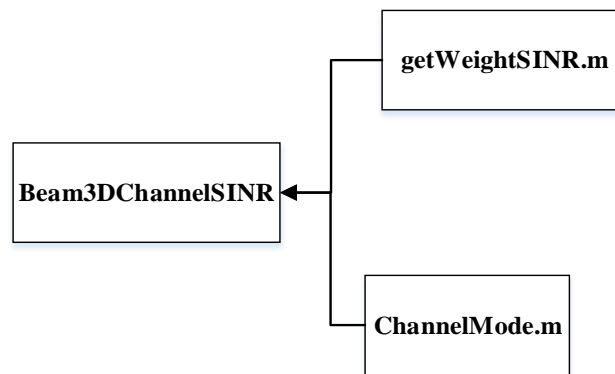


Figure B- 30: The flow chart of the function Beam3DChannelSINR

### B.3.1.1.1 Function getWeightSINR

- **Function [Weight, Num, xyzUE, Center] = getWeightSINR( Nsim, nFace, nArea, Weight\_Ones)**

Call the function **getWeightSINR.m** from the function **Beam3DChannelSINR.m**. The weighting matrix for antenna array is read from the structure variable **WeightLSM** from the file 'data\ WeightwA.mat'. The parameters are explained in the Table B-11.

Table B- 11: The parameters the function getWeightSINR

Parameters	Meaning
Weight	The weighting matrix as output
Num	The size of antenna array as output
xyzUE	The location of UEs as output
Center	The center of cluster for the beam as

	output
Nsim	The time of running simulation
Nbeam	The number of beams
nFace	The number of faces
nArea	The number of areas
Weight_Ones	The chosen of the weighting matrix

### B.3.1.1.2 Function ChannelMode

- **Function [h] = ChannelMode( Nsim, nFace, nBeam, nUser, NIRF, L, N, M, Time)**

This function is same as the function with the same name in cluster user program.

### B.3.1.1.2.1 Function Channel3DMode

Uses Functions:

#### 1. FunctionChannelModel

##### 1.1 FunctionArrDepangle

##### 1.2 FunctionfieldPattern

##### 1.3 Functionexplambda

##### 1.4 Functionxpr

##### 1.5 FunctionChannelLoS

##### 1.5.1 Function fieldPatternLoS

##### 1.5.2 Function xpr

##### 1.5.3 Function explambdaLoS

##### 1.6 Functionpathloss

##### 1.7 FunctionprobLoS

- **Function [Channel, Nz, Ny, N\_AntUE] = Channel3DMode( Nsim, nFace, nArea, nUser, Tnsec )**

This function is same as the function with the same name in cluster user program.

- **Function [Hus, angleAD] = ChannelModel(parset, fixpar, Envpar, Tnsec)**

This function is same as the function with the same name in cluster user program. However, the PL and the LOS probabilities for the mm-wave system need be calculated the carrier frequency is changed to 28 GHz or 73 GHz. Then the new calculation equation for the LOS probabilities, PL and shadowing for the mm-wave system can be calculated, which are the function **probLoS.m** and the function **pathloss.m**.

- **Function [angleAD] = ArrDepangle(parset, fixpar, Envpar)**

This function is same as the function with the same name in cluster user program.

- **Function [FieldData] = fieldPattern(Envpar, angleAD)**

This function is same as the function with the same name in cluster user program.

- **Function [ExpLambda\_NLoS, ExpLambda\_LoS] = explambda(typescen, Envpar, angleAD)**

This function is same as the function with the same name in cluster user program.

- **Function [Exp] = xpr(typescen, typepath, fixpar)**

This function is same as the function with the same name in cluster user program.

- **Function [HusLoS] = ChannelLoS(TypeScen, TypePath, fixpar, Envpar, angleAD )**

This function is same as the function with the same name in cluster user program.

- **Function [FieldTxLoS, FieldRxLoS] = fieldPatternLoS(Envpar, angleAD)**

This function is same as the function with the same name in cluster user program.

- **Function [Exp] = xpr(typescen, typepath, fixpar)**

This function is same as the function with the same name in cluster user program.

- **Function explambdaLoS**

This function is same as the function with the same name in cluster user program.

- **Function [PL, SF] = pathloss(Envpar, d3D, d2D, hUT, hBS, TypeCluster)**

Call the function **pathloss.m** from the function **ChannelModel.m**, which is calculating the PL and shadowing for the channel in mm-wave system. The parameters in the equation for PL is based on the Tables 7.2-1 of the “3GPP TR36.873”, which is modified the parameters in the equation of the PL and shadowing for the mm-wave system because the carrier frequency is changed to 28 GHz or 73 GHz . The parameters are explained in the Table B-12.

**Table B- 12: The parameters in the function pathloss**

<b>Parameters</b>	<b>Meaning</b>
PL	Path loss as output
SF	Shadow fading as output
Envpar	The parameters for the network environment
d3D	The 3D distance in 3D Channel Model
d2D	The 2D distance in 3D Channel Model
h_UT	The height of UE in 3D Channel Model
h_BS	The height of BS in 3D Channel Model
TypeCluster	The type of the path : NLOS or LOS

- **Function [PLOS] = probLoS( Envpar, TypeScen )**

Call the function **probLoS.m** from the function **ChannelModel.m**, which is a new calculation equation for the LOS probabilities for the mm-wave system because the carrier frequency is changed to 28 GHz or 73 GHz. The parameters “Envpar” is the parameters for the network environment and “TypeScen” is the environment selection, 3D UMi or 3D UMa.

### **B.3.1.2 Function receivedSignalConv**

- **Function [Rxx, W] = receivedSignalConv(ht, Weight, txSignal, Nfft)**

This function is same as the function with the same name in cluster user program.

### B.3.1.3 Function calculateBER

- Function `[nErrors, numData] = calculateBER(refData, rxData, nErrors, numData, ncw)`

This function is same as the function with the same name in cluster user program.

## B.4 mmReadBERStart\_Callback (hObject, eventdata, handles)

Call the function “`mmReadBERStart_Callback`” in `main.m`, which is a radio button in `main.fig`. In this function, the program reads the data of the BER for each user from the file 'data\ BER1.mat', 'data\ BER2.mat' and show the results in the figures. The flow chart of functions is shown in Figure B-31.

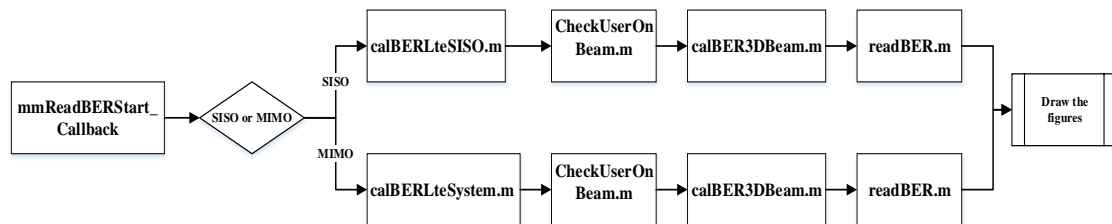


Figure B- 31: The flow chart of function `mmReadBERStart_Callback`

### B.4.1 Function calBERLteSystem

- Function `[simBER] = calBERLteSystem(enb, SNRIn, NRxAnt, MIMOCorr )`

Call the function `calBERLteSystem.m` from the function “`mmReadBERStart_Callback`”, which generates the LTE MIMO system and calculates the BER for the system. Moreover, it shows the results in the figures, which draws the constellation figure for receiver and the mean of BER for LTE system. The parameters are explained in the Table B-13. The flow chart of functions is shown in Figure B-32.



**Table B- 13: The parameters in the function calBERLteSystem**

<b>Parameters</b>	<b>Meaning</b>
simBER	The BER of simulation as output
enb	The structure variable from the RMC R.0-9 in Matlab 2016b
SNRIn	The setting SNR from GUI
NRxAnt	The size of antenna array
MIMOCorr	The type of the MIMO correlation

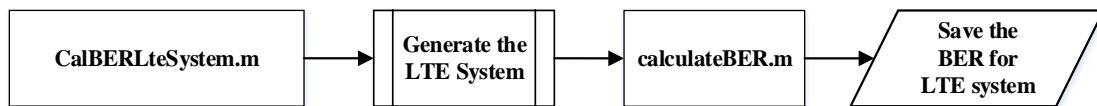


**Figure B- 32: The flow chart of the function calBERLteSystem**

#### **B.4.1.1 Function calculateBER**

- **Function [nErrors, numData] = calculateBER(refData, rxData, nErrors, numData, ncw)**

Call the function **calculateBER.m** from the function **calBERLteSystem.m**, which is the calculation of BER for the transmitting signals and the received signals. The BER for all UEs are determined, in which the BER are saved in “nErrors”.

#### **B.4.2 Function calBERLteSISO**

- **Function [ simBER ] = calBERLteSISO( enb, SNRIn )**

Call the function **calBERLteSISO.m** from the function “**mmReadBERStart\_Callback**”, which generates the LTE SISO system and calculates the BER for the system. Moreover, it shows the results in the figures, which draws the constellation figure for receiver and the mean of BER for LTE system. The parameters “enb” is the structure variable from the RMC R.0-9 in Matlab 2016band “SNRIn” is the setting SNR from GUI. The flow chart of functions is shown in Figure B-33.

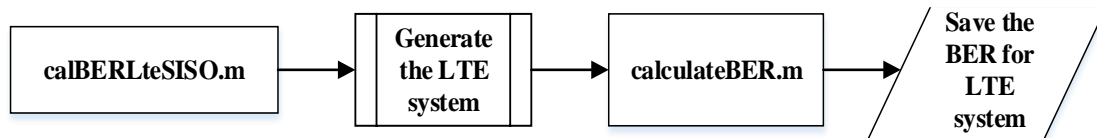


Figure B- 33: The flow chart of the function calBERLteSISO

### B.4.3 Function CheckUserOnBeam

- **Function [ N1, N2, N3, N4 ] = CheckUserOnBeam(Nsim1, Nuser)**

Call the function **CheckUserOnBeam.m** from the function “**mmReadBERStart\_Callback**”. In this function, one UE, which is in an appointed beam, can be selected and checked it whether is covered by beam. The function reads the information data for UEs. The parameters are explained in the Table B-14.

Table B- 14: The parameters in the function CheckUserOnBeam

Parameters	Meaning
N1	The order time for running simulation as output
N2	The order number of face as output
N3	The order number of beam as output
N4	The order number of UEs as output
Nsim1	The number of time for running simulation
Nuser	The number of UEs

### B.4.4 Function calBER3DBeam

- **Function [simBER] = calBER3DBeam(enb, SNRIn, SINRdB, Nsim, Nface, Nbeam, nUser, W12)**

Call the function **calBER3DBeam.m** from the function “**mmReadBERStart\_Callback**”. The function calculates the BER for mm-wave system, which is similar to **CalBerPDFOn3DBeam.m**. In this function, the constellation figure and the figure of BER for millimeter-wave systems in two weighted states has been shown. The

parameters are explained in the Table B-15. The flow chart of functions is shown in Figure B-34.

**Table B- 15: The parameters in the function calBER3DBeam**

<b>Parameters</b>	<b>Meaning</b>
simBER	The BER for mm-wave system as output
enb	The structure variable from the RMC R.0-9 in Matlab 2016b
SNRIn	The setting SNR from GUI
SINRdB	The loading SINR from the files
Nsim	The time of running simulation
Nface	The number of faces
Nbeam	The number of beams
nUser	The number of UEs
W12	The chosen of the weighting matrix

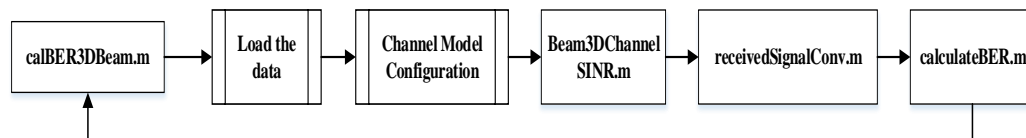


**Figure B- 34: The flow chart of the function calBER3DBeam**

### B.4.5 Function readBER

- **Function [medianBER,p5BER,p95BER] = readBER(SNRdB, Prc, W12)**

Call the function **readBER.m** from the function “**mmReadBERStart \_Callback**”. The function reads the BER data from the file 'data\ BER1.mat' and 'data\ BER2.mat'. The structure variable **simBER** has been read to show the CDF and PDF figures of BER for each user, which is based on the chosen percentile value. The parameters are explained in the Table B-16.

Table B- 16: The parameters in the function readBER

Parameters	Meaning
medianBER	The BER in median values of percentile value for UE as output
p5BER	The BER in minimum values of percentile value for UE as output
p95BER	The BER in maximum values of percentile for UE as output
SNRdB	The SNR for calculation
Prc	The interval values of percentile
W12	The chosen of the weighting matrix

## B.5 Function CompBERStart\_Callback (hObject, eventdata, handles)

Call the function “**CompBERStart\_Callback**” in **main.m**, which is a radio button in **main.fig**. In this function, the CDF of BER, which are from them m-wave system by the new weighting method and the mm-wave system by the equal weighting matrix, has been compared in one figure. The flow chart of functions is shown in Figure B-35.

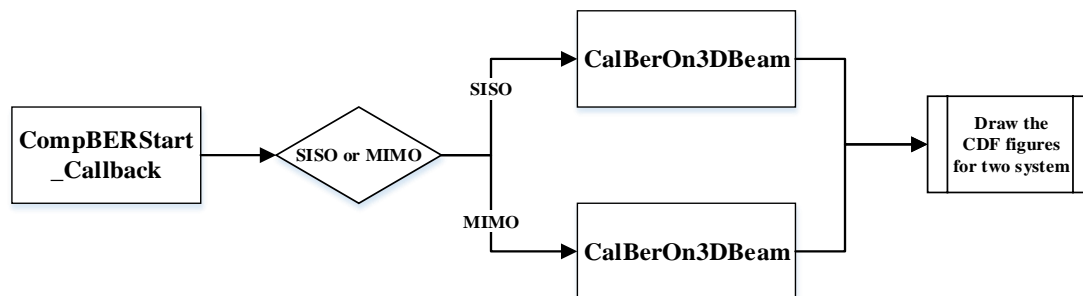


Figure B- 35: The flow chart of the function CompBERStart\_Callback

### B.5.1 Function CalBerOn3DBeam

- **Function [simBER] = CalBerOn3DBeam(SNRIn, enb, Weight\_Ones)**

Call the function **CalBerOn3DBeam.m** from the function “**CompBERStart\_Callback**”. The function calculates the BER for the mm-wave system, which is similar to **CalBerOn3DBeam.m**. The parameters are explained in the Table B-17. The flow chart of functions is shown in Figure B-36.

Table B- 17: The parameters in the function CalBerOn3DBeam

Parameters	Meaning
simBER	The BER for mm-wave system as output
SNRIn	The setting SNR from GUI
enb	The structure variable from the RMC R.0-9 in Matlab 2016b
Weight_Ones	The chosen of the weighting matrix

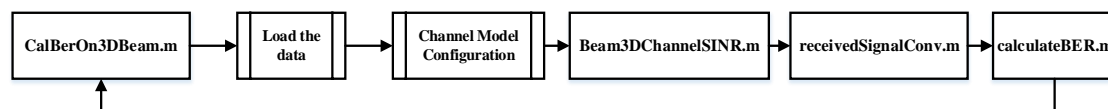


Figure B- 36: The flow chart of the function CalBerOn3DBeam

### B.6 Function ReadCompBER\_Callback (hObject, eventdata, handles)

Call the function “**ReadCompBER\_Callback**” in **main.m**, which is a radio button in **main.fig**. This function drawing the CDF figure is based on loading the data from the files 'data\simBER1' and 'data\simBER2', which are the BERdata for the two mm-wave system. The flow chart of functions is shown in Figure B-37.

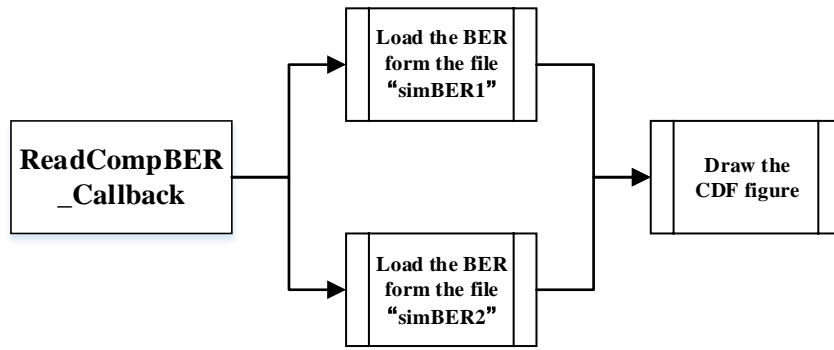


Figure B- 37: The flow chart of the function ReadCompBER\_Callback